UNIVERSITY OF SOUTHAMPTON

DYNAMIC MODELLING OF BEAM-PLATE SYSTEMS IN THE MID-FREQUENCY REGION

by

Ji Woo Yoo

Institute of Sound and Vibration Research
Faculty of Engineering, Science and Mathematics

Thesis submitted for the degree of
Doctor of Philosophy

June 2005

UNIVERSITY OF SOUTHAMPTON

ABSTRACT

FACULTY OF ENGINEERING, SCIENCE AND MATHEMATICS
INSTITUTE OF SOUND AND VIBRATION RESEARCH

Doctor of Philosophy

DYNAMIC MODELLING OF BEAM-PLATE SYSTEMS IN THE MID-FREQUENCY REGION

By Ji Woo Yoo

The mid-frequency region, where neither a low frequency deterministic method nor a high frequency statistical method may be amenable requires special treatment. For structures such as automotive vehicles, ships and aircraft, this region corresponds to an important part of perceived sound spectrum, and it is necessary to develop practical methods to predict the response in this region. This thesis develops and compares approaches that can deal with built-up structures in the mid-frequency range.

Most previous work on this region has been limited in application to a simple structure, for example, a one-dimensional system or a single beam coupled to a plate so that its applicability to more complex structures has yet to be determined.

Thus, an objective of this thesis is to develop approaches that can deal with more complicated structures in the mid-frequency region. Two principal configurations considered are a fully framed rectangular plate and a rectangular plate with two beams on opposite parallel edges. While the beams are relatively stiff, the plate is more flexible. Such systems are typical components in industrial applications and it is important to identify their dynamic behaviour at the mid and high frequencies.

The analytical models considered are based on a wave method, proposed by Grice and Pinnington. The beam is assumed infinitely stiff to torsion and thus the plate edge at a junction is sliding. This method starts from free wavenumbers of subsystems and uses an approximate impedance for the plate in determining the coupled beam wavenumbers. It is reasonable as long as the beam is much stiffer than the plate. This approximate wave method is enhanced by introducing Muller's method to solve for the wavenumbers.

The model is extended from a single-beam-plate system, to a plate with two parallel beams which is modelled using a symmetric-antisymmetric wave model, and a plate surrounded by four beams which is modelled using a plate-decoupled wave model. The modelling techniques for the two systems are different, although a similar wave approach is used. Because the wave methods provide an approximate response, a Fourier technique and a modal method based on simplified boundary conditions are also considered for comparison. These provide exact responses for the two-beam-plate and four-beam-plate systems respectively for the particular boundary conditions. The wave method can be applied more generally and is computationally more efficient but involves approximations that are not always justified. For example, mobilities show some discrepancy when the coupled beam wavenumbers found from the travelling wave have a high rate of decay.

An experimental study is performed to verify the analytical models. Comparisons based on power and subsystem energy ratios show that the wave models replicate well the experimental results at mid and high frequencies. Also, the modal and Fourier models show good agreement at these frequencies, which justifies their use of simplified boundary conditions. A wavenumber correlation technique has been used to verify experimentally that the wavenumbers in the plate follow those of the beam in the direction parallel to the beam.

Table of Contents

Acknowledgements

I would like to dedicate this thesis to my wife Yun Kyong. She worked harder and worried more than myself, as also a friend and colleague. Without her immense help, all this work would not be possible.

My supervisors, Prof. David J. Thompson and Dr. Neil S. Ferguson, are teachers of whom I cannot imagine better. My greatest gratitude should go to them. They have taught me many things from the viewpoint of life as well as in study. I am also grateful to them for the financial arrangement and support.

I wish to acknowledge Prof. Brian R. Mace and Dr. Tim P. Waters who gave me invaluable comments and advice during my study. Also, I really thank Ms. Anne-Marie McDonnell for her warm help.

I would like to share my pleasure with my father and mother who have always been concerned for their son and my father and mother-in-law who believe in their son. I also thank my brothers and sisters and especially my brother-in-law and his wife.

During living in the United Kingdom, the Korean colleagues and friends who have been and are in Southampton gave me great comfort and consolation. I must express my gratitude to them.

List of Symbols

$\mathbf{A}$	modal correlation matrix
A	wave amplitude (m); cross-sectional area
B	wave amplitude (m)
C	wave amplitude (m); constant
D	wave amplitude (m); beam stiffness (Nm^2); plate stiffness (Nm)
E	Young's modulus of elasticity (N/m^2); energy
$\mathbf{F}$	force vector
F_0	amplitude of force (N)
$\overline{F}_0$	mean square force of a point force (N)
F_i	spatial Fourier transform of force f_i (N/m)
$\mathbf{I}$	identity matrix
I	second moment of area ($=bh^3/12$)
$\mathbf{K}$	stiffness matrix
K	generalised stiffness; function stiffness
L	length or width (m)
$\mathbf{M}$	mass matrix
M	generalised mass; function mass; maximum mode number; amplitude of bending moment; number of sampled data point
N	maximum mode number; number of sampled data point
P	power (Nm/s)
P_{dis}	dissipated power
P_{in}	input power
$P_{i\rightarrow j}$	net power transferred from subsystem i to subsystem j
T	kinetic energy
U	potential (strain) energy
W	Spatial Fourier transform of displacement w (m)
Y	structural mobility (m/sN)
Y_0	point mobility

$\mathbf{Z}$	impedance matrix
Z_b	beam impedance in flexure ($= 2\rho A c_B(1+i)$)
Z_{mass}	impedance of a point mass ($= i\omega m$)
Z'_p	line impedance of a plate (Ns/m^2)
a	constant
b	thickness of a beam (mm)
c_B	phase velocity of a flexural wave
e	frequency and space-averaged error (dB); residual
f	frequency (Hz);
f_c	centre frequency of band (Hz)
f_l	lower frequency of band (Hz)
f_u	upper frequency of band (Hz)
f_i	force per unit length (N/m)
h	height of a beam (mm)
i	$\sqrt{-1}$
k_b	uncoupled beam wavenumber (rad/m)
k_e	coupled nearfield trace wavenumber in y direction (rad/m)
k_p	uncoupled free wavenumber in a plate (rad/m)
k_x	coupled travelling trace wavenumber in x direction (rad/m)
$k_{x,n}$	$n\pi/L_x$
k_y	coupled travelling trace wavenumber in y direction (rad/m)
m	mode number; mass (kg)
m'_b	mass per unit length of a beam (kg/m)
m''_p	mass per unit area of a plate (kg/m^2)
n	mode number; Fourier component number
$\mathbf{q}$	vector containing q
q	generalised coordinate
r	mode number

$\tilde{r}$	complex reflection coefficient
s	mode number
t	thickness (mm); time (s)
v	velocity response (m/s)
w	displacement (m)
x, y, z	Cartesian coordinates (m)
Υ	correlation function
$\mathbf{\Psi}$	matrix containing mode shape function ψ
$\boldsymbol{\beta}$	modal correlation matrix
$\tilde{\beta}$	wave attenuation coefficient
γ	non-dimensional wavenumber ($= k_x/k_b$)
γ_p	non-dimensional wavenumber ($= k_x/k_p$)
δ	Dirac delta function; Kronecker delta; constant
η	structural loss factor (-)
λ	wavelength (m)
ν	Poisson's ratio
ξ	$k_b/\tilde{k}_p$
ρ	density (kg/m^3)
σ	constant
τ	constant
ϕ	mode shape function; $\sqrt{(\gamma\xi)^2+1}$
χ	orthogonal function
ψ	mode shape function; $\sqrt{(\gamma\xi)^2-1}$
μ	$m_p''/\left(m_b' k_p\right)$ (-); mean
ω	radian frequency (rad/s)
$\langle\ \rangle$	spatial average
$\bar{(\ )}$	frequency average
$\tilde{}$	complex quantities

CHAPTER 1

INTRODUCTION

1.1 Background

Since the industrial revolution started in the United Kingdom in the 18th century, vibration, noise and related problems have often been critical issues in most industrial, commercial and domestic situations [1]. In addition, the increasing importance of social and environmentally friendly regulations ensures that noise and vibration must be given a high priority in industry [1, 2]. From the industrial viewpoint and for the welfare of people, this might become more critical in future.

Low frequency dynamics that provides a basic theory for dealing with a noise and vibration problem can often be considered using simple lumped parameter systems analysed using Newton's law of motion. As the frequency range is extended, more complex analytical and numerical models are required, a typical example of which is the widely applied Finite Element Method (FEM) [3-10]. In this, a discretised model of a continuous system is produced using elements that incorporate stiffness, mass and dissipation effects. FE is basically suitable for low frequency analysis because higher frequency calculations require more elements as the wavelength reduces. There is also a more fundamental reason that prevents the higher frequency application. At high frequencies the dynamic response is increasingly sensitive to structural details and consequently there is considerable variability in the response due to uncertainties [11]. This means that the exact modelling of a particular system is limited and impractical [12] and thus high frequency analysis should be carried out in a different way, i.e. a statistical approach which provides more useful spatial and frequency average behaviour.

In this context alternative methods were developed to overcome the disadvantages of the low frequency technique such as FE, the most widely accepted being

Statistical Energy Analysis (SEA) [12-17]. In SEA, the system is considered to be an assembly of subsystems and each subsystem is assigned a single energy degree of freedom [15]. The coupling loss factor (CLF) describes the power transferred through a junction between subsystems. As a probabilistic method, SEA requires a minimum number of modes in each subsystem and it is assumed that subsystems are weakly coupled. These inherent characteristics of SEA imply that it is more suitable for high frequency analyses.

An alternative energy based method, the so-called Energy Flow Method (EFM) has been developed [28-34]. However, the application is also limited to the higher frequency regions in general and some difficulties remain.

Between the low and high frequency is called the mid-frequency region, in which neither method mentioned above is suitable. Therefore, much recent research has attempted to find new methods suitable for mid-frequency analysis. FE-based techniques involving the component mode synthesis (CMS) [35-39], wave methods [40, 41], fuzzy structure theory [42-46] and a mode-based approach [47-49] have been proposed. In addition, some methods combine the advantages of the conventional methods such as FE with the energy flow method (EFM) or wave methods. Theses are called hybrid methods [50-56]. These methods are discussed in more detail in the following sections.

1.2 Low frequency methods

Low frequency analysis has been traditionally important because it represents the fundamental characteristics of a structure and some useful and powerful numerical methods have been developed for this analysis range.

The most common of these is the finite element method. It is widely used in most companies manufacturing mechanical engineering applications. This is primarily due to the increasing dependence on virtual prototyping using FE instead of many

physical experiments. Also both the static and dynamic characteristics of a product can be predicted before manufacturing and other performance, optimisation and design calculations can be considered. For example, it is generally used in the automotive industry to predict body vibrations and interior noise in the low frequency region [5-7]. In an FE model the structure is divided into a finite number of elements, often hundreds of thousands, and an overall stiffness and mass matrix is determined in terms of degrees of freedom (e.g. displacements and rotations) for each element. This is a deterministic method because in principle it is possible to predict the exact behaviour of the system for given material properties.

In general, it is known that more than four linear elements are needed per half bending wavelength to predict and replicate the continuous deformation [3, 4]. The accuracy of the result can usually be improved by increasing the number of elements [8]. This means that for more accurate results in the higher frequency range, a large number of elements should be included. Thus, it is more appropriate for low frequency analysis. This limitation may partially be solved by the significant development of computer speed and memory allowing enlarged frequency ranges to be solved. Also, recent new developments have led to higher order elements being developed [9, 10]. These Hierarchical Finite Elements use higher order polynomial or slope functions which result in fewer elements per wavelength and can result in smaller computational problems. However, even with such a large size of model, predictions can be inaccurate due to the uncertainties of the system. For example, the response of the structure can be very sensitive to small fabrication details so that the dynamic characteristics seem significantly different at high frequencies. Such an example is shown in Figure 1.1 where the measured noise levels in the cabin of 57 nominally identical trucks due to a force input at the wheel show large variations even at frequencies that are not particularly high [11]. If an FE model were made of one of these variants it would not accurately represent the others.

Thus, although extending the frequency range is possible in principle, the variability in the results at high frequencies make this option inappropriate and

undesirable [17]. In such cases the structural analysis often needs to be treated as providing a mean value estimate rather than the detailed response of the structure. Typically one could then average over a number of results from similar FE models but this is computationally expensive and inappropriate. For this reason various methods have been developed, amongst which the most widely accepted is Statistical Energy Analysis (SEA) [12-17].

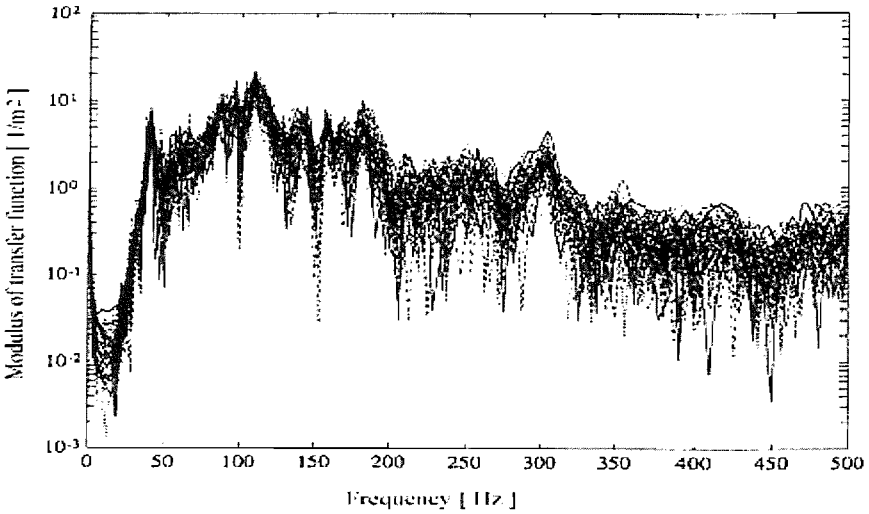

Figure 1.1. Modulus of transfer functions between input force at front left wheel and sound pressure level at the location of driver's head measured on 57 nominally identical vehicles [11].

1.3 High frequency methods

1.3.1 Statistical Energy Analysis: a general overview

In SEA, the system is generally divided into a number of subsystems, the response of which is described in terms of energy. Nominally identical subsystems may have the same gross physical and geometrical properties, but modal characteristics vary due to differences in detailed properties. If they are randomly different in a statistical sense, then the characteristics of the subsystem can be defined in terms of the ensemble average of many such similar but not identical systems [15]. Then, the energy flow between subsystems is found considering a statistical approach

rather than deterministic quantities such as exact natural frequencies and mode shapes.

Although the results are evaluated strictly in terms of ensemble averages, the application based on the ensemble is often impractical. It is known that the variance of the response over the ensemble decreases when the frequency averaging bandwidth increases [15]. Thus, the frequency average technique can be used to approximate the ensemble average if the system has high modal overlap or wide analysis bands are used. The frequency average arises from analysis based on a frequency band, for example an octave or one-third octave band.

The simplest SEA model consists of two subsystems. The time-averaged energy and the power balance relationship of such a system is shown schematically in Figure 1.2 below.

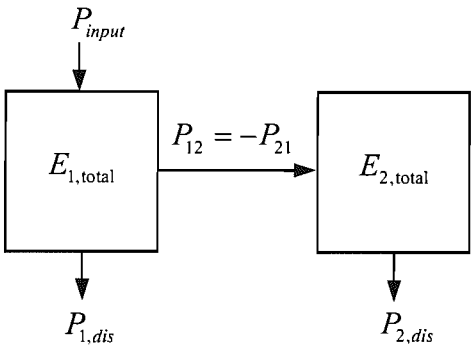

Figure 1.2. Power balance relationship of a coupled structure consisting of subsystems 1 and 2. E is the stored energy in each subsystem, P is the dissipated or transferred net power and subscripts indicate the corresponding subsystems in the coupled system.

The power transferred between subsystems is related to the difference between the mean modal stored energy in the source and receiver subsystems and the coupling loss factor, CLF. This is defined in an analogous way to the dissipation loss factor (DLF) [12, 13]. The values of the CLFs for particular connections are highly

dependent on the physical and geometrical properties and may require numerical calculations [18]. Values can also be estimated using a wave method [19, 20].

In SEA it is assumed that the response is spatially diffuse within each subsystem, so that only the total vibrational energy in each subsystem is important. Because each subsystem or substructure corresponds to only one element of the solution matrix, it is a relatively simple, efficient and low cost method. However, in practical applications there are also some difficulties. One of them is to find the relevant coupling loss factors. To ensure more accurate results for practical structures, more diverse coupling loss factors that include more dynamic characteristics of the corresponding structures should be defined, so that their variability due to uncertainties can be identified [21].

Ideally for application of SEA the subsystems or substructures should be weakly coupled. Coupling is generally considered weak if the ratio of the coupling loss factor to the internal loss factor for the subsystem is substantially less than unity [22]. The response based on SEA depends strongly on the modal overlap. The modal overlap is the ratio of the half-power bandwidth to the average spacing between resonances [12]. If this factor is in the region of unity or greater then no clear resonance peaks can be seen, since the resonance peaks tend to merge together. As variability of the response due to structural uncertainties is of concern, it is preferable to have high modal overlap that generally leads the variance of the response to be low [15]. In addition, for any particular frequency band each substructure should contain a minimum number of modes whose natural frequency falls within the band and there should ideally be equi-partition of vibrational energy between the modes of a substructure [16].

Because of such assumptions mentioned above, the accuracy of the predicted average energy is limited particularly for a system containing components carrying a long wavelength or having a low modal density. This results in a low frequency limit for the applicability of SEA in such cases.

SEA is thus generally used for the high frequency analysis in various areas such as buildings [14], aerospace applications [23] and more recently automotive vehicles. One successful example of the latter was given by Fraser [24], in which wave intensity analysis proposed by Langley [57, 58] was used to model a curved panel and a complex joint modelling technique was studied. Then, the energy level difference of certain panels connected through a joint, such as the roof and the windscreen or the windscreen and the firewall, was predicted in an SEA framework. The sound pressure level (SPL) in the interior saloon due to an engine excitation was predicted by the complex joint SEA model. The result showed good agreement with experiment in terms of one-third octave bands in the frequency range of 100 to 6300 Hz and the most important noise paths were identified.

Another application to an automotive vehicle was carried out by Yamazaki et al [25], where an FE model was used in the calculation of the coupling loss factors. As it is difficult to find the experimental modal density of a complex structure such as an automotive body-in-white, the modal density of each subsystem of the body was determined from the normal mode analysis with an FE model. The coupling loss factors were obtained using the equation for infinite plates connected at a line junction and the effect of the power reflection by the coupled structure was ignored. Thus, in fact they were not calculated in terms of a power balance equation. Although the result is only approximate, the coupling loss factor shows reasonable agreement compared with the experiment above about 500 Hz.

1.3.2 Statistical Energy Analysis: variability at low frequency

The previous studies based on SEA are important because, although a statistical model is normally acceptable for high frequency analysis, it is also helpful to understand the physical behaviour of the structure in the low and mid-frequency regions. Thus, SEA-related studies previously published, especially studies dealing with the variability of the coupling loss factors are discussed here because most difficulties in an SEA application are related to such variability due to uncertainties.

An investigation into the variability of the CLF was conducted by Wester and Mace [26]. They used an explicit ensemble average formulation to analyse two line-coupled finite rectangular plates. The response of the system was described using a wave approach. The subsystem was assumed to be drawn from an ensemble in which the reflection coefficient phase lag is uniformly distributed as a random variable. Accordingly, the ensemble power was presented and compared with the estimates of the CLFs obtained using traditional SEA methods, e.g. infinite plate wave transmission. It was shown that the traditional SEA hypothesis of proportionality between the coupling power and the difference in subsystem mean modal energies is exact for the ensemble average response of the plate systems, regardless of the strength of coupling. Also a CLF traditionally calculated for use in SEA by a wave method, in which semi-infinite subsystems and diffuse fields are assumed, was found generally to over-estimate the exact value based on the ensemble average predictions at low frequencies (low modal overlap). At these low frequencies the subsystems are described as being strongly coupled.

Fahy and Mohammed [27] investigated the relationship between the CLF, modal overlap factor and the variance of the power flow for a coupled plate system using a computational experiment. For the coupled plate system presented, it was shown that it is necessary to have at least five resonance frequencies in a frequency band for reliable estimates of the CLF to be obtained. In addition, the estimates of the CLF based on a diffuse field transmission coefficient generally exceed the actual value when the geometric average modal overlap factor of the two subsystems is much less than unity. Accordingly, the computational examples showed that the CLF derived from tests on one physical sample could be unrepresentative of the ensemble average value when modal overlap factors are small.

The variability in the CLF of two coupled rectangular plates was investigated by Park [21] using the dynamic stiffness method. In order to quantify the variability of the effective CLF, a wide range of parameter variations such as the thickness ratio, the length ratio, the length-to-width ratio and damping loss factor were studied

using finite plate simulations. Variations in both modal density and modal overlap were considered, either together or separately. Although the variability of the effective CLFs reduced as frequency increased, it was found that significant variability still remained when modal overlap is greater than about 0.4. Upper and lower bounds for the CLF developed by Craik et al [59] were considered. It was shown that better agreement is found when the modal overlap of both systems is taken into account, rather than that of the receiver alone, as originally proposed by Craik et al [59]. Also the variance was investigated to find the variability of the effective CLF in terms of the combined modal overlap factor and combined number of modes for each subsystem. An empirical formula for the variance of the effective CLF was derived, which showed improved confidence intervals of the CLFs compared with previously published estimates [59, 60].

1.3.3 Energy flow method and energy finite element method

An alternative method to SEA, a so-called energy method (energy flow method, EFM) is in use to solve high frequency problems. As SEA can only define a single energy value for each subsystem, the spatial information within an SEA subsystem cannot be found. Although the division of subsystems into smaller ones may partially solve this limitation, in general these become strongly coupled and the same energy levels are obtained for the divided components. To overcome this limitation Nefske and Sung [28] proposed a power flow analysis, which is analogous to the flow of thermal energy in heat conduction. Based on this hypothesis, Wohlever and Bernhard [29] developed an energy flow method for one-dimensional systems. On the assumptions that a structure has light damping and that the kinetic energy density and potential energy density are equal, a second order differential equation governing the energy distribution was developed and applied to coupled rod or coupled beam systems.

Bouthier and Bernhard [30] also applied this method to membranes where the energy equation is approximate or relies on the assumption that one is in the far

field where the response can be reasonably described in terms of plane waves. To get an approximate energy distribution, an equation for the time-averaged energy density was used with a smoothing operation which means a space-averaging procedure over the span of the trace wavelength. The accuracy of this method is improved as the frequency of excitation increases, but at low frequency the approximations are not suitable because there are not enough modes in the frequency band of interest.

A more complicated system consisting of a rectangular plate and finite beams was investigated by Seo et al [31] using the energy flow method in which several parallel beams were coupled to a simply supported plate. Although the power transmission and reflection coefficients at a beam-plate junction and the power input were calculated using the assumption of a semi-infinite plate, the energy density distributions and the power flow intensity were successfully predicted, in terms of the global decay and the attenuation patterns of the energy density.

Langley [32] investigated the use of EFM for two-dimensional structures and showed some difficulties for the present case. For a point load, the direct field response predicted by EFM does not match the known exact solution. This is especially important when the structure is heavily damped. Also it was emphasised that the far field energy density in EFM is proportional to $1/\sqrt{r}$ with r the radius from the loading point, while the exact result is proportional to $1/r$. It is known that such difficulties do not arise for one-dimensional systems.

In application of the energy flow method, a finite element approach was employed by Vlahopoulos et al [33]. This is called the Energy Finite Element Method (EFEM). It was based on the governing differential equations with respect to energy density variables. Only the propagating wave of a plate is considered. The finite element formulation is utilised for a numerical solution. In EFEM, a discontinuity occurs if the geometry and material properties are changed such as a junction where different members meet. Thus, a junction element was developed to connect such discontinuities, the coefficients of which are computed from

analytical solution of semi-infinite members connected to each other and by the continuity of the power flow across the junction. Where it is continuous between elements the energy density was found in the conventional finite element manner. The calculated energy ratio in one-third octave bands for a scale model of an engine foundation and a large scale ship structure shows similar agreement with that of conventional SEA above about 4000 Hz. The numerical result also showed that the spatial variation of the energy density can easily be identified using EFEM.

It is traditionally important to define the joints particularly of automotive vehicles, especially spot-welded joints. The development and evaluation of the power transfer coefficient in the EFEM framework was carried out by Vlahopoulos et al [34] to predict the behaviour of spot-welded joints in an automotive structure. In order to derive the power transmission coefficient, the connected members are generally considered semi-infinite, similar to SEA. However, although the conventional FEM was utilised to compute the power characteristics, the semi-infinite assumption was not used. Instead, a numerical iterative algorithm was adopted. The technique presented showed better agreement in comparisons of energy ratio of the two-plate coupled system via spot-welding. This energy flow approach via the FE method shows the possibility of a hybrid method incorporating an energy method with FE, which will be discussed further later in this chapter.

Another type of energy flow method was developed for a jointed beam structure by Shankar and Keane [61, 62]. Under some limiting conditions, for example, the beams are not allowed to be coupled at the mid-span and the boundary conditions are only hinged or clamped conditions, the average energy levels were studied using the receptances at the grid of joints between beams. The behaviour of the global structure made of rigidly jointed beams was predicted from Green's functions of the individual uncoupled beams. This approach has some advantages, for example, local damping can be used for the corresponding substructure and the finite element method can be used. However, difficulties in the convergence of the Green's function can require the inclusion of a large number of modes.

1.4 Mid-frequency methods

In the mid-frequency region the low frequency characteristics and methods have increasing uncertainties whilst an SEA response calculation is not strictly applicable. This can be due to strong coupling, the presence of global modes or a small number of modes. A particular problem arises in structures containing a mixture of stiff and flexible elements. The stiff elements may exhibit 'low frequency' behaviour up to quite high frequencies whereas the flexible components may have 'high frequency' behaviour from quite low frequencies. Thus such structures have a very broad mid-frequency region where neither conventional approach is satisfactory.

There has been much effort to overcome the limitations and to find suitable methods for this region and some of these previous studies are described here.

1.4.1 CMS-based method

Some efforts have been made to extend the frequency region of interest for FE models. Mace and Shorter [35] used FE to find energy-related quantities. This involved using a global modal decomposition and a reordering of the subsequent numerical calculation. For frequency-averaged response quantities and spatially independent excitation such as 'rain-on-the-roof', cost-reduced integral forms were presented as only a few terms including global modal receptance are frequency dependent. There is further benefit for a lightly damped system and with an excitation force of known power spectral density. It was shown that significantly fewer component modal degrees of freedom based on the component mode synthesis (CMS) approach [63] were required and hence less computation is involved.

CMS was originally developed to reduce the number of degrees of freedom (DOF) in FE analysis and models [3]. The most general method among the CMS is known

as a Craig-Bampton method [63]. In CMS, the response of a system is found in terms of the modal degrees of freedom (DOF) of the subsystems (called components). Different CMS approaches exist where the modes of the subsystems are calculated either with free or fixed interface conditions at their boundaries. In addition to these modes, additional 'constraint modes' are introduced to allow for interface motion. The overall model is then transformed in terms of the modal and boundary degrees of freedom, significantly smaller in size than the original number of DOFs. Very good convergence can be obtained for a reasonably small number of component modes.

The Craig-Bampton method was adapted by Castanier et al [36] to give a more efficient numerical analysis based on FE. In conventional CMS methods if the FE mesh is fine, the size of the CMS model increases as the number of constraint mode degrees of freedom increases. The size of the CMS model can be reduced by performing an eigenvalue analysis on the constraint mode partitions. So-called characteristic constraint modes were produced, which represent the characteristic motion of the interface boundary between substructures. Thus, the technique involves a secondary modal analysis. A refinement of the finite element mesh would increase the accuracy without requiring an increase in the size of a numerical model consisting of the characteristic constraint modes. The characteristic constraint modes provide the principal modes of deformation for the coupling interface. Thus, this technique presents important physical insight into the energy transmission between substructures, in which the characteristic constraint modes may be suitable for the efficient calculation of power flow in a complex structure, due to the compact representation of the interface motion.

This enhanced CMS technique was thus used for predicting the power flow statistics due to uncertainties [37]. The outward power flow from a subsystem was formulated in terms of the characteristic constraint modes. The uncertainties were incorporated into the subsystem by assuming that a group of component modes is associated with a random variable with uniform distribution. The technique was used on a complex tracked vehicle. The statistical treatment provides efficient and

accurate modelling of parameter uncertainties, which is critical for mid-frequency vibration analysis.

A local modal/perturbational method was introduced by Mace and Shorter [38], which enables the statistics of the FRF to be predicted for a system whose properties are uncertain. The global modes of the baseline system were found in terms of all of subsystem modes using fixed interface component modes. It was assumed that the uncertainty exists in the local mode properties of the subsystem, not in physical properties of the original system. Thus, here the ensemble was defined in terms of the component modal properties such as the mass and stiffness matrix in the component modal equations. Correspondingly, each member system in the ensemble was defined by its eigenvalues. A linear perturbation was found which relates small changes in the local mode properties to those in the global mode properties. A Monte Carlo simulation was used to estimate the FRF statistics. Two spring-coupled rods were considered as the numerical example.

Soize and Mziou [39] suggested an alternative approach in dynamic substructuring for numerical calculation of complex structures in the mid-frequency range. This was also based on the Craig-Bampton decomposition. For a damped substructure with fixed coupling interface, the eigenfunctions of the kinetic energy in a certain frequency bandwidth in the mid-frequency region were found from the eigenvalue problem. It was shown that the eigenvalues of the substructure rapidly decrease for the present case. Then, only a few larger eigenvalues were used to construct the reduced matrix model of each substructure. The extension of the method seems promising as the matrix reduction can be applied to any boundary condition on the coupling interface. However, how the mid-frequency region and a corresponding bandwidth can be defined, especially in terms of obtaining such eigenvalues, is not clear.

1.4.2 Wave methods

A wave approach based on the reflection and transmission of a wave along a structure and at its joints can also be used. Hugin [40] described the response and transmitted power of bending waves in structures consisting of beams under the assumption that the influence of the near fields is negligible.

Grice and Pinnington [41] used a wave analysis to study a built-up structure consisting of a stiff beam and flexible plate in which the beam is seen as a source and the plate as a receiver. If the flexural wavenumber in the plate is at least twice as large as the coupled wavenumber in the beam, the plate can be idealized as a set of independent plate strips that have a locally reacting impedance [64]. Then the dynamic behaviour of the beam can be described in terms of the locally reacting impedance of the plate and the dispersion relationship of the coupled structure. As the coupled structure can be divided into a component carrying long wavelengths (beam) and one carrying short wavelengths (plate), one can expect that each substructure can be analysed by different methods. This leads to a hybrid method that will be discussed and developed later.

1.4.3 Fuzzy structure theory

For the analysis of the mid-frequency range, Soize [42] introduced fuzzy structure theory. A fuzzy structure is defined as the set of uncertain substructures which are attached to a master structure but are not accessible by classical modelling and are therefore modelled by probabilistic concepts [43]. For the low frequency dynamic analysis, the modelling of the fuzzy structure is commonly made with a system of masses [44], which may not be suitable for the mid-frequencies. Therefore, the dynamic effects that the fuzzy has on the master system were considered in [43]. For this, a probabilistic (fuzzy) boundary impedance that models the effects of the fuzzy structure on the master system was sought. Two different constitutive laws were proposed to construct the impedances [42].

The first type of impedance is independent of the spatial variable along the common boundary (or interface) between the master and the fuzzy systems. The parameters of simple oscillators were modelled by random variables and consequently a random family of oscillators was generated probabilistically. The mechanical parameters, which are the mass and damping and modal density of the fuzzy part, were modelled by mutually independent random variables. A parameter was introduced to control the distribution of these mechanical parameters.

The second type of impedance can be described as an impedance dependent on the spatial variable along the interface. It was modelled by a mass attached to the boundary via a set of oscillators, each of which has absolute displacement (so-called spatial memory). It comprises the equivalent coupling loss factor as well as the mechanical random parameters mentioned above.

Then, the second fuzzy impedance proposed in [42] was used to model the fuzzy substructures attached to the master system through a continuous common boundary (junction) [45]. A system was investigated consisting of six rectangular plates, four of which are coupled perpendicularly to two coplanar plates. The fuzzy theory gives the simpler boundary value problem related to the master plate attached to the fuzzy substructures. Thus, the impedance of the boundary junction was described in terms of the fuzzy impedance. The variables are mass, damping, modal density and equivalent coupling factor. The mean response function calculated by the fuzzy theory gave a good estimation. Some important problems remain such as fitting the fuzzy parameters upon real structures and the choice of the probability density distribution for the fuzzy parameters [45].

Strasberg and Feit [46] derived a simple expression for the vibration damping induced by a multitude of small sprung masses without using a probabilistic approach and applied this to a simple structure consisting of a beam and a plate. From these studies it is observed that the fuzzy structure behaves mainly as

damping to the master structure and the level of the damping is independent of the dissipation factor of the attachments.

In practice, because a structure is divided into a master structure and a fuzzy structure, application is limited to relatively simple structures or structures with a clear division between master and fuzzy components.

1.4.4 Power mode and mode-based approaches

Ji et al [47] proposed a power mode approach in which the vibrational power transmitted to a receiver, such as a flexible plate, by N discrete point forces, can be considered as that transmitted by N independent force contributions involving eigenvectors and eigenvalues that are found from the receiver mobility matrix. The initial idea was originally suggested by Jianxin et al [65] in which the bound of power transmission can be simply defined using the characteristics of the eigenvalues. The power mode approach provides the lower and upper bounds of the power transmitted to the plate using the mean and standard deviation of the eigenvalues. This showed the approximate power transmission can be found simply when the wavelength of the plate is very short and the correlation between individual excitations can be neglected. Thus, this showed possible application to mid and high frequency analyses where the plate is regarded as a flexible receiver system coupled to a stiff system.

The power mode approach was extended to a built-up structure consisting of a stiff beam (source) and a flexible plate (receiver) connected through a discrete coupling [48]. Approximate upper and lower bounds of power transmission were again found. The range between them is closely related to the mobility mismatch between the source and the receiver. A larger mismatch, corresponding to a stiffer source compared with the receiver, results in a narrower range. If the receiver structure is much more flexible than the source, the approximate power transmission can be given simply, incorporating the mobilities of the uncoupled source and receiver.

The approximate frequency average of the power transmission was also found using the characteristic point mobility, which is equal to the point mobility of an infinite plate. The numerical results showed that the accuracy increases as the mobility mismatch increases, whilst requiring much less calculation effort than an exact description and solution.

Ji also proposed a mode-based method [49] where a set of basis functions was introduced for interface decomposition between a stiff beam and a flexible plate. The equilibrium and continuity boundary conditions are enforced along the interface. Then, the dynamic response of the coupled beam and the power transmitted to the plate can be expressed in terms of uncoupled modal properties of the beam and the plate as well as the modal correlation matrix between them. The numerical analysis was performed for a flexible rectangular plate in simply supported conditions, coupled to a stiff beam. Cases when the plate is rotated relative to the beam or when a larger plate is coupled were also considered for comparison. The numerical results showed that the dimensions or the boundary conditions of the plate are less important for determining the general vibration response as the response is predominantly controlled by the beam. The mode-based method can also be used for a flexible plate which is approximated in an asymptotic way such as a simple standing wave model, especially in a frequency average sense.

1.4.5 Hybrid methods for mid-frequency analysis

Considering the advantages and disadvantages of the deterministic and probabilistic methods, it seems natural to develop a hybrid method, for example combining the features of the finite element method and statistical energy analysis.

Langley and Bremner have developed a novel hybrid method [50]. In this method, the degrees of freedom of a system are partitioned into a global set and a local set. The important assumption is that the local modes have a high degree of modal

overlap and the main effect of the local modes is to add damping and an effective mass to the global modes, which can be referred to as a fuzzy structure. Then, the long wavelength component is modelled deterministically, while the short wavelength component is modelled using SEA so that each subsystem can be assigned a single degree of freedom corresponding to the vibrational energy of the local modes. An example for a simple rod system was presented in [50] and it was shown that the method can be used to predict the dynamic behaviour in low and high frequency regions. However, application to other systems is not straightforward.

A hybrid method incorporating both FE and SEA in a different way was proposed recently by Langley and Shorter [51], where separate direct and reverberant fields are introduced. An advantage of this method is that a conventional FE model can readily be used. All degrees of freedom of the FE model are divided into those associated with SEA subsystems (e.g. flexural motion with short wavelength) except at subsystem boundaries and those of the deterministic part (e.g. in-plane motion with long wavelength). Then, a direct field dynamic stiffness matrix that will be coupled to the FE model is constructed for each subsystem in terms of the subsystem boundary degrees of freedom. The forces arising from the SEA subsystem are separated into those producing a direct field and those producing a reverberant field. The response is found from equations coupling FE and SEA methodologies. As FE is not used to calculate the short wave response of the subsystems, computation time significantly reduces. A beam framework with three plates was investigated. The response due to a point force shows good agreement between the hybrid method and Monte Carlo simulation based on a FE model. Further study for the extension of the hybrid method is in progress.

The theoretical development of a hybrid finite element method was introduced by Vlahopoulos and Zhao [52, 53]. This combines the conventional finite element method (FEM) with the Energy Finite Element Method (EFEM, see section 1.3.3) to achieve a numerical solution to mid-frequency vibrations. So-called 'long members' and 'short members' were defined. The long members that contain

wavelengths shorter than the corresponding system were modelled by the EFEM. The short members that contain wavelengths longer than the corresponding system were modelled by conventional FE. Uncertainties are imposed on the long member by using different lengths. The primary concept of this hybrid method is to utilise low-frequency models (FEM) for deriving energy information for the short members and to integrate them with EFEM. Thus, this method involves two sets of data. The first set comprises power transfer coefficients for each EFEM members at a joint (with a short member). The second comprises relationships between the primary variable of the EFEM model at a joint and the primary variables of the FE model at the same joint.

The method was applied to coaxially coupled beam systems [52] and systems consisting of two or three beams connected at an arbitrary angle [53]. In the latter case the member possessing the bending wave was considered as a long member whilst the longitudinal wave member was considered as a short member. Although applications are limited to simple structures of beams, the method showed good agreement with the analytical solution in the mid-frequency region where the EFEM results are inaccurate as the resonant effects of the short members are important to the overall behaviour.

The wave approach for the investigation of a structure consisting of a so-called spine and receiver, introduced by Grice and Pinnington [41], was extended to a hybrid method [54] where the plate is modelled as a number of plate strip impedances. Meanwhile, a finite element method was used for modelling the beam. The hybrid approach was used to calculate the response of two different plate-beam systems, with a rectangular plate and a trapezoidal plate, and good agreement with measurements was shown. This hybrid method was then extended to a box structure [55], in which the finite element method was used to predict a long-wave response and analytical impedances were considered to calculate short flexural waves. This method seems useful for the simple structure combination considered, but it has yet to be extended to a more general approach to deal with practical structures.

Another hybrid method incorporating a mode shape function and a Fourier transform was presented by Ji et al [56], in which a stiff beam is defined deterministically in terms of its modes, whereas a plate having a high mode count is treated approximately by assuming that it extends to infinity. The conventional Fourier transform method can yield the line impedance of an infinite plate in the wavenumber domain. It was assumed the contribution outside the plate interface region is negligible in the Fourier integral. Equilibrium and continuities were approximated along the interface between the beam and the plate in the wavenumber domain by a Fourier transform method. Then, assuming the cross coupling between beam mode shape functions can be ignored, the coupling relationship could be found in terms of the plate line impedance and the mode shape of the uncoupled beam in the wavenumber domain. The numerical results showed that the exact details regarding boundary conditions, size and shape of a very flexible receiver, tend to be less important when the dynamic mismatch, such as given by a large wavenumber ratio, of the system increases. Thus, it can be useful to deal with beam-plate coupled systems where the exact dynamic properties of the plate receivers may not be available.

1.4.6 Other studies for mid-frequency investigation

Vibrational power-flow techniques were proposed by Cuschieri [66] for the mid-frequency analysis of two-dimensional plate-like coupled structures joined along a common edge. Since the mobility functions were defined for the individual substructures, it was not necessary to consider the global structure, but each substructure was considered separately. The input power and transmitted power were obtained from the input and transfer mobilities. The flexural response in the two plates was calculated when the joint is simply supported for convenience. The numerical results are in reasonable agreement with those obtained using FE or SEA. The aspect of the uncertainty was neglected in the application.

Savin [67] showed an experimental study of a three-dimensional complex structure, consisting of beams and plates. He proposed that the medium frequency range is the range where the modal density exhibits important variations from one band to another and vibration of a complex structure at these frequencies is characterised by the superposition of some global modes and local modes. He pointed out that local modes are not necessarily modes having high natural frequencies but can exist even at relatively low frequencies with high modal densities, for example in a three-dimensional truss structure.

1.5 Analysis of four-beam coupled structures

The most important structure considered in the present study consists of four beams and a rectangular plate. There are some published studies on such a framed structure. Takabatake and Nagareda [68] studied the framed structure, where the behaviour of the plate was the primary focus. The plate supported with edge beams was replaced by a plate with edges elastically restrained against translation and rotation. Using relationships between these different boundary conditions, the shape functions in the plate use the beam shape functions corresponding to supports with equivalent translational and torsional stiffness. The closed form approximate solutions for static and dynamic problems of a rectangular plate with edge beams were developed using the Galerkin method, in which the mass effect of the beam was neglected.

The static and dynamic characteristics of a rectangular plate with edge beams were evaluated using a Ritz vector approach by Yang and Gupta [69]. The effect of elastic edge restraints was accounted for by including appropriate integrals for the beams in the expressions for the total kinetic and potential energies, although the procedure to develop the modal mass and modal stiffness was not clearly explained. The various types of boundary conditions at the beams were considered by the corresponding Ritz vectors. The contribution of beam mass to the total kinetic energy was also considered.

Various analytical methods proposed for mid-frequency analysis have been reviewed. As seen and discussed, their applications are generally placed on simple academic systems for example, one-dimensional systems [38, 52] and a single beam and plate [41, 46, 54, 56]. A more complicated system such as a framed structure was only studied in terms of a fundamental dynamic behaviour [68, 69]. For other analytical research concerning the mid-frequency region, it seems that further study is necessary for more general applications [39, 45, 50]. Thus, such evaluation provides the motivation of the present research and a more straightforward and practical approach is sought for a complex industrial application.

1.6 Aims and scope of thesis

An objective of this thesis is, therefore, to consider another possibility for mid-frequency analysis of more complicated structures, in particular two-beam and four-beam coupled systems, which might increase the applicability of the technique for practical industrial application. Typically such systems are principal components in an automotive vehicle, aircraft fuselage, ship hull etc.

As presented in section 1.5, there are few previous studies that deal with such systems consisting of two beams or four beams coupled to a rectangular plate. The closest example may be the study by Grice and Pinnington in which a hybrid technique incorporating FEM and an analytical impedance based on the wave approach was used to analyse a box structure [55].

It should be noted that, as the mid-frequency region was defined as the region where neither deterministic nor statistical methods can be used reliably. This region is dependent on the structural system under investigation. For example, the mid-frequency regions for a beam having a large second moment of area and a thin flexible plate would be different. When coupled together, the mid-frequency region of the combined structure can be very broad.

Some researchers have defined the low frequency region as where a deterministic method is suitable, and the high frequency region as suitable for a statistical method. Then, the mid-frequency region can be defined as the frequency range where some of the components of a system are suitable for the deterministic method while other members are suitable for the statistical method in this thesis. The mid-frequency region can be considered as the range where stiff beams show low frequency behaviour while flexible plates show high frequency behaviour.

Such a system consisting of beams and plates is a most practical industrial structure and thus although still idealised it is expected that the present research will be very applicable. Figure 1.3 shows an automotive body-in-white [8]. One can find such a beam-plate system is widely present in the vehicle body, for example as highlighted by circles indicating the roof, floor and parcel shelf.

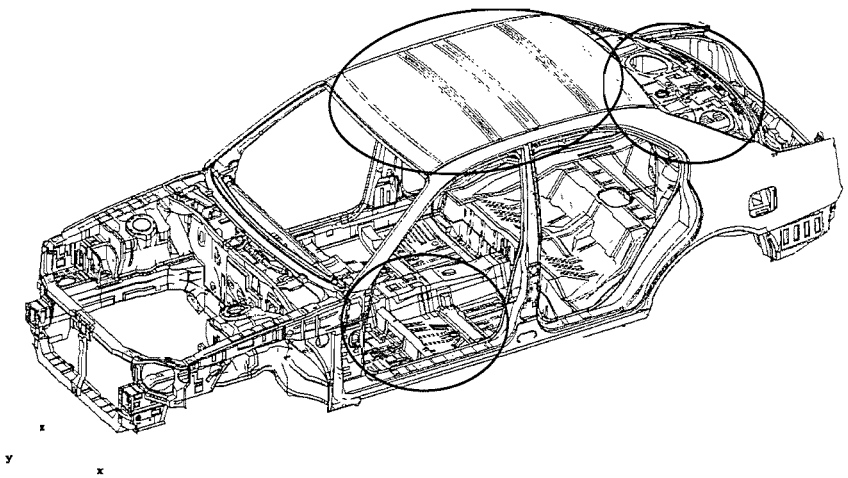

Figure 1.3 A typical automotive body-in-white [8]. The circles indicate structures consisting of two or four stiff beams coupled to a flexible plate.

The main aim of the thesis is to develop analytical methods that can be applied to the mid-frequency region of coupled beam / plate structures. The emphasis is placed on structures consisting of several beams and a rectangular plate as well as a simple beam and plate system previously studied by other researchers [41, 46, 54, 56]. Such analysis provides insight into the dynamic behaviour of coupled systems

of beams and plates that is often difficult to obtain from numerical methods. Although no application is considered here of an engineering structure such as the automotive body-in-white shown in Figure 1.3, it is expected that the study can be utilised as a basis for mid-frequency analysis of such structures.

Both exact and approximate methods will be considered to obtain the dynamic response of such coupled systems. The exact methods are a mode-based method and a Fourier transform technique. These will provide exact solutions that can be used for benchmarking purposes but will be limited to specific sets of boundary conditions. An approximate wave method is then considered which allows much greater flexibility in terms of geometry and boundary conditions.

The analytical models to describe the motion of two beams coupled to a plate are developed using both the Fourier transform technique and a wave approach. A modal method and the wave method are used to model the framed four-beam-plate system. The wave methods are approximate but practically suitable for the mid-frequency analysis. It should be noted that the modelling techniques for the two-beam system and the four-beam system introduced later are different although they are based on a similar wave approach. Thus, they may be separately mentioned as the symmetric-antisymmetric wave model and the plate-decoupled wave model. The conventional wave method [41] is enhanced for this purpose.

The novelty of this thesis can be summarised as follows.
(i) Introduction of sliding boundary conditions on the plate edges and beam ends: this allows both an external excitation on an arbitrary location and a simplification for analyses based on the modal and Fourier methods.
(ii) The damping and mass effect of the plate on the coupled beam is identified in the wavenumber domain.
(iii) Enhancement of the wave method: Muller's method is utilised for obtaining complex roots of a dispersion wave equation, which does not converge in the conventional wave method based on a simple iteration.

(iv) Identification of a plate impedance corresponding to a beam nearfield wave in the wave model: it is found that this plate impedance has the same form as that corresponding to a travelling wave, but different values.
(v) Application of a symmetric and anti-symmetric technique in the beam-plate-beam system: this is commonly used, for example, in FE, but is introduced here in the wave model and can be realised by simply changing the reflection coefficient in the plate impedance equation.
(vi) Representation of the framed system by introducing four decoupled plates in the wave model: the four beams surrounding the rectangular plate are described using four separate plates, each of them being coupled to the corresponding beam. The power investigation shows that this is a reasonable representation, although a difference is found for the beam furthest from the excitation point due to the lack of the physical connection by the plate.
(vii) Experimental verification of wavenumbers in the beam-plate-beam system: it is found that wavenumbers of the rectangular plate in the beam direction are dominated by the stiff beam wavenumber.
(viii) Limitations of the wave method are found: it is found that the wave method provides only approximate results of the power transfer and dissipated power of subsystems. Also, if the wave model is based on separate plate impedances corresponding to the travelling and nearfield waves in the beam a violation of energy conservation occurs.

Throughout this thesis, it is assumed that the beams are infinitely stiff to torsion and a plate is rigidly attached to the beams. Consequently, the corresponding edges of the plate are in sliding. Such a boundary condition can also approximate a real structure such as a beam-ribbed floor structure (e.g. the structure shown in [31]) where several parallel beams are attached to a flat plate, as the presence of a plate on both sides of a beam introduces structural symmetry.

The beams are modelled based on Euler-Bernoulli beam theory and an isotropic plate [70] is assumed throughout in this thesis. As this study concerns the mid-frequency region of a coupled beam-plate system and in-plane motion in the plate

and beam occurs at relatively higher frequencies [50], only flexural motion for both the beam and plate is taken into account.

The chapters are arranged as follows.

As an introductory step before dealing with the complicated systems, Chapter 2 introduces a simpler system consisting of a single beam and a plate. A modal method is introduced which will be used as a reference model for comparison with approximate methods developed later. Using sliding boundary conditions one can greatly simplify the analysis of a single beam coupled to a rectangular plate by ensuring that the mode shapes of the beam and plate match. Simple analytical expressions are available for the mode shapes, which are separable solutions for the plate in the two coordinate directions. Use of the sliding boundary condition also allows point forces to be placed at the edges, which is not possible with simple supports. The convergence of the modal method is studied and, for modes in the direction parallel to the beam, is found to depend on the wavenumbers in the stiffer beam rather than the more flexible plate.

In Chapter 3 a Fourier approach is used to study the same system. The mass and damping effect of the coupled plate is shown in the wavenumber domain. The range of integration required for a specified accuracy is established in terms of the wavenumber of the beam.

Chapter 4 presents and discusses an approximate wave method. Approximate solutions for the wave motion and forced response are obtained by modelling the stiff structure using a wave approach in which the wavenumber is modified by the local impedance of the flexible structure. To estimate the wavenumbers at certain frequencies Muller's method is introduced to give improved convergence. Solving separately for the propagating and nearfield wavenumbers of the coupled system, it is found that a non-physical system is created in which power balance is not respected. This can largely be overcome by using the same wavenumber for both

waves. In such a case, it is found that the power dissipated in the plate is an underestimate due to the approximations of the wave method.

Chapter 5 extends the analysis to a coupled system consisting of two parallel beams and a rectangular plate. The Fourier method discussed in Chapter 3 is used for such a system, and can analyse the system irrespective of whether the beams are identical or not. A symmetric-anti-symmetric technique is used to simplify the analysis for the wave method. Consequently, the wave method is here limited to identical parallel beams. From the power balance investigation it is shown that the wave method gives only approximate results of the power transfer and the dissipated power. Nevertheless, the difference seems mostly small and the validity of the wave method is presented.

Chapter 6 is concerned with a more complex coupled system consisting of four beams and a rectangular plate. The modal method introduced in Chapter 2 is extended to cover such a system and provides an exact response for the present (sliding) boundary conditions. For a framework of beams surrounding the plate, an approximate wave model is presented as a set of connected beams each loaded with an independent plate. This allows non-identical beams in the modelling. Use of a semi-infinite plate loading the beam framework is also considered but shown to lead to an over-estimate of the damping in the system. However, the actual boundary conditions used at the far side of the plate are shown not to be important for the frequency-averaged response.

In Chapter 7 experimental work is presented concentrating on two-beam and four-beam plate coupled systems. Experimental validation is shown for the power flow calculation based on the wave method, even though the boundary conditions differ from those in the numerical model. This shows the usefulness of the sliding boundary conditions used in the model. A comparison using the energy ratio between subsystems also shows the validity of the numerical methods, especially the wave method, although wave models only provide an approximate response. From measurements with a scanning laser vibrometer and using wavenumber

estimation techniques, the wavenumbers in a coupled beam-plate structure are shown to be dominated by the stiff beam system in the direction parallel to the beam, as expected and predicted theoretically. This is important in justifying the use of the wave method.

The conclusions are summarised and the related important results are integrated into Chapter 8. Future studies that could be extensions of this work are also discussed.

CHAPTER 2

MODAL METHOD FOR COUPLED STRUCTURES

2.1 Introduction

As reviewed in the previous chapter, there are a number of analytical and numerical approaches that have been developed to analyse the behaviour of coupled structures consisting of stiff and flexible components, such as beams and plates. In later chapters of this thesis, approaches such as a wave method and a Fourier transform technique will be developed and applied to such structures. Before introducing these more novel approaches, a brief overview of a modal method will be given, which is widely used in many texts to describe the motion of a simple beam or plate. This provides an excellent analytical benchmark and also highlights some important dynamic characteristics when applied to simple structures.

A mode-based method, in which the dynamic response of a coupled structure is described in terms of the mode shape functions of the components, is given in many texts [71-73]. In this chapter a coupled structure comprising a single beam and a single plate is considered, with a relatively straightforward extension to a structure containing several beams given in later chapters.

Although various kinds of boundary conditions for the ends of a beam and the edges of a plate can be used, sliding boundary conditions have been considered for the beam and plate here. There are several reasons for choosing sliding conditions. Firstly, this gives exact analytical mode shape functions and natural frequencies. Secondly the complexity of the analysis can be significantly reduced. Third, unlike simple supports, a point force can still be applied to the plate edges. In principle the modal approach is valid for arbitrary boundary conditions and it is not a necessary condition that both structural components, in this case the beam and plate, have identical mode shapes. It is sufficient only to enforce the equilibrium and continuity conditions at the junction or interface of the individual structural

components. However, the focus of the research is on the mid to high frequency prediction, whereas the effect of imposing particular boundary conditions is noticeable mainly at low frequencies. There are less differences with results from other boundary conditions as the frequency increases so that the actual boundary conditions are less important [26, 49].

A brief presentation of the theoretical basis of the modal method and a general coupling technique involving basis functions of the interface are described. Then application to the beam-plate coupled system is highlighted. Some numerical results are shown and compared with those of a Finite Element (FE) model, including results demonstrating the convergence of the response with the number of modes included. This has implications for predicting the effect of a stiff beam when coupled to a more flexible plate. Before introducing the coupled model, a modal description of the uncoupled beam and plate vibrations is given.

2.2 A modal description for flexural beam vibration

2.2.1 Mode shape function and natural frequencies

It is well known [74] that the dynamic response of an one-dimensional elastic structure, such as a beam, at position x and time t can be expressed as

$$w(x,t) = \sum_m \phi_m(x)\, q_m(t) \tag{2.1}$$

where $w(x,t)$ is the displacement, $q_m(t)$ is the generalised coordinate for the mode m and $\phi_m(x)$ is the corresponding mode shape function of the structure for the specified boundary conditions. The modal expansion given in equation (2.1) is valid for arbitrary motion as well as harmonic steady state motion. Strictly for a continuous structure the summation is over the infinite number of modes of the structure.

For a uniform beam in flexure the general expression for the normal mode or characteristic function is given by [74]

$$\phi(x) = C_1 \cos k_x x + C_2 \sin k_x x + C_3 \cosh k_x x + C_4 \sinh k_x x \tag{2.2}$$

where k_x is the flexural wavenumber, related to the natural frequencies by

$$m_b' \omega_m^2 = k_x^4 D_b \tag{2.3}$$

where D_b is the bending stiffness, ω_m is the m th natural frequency and m_b' is the mass per unit length of the beam assuming a uniform cross-sectional area. Using the general solution, such as equation (2.2), the mode shape functions for arbitrary boundary conditions can be found [74]. Solving the resulting characteristic equation provides the corresponding values of k_x for the particular modes.

For a beam of length L_x with both ends of the beam $x = 0$ and $x = L_x$ considered to be in sliding conditions, the corresponding boundary conditions are zero rotation and shear force. Applying these conditions to (2.2), it is found that $C_2 = C_3 = C_4 = 0$ and the wavenumbers at the natural frequencies can be found as [75, 76]

$$k_x = \frac{m\pi}{L_x} \quad \text{for } m = 0, 1, 2, 3, \cdots \tag{2.4}$$

where $m = 0$ corresponds to the rigid fundamental mode of a sliding beam. The resulting mode shape from equation (2.2) is

$$\phi_m(x) = \cos k_x x = \cos \frac{m\pi x}{L_x}. \tag{2.5}$$

The response of the structure, given the chosen shape functions, requires the generalised coordinate $q_m(t)$ to be determined as a solution of the modal equations of motion. The equations can be derived using Lagrange's equations [73]. The steady state solution for the generalised coordinate $\tilde{q}_m$ is found to be [73]

$$\tilde{q}_m = \frac{\tilde{F}_m}{M_m^b\left(\omega_m^2 - \omega^2\right)} \tag{2.6}$$

where $\tilde{F}_m$ is the harmonic generalised force amplitude corresponding to the generalised coordinate $\tilde{q}_m$, M_m^b is the modal mass, ω_m is the natural frequencies of mode m and $\tilde{}$ is used for complex quantities. The generalised force is given by

$$F_m(t) = \int_0^{L_x} f(x,t)\phi_m(x)dx\,. \tag{2.7}$$

which for a point force $\tilde{F}_0$ at x_1 is given by $\tilde{F}_m(t) = \tilde{F}_0\phi_m(x_1)e^{i\omega t}$. The modal mass is obtained by

$$M_m^b = \int_0^{L_x} m_b'\phi_m^2 dx\,. \tag{2.8}$$

For the mode shape given in equation (2.5) $M_m^b = m_b' L_x/2$ for $m \geq 1$ and $m_b' L_x$ for $m = 0$. The natural frequencies ω_m can be found from equations (2.3) and (2.4) as

$$\omega_m^2 = \left(\frac{m\pi}{L_x}\right)^4 \frac{D_b}{m_b'} \text{ for } m = 0,1,2,\cdots \tag{2.9}$$

where $m = 0$ represents the rigid body mode for the sliding boundary condition considered.

2.2.2 Introduction of hysteretic damping

If structural damping is introduced to the beam via a complex Young's modulus $\tilde{E} = E\left(1+i\eta\right)$, the corresponding bending stiffness $\tilde{D}_b$ is then given by

$$\tilde{D}_b = D_b\left(1+i\eta_b\right) \tag{2.10}$$

where η_b is structural loss factor. Then, equation (2.6) is changed to include the damping as follows.

$$\tilde{q}_m = \frac{\tilde{F}_m}{M_m^b \left[\omega_m^2 \left(1 + i\eta_b\right) - \omega^2 \right]}. \tag{2.11}$$

2.3 A modal description for plate vibration

Similar to equation (2.1), the flexural displacement of a two-dimensional structure such as a plate having an arbitrary shape can also be represented using an infinite series as

$$w_p(x, y, t) = \sum_r \psi_r(x, y) q_r(t) \tag{2.12}$$

where $\psi_r(x, y)$ is a shape function of the plate, $q_r(t)$ is the corresponding generalised coordinate.

Limiting the plate to a rectangular shape, its mode shapes can be either exactly or approximately represented by combination of shape functions in the two perpendicular directions. Thus, the mode shape of the rectangular plate $\psi_r(x, y)$ can be expressed as the product of two separable functions so that each depends on a single spatial variable x or y i.e.

$$\psi_r(x, y) = \phi_{m_r}(x)\phi_{n_r}(y) = \phi_{m_r}\phi_{n_r} \tag{2.13}$$

where $\phi_{m_r}(x)$ and $\phi_{n_r}(y)$ are selected as two linearly independent sets satisfying all of the appropriate boundary conditions and m_r and n_r are integers representing the orders of the separable functions for mode r. In the general case, the separable solution is an approximate approach as it is only in the special cases where a pair of opposite parallel edges are either simply supported or sliding that the governing equation of motion for a rectangular isotropic plate can be solved exactly by this type of separable expansion.

If all edges of the rectangular plate are sliding then the corresponding separable functions are exact and given by

$$\phi_{m_r} = \cos k_x x\,,\ \phi_{n_r} = \cos k_y y \tag{2.14}$$

where

$$\begin{aligned} k_x &= m_r \pi / L_x \ \text{ for } m_r = 0,1,2,\cdots \\ k_y &= n_r \pi / L_y \ \text{ for } n_r = 0,1,2,\cdots . \end{aligned} \tag{2.15}$$

Similar to the beam in the previous section, assuming harmonic excitation and response at frequency ω and introducing structural damping to the plate results in

$$\tilde{q}_r = \frac{\tilde{F}_r}{M_r^p\left[\omega_r^2\left(1+i\eta_p\right)-\omega^2\right]} \tag{2.16}$$

where η_p is the structural loss factor of the plate, $\tilde{F}_r$ is the generalised force amplitude given by $F_r = \int_0^{L_x}\int_0^{L_y} f(x,y,t)\psi_r(x,y)\,dxdy$, or

$$\tilde{F}_r = \tilde{F}_0 \phi_{m_r}(x_1)\phi_{n_r}(y_1) \tag{2.17}$$

for a point force at (x_1, y_1), and the modal mass is given by $M_r^p = \int_0^{L_y}\int_0^{L_x} m_p'' \psi_r^2\,dxdy$.

2.4 General coupling based on modal method

In this section a structural coupling technique based on the modal method is discussed. Although in this thesis the emphasis is placed on a coupled structure consisting of beams and a plate for sliding boundary conditions, the coupling in a general situation is presented first. The derivation is similar to Ji [49] but uses a dynamic stiffness approach rather than a mobility approach.

Consider a coupled structure consisting of two subsystems attached through arbitrary continuous interfaces indicated by the thick line shown in Figure 2.1 (a). It is assumed for simplicity that the subsystems are undamped, although the damped system can also be realised simply as explained in section 2.2.2 by introducing a loss factor. For consistency with the following sections, the upper subsystem is described as system '*b*' and the lower subsystem as system '*p*', although at this stage the subsystems can have arbitrary shapes. If an external force f_e is applied to system b then the coupled system can be divided as shown schematically in Figure 2.1 (b) where f_i^b and f_i^p are the forces acting on each subsystem through the interface. Although they will be enforced to be the same by an equilibrium condition, they are initially described separately to explain the general coupling procedure.

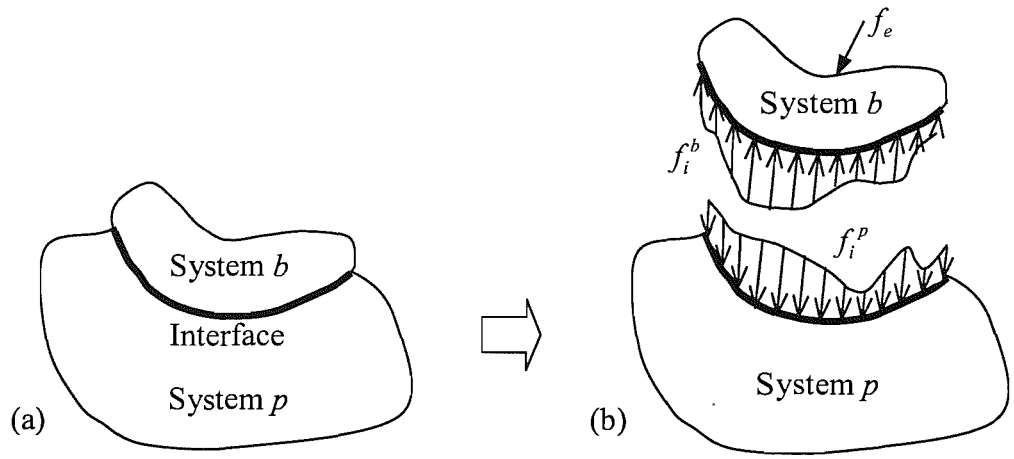

Figure 2.1. The coupled system and its force relationship between subsystems.

2.4.1 Modal method of subsystems

The dynamic displacement of the uncoupled subsystem b can be written, similar to equation (2.1), as

$$w_b(\mathbf{x}_b) = \sum_m \phi_m^b(\mathbf{x}_b) q_m^b(t) \tag{2.18}$$

where $w_b(\mathbf{x}_b)$ is the displacement, ϕ_m^b is the mth mode shape function, q_m^b is the mth generalised coordinate and $\mathbf{x}_b$ is the local coordinate of subsystem b which is given in a vector form. Then, assuming time-harmonic motion, the steady state solution, similar to equation (2.6), is found as (see [49] for details)

$$\tilde{q}_m^b = \frac{F_{e,m}^b - F_{i,m}^b}{M_m^b\left(\omega_{b,m}^2 - \omega^2\right)} = \frac{1}{Z_m^b}\left(F_{e,m}^b - F_{i,m}^b\right). \tag{2.19}$$

where M_m^b is the modal mass, and $\omega_{b,m}$ is the natural frequency of the uncoupled subsystem b. Z_m^b is the dynamic stiffness corresponding to mode m, $Z_m^b = M_m^b\left(\omega_{b,m}^2 - \omega^2\right)$. Also, the corresponding generalised external and interface forces of the mth mode are respectively

$$F_{e,m} = \int_{D_b^e} f_e(\mathbf{x}_b^e)\phi_m^b(\mathbf{x}_b^e)d\mathbf{x}_b^e \tag{2.20}$$

and

$$F_{i,m}^b = \int_{D_b^i} f_i^b(\mathbf{x}_b^i)\phi_m^b(\mathbf{x}_b^i)d\mathbf{x}_b^i \tag{2.21}$$

where D_b^e and D_b^i are the respective domains where the external force is applied and the interface force occurs and $\mathbf{x}_b^e$ and $\mathbf{x}_b^i$ are the corresponding local coordinates. Equation (2.19) can be presented in a matrix form as

$$\mathbf{q}_b = \mathbf{Z}_b^{-1}\left(\mathbf{F}_e^b - \mathbf{F}_i^b\right) \tag{2.22}$$

where $\mathbf{Z}_b$ is a diagonal matrix of modal stiffnesses. Then, the motion of subsystem b can be found from equations (2.18) and (2.22). It should be noted that the exact response is found from the sum of an infinite number of modes. However, for practical reasons an appropriate finite number should be considered.

In a similar manner the displacement w_p of subsystem p is given by

$$w_p(\mathbf{x}_p) = \sum_r \psi_r^p(\mathbf{x}_p) q_r^p(t) \tag{2.23}$$

where ψ_r^p is the rth mode shape function, q_r^p is the corresponding generalised coordinate and $\mathbf{x}_p$ is the local coordinate of the uncoupled subsystem p. Similar to subsystem b, the modal solution of the uncoupled system can be found as

$$\mathbf{q}_p = \mathbf{Z}_p^{-1}\mathbf{F}_i^p \tag{2.24}$$

where $\mathbf{Z}_p$ is a diagonal matrix of modal dynamic stiffnesses of the form

$$Z_r^p = M_r^p\left(\omega_{p,r}^2 - \omega^2\right) \tag{2.25}$$

where M_r^p is the modal mass of subsystem p and the generalised interface force is

$$F_{i,r}^p = \int_{D_p^i} f_i^p(\mathbf{x}_p^i)\psi_r^p(\mathbf{x}_p^i)d\mathbf{x}_p^i \tag{2.26}$$

where D_p^i is the interface domain and $\mathbf{x}_p^i$ is the local coordinate where the interface force occurs in subsystem p.

2.4.2 Structural response based on the general modal coupling

Consider the interface force f_i applied at the local coordinate $\mathbf{x}_i$ and the corresponding displacement at $\mathbf{x}_i$, $w_i(\mathbf{x}_i)$. This force and displacement can be presented in terms of a set of complete orthogonal basis functions, $\chi_k(\mathbf{x}_i)$ spanning the interface domain, as

$$f_i(\mathbf{x}_i) = \sum_k \chi_k(\mathbf{x}_i)F_{i,k} \tag{2.27}$$

$$w_i(\mathbf{x}_i) = \sum_k \chi_k(\mathbf{x}_i)q_{i,k} \tag{2.28}$$

where $F_{i,k}$ is the kth generalised interface force and $q_{i,k}$ is the kth generalised interface coordinate. One can see that the actual interface force and displacement

are now decomposed in terms of the generalised interface coordinates. Such expressions for the force and displacement can be utilised for a general coupling situation, for example, when the mode shape functions of subsystems are different and their interaction through the interface needs to be identified. As the basis functions are orthogonal

$$\int_{D_i} \chi_k \chi_{k'} d\mathbf{x}_i = \delta_{kk'} X_k \tag{2.29}$$

where D_i is the interface region, $\delta_{kk'}$ is the Kronecker delta and X_k depends on the normalisation of χ. Note that for practical cases the sum in equations (2.27) and (2.28) is also truncated to a finite number of basis functions.

Then, the motion of the coupled system can be described in terms of the force equilibrium and the continuity of the displacement through the interface, which are

$$f_i(\mathbf{x}_i) = f_i^b(\mathbf{x}_b^i) = f_i^p(\mathbf{x}_p^i), \tag{2.30}$$

$$w_i(\mathbf{x}_i) = w_b(\mathbf{x}_b^i) = w_p(\mathbf{x}_p^i). \tag{2.31}$$

Combining equations (2.21), (2.27) and (2.30) results in

$$F_{i,m}^b = \sum_k F_{i,k} \int_{D_b^i} \phi_m^b(\mathbf{x}_b^i) \chi_k(\mathbf{x}_i) d\mathbf{x}_b^i \tag{2.32}$$

or in a matrix form

$$\mathbf{F}_i^b = \boldsymbol{\beta}_b \mathbf{F}_i \tag{2.33}$$

where the matrix of factors $\boldsymbol{\beta}_b$ is given by

$$\beta_{mk}^b = \int_{D_b^i} \phi_m^b(\mathbf{x}_b^i) \chi_k(\mathbf{x}_i) d\mathbf{x}_b^i . \tag{2.34}$$

Thus, $\boldsymbol{\beta}_b$ is a matrix of modal correlations between the modes of subsystem b and the basis functions of the interface. Then from equation (2.33), equation (2.22) becomes

$$\mathbf{q}_b = \mathbf{Z}_b^{-1}\left(\mathbf{F}_e^b - \boldsymbol{\beta}_b \mathbf{F}_i\right). \tag{2.35}$$

Similarly, combining equations (2.26), (2.27) and (2.30) gives

$$\mathbf{F}_i^p = \boldsymbol{\beta}_p \mathbf{F}_i \tag{2.36}$$

where

$$\beta_{rk}^p = \int_{D_p^i} \psi_r^p(\mathbf{x}_p^i)\chi_k(\mathbf{x}_i)d\mathbf{x}_p^i. \tag{2.37}$$

Thus from equation (2.36), equation (2.24) becomes

$$\mathbf{q}_p = \mathbf{Z}_p^{-1}\boldsymbol{\beta}_p \mathbf{F}_i. \tag{2.38}$$

As continuity should hold at the interface, equation (2.31),

$$\sum_m \phi_m^b(\mathbf{x}_b^i)q_m^b = \sum_r \psi_r^p(\mathbf{x}_p^i)q_r^p = \sum_k \chi_k(\mathbf{x}_i)q_k^i. \tag{2.39}$$

Multiplying equation (2.39) by $\chi_k(\mathbf{x}_i)$ and integrating over the interface using equations (2.34) and (2.37) gives the relationship between the beam and plate as

$$\boldsymbol{\beta}_b^T \mathbf{q}_b = \boldsymbol{\beta}_p^T \mathbf{q}_p. \tag{2.40}$$

Equation (2.40) can be used to eliminate $\mathbf{q}_p$, substitute into (2.38) to express $\mathbf{F}_i$ in terms of $\mathbf{q}_b$ and then into (2.35) to find $\mathbf{q}_b$ in terms of the externally applied force $\mathbf{F}_e^b$.

Taking the special case where the beam mode shapes can be used as the interface basis functions

$$\chi_k = C_k \phi_k^b \tag{2.41}$$

for some constant C_k chosen to ensure

$$\boldsymbol{\beta}_b = \mathbf{I}. \tag{2.42}$$

Thus, if $\phi_k^b = \cos(k\pi x/L_x)$ the constant C_k is

$$C_k = \begin{cases} 1/L_x & \text{for } k = 0 \\ 2/L_x & \text{for } k \geq 1 \end{cases}. \tag{2.43}$$

Thus, the above equations (2.35), (2.38) and (2.40) reduce to, respectively

$$\mathbf{Z}_b \mathbf{q}_b = \mathbf{F}_e^b - \mathbf{F}_i, \tag{2.44}$$

$$\mathbf{Z}_p \mathbf{q}_p = \boldsymbol{\beta}_p \mathbf{F}_i, \tag{2.45}$$

$$\mathbf{q}_b = \boldsymbol{\beta}_p^T \mathbf{q}_p. \tag{2.46}$$

Expressing the response in terms of $\mathbf{q}_p$ leads to

$$\mathbf{q}_p = \left(\mathbf{Z}_p + \boldsymbol{\beta}_p \mathbf{Z}_b \boldsymbol{\beta}_p^T\right)^{-1} \boldsymbol{\beta}_p \mathbf{F}_e^b, \tag{2.47}$$

and thus

$$\mathbf{q}_b = \boldsymbol{\beta}_p^T \left(\mathbf{Z}_p + \boldsymbol{\beta}_p \mathbf{Z}_b \boldsymbol{\beta}_p^T\right)^{-1} \boldsymbol{\beta}_p \mathbf{F}_e^b. \tag{2.48}$$

Such a special case can be realised when a beam is attached at the edge of a rectangular plate where the edge motion is described using the shape function of the beam and thus a basis function is not necessary. This coupling case will be explained in the following section.

2.5 A modal formulation for the coupled motion of a system comprising a single beam attached to a plate

2.5.1 A single beam coupled to a rectangular plate

The vibrational behaviour of a coupled structure consisting of a single beam and a rectangular plate, as shown in Figure 2.2, is investigated next. The motion of the uncoupled beam and the plate can be represented using the mode shape functions described previously. The behaviour of the coupled system can also be described in terms of the mode shapes. It is not necessary to obtain the modes of the coupled structure itself, as the relevant separate modal matrices of the uncoupled structures will be used as presented in sections 2.2 and 2.3. The motion of the coupled structure is obtained by the above coupling technique.

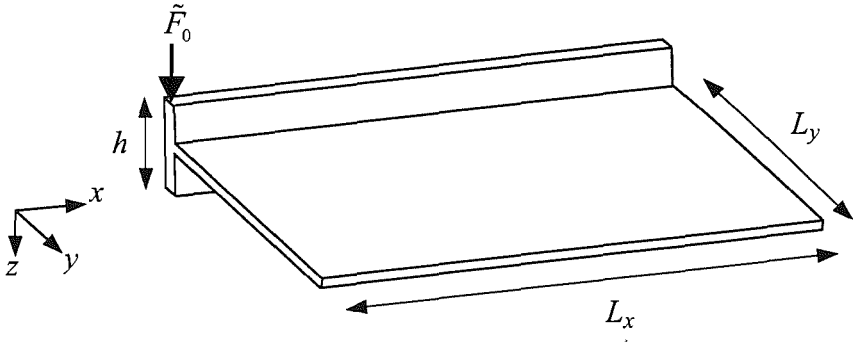

Figure 2.2. A coupled structure consisting of a finite beam attached to a finite rectangular plate.

For simplicity, the beam is assumed infinitely stiff to torsion and all edges of the plate are also assumed to be sliding. Similar to the uncoupled plate, it is assumed in the following that the plate response is given using a separable solution. Thus, the two sets of functions in the two directions correspond to the mode shape functions of a beam with sliding ends. Then, as these mode shape functions are orthogonal, no other basis functions are required for the general coupling situation in representing the motion of this coupled system.

2.5.2 Solution in terms of generalised coordinates

The flexural displacement of the plate with a single beam attached is written as

$$w_p(x,y,t) = \sum_r \psi_r(x,y) q_r(t) \tag{2.49}$$

where ψ_r are the rth mode shapes of the uncoupled plate and q_r are generalised coordinates. The displacement of the beam is given by

$$w_b(x,t) = w_p(x,0,t) \tag{2.50}$$

due to continuity at the plate edge.

Now the response of the coupled structure is expressed in terms of the generalised coordinates of the plate. The modal correlation functions, equation (2.37) can be written as

$$\beta_{rk}^p = C_k \int_{D_p^i} \psi_r^p(\mathbf{x}^i)\phi_k^b(\mathbf{x}^i)\, d\mathbf{x}^i . \tag{2.51}$$

As the mode shapes of the plate are written in terms of the function ϕ (equation (2.13))

$$\beta_{rk}^p = C_k \int_0^{L_x} \phi_{m_r}(x)\phi_{n_r}(0)\phi_k(x)dx = \delta_{m_r k} . \tag{2.52}$$

since $\phi_{n_r}(0) = 1$. The maximum number of modes m and k may be chosen to be the same. The corresponding maximum mode numbers M and N need to be determined for practical use, which also corresponds to the maximum mode number R.

The dynamic stiffness matrix in equation (2.47) to be assembled

$$\mathbf{Z} = \mathbf{Z}_p + \boldsymbol{\beta}_p \mathbf{Z}_b \boldsymbol{\beta}_p^T \tag{2.53}$$

or in terms of modal mass and stiffness matrices

$$\mathbf{Z} = \mathbf{K}_p + \boldsymbol{\beta}_p \mathbf{K}_b \boldsymbol{\beta}_p^T - \omega^2 \mathbf{M}_p - \omega^2 \boldsymbol{\beta}_p \mathbf{M}_b \boldsymbol{\beta}_p^T \tag{2.54}$$

where $K_{p,r} = \omega_{p,r}^2 M_{p,r}$ and $K_{b,m} = \omega_{b,m}^2 M_{b,m}$. Note that $\mathbf{M} = \mathbf{M}_p + \boldsymbol{\beta}_p \mathbf{M}_b \boldsymbol{\beta}_p^T$ is an assembled mass matrix and $\mathbf{K} = \mathbf{K}_p + \boldsymbol{\beta}_p \mathbf{K}_b \boldsymbol{\beta}_p^T$ the corresponding stiffness matrix. $\mathbf{F} = \boldsymbol{\beta}_p \mathbf{F}_e^b$ is the generalised force vector in plate modal coordinate.

Introducing the hysteretic damping to the system by making the stiffness matrices complex, the generalised coordinates of equation (2.47) can then be obtained in terms of the generalised mass, stiffness matrix and the force matrix as follows.

$$\tilde{\mathbf{q}} = \left(\tilde{\mathbf{K}} - \omega^2 \mathbf{M}\right)^{-1} \tilde{\mathbf{F}}. \tag{2.55}$$

2.6 Results

Numerical analysis is carried out based on the modal method for the beam-plate structure shown in Figure 2.2. The torsional stiffness of the beam is assumed infinite and the boundary conditions assumed are sliding beam ends and plate edges. The beam is located symmetrically with respect to the plate, so that its neutral axis lies in the centre of the beam and the second moment of area I of the beam cross-section is given by $I = bh^3/12$.

It is first necessary to determine maximum mode numbers (M, N) for a practical application of the modal method by investigating convergence. In the convergence study some important physical phenomena of the coupled system are identified. Using the chosen mode numbers the response of the coupled system is compared with that based on the finite element method (FEM).

Table 2.1 shows the material properties and dimensions used for the coupled structure. Perspex is considered and the material properties are the same as

presented by Grice and Pinnington [41]. For reasons of comparison with later models, the wavenumbers of the subsystems are chosen to represent a system in which the free plate wavenumber is at least about twice the coupled beam wavenumber. The ratio of the free wavenumber of the uncoupled plate to the uncoupled beam (k_p/k_b) is 3.26, which is sufficiently large (see also section 4.2.5). Note that, however, this is not a limitation of the modal method. The corresponding free wavenumbers are shown in Figure 2.3.

Table 2.1. Material properties and dimensions of the coupled system consisting of a beam and a rectangular plate shown in Figure 2.2.

Material	Perspex
Young's modulus, E (GNm^{-2})	4.4
Poisson's ratio, ν	0.38
Density, ρ (kgm^{-3})	1152.0
Beam length, L_x (m)	2.0
Beam thickness, b (mm)	5.9
Plate width, L_y (m)	0.75
Plate thickness, t_p (mm)	5.9
Height of beam, h (mm)	68.0
Damping loss factor of beam, η_b	0.05
Damping loss factor of plate, η_p	0.05

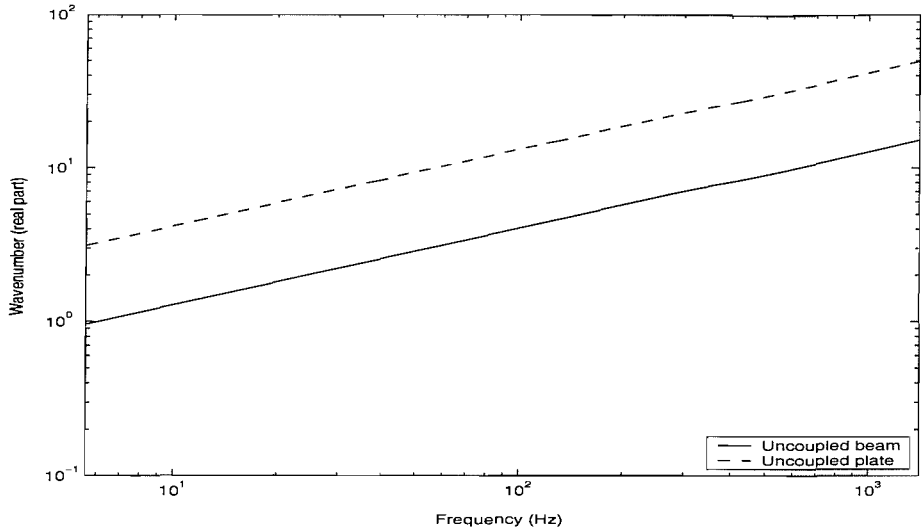

Figure 2.3. Wavenumbers of the uncoupled subsystems.

The frequency range of interest in numerical analysis is chosen as 5.6 – 1412 Hz (data points of 457 are used in this range). This is basically a similar to the range of 10 – 1000 Hz used by Grice and Pinnington [41]. However, in this thesis an average expression such as octave or one-third octave bands will often be used and thus the frequency range is adjusted for convenience to cover complete bands. The number of frequency data points used in each one-third octave band is 19. In this frequency range, the uncoupled beam has 10 modes with the first resonance frequency at 15.1 Hz (the rigid body mode at zero Hz being incorporated into the modal sum and calculation). Meanwhile, the first three resonance frequencies of the uncoupled plate are 1.4, 5.7 and 10.0 Hz and there are more than 300 modes in the frequency range considered, the modal density being about 0.4 modes per Hz. The modal overlap of the plate is greater than unity above about 50 Hz. Thus the beam and plate might be suitable for low and high frequency analyses respectively, which provides an insight for mid-frequency analysis.

2.6.1 Investigation of convergence

The analytical modal procedure presented in section 2.5 provides an exact response only when an infinite number of modes are included in the calculation. For practical calculations, a reasonable range should be chosen such that there is an acceptable error in the response.

The response calculated when the number of modes is very large is taken as a reference, for comparison with the calculations based on a more practical number of modes. Here, the maximum mode number of 200 for each direction is considered as a reference case ($M = N = 200$), which results in 40401 modes in the motion of the coupled structure. This should provide an accurate prediction of the coupled modal response in the present frequency range of 5.6 – 1415 Hz. The FEM predicts 316 coupled modes in this frequency range. Assuming the reference case gives an exact response, the convergence of the modal method is investigated in terms of the evaluation of the spatially averaged kinetic energy.

To obtain an estimate of the space-averaged kinetic energy of the plate, 20 points are randomly selected when an external point force is applied at the end of the beam (see Figure 2.2)*. It is assumed that the response calculated using the maximum mode number of 200 in each direction is exact. This space-averaged kinetic energy for a unit amplitude force is shown in Figure 2.4. Although the modal density of the present plate is about 0.4 modes/Hz, individual modes cannot be distinguished separately at high frequency because of high modal overlap.

* Although 20 points are insufficient to give an accurate estimate of the energy [21] by using the same points in each case the influence of these points is eliminated.

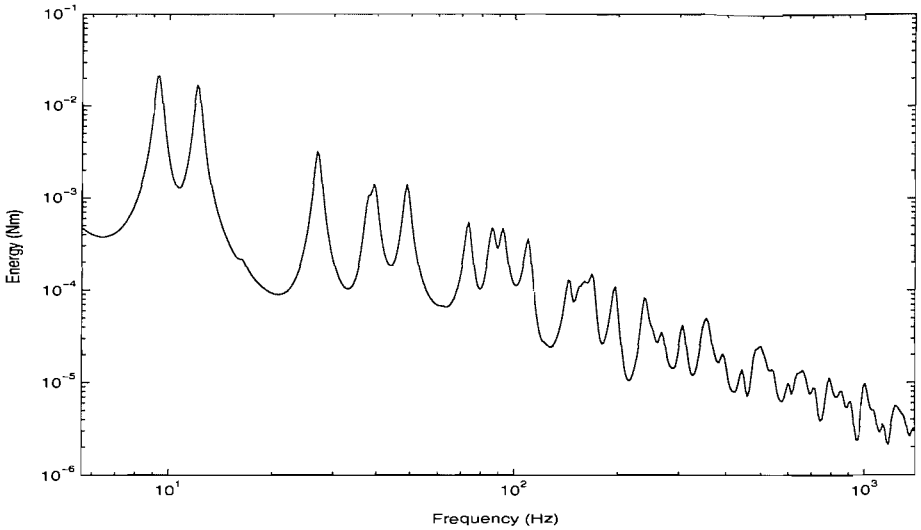

Figure 2.4. Kinetic energy averaged over 20 points of the plate of the coupled system as in Figure 2.2. Unit excitation at $x = 0.0$ m, $y = 0.0$ m (beam left hand end). $M = N = 200$.

The relative error in the kinetic energy estimate at a certain frequency is given as

$$E_\omega = E(\omega) = \left|\left\langle T_{exact}(\omega)\right\rangle - \left\langle T_{MN}(\omega)\right\rangle\right| \Big/ \left\langle T_{exact}(\omega)\right\rangle \tag{2.56}$$

where $\left\langle T_{exact}(\omega)\right\rangle$ is the accurate estimate of the space-averaged kinetic energy of the plate and $\left\langle T_{MN}(\omega)\right\rangle$ is that resulting from a finite modal summation. Then, the frequency-averaged error e in dB is given as

$$e(\mathrm{dB}) = 10\log_{10}\overline{E}_\omega \tag{2.57}$$

where $\overline{E}_\omega$ is the frequency-averaged value of E_ω. For illustration this is evaluated as a one-third octave band average for bands with centre frequencies of 20, 100, 1000 and 1250 Hz.

The convergence is examined by evaluating the mean error e when the maximum mode numbers, M and N are incrementally changed for the x and y directions respectively, at intervals of 2.

The error distribution in the 20 Hz one-third octave band is shown in Figure 2.5. It is interesting that the mean error reduces rapidly as the number of modes in the x direction is increased, especially for maximum mode numbers M of 6, 12 and 24, whilst for the error in the y direction the reduction is more gradual. This effect is related to the motion of the stiffer beam which lies along the x axis.

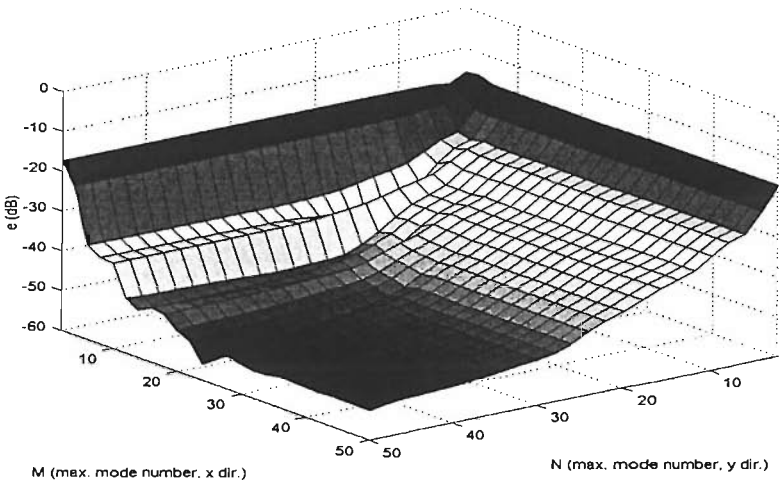

Figure 2.5. Error distribution in terms of the one-third octave band average energy based on the modal method. Centre frequency of 20 Hz. Reference values from $M = N = 200$ using the modal method.

As the mean error is evaluated using the plate response, it seems reasonable to introduce a non-dimensional wavenumber in terms of the plate free wavenumber. The centre frequency of the one-third octave band is used to derive the non-dimensional wavenumber. Note that the introduction of the centre frequency here is only for a consistent expression in this study using one-third octave bands. This non-dimensional wavenumber is given by

$$\gamma_{p,x} = k_x / k_{p,c} = M\pi / \left(L_x k_{p,c}\right),\ \gamma_{p,y} = k_y / k_{p,c} = N\pi / \left(L_y k_{p,c}\right) \tag{2.58}$$

where M and N are the maximum mode numbers in the x and y directions, L_x is the length of the beam, L_y is the width of the plate and $k_{p,c}^4 = m_p'' \omega_c^2 / D_p$ is the plate free wavenumber at the centre frequency $\omega_c \left(= 2\pi f_c\right)$.

In a similar manner, a normalised wavenumber with respect to the beam free wavenumber can be introduced. This is helpful to understand the relationship between the motions of the beam and the plate. Consider such a wavenumber normalised by the beam free wavenumber in the one-third octave band centre frequency. In the present one-third octave band ($f_c = 20$ Hz), the beam wavenumber is $k_{b,c} = 1.81$ rad/m and thus, the normalised wavenumber with respect to the free beam wavenumber gives factors of about 5, 10 and 20 corresponding to $M = 6, 12$ and 24 respectively.

Another example is shown in Figure 2.6 corresponding to the one-third octave band average error in the energy at 1 kHz. The beam wavenumber in this band is 12.8 rad/m. Comparing this result with Figure 2.5, one can observe that the error is larger. It is natural to expect that using a particular maximum mode number gives a lower error at low frequencies than at high frequencies, as the maximum mode number can more adequately describe the motion at low frequencies. As the free plate and beam wavenumbers increase, more modes are required to represent the motion.

The overall observation is that the reduction in the mean error is more rapid as the number of modes is increased in the x direction than for the y direction. A rapid reduction is found at $M = 10$. The corresponding normalised wavenumber with respect to the beam wavenumber is about 1. Thus, it appears that the mean error significantly reduces when the trace wavenumber $k_x \left(= M\pi / L_x\right)$ becomes greater than the beam wavenumber k_b in the corresponding frequency band. Note that the error is obtained using space-averaged responses on the plate, not on the beam. Thus, this gives the important result that the motion of the flexible plate is heavily influenced by the motion of the stiff beam in this direction (parallel to the beam). This enables a hypothesis to be proposed that in any subsequent wave method the motion of the plate in this direction is dominated or heavily influenced by the coupled beam wavenumber.

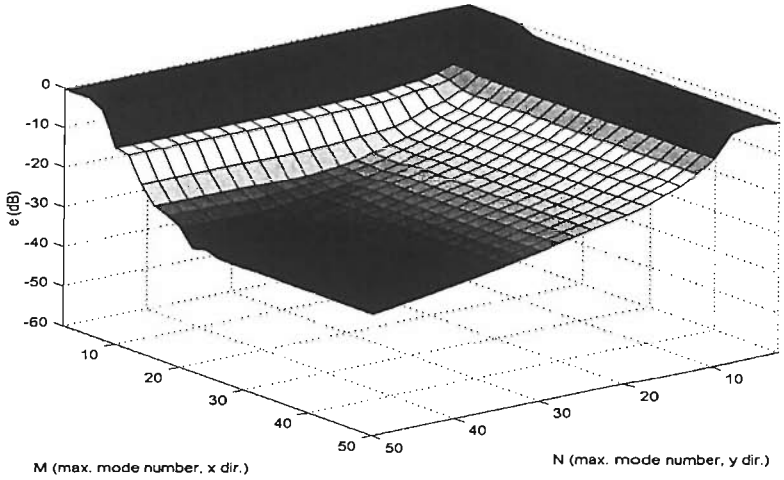

Figure 2.6. Error distribution in terms of the one-third octave band average based on the modal method. Centre frequency of 1 kHz.

Clearly, using more modes results in a more accurate response prediction. It is also clear that the response at higher frequencies needs more modes for a given accuracy than at lower frequencies. Thus, it is necessary to choose a maximum mode number to be used for a practical application, which is also dependent on the frequency range of interest. Accordingly, a physical quantity that is less dependent on the frequency range needs to be introduced rather than a maximum mode number.

A contour plot of the mean errors shown in Figure 2.6 is given in Figure 2.7 in terms of the non-dimensional wavenumbers $\gamma_{p,x}$ and $\gamma_{p,y}$. The thick black line indicates a mean error of about –20 dB (about 1.0 %) in the corresponding one-third octave band.

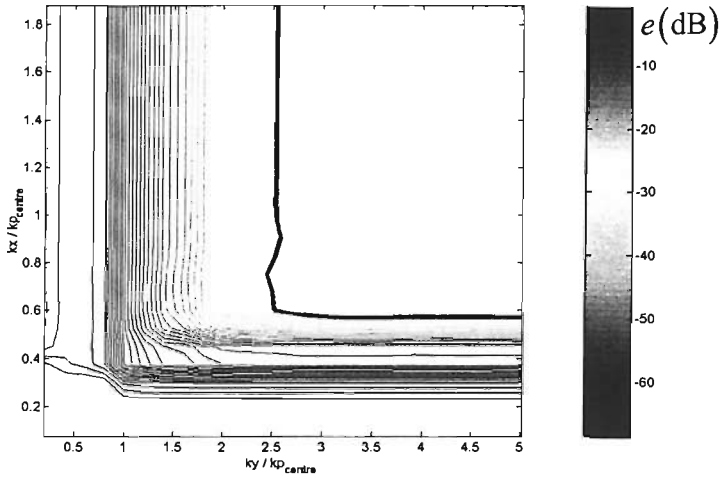

Figure 2.7. Contours of the one-third octave band average error as a function of the non-dimensional wavenumbers in the modal method. Centre frequency of 1 kHz.

Another example of the contours corresponding to the centre frequency of 100 Hz is shown in Figure 2.8, also in terms of non-dimensional wavenumbers. The thick black line again indicates an error of about –20 dB.

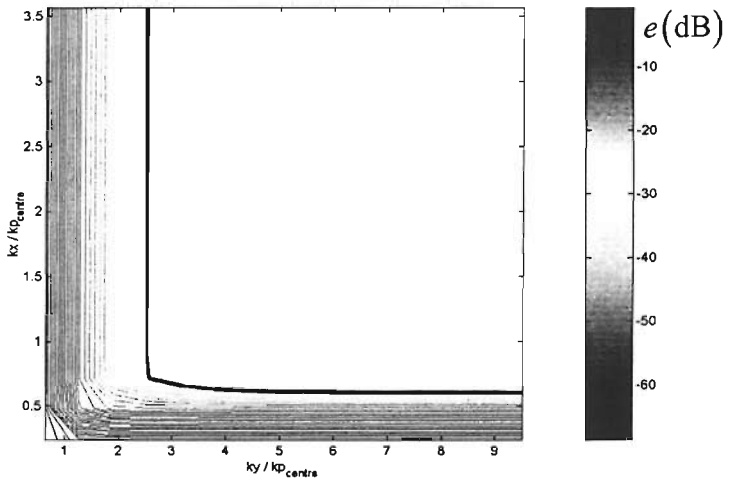

Figure 2.8. Contours of the one-third octave band average error as a function of the non-dimensional wavenumbers in the modal method. Centre frequency of 100 Hz.

Comparing Figures 2.7 and 2.8, one can find that the error of –20 dB occurs at very similar non-dimensional wavenumbers, say about $\gamma_{p,x} \approx 0.6$ or $\gamma_{p,y} \approx 2.5$. Note that while convergence occurs when the wavenumber is about 2.5 times the free

plate wavenumber in the y direction, the same convergence occurs when the wavenumber is smaller than the free plate wavenumber in the x direction. This confirms that the beam dominates the plate motion in this direction. Similar phenomena are also found for other frequency bands considered (f_c = 20 Hz and 1250 Hz). As expected, the non-dimensional wavenumber appears to be a very useful indicator, which seems independent of frequency. If an error of –20 dB is chosen on practical grounds*, the non-dimensional wavenumbers assist in specifying the modal order limits for the required accuracy from the modal approach. Further, in the present coupled structure, the motion in the x direction, parallel to the beam, is strongly related to the motion of beam, which gives the assumption of $k_x \approx k_b$. Then, as $k_p/k_b = 3.26 \gg 1$, using the wavenumber trace matching of $k_y^2 = k_p^2 - k_x^2$, the ratio of the trace wavenumbers can be found as $k_y/k_x \approx 3.1$. Thus, the location having this ratio, somewhere in the black line in Figures 2.7 and 2.8 for the error of –20 dB, can be found. This gives unique non-dimensional wavenumbers of $\gamma_{p,y} = 2.53$ and $\gamma_{p,x} = 0.78$ in Figure 2.7. In the same manner, non-dimensional wavenumbers producing the error of about –20 dB in different frequency bands are evaluated and summarised in Table 2.2.

Table 2.2. Relationship between the maximum mode number and non-dimensional wavenumber in various one-third octave bands for a mean error of –20 dB.

f_c	$\gamma_{p,x}$	$\gamma_{p,y}$	M	N
20 Hz	0.71	2.31	3	4
100 Hz	0.79	2.57	7	9
1000 Hz	0.78	2.53	21	26
1250 Hz	0.69	2.25	21	26

The M and N values given in the table are the minimum to give the corresponding non-dimensional wavenumbers for the particular plate dimensions

* An error of –20 dB, or 1% in the energy corresponds to ±0.04 dB accuracy.

(2.0 × 0.75 m). Thus, for the whole frequency range of 5.6 – 1412 Hz, it is recommended to use $M \times N = 21 \times 26$. The mean error in the whole frequency range of 5.6 – 1412 Hz is about –27.3 dB (0.18 %). For further study the maximum numbers of $M = N = 26$ are used for convenience.

2.6.2 Comparison of the modal method for beam-plate coupled system with FE

Numerical results based on the modal method presented in the previous sections are presented here. The maximum number of modes used in the modal method is 26 for both directions x and y. A comparison is made between the modal method and results obtained using a commercial Finite Element (FE) program for structural analysis. The same boundary conditions of sliding beam-ends and plate edges are used in both methods. Euler-Bernoulli FE beam elements (133 elements) and thin shell elements are used. It is generally known that at least 8 elements per wavelength are necessary to describe an appropriate motion of a structure [3] and thus the thin shell element size of 15 mm is used for the plate. The plate wavelength at 1412 Hz is 0.126 m. The FE model used is shown in Figure 2.9 where the thick solid line is added to distinguish the beam from the plate. The total number of elements is 6783. A hysteretic damping factor η of 0.05 is used for the beam and plate. The material properties are as in Table 2.1.

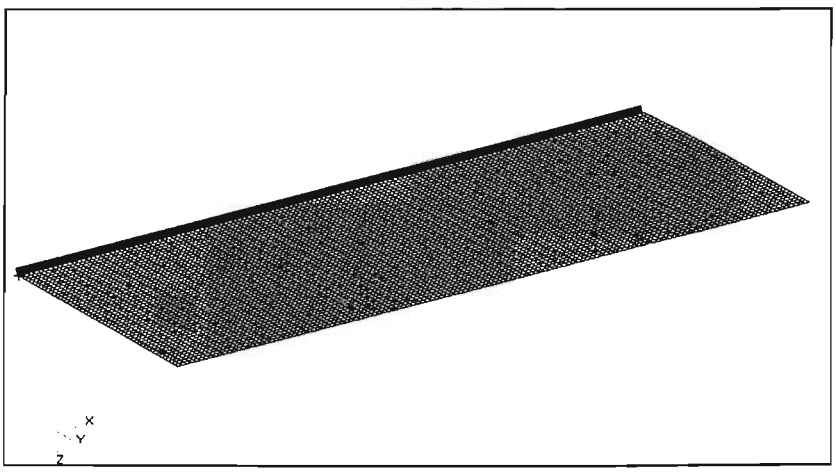

Figure 2.9. A finite element model used for the numerical comparison with the modal method.

The results presented consist of mobilities where a point force is applied at one end of the beam. The point mobilities are compared in Figure 2.10 and the transfer mobilities to an arbitrary point on the plate are compared in Figure 2.11. The two methods are in excellent agreement, with differences only noticeable at the high frequencies. Note that the FE results should be considered approximate at high frequencies.

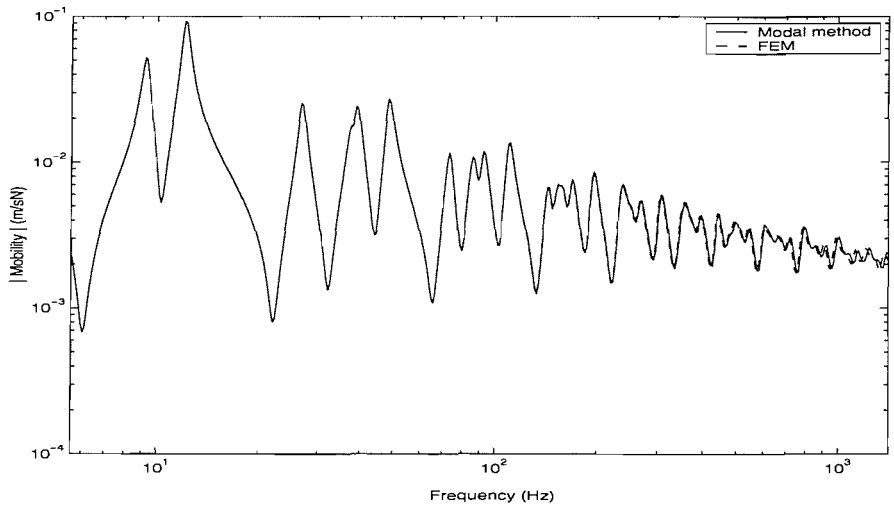

Figure 2.10. Point mobilities from the modal method and the FEM. Excitation and response at $x = 0.0$ m, $y = 0.0$ m (beam left hand end).

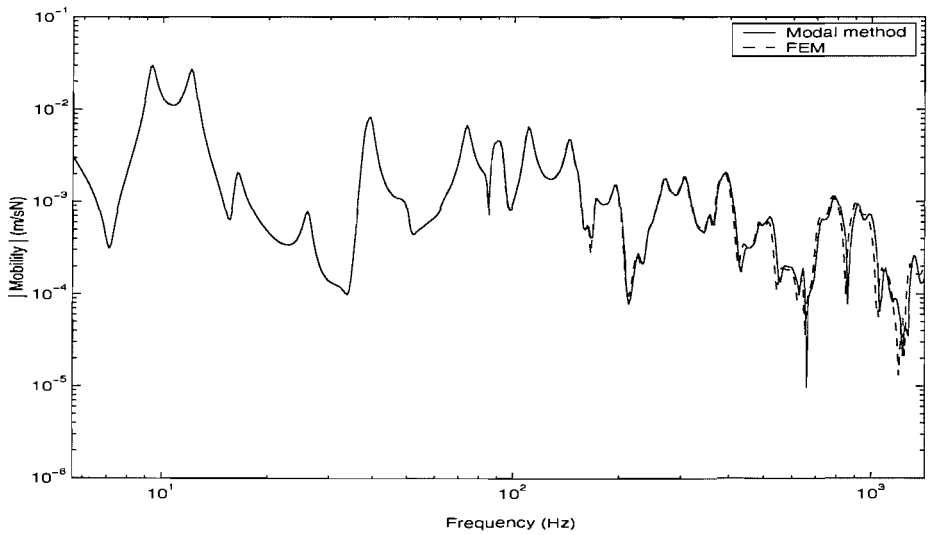

Figure 2.11. Transfer mobilities from the modal method and the FEM. Excitation at $x = 0.0$ m, $y = 0.0$ m (beam left hand end) and response of the plate at $x = 1.50$ m, $y = 0.49$ m.

The results presented in Figures 2.10 and 2.11 confirm the validity of using the modal model that has been developed and the coupling technique for a stiff beam connected to a flexible plate using mode shape functions based on separation of the variables.

2.7 Conclusions

The modal method presented in this chapter, for coupling a stiff beam to a flexible rectangular plate, produces some important results that will be used for further studies.

The modal method gives excellent predictions of the coupled response such as mobilities. The modal coupling technique allows the known mode shape functions of the corresponding subsystems to be used, instead of finding the modes of the coupled system. The approach based on the variable separation is especially useful to analyse the coupled system incorporating a rectangular plate. Also by assuming sliding boundary conditions of the plate edges the complexity of the modal method is reduced with simple analytical modes which are the same for plate and beam along their common boundary and simplicity in the algebraic derivation and numerical implementation. While the same could be achieved using simple supports, sliding boundaries allow an external force to be considered on the beam.

Such a technique can also be utilised for more complex systems consisting of several beams, to provide an accurate response to be used for comparison with alternative approximate methods developed later. The number of modes required in the modal method in order to obtain an accurate response was examined. The convergence in one-third octave bands was studied in terms of the non-dimensional wavenumbers. Convergence is achieved to within –20 dB when modes are included up to a wavenumber approximately 2.5 times the free plate wavenumber in the y direction and 2.5 times the free beam wavenumber in the x direction.

In the convergence study, it was shown that the behaviour of the flexible rectangular plate in the direction parallel to the stiffer beam is mostly governed by the stiff beam. The response in that direction also requires fewer modes in order to represent the behaviour well. This important result has implications for the wave method considered in later chapters.

The mode-based method could be extended to the more general case using the uncoupled modes of the separate beam and plate. The modes could be numerical rather than analytical and need not be for the same boundary conditions or expressible as separate functions in the orthogonal directions [49].

CHAPTER 3
A FOURIER TECHNIQUE FOR STRUCTURES WITH CONSTANT GEOMETRY IN ONE DIRECTION

3.1 Introduction

The dynamic behaviour of a coupled structure consisting of a single beam and a plate was analysed in Chapter 2 using a modal method. In this chapter, a similar coupled structure is investigated using a Fourier transform technique. This approach will show some important physical phenomena of the coupling between the beam and the plate, which were difficult to determine using the modal method. The Fourier method considers all possible real values for the wavenumber k_x in the direction of the beam.

In the previous chapter, it was assumed that the beam attached to the plate has infinite torsional stiffness. A sliding condition was also considered at the ends of the beam. These assumptions are also made in this chapter. However, it is assumed that the opposite edge of the plate, parallel to the beam, is pinned. This shows an advantage of the Fourier transform technique in comparison with the modal method, as other boundary conditions such as sliding or free condition can simply be adopted instead. Also the corresponding results will be used in the next chapter for comparison with those obtained by the approximate wave method where the pinned opposite edge is considered.

This chapter mainly deals with the case of excitation on the beam of the coupled beam-plate structure (the plate-excited case can be considered in a similar way). The structural behaviour is presented for the coupled structure consisting of an infinite beam and a semi-infinite plate. The dynamic characteristics of the structure are examined in terms of the spatial Fourier transformed response and some physical meanings are given. Both numerical quadrature and FFT implementations

of the Fourier transform are considered. Following this, an infinite beam connected to a finite width plate is considered. Then, a Fourier series approach is applied to obtain the response of a finite beam coupled to a finite plate.

The results of the analysis are compared and validated against those obtained using the FEM. Furthermore, power relationships based on the Fourier transform method are presented and some comments are given relating to the studies that will follow later.

3.2 Infinite beam coupled to semi-infinite plate

3.2.1 Wavenumber relationship

Consider an infinite beam coupled to a plate of semi-infinite width and infinite length shown in Figure 3.1. Harmonic motion at frequency ω is assumed throughout with a time dependence of $e^{i\omega t}$. It is assumed that the beam is infinitely stiff to torsion along $y = 0$.

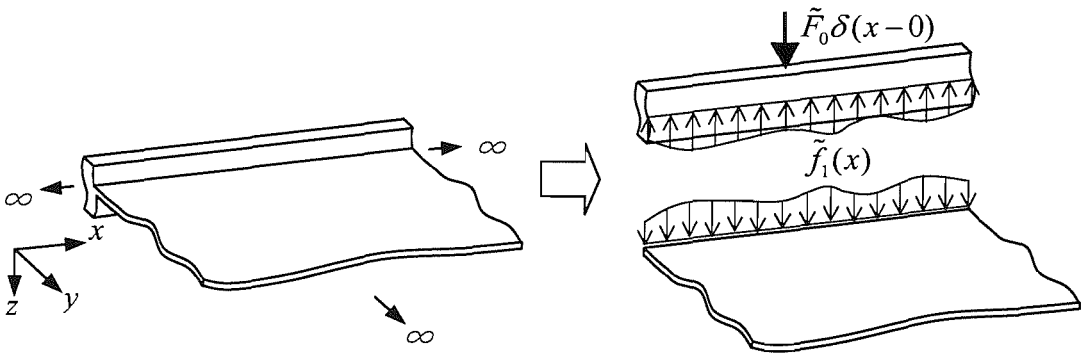

Figure 3.1. A coupled structure consisting of an infinite beam attached to a plate of semi-infinite width.

Firstly, considering the uncoupled free vibration of the beam at frequency ω, the relevant equation of motion of the beam with damping is [70]

$$\tilde{D}_b \frac{d^4 \tilde{w}_b(x)}{dx^4} - m_b' \omega^2 \tilde{w}_b(x) = 0 \tag{3.1}$$

where $\tilde{w}_b$ is the complex displacement amplitude of the beam vibration, m_b' is the mass per unit length and $\tilde{D}_b$ is the bending stiffness given by $\tilde{E}_b I$, with $\tilde{E}_b \left(= E_b \left(1 + i\eta_b\right)\right)$ Young's modulus with damping and I the second moment of area of the beam. The damped free beam wavenumber satisfies $\tilde{D}_b \tilde{k}_b^4 = m_b' \omega^2$.

When the semi-infinite plate and the infinite beam are joined along the line $y = 0$, a force per unit length $\tilde{f}_1(x)$ acts between them as shown in Figure 3.1. An external force acting on the beam at $x = 0$ is defined by a point force $\tilde{F}_0 \delta(x - 0)$ where $\delta(x - 0)$ represents a delta function. Then equation (3.1) becomes

$$\tilde{D}_b \frac{d^4 \tilde{w}_b(x)}{dx^4} - m_b' \omega^2 \tilde{w}_b(x) = \tilde{F}_0 \delta(x - 0) - \tilde{f}_1(x) \tag{3.2}$$

Spatial Fourier transform pairs are defined by the relationship between the coordinate x and real wavenumber k_x in the x direction as follows.

$$\tilde{W}_b(k_x) = \int_{-\infty}^{\infty} \tilde{w}_b(x) e^{-ik_x x} dx, \tag{3.3}$$

$$\tilde{w}_b(x) = \frac{1}{2\pi} \int_{-\infty}^{\infty} \tilde{W}_b(k_x) e^{ik_x x} dk_x. \tag{3.4}$$

For spatial derivatives of the functions one has

$$\begin{aligned} ik_x \tilde{W}_b(k_x) &= \int_{-\infty}^{\infty} \frac{d\tilde{w}_b(x)}{dx} e^{-ik_x x} dx, \\ -k_x^2 \tilde{W}_b(k_x) &= \int_{-\infty}^{\infty} \frac{d^2 \tilde{w}_b(x)}{dx^2} e^{-ik_x x} dx. \end{aligned} \tag{3.5}$$

Therefore, the spatial Fourier transform of equation (3.2) gives

$$\tilde{D}_b\left(k_x^4-\tilde{k}_b^4\right)\tilde{W}_b(k_x)=\tilde{F}_0-\tilde{F}_1(k_x). \tag{3.6}$$

where $\tilde{F}_1(k_x)$ is the Fourier transform of $\tilde{f}_1(x)$.

The equation of motion of the free plate with damping is [77]

$$\tilde{D}_p\left(\frac{\partial^4\tilde{w}_p(x,y)}{\partial x^4}+2\frac{\partial^4\tilde{w}_p(x,y)}{\partial x^2\partial y^2}+\frac{\partial^4\tilde{w}_p(x,y)}{\partial y^4}\right)-m_p''\omega^2\tilde{w}_p(x,y)=0 \tag{3.7}$$

where $\tilde{D}_p$ is the complex plate bending stiffness given by $\tilde{D}_p=\tilde{E}_p t_p^3/12(1-\nu^2)$, ν is Poisson's ratio, t_p is the thickness and m_p'' is the mass per unit area of the plate. This leads to damped free wave solutions with wavenumber $\tilde{k}_p^4=m_p''\omega^2/\tilde{D}_p$.

If the motion of the plate is defined by a wavenumber k_x in the x direction, the response can be written as $\tilde{W}_p(k_x,y)$. The complete response at position y can thus be given by the Fourier transform

$$\tilde{w}_p(x,y)=\frac{1}{2\pi}\int_{-\infty}^{\infty}\tilde{W}_p(k_x,y)e^{ik_x x}dk_x, \tag{3.8}$$

which has an inverse Fourier transform

$$\tilde{W}_p(k_x,y)=\int_{-\infty}^{\infty}\tilde{w}_p(x,y)e^{-ik_x x}dx. \tag{3.9}$$

Now the Fourier transform of equation (3.7) is

$$\tilde{D}_p\left\{k_x^4\tilde{W}_p(k_x,y)-2k_x^2\frac{\partial^2\tilde{W}_p(k_x,y)}{\partial y^2}+\frac{\partial^4\tilde{W}_p(k_x,y)}{\partial y^4}\right\}-m_p''\omega^2\tilde{W}_p(k_x,y)=0, \tag{3.10}$$

which can be written as

$$k_x^4\tilde{W}_p(k_x,y)-2k_x^2\frac{\partial^2\tilde{W}_p(k_x,y)}{\partial y^2}+\frac{\partial^4\tilde{W}_p(k_x,y)}{\partial y^4}-\tilde{k}_p^4\tilde{W}_p(k_x,y)=0. \tag{3.11}$$

Consider a solution for a harmonic wave in the plate of the form

$$\tilde{W}_p(k_x, y) = \tilde{B}_1 e^{\tilde{k}_y y} \tag{3.12}$$

where $\tilde{k}_y$ is the trace wavenumber for the wave radiating into the plate normal to the beam. Substituting equation (3.12) into equation (3.11) gives

$$k_x^4 - 2k_x^2\tilde{k}_y^2 + \tilde{k}_y^4 - \tilde{k}_p^4 = 0$$

or

$$\tilde{k}_y^2 = k_x^2 \pm \tilde{k}_p^2. \tag{3.13}$$

Therefore, if the negative square root is assumed for waves propagating or decaying away from the junction (i.e. with a negative real part), two different types of wavenumber in the plate are found to be

$$\tilde{k}_y = -\sqrt{k_x^2 - \tilde{k}_p^2} = \tilde{k}_{y1}, \tag{3.14 a}$$

$$\tilde{k}_y = -\sqrt{k_x^2 + \tilde{k}_p^2} = \tilde{k}_{y2}. \tag{3.14 b}$$

If $|k_x| < |\tilde{k}_p|$, then wavenumber $\tilde{k}_{y1}$ may be considered to represent a wave propagating outward into the plate (if k_p is real then k_{y1} is imaginary for $k_x < k_p$) and $\tilde{k}_{y2}$ is considered as a nearfield wave decaying outward from the beam. Conversely, if $|k_x| > |\tilde{k}_p|$, then both may be considered as nearfield waves.

Consequently the travelling and nearfield waves for the plate can be written as

$$\tilde{W}_p(k_x, y) = \tilde{B}_1 e^{\tilde{k}_{y1} y} + \tilde{B}_2 e^{\tilde{k}_{y2} y}. \tag{3.15}$$

The waves with wavenumber $-\tilde{k}_{y1}$ and $-\tilde{k}_{y2}$ cannot exist on a semi-infinite plate for excitation on the beam.

3.2.2 Response of the coupled beam

Having obtained the wavenumber relationship of the coupled structure, the response of the structure can be obtained from the boundary conditions expressed in the wavenumber domain. The boundary conditions when a semi-infinite plate is attached at its edge to the beam are:

(i) Continuity equation; equal displacement

$$\tilde{W}_b(k_x) = \tilde{W}_p(k_x, y)\Big|_{y=0} = \tilde{B}_1 + \tilde{B}_2 . \tag{3.16}$$

(ii) Sliding condition for the plate; the beam is assumed infinitely stiff to torsion along y=0

$$\frac{\partial \tilde{W}_p(k_x, y)}{\partial y}\bigg|_{y=0} = \tilde{B}_1 \tilde{k}_{y1} + \tilde{B}_2 \tilde{k}_{y2} = 0 . \tag{3.17}$$

(iii) Force equilibrium condition; the force on the plate is equal and opposite to the force on the beam

$$\tilde{D}_p \left[\frac{\partial^3 \tilde{W}_p(k_x, y)}{\partial y^3} - k_x^2 (2-\nu) \frac{\partial \tilde{W}_p(k_x, y)}{\partial y} \right]_{y=0} = \tilde{F}_1(k_x) . \tag{3.18}$$

From boundary condition (ii),

$$\tilde{B}_1 = -\frac{\tilde{k}_{y2}}{\tilde{k}_{y1}} \tilde{B}_2 . \tag{3.19}$$

Equation (3.16) for the boundary condition (i) becomes

$$\tilde{W}_b(k_x) = \left(1 - \frac{\tilde{k}_{y2}}{\tilde{k}_{y1}} \right) \tilde{B}_2 . \tag{3.20}$$

From equations (3.17) and (3.18),

$$\tilde{F}_1(k_x) = \tilde{D}_p \left[\frac{\partial^3 \tilde{W}_p(k_x, y)}{\partial y^3} \right]_{y=0} = \tilde{D}_p \left(\tilde{B}_1 \tilde{k}_{y1}^3 + \tilde{B}_2 \tilde{k}_{y2}^3 \right) . \tag{3.21}$$

Substituting equation (3.19) into this gives

$$\tilde{F}_1(k_x) = -\tilde{D}_p \tilde{k}_{y1} \tilde{k}_{y2} \left(\tilde{k}_{y1} + \tilde{k}_{y2} \right) \left(1 - \frac{\tilde{k}_{y2}}{\tilde{k}_{y1}} \right) \tilde{B}_2 . \tag{3.22}$$

From equation (3.20), this can be expressed in terms of $\tilde{W}_b(k_x)$ as follows.

$$\tilde{F}_1(k_x) = -\tilde{D}_p \tilde{k}_{y1} \tilde{k}_{y2} \left(\tilde{k}_{y1} + \tilde{k}_{y2} \right) \tilde{W}_b(k_x) . \tag{3.23}$$

Equation (3.6), representing motion of the coupled structure, becomes, on substituting for the interaction force

$$\tilde{W}_b(k_x) = \frac{\tilde{F}_0 / \tilde{D}_b}{k_x^4 - \tilde{k}_b^4 - \tilde{D}_p \tilde{k}_{y1} \tilde{k}_{y2} \left(\tilde{k}_{y1} + \tilde{k}_{y2} \right) / \tilde{D}_b} . \tag{3.24}$$

The displacement of the beam at position x is given by the inverse Fourier transform, equation (3.4),

$$\tilde{w}_b(x) = \frac{\tilde{F}_0}{2\pi \tilde{D}_b} \int_{-\infty}^{\infty} \frac{1}{k_x^4 - \tilde{k}_b^4 - \tilde{D}_p \tilde{k}_{y1} \tilde{k}_{y2} \left(\tilde{k}_{y1} + \tilde{k}_{y2} \right) / \tilde{D}_b} e^{ik_x x} dk_x . \tag{3.25}$$

Note that the meaningful range of k_x for the integral depends on the uncoupled beam wavenumber $\tilde{k}_b$, as will be shown later. By introducing a new variable γ, defined as the ratio of the coupled wavenumber k_x to the uncoupled real wavenumber k_b ($\gamma = k_x / k_b$), consideration of both k_x and k_b can be simplified.

Also, as the plate wavenumbers $\tilde{k}_{y1}$ and $\tilde{k}_{y2}$ include the wavenumber k_x, another variable is introduced as follows.

$$\xi = \frac{k_b}{\tilde{k}_p} . \tag{3.26}$$

Then, as $\gamma\xi = k_x / \tilde{k}_p$, the third term of the denominator of equation (3.25) divided by k_b^4 is

$$-\tilde{D}_p\tilde{k}_{y1}\tilde{k}_{y2}\left(\tilde{k}_{y1}+\tilde{k}_{y2}\right)\Big/\left(\tilde{D}_b k_b^4\right)$$
$$=m_p''\sqrt{(\gamma\xi)^4-1}\left(\sqrt{(\gamma\xi)^2-1}+\sqrt{(\gamma\xi)^2+1}\right)\Big/\left[m_b'\tilde{k}_p\left(1+i\eta_b\right)\right]. \tag{3.27}$$

To simplify, if new variables ϕ, ψ and μ are given by

$$\phi=\sqrt{(\gamma\xi)^2+1},\ \psi=\sqrt{(\gamma\xi)^2-1},\ \mu=m_p''\Big/\left(m_b'\tilde{k}_p\right) \tag{3.28}$$

then, equation (3.27) becomes

$$-\tilde{D}_p\tilde{k}_{y1}\tilde{k}_{y2}\left(\tilde{k}_{y1}+\tilde{k}_{y2}\right)\Big/\left(\tilde{D}_b k_b^4\right)=\mu\phi\psi\left(\phi+\psi\right)/\left(1+i\eta_b\right). \tag{3.29}$$

Thus, assuming small damping $\tilde{k}_b^4/k_b^4\approx 1-i\eta_b$, equation (3.25) becomes

$$\tilde{w}_b(x)\simeq\frac{\tilde{F}_0}{2\pi\tilde{D}_b k_b^3}\int_{-\infty}^{\infty}\frac{e^{ik_b x\gamma}d\gamma}{\gamma^4-\left(1-i\eta_b\right)+\mu\phi\psi\left(\phi+\psi\right)\left(1-i\eta_b\right)} \tag{3.30}$$

3.2.3 Discussion

If the plate is removed from the beam, then the third term of the denominator of equation (3.25) is equal to zero, and the response should be that of a forced uncoupled beam. Then, the corresponding equation becomes

$$\tilde{w}_b(x)=\frac{\tilde{F}_0}{2\pi\tilde{D}_b}\int_{-\infty}^{\infty}\frac{e^{ik_x x}}{k_x^4-\tilde{k}_b^4}dk_x. \tag{3.31}$$

In terms of the non-dimensional wavenumber $\gamma(=k_x/k_b)$, equation (3.31) becomes

$$\tilde{w}_b(x)=\frac{\tilde{F}_0}{2\pi\tilde{D}_b k_b^3}\int_{-\infty}^{\infty}\frac{e^{ik_b x\gamma}d\gamma}{\gamma^4-\left(1-i\eta_b\right)}. \tag{3.32}$$

The solution to this can be obtained analytically. First of all, note that the integrand has four poles at $k_x=\pm\tilde{k}_b$ and $\pm i\tilde{k}_b$ which are complex numbers. Accordingly, they can be represented in the complex plane as shown in Figure 3.2. The integrand goes to zero as $|k_x|\to+\infty$ for $\mathrm{Im}(k_x)>0$, so the contour is closed in the upper half

plane (anticlockwise) as shown. Contour integration can be applied in this upper half plane letting the magnitude $R = |k_x|$ go to infinity.

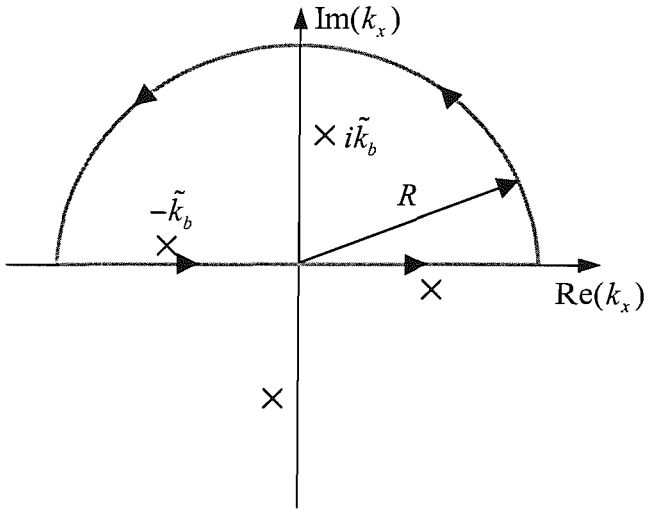

Figure 3.2. Poles of the uncoupled beam and the path of the corresponding contour integral.

As the poles are at complex values of k_x, it can be seen that the contour encloses only two poles, $k_x = i\tilde{k}_b$ and $-\tilde{k}_b$. Then, the integral can be evaluated using the residue theorem [78] as

$$\int_{-\infty}^{\infty} \frac{e^{ik_x x}}{k_x^4 - \tilde{k}_b^4} dk_x = 2\pi i \sum \text{Res}\left(\frac{e^{ik_x x}}{k_x^4 - \tilde{k}_b^4} \right) = \frac{2\pi}{4\tilde{k}_b^3}\left(-e^{-\tilde{k}_b x} - ie^{-i\tilde{k}_b x} \right). \tag{3.33}$$

as the contribution from the semi-circular arc on the contour can be shown to be zero in the limit. Finally, the analytical solution for the forced uncoupled beam is

$$\tilde{w}_b(x) = \frac{\tilde{F}_0}{\tilde{D}_b 4\tilde{k}_b^3}\left(-e^{-\tilde{k}_b x} - ie^{-i\tilde{k}_b x} \right), \; x \geq 0 \tag{3.34}$$

which is the well-known solution for the forced infinite beam [79]. Such an analytical integration could be considered for a beam-plate coupled system consisting of infinite structures, although in this thesis the response of a beam-plate system is found numerically. Such an example was given by Lamb, Jr [80] who found the analytical response of an infinite beam coupled to the centre of a plate using the Cauchy integral theorem, where the contribution of both poles and branch cuts was taken into account.

As can be seen in equation (3.31), the denominator is minimized when $k_x = k_b$, and correspondingly the beam response will have a peak at this wavenumber. In the same manner, equation (3.25) shows how the response of the beam can be obtained from the inverse Fourier transform over wavenumber k_x for the case when the plate is attached to the beam. The Fourier transformed beam response will be maximum when $k_x \approx k_b$, although the exact value depends on the third term of the denominator.

The physical meaning of the third term in equation (3.30) can be identified. Assuming the beam and the plate are undamped, and if $|k_x| \ll |k_p|$, then the third term is approximately

$$\mu\phi\psi(\phi+\psi) \approx \frac{m_p''(-1+i)}{m_b' k_p}. \tag{3.35}$$

Thus this complex term introduces damping to the beam as well as a mass effect. That is, the imaginary part has a damping-like effect. Also, the real part can be regarded as a mass-like term and will shift the peak response to a wavenumber slightly above k_b. If $m_b' \ll m_p''/k_p$ then the effect of this term will be large. In fact, m_p''/k_p is the mass, per unit length along the beam, of a plate having a width of approximately one-sixth of the plate wavelength [41]. Therefore, its effect becomes small as frequency increases due to the factor $1/k_p$. The subsequent numerical results in section 3.2.6 will clearly show these effects.

3.2.4 Results: uncoupled beam in wavenumber domain

Before presenting numerical results for the coupled beam-plate structure, it is worthwhile to consider an uncoupled infinite beam as described in the previous section. The response of the uncoupled beam can be simply obtained from equation (3.31). The dimensions of the uncoupled beam are chosen as those presented in Table 2.1 except that the beam is assumed infinitely long.

The external point force $\tilde{F}_0 = 1$ is applied at $x = 0$. Although, to obtain the exact response, it may be possible to consider the whole range of the wavenumber, from $-\infty$ to ∞ as presented in equation (3.31), it seems more practical to choose an appropriate integration range. This is because the range chosen can readily be used for a Fourier series to be used for a finite coupled system (see section 3.4.1), although a convergence test is necessary. This will be discussed in the following sections. Initially a large but finite range of the wavenumber k_x is chosen, between -100 and $+100$ rad/m. Then $\tilde{W}_b(k_x)$ can be evaluated for different values of k_x and k_b when the third term of the denominator of equation (3.24) equals zero.

The modulus of the transformed displacement of the uncoupled beam based on equation (3.24) is shown in Figure 3.3 for a frequency of 5.6 Hz.

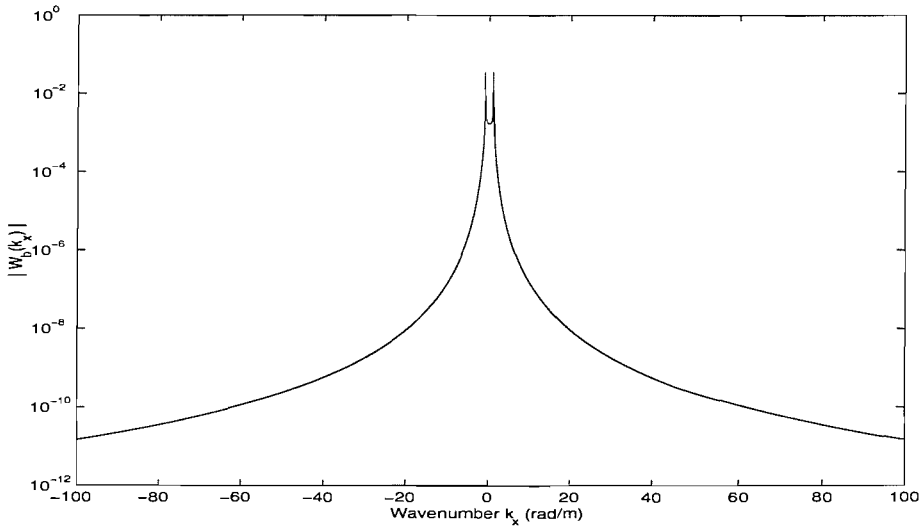

Figure 3.3. Fourier transformed displacement of the uncoupled beam at 5.6 Hz. k_b = 0.96 rad/m.

Figure 3.3 shows that the response of the uncoupled beam as a function of the wavenumber k_x is symmetric. The pole of equation (3.24) is identified at $k_x = \pm 0.96$ rad/m, corresponding to the uncoupled wavenumber k_b = 0.96 rad/m at this frequency, which minimises the denominator. Note that the pole lies in the

complex plane near this value of k_x leading to a peak in $|\tilde{W}_b(k_x)|$ at this value limited by damping.

Truncating the integral at $k_x = \pm 100$ rad/m appears to be justified from the low response levels and small contribution at these values of k_x.

Figure 3.4 shows the Fourier transformed displacement of the uncoupled beam at 1412 Hz. The corresponding pole occurs at $k_x = \pm 15.2$ rad/m. Again the peaks at the pole do not tend to infinity due to the damping in the beam.

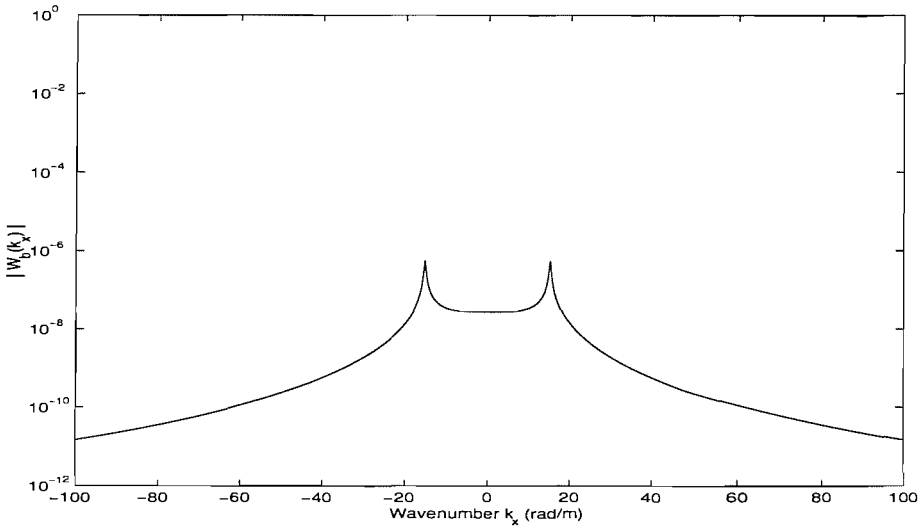

Figure 3.4. Fourier transformed displacement of the uncoupled beam at 1412 Hz. k_b = 15.2 rad/m.

3.2.5 Results: Fourier transform of uncoupled beam

Using the Fourier transformed response presented, the forced frequency response function can be obtained from equation (3.31). The analytical solution is presented in equation (3.34) and is used for comparison. To evaluate the integral, the function QUADL [81] of MATLAB was used, which is based on an adaptive Lobatto quadrature.

An appropriate wavenumber range to be considered in the integration is inferred. Because the uncoupled beam wavenumber k_b depends on frequency, it seems more reasonable to use equation (3.32) including the non-dimensional wavenumber $\gamma (= k_x / k_b)$ to determine the wavenumber range. In Figure 3.5, the inverse Fourier transformed response at the point of excitation divided by the corresponding analytical result based on equation (3.34) is shown. The inverse Fourier transformed results depend on the different ranges of the non-dimensional wavenumber. The actual response itself, is shown later in Figure 3.14 where the response is shown in terms of mobility.

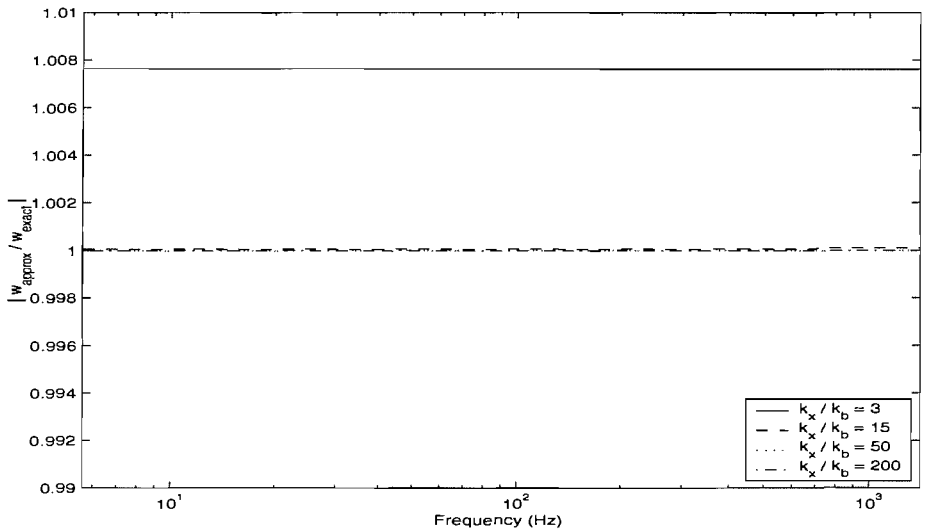

Figure 3.5. Error of the displacement of the uncoupled infinite beam at the excitation point when different ranges of non-dimensional wavenumber γ are considered in the inverse Fourier transform. The responses are divided by the analytical displacement given in equation (3.34).

As can be seen, the inverse Fourier transformed response for the case $-3 \le \gamma \le 3$ is already close to the analytical result, with an error of 0.8%, reducing to about 0.01% for $-15 \le \gamma \le 15$. When the range for γ is considered from -50 to $+50$, the error is approximately 0.0002% (0.000002% for $-200 \le \gamma \le 200$). A further investigation of convergence is carried out for the coupled beam case in the next section to determine an appropriate range of the non-dimensional wavenumber for that case.

3.2.6 Results: coupled beam in wavenumber domain

Attaching the semi-infinite plate to the beam one can compare how the response is affected. The material properties and all dimensions are as presented in Table 2.1, except that the beam is infinite and the plate is semi-infinite.

To examine the relationship between the response of the coupled beam and the wavenumber k_x, the response $\tilde{W}_b(k_x)$ obtained from equation (3.24) is first presented. Figure 3.6 shows the modulus of the transformed displacement of the coupled beam for a frequency of 5.6 Hz.

Comparing Figures 3.3 and 3.6, it is clear that the coupled beam is influenced by the damping effect of the plate near the peaks, which are less sharp. While the uncoupled wavenumber $k_b = 0.96$ rad/m, the peak in Figure 3.6 occurs at $k_x \approx \pm 1.4$ rad/m. This means that the pole of the coupled wavenumber occurs at a larger wavenumber due to the influence of the plate, and this is mainly related to the added mass effect of the plate.

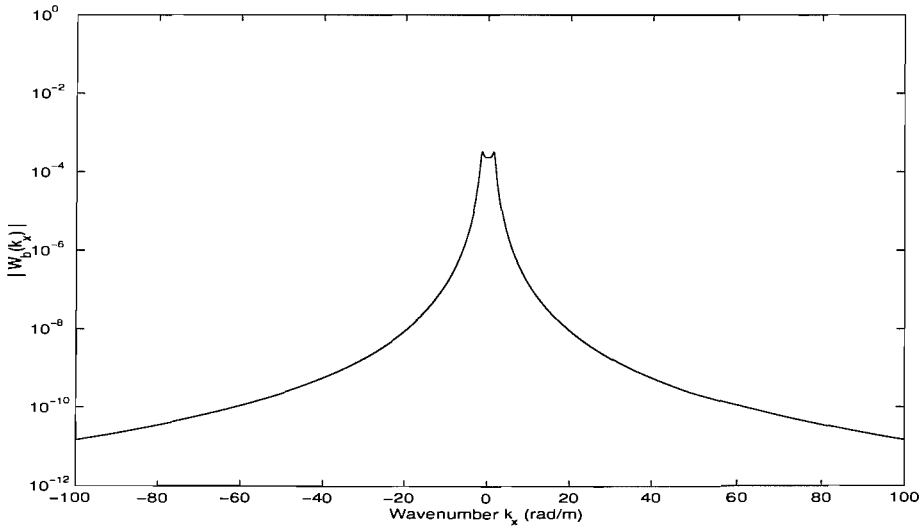

Figure 3.6. Fourier transformed displacement of the coupled beam as in Figure 3.1 at 5.6 Hz. $k_b = 0.96$ rad/m. $m_p''/\left(m_b' k_p\right) = 4.7$.

The mass and damping effects of the third term in equation (3.24) can be simply compared by including either the real part or the imaginary part of the third term separately. Figure 3.7 shows these results. It can be seen that the mass effect shifts the peak to a wavenumber above k_b and the effective damping due to the plate reduces the peak amplitude and broadens the peaks.

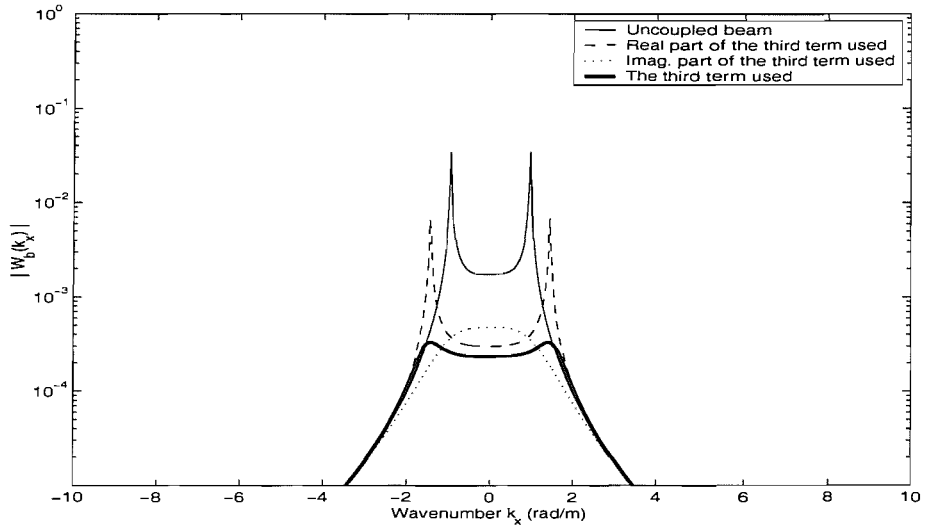

Figure 3.7. The effect of the complex third term in the denominator of equation (3.24) at 5.6 Hz in the wavenumber domain.

Figure 3.8 shows the transformed displacement response at 1412 Hz. The peak occurs at $k_x \approx \pm 16.1$ rad/m which is closer to the corresponding uncoupled value of $k_b = 15.2$ rad/m. That is, the relative difference between the values of k_b and k_x is smaller at 1412 Hz than at 5.6 Hz. As explained before, this is because the mass effect of the plate is reduced as frequency increases due to the k_p term. This can be confirmed by comparing the values of $\mu = m_p'' / \left(m_b' k_p \right)$, which changes from 4.7 at 5.6 Hz to 0.3 at 1412 Hz.

As the uncoupled beam wavenumber k_b depends on frequency, to obtain the correct response of $\tilde{w}_b$ the wavenumber range of $\tilde{W}_b(k_x)$ to be considered should be changed according to the frequency, i.e. $\tilde{W}_b(k_x)$ is not only a function of k_x but

also of k_b as seen in Figures 3.6 and 3.8. Therefore, it is necessary to consider the response from the point of view of both k_x and k_b. By introducing the non-dimensional wavenumber $\gamma = k_x/k_b$ as before, the relationship between the response and k_x and $\tilde{k}_b$ can be examined.

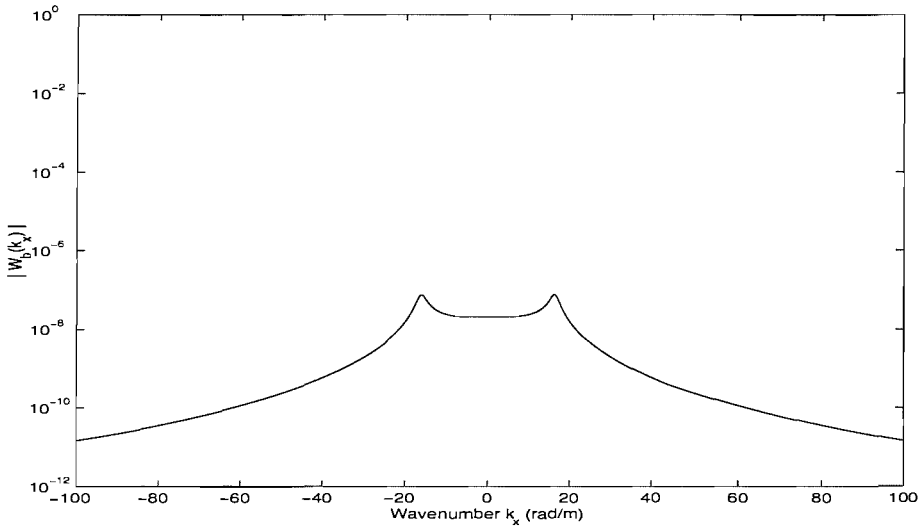

Figure 3.8. Fourier transformed displacement of the coupled infinite beam and plate as in Figure 3.1 at 1412 Hz. k_b = 15.2 rad/m. $m_p''/\left(m_b' k_p\right)$ = 0.3.

$\tilde{W}_b(k_x)$ is shown in terms of γ in Figure 3.9. Note that it is possible to truncate the range of integration by identifying a sufficiently low level response with respect to the maximum Fourier transformed response. For example, if the non-dimensional wavenumber range is chosen to cover a range of 60 dB with respect to the maximum response, this would seem to be a reasonable range to estimate the most significant contribution. The corresponding non-dimensional wavenumber range is approximately ±50 at 5.6 Hz and ±25 at 1412 Hz. A further study follows.

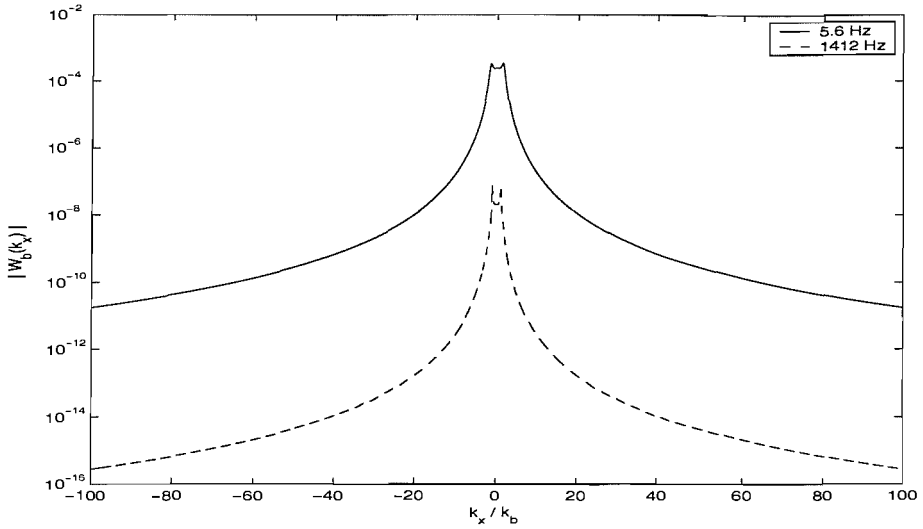

Figure 3.9. Fourier transformed displacement of the coupled infinite beam and plate as in Figure 3.1 with non-dimensional wavenumber at 5.6 Hz and 1412 Hz.

3.2.7 Results: Fourier transform of coupled beam

To choose an appropriate range of the non-dimensional wavenumber, the drive point response amplitude of the coupled structure is used. Assuming the amplitude based on the range of $\gamma = \pm 200$ is exact, the accuracy of the response is examined for different integration ranges. The response amplitudes are calculated based on equation (3.30), which is derived in terms of the non-dimensional wavenumber γ in the inverse Fourier transform. The function QUADL was used as previously for the evaluation of the integral and the corresponding results are shown in Figure 3.10. This indicates that the response amplitude is predicted reliably for a small range of non-dimensional wavenumber. When the non-dimensional wavenumber range for γ is between ± 3 the response is already close (error of 1.2% at 5.6 Hz) to that for the case when $\gamma = \pm 200$ is used. Maximum errors of 0.06%, 0.009% and 0.0004% are found for $\gamma = \pm 8$, $\gamma = \pm 15$ and $\gamma = \pm 50$ respectively. The corresponding point mobility is shown later in Figure 3.14.

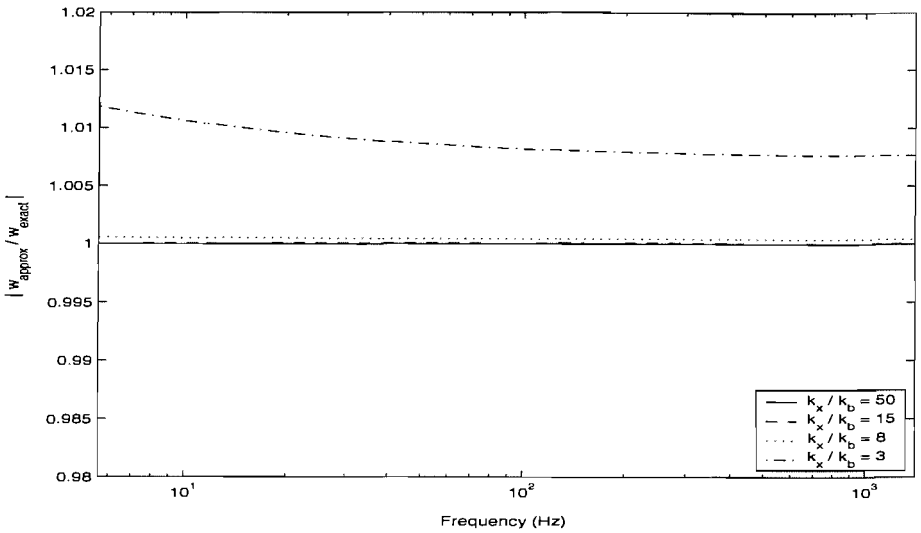

Figure 3.10. Error of the displacement of the coupled infinite beam and plate as in Figure 3.1 at the excitation point when different ranges of non-dimensional wavenumber γ are considered in the inverse Fourier transform. The results for $\gamma = \pm 200$ is used as a reference.

The errors are shown in Figure 3.11 as a function of the integration range at three different frequencies, 5.6 Hz, 100 Hz, and 1412 Hz. Clearly, it can be seen that the differences are reduced as the integration range is increased. Although a greater range results in smaller errors, it also requires much more computation time. Therefore, a compromise is required. If the non-dimensional wavenumber range chosen is -15 to $+15$ the errors for the frequencies considered are less than 0.01% in Figure 3.11, which can be regarded as acceptable accuracy*. This range is used for further studies where the frequency range of 5.6 – 1412 Hz is considered. The chosen non-dimensional wavenumber of $\gamma = \pm 15$ are about 40 and 51 dB below the maximum at the frequencies of 5.6 and 1412 Hz respectively. Thus, an alternative requirement of at least 40 dB attenuation can be used instead of the fixed non-dimensional wavenumber range of $\gamma = \pm 15$.

* This gives responses with precision ± 0.0009 dB.

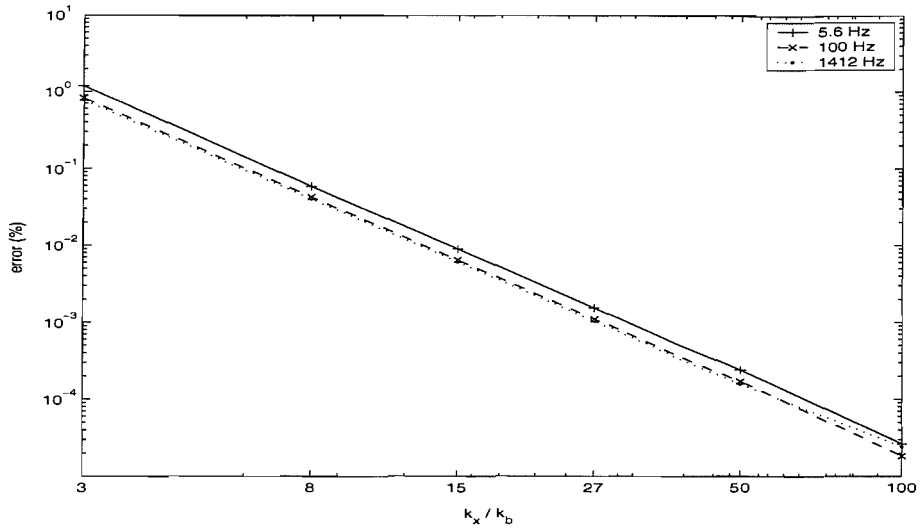

Figure 3.11. The errors of the displacement dependent on the integration range of the non-dimensional wavenumber (The result based on the range of $\gamma = \pm 200$ is assumed to be the exact value).

Instead of adaptive quadrature, the Fast Fourier Transform (FFT) can be used to evaluate $\tilde{w}_b(x)$. The advantage of the FFT is that results can be obtained more rapidly than using an adaptive quadrature. However, consideration should be given to the data resolution of $\tilde{W}_b(k_x)$. If $\tilde{W}_b(k_x)$ is not calculated with sufficient resolution in terms of k_x, then some important data can be lost, particularly at the peaks, and this results in inaccurate predictions. The relationship between the data resolution of $\tilde{W}_b(k_x)$ and the response $\tilde{w}_b(x)$ has therefore been studied.

Data resolution Δk_x in the FFT defines the response ranges of $\tilde{w}_b(x)$ as follows [82].

$$x_{\max} = \frac{2\pi}{\Delta k_x}. \tag{3.36}$$

In fact, because the results calculated using the FFT are symmetric with respect to $x = 0$, only half of the inverse Fourier transforms are shown and their limit can be defined by

$$x_{fold} = \frac{x_{\max}}{2} = \frac{\pi}{\Delta k_x}. \tag{3.37}$$

Using the symmetric Fourier transformed displacement, such as that shown in Figure 3.9, the FFT gives the response at all positions x. Figures 3.12 and 3.13 present these results, which show the real part of the displacement of the coupled beam as a function of position x. For both cases, the same non-dimensional wavenumber range $\gamma = -15$ to $+15$ is used. Because the same resolution of non-dimensional wavenumber is used, the resolution of the wavenumber Δk_x is effectively adjusted based on k_b. In this case the number of values of wavenumber k_x used is 2561, independent of frequency, and Δk_x is chosen to be $0.012k_b$.

In both figures it can be seen that the response decays to a negligible level well within the range limited by x_{fold}. Therefore, the value chosen for Δk_x based on the non-dimensional wavenumber seems to be reasonable for obtaining an accurate response. A larger value of Δk_x would give the same response but truncated to a smaller value of x_{fold}.

Note that the displacement at 5.6 Hz decays in a smaller number of cycles than the 1412 Hz case. As mentioned previously, this is also related to the damping effect of the plate. The value of $\mu = m_p'' / \left(m_b' k_p \right)$ at 5.6 Hz is larger than that at 1412 Hz, the effective damping due to the plate is greater at the lower frequency (see equation (3.35)).

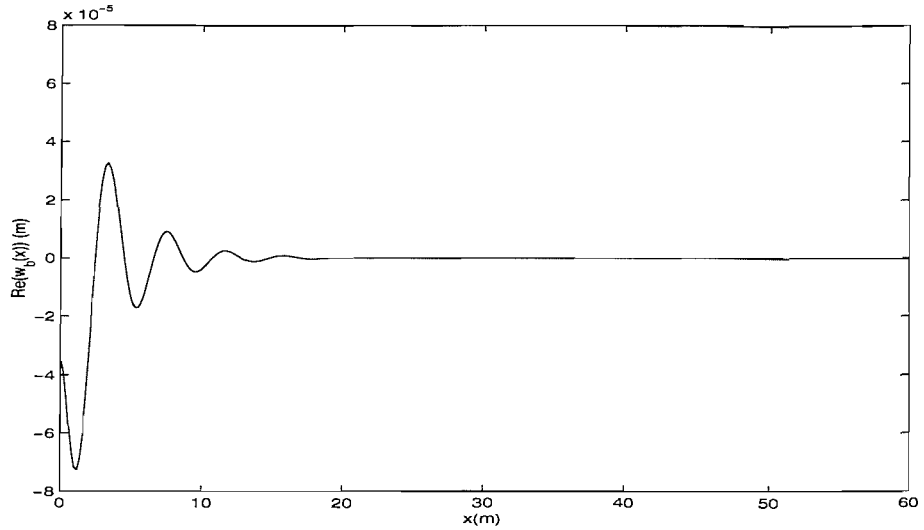

Figure 3.12. Real part of displacement of the coupled infinite beam as in Figure 3.1 at 5.6 Hz. Non-dimensional wavenumber range used is $\gamma = -15$ to $+15$, $k_x = -14.3$ to $+14.3$ rad/m, $\Delta k_x = 0.0122$ rad/m, $x_{fold} = 280$ m, $m_p''/\left(m_b' k_p\right) = 4.7$.

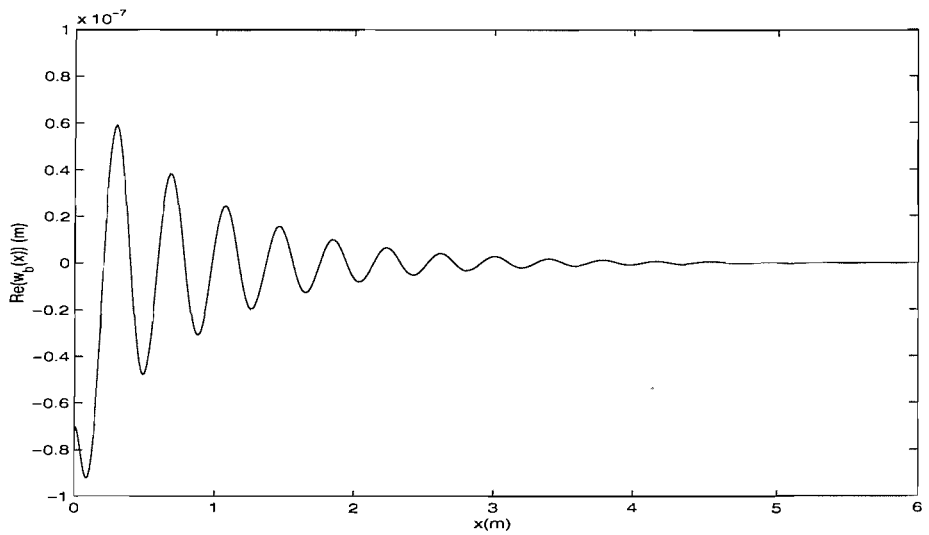

Figure 3.13. Real part of displacement of the coupled infinite beam as in Figure 3.1 at 1412 Hz. Non-dimensional wavenumber range used is $\gamma = -15$ to $+15$, $k_x = -228$ to $+228$ rad/m, $\Delta k_x = 0.1782$ rad/m, $x_{fold} = 17.6$ m, $m_p''/\left(m_b' k_p\right) = 0.3$.

The response at $x = 0$ based on the discrete FFT is compared in Figure 3.14 with that calculated by the Fourier transform method, for which QUADL is used. The same integration range of the non-dimensional wavenumber $\gamma = -15$ to $+15$ is used. Because a unit point force is applied, the velocity response is equivalent to

the point mobility of the infinite beam coupled to the semi-infinite plate. Figure 3.14 shows good agreement in both the amplitude and phase of the point mobilities for the two methods (the two lines are indistingushable). Maximum differences of 0.1% and 1.2×10^{-4} radian respectively are found at 5.6 Hz, due to different integration methods used.

Finally, the effect of the plate on the beam is investigated by comparing the point mobility and the corresponding phase of the coupled beam and the uncoupled beam. The Fourier transform method is used for this where the non-dimensional wavenumber range $\gamma=-15$ to $+15$ is used. The corresponding results are also shown in Figure 3.14. It can be seen that the mobility level of the coupled beam is lower than that of the uncoupled beam because of the mass effect of the plate. As explained in section 3.2.3 the effective mass of the plate corresponds to a width of about one-sixth of the plate wavelength at the corresponding frequency. Thus, it can be seen that its effect reduces with increasing frequency. Also, due to the damping effect of the plate the phase lag increases with increasing frequency, the phase of the uncoupled beam being $-\pi/4$. For reference, the point mobility of the uncoupled plate is also shown in the same figure, which is calculated by $1/\left(4\sqrt{D_p m_p''}\right)$ for excitation at a sliding edge. It forms a low frequency asymptote to the mobility of the coupled system, although the beam mass of the coupled system results in difference in the level.

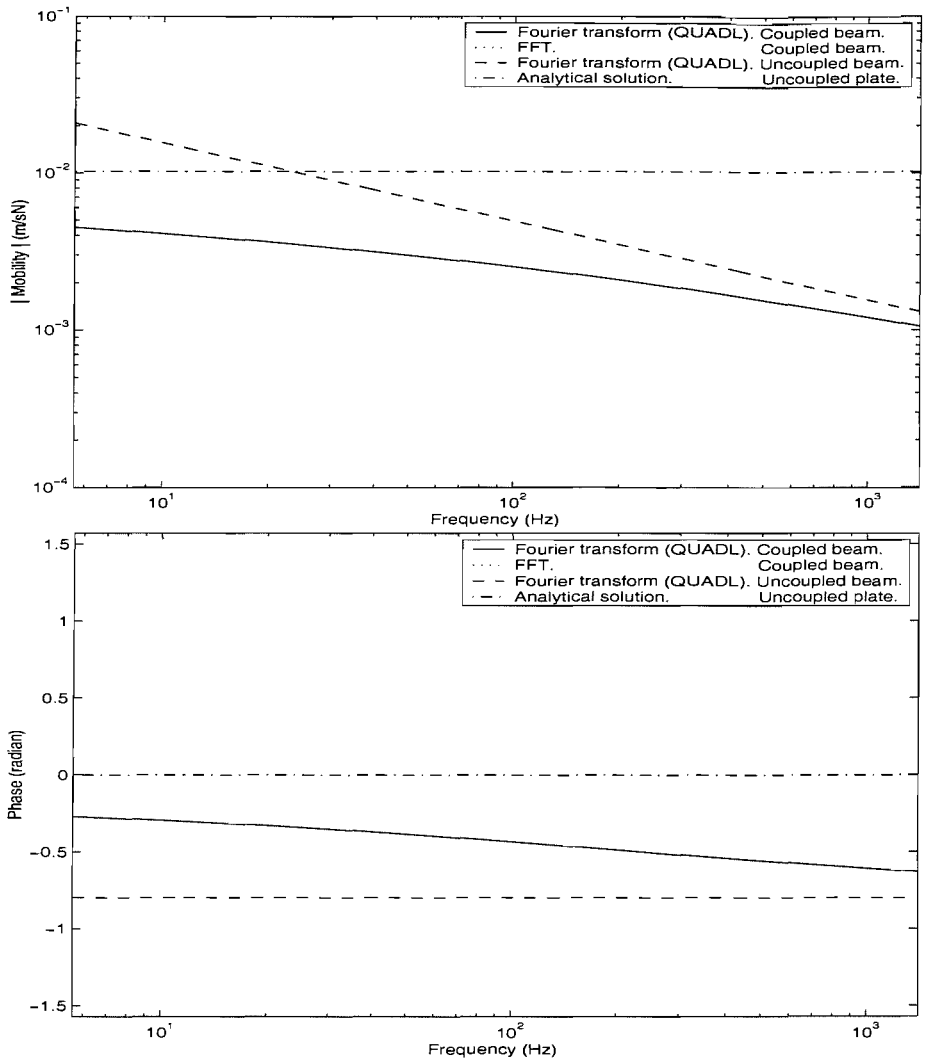

Figure 3.14. The amplitude and phase of the point mobility for an infinite beam coupled to a semi-infinite plate, uncoupled beam and uncoupled plate ($\eta_b = \eta_p = 0.05$). Non-dimensional wavenumber range $\gamma = -15$ to $+15$ is considered in the Fourier transform and FFT.

3.3 Infinite beam coupled to finite width plate

3.3.1 Structural coupling

In this section, a coupled structure is considered consisting of an infinite beam and a plate of finite width as shown in Figure 3.15. A pinned boundary condition is considered along the opposite edge of the plate parallel to the beam.

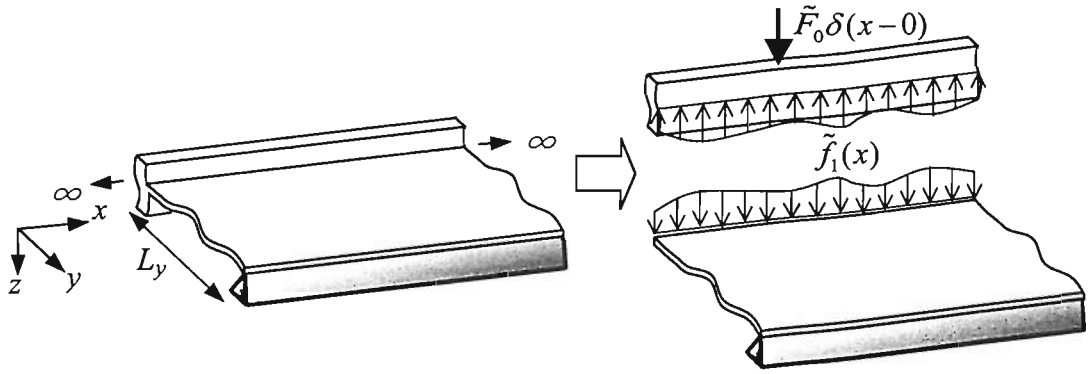

Figure 3.15. A coupled structure consisting of an infinite beam attached to a finite width plate.

Including the reflected travelling wave and nearfield wave generated at the opposite edge of the finite plate, equation (3.15) can be extended, as follows,

$$\tilde{W}_p(k_x, y) = \tilde{B}_1 e^{\tilde{k}_{y1} y} + \tilde{B}_2 e^{\tilde{k}_{y2} y} + \tilde{B}_3 e^{-\tilde{k}_{y1} y} + \tilde{B}_4 e^{-\tilde{k}_{y2} y} \tag{3.38}$$

where $\tilde{B}_3$ is the amplitude of the reflected propagating wave and $\tilde{B}_4$ is the amplitude of the nearfield wave which is generated at the opposite edge of the plate.

All boundary conditions between the plate and beam are assumed to be the same as presented in the previous section. From boundary condition (i),

$$\tilde{W}_b(k_x) = \tilde{W}_p(k_x, y)\Big|_{y=0} = \left(\tilde{B}_1 + \tilde{B}_2 + \tilde{B}_3 + \tilde{B}_4\right). \tag{3.39}$$

From boundary condition (ii),

$$\left.\frac{\partial \tilde{W}_p(k_x, y)}{\partial y}\right|_{y=0} = \tilde{k}_{y1}\tilde{B}_1 + \tilde{k}_{y2}\tilde{B}_2 - \tilde{k}_{y1}\tilde{B}_3 - \tilde{k}_{y2}\tilde{B}_4 = 0, \tag{3.40}$$

and from the force equilibrium condition,

$$\tilde{F}_1(k_x) = \tilde{D}_p\left[\frac{\partial^3 \tilde{W}_p(k_x, y)}{\partial y^3}\right]_{y=0} = \tilde{D}_p\left[\tilde{k}_{y1}^3\tilde{B}_1 + \tilde{k}_{y2}^3\tilde{B}_2 - \tilde{k}_{y1}^3\tilde{B}_3 - \tilde{k}_{y2}^3\tilde{B}_4\right]. \tag{3.41}$$

It is necessary to introduce two more boundary conditions because there are two more unknown variables $\tilde{B}_3$ and $\tilde{B}_4$.

(iv) Pinned condition at the opposite edge of the plate at $y = L_y$,

$$\tilde{W}_p(k_x, y)\Big|_{y=L_y} = e^{\tilde{k}_{y1}L_y}\tilde{B}_1 + e^{\tilde{k}_{y2}L_y}\tilde{B}_2 + e^{-\tilde{k}_{y1}L_y}\tilde{B}_3 + e^{-\tilde{k}_{y2}L_y}\tilde{B}_4 = 0. \tag{3.42}$$

(v) The pinned condition also yields

$$\left.\frac{\partial^2 \tilde{W}_p(k_x, y)}{\partial y^2}\right|_{y=L_y} = 0 = \tilde{k}_{y1}^2\left(e^{\tilde{k}_{y1}L_y}\tilde{B}_1 + e^{-\tilde{k}_{y1}L_y}\tilde{B}_3\right) + \tilde{k}_{y2}^2\left(e^{\tilde{k}_{y2}L_y}\tilde{B}_2 + e^{-\tilde{k}_{y2}L_y}\tilde{B}_4\right). \tag{3.43}$$

As $\tilde{k}_{y1} \neq \tilde{k}_{y2}$ these yield

$$\begin{aligned} \tilde{B}_3/\tilde{B}_1 &= e^{2\tilde{k}_{y1}L_y} = \tilde{\beta}_{y1}, \\ \tilde{B}_4/\tilde{B}_2 &= e^{2\tilde{k}_{y2}L_y} = \tilde{\beta}_{y2}. \end{aligned} \tag{3.44}$$

Substituting these into equation (3.40), the relationship between $\tilde{B}_1$ and $\tilde{B}_2$ is obtained.

$$\tilde{B}_2 = -\frac{\tilde{k}_{y1}\left(1+\tilde{\beta}_{y1}\right)}{\tilde{k}_{y2}\left(1+\tilde{\beta}_{y2}\right)}\tilde{B}_1. \tag{3.45}$$

Therefore, equation (3.39) becomes

$$\tilde{W}_b(k_x) = \frac{-\tilde{k}_{y1}\left(1+\tilde{\beta}_{y1}\right)\left(1-\tilde{\beta}_{y2}\right) + \tilde{k}_{y2}\left(1-\tilde{\beta}_{y1}\right)\left(1+\tilde{\beta}_{y2}\right)}{\tilde{k}_{y2}\left(1+\tilde{\beta}_{y2}\right)}\tilde{B}_1. \tag{3.46}$$

Similarly the equation for force equilibrium condition is expressed as

$$\begin{aligned} \tilde{F}_1(k_x) &= \tilde{D}_p\left[\tilde{k}_{y1}^3\left(1+\tilde{\beta}_{y1}\right)\tilde{B}_1 + \tilde{k}_{y2}^3\left(1+\tilde{\beta}_{y2}\right)\tilde{B}_2\right]. \\ &= \tilde{D}_p \frac{\tilde{k}_{y1}\tilde{k}_{y2}\left(\tilde{k}_{y1}^2 - \tilde{k}_{y2}^2\right)}{-\tilde{k}_{y1}\left(1-\tilde{\beta}_{y2}\right)/\left(1+\tilde{\beta}_{y2}\right) + \tilde{k}_{y2}\left(1-\tilde{\beta}_{y1}\right)/\left(1+\tilde{\beta}_{y1}\right)}\tilde{W}_b(k_x). \end{aligned} \tag{3.47}$$

As $\left(1-\tilde{\beta}_{y2}\right)/\left(1+\tilde{\beta}_{y2}\right) = -\tanh\left(\tilde{k}_{y2}L_y\right)$ and $\left(1-\tilde{\beta}_{y1}\right)/\left(1+\tilde{\beta}_{y1}\right) = -\tanh\left(\tilde{k}_{y1}L_y\right)$, equation (3.47) can be expressed more simply as

$$\tilde{F}_1(k_x) = \tilde{D}_p \frac{\tilde{k}_{y1}\tilde{k}_{y2}\left(\tilde{k}_{y1}^2 - \tilde{k}_{y2}^2\right)}{\tilde{k}_{y1}\tanh\left(\tilde{k}_{y2}L_y\right) - \tilde{k}_{y2}\tanh\left(\tilde{k}_{y1}L_y\right)} \tilde{W}_b(k_x). \tag{3.48}$$

Finally substituting for the reaction force of the finite width plate $\tilde{F}_1(k_x)$ into equation (3.6), for the coupled structure shown in Figure 3.15, one has the transformed beam response

$$\tilde{W}_b(k_x) = \frac{\tilde{F}_0}{\tilde{D}_b k_x^4 - m_b'\omega^2 + \tilde{H}(k_x)} \tag{3.49}$$

where $\tilde{H}(k_x)$ is defined as

$$\tilde{H}(k_x) = \tilde{D}_p \frac{\tilde{k}_{y1}\tilde{k}_{y2}\left(\tilde{k}_{y1}^2 - \tilde{k}_{y2}^2\right)}{\tilde{k}_{y1}\tanh\left(\tilde{k}_{y2}L_y\right) - \tilde{k}_{y2}\tanh\left(\tilde{k}_{y1}L_y\right)}. \tag{3.50}$$

3.3.2 Results

Numerical simulation was carried out using equation (3.49) for the coupled structure as in Figure 3.15. The material properties and dimensions are as in Table 2.1

For comparison with the numerical results, FEM is used, which can describe approximately such an infinite system by imposing a damping effect on the finite system. The FE model is constructed in a similar manner as in section 2.6.2. Thus, the Euler-Bernoulli FE beam elements and thin shell elements are used and their size is as explained in the same section. The opposite edge of the plate, parallel to the beam, is considered to be pinned. To approximate and compare with the semi-infinite beam structure, a beam of length 8.0 m is modelled. Accordingly the length of the plate also becomes 8.0 m. One end of the beam at $x = 0$, where the external force is applied, and the corresponding plate edge, are assumed to be sliding to represent symmetry. The other end and the corresponding plate edge are modelled as free. To simulate an anechoic termination of the free end, structural damping of between 0.05 and 0.65 is added gradually in both the beam and plate along the final 2.0 m length.

The numerical response based on the Fourier transform method is symmetric in shape with respect to $x = 0$. Therefore, the point mobility of the FE model with the sliding condition is twice that of the fully infinite structure, as the sliding condition requires symmetry and accordingly, only half the force is necessary for the half model. These point mobilities are compared in Figure 3.16.

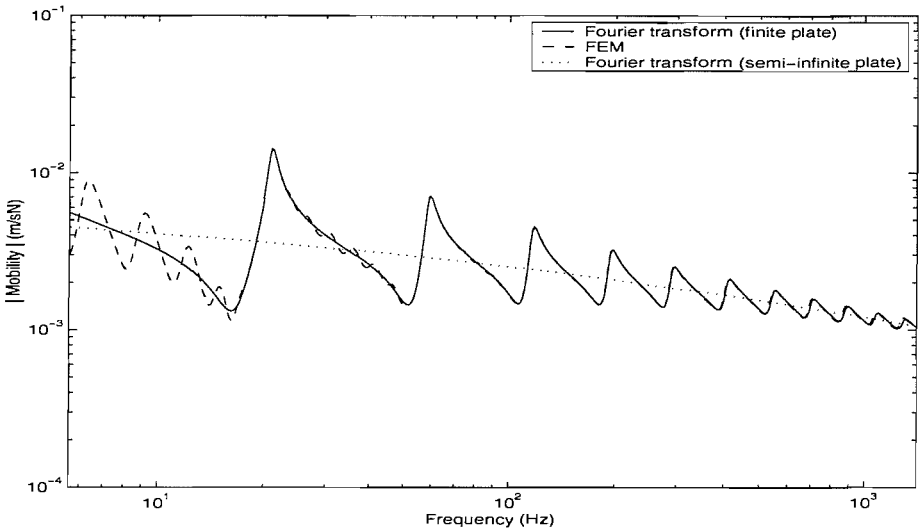

Figure 3.16. Point mobility calculated by Fourier transform and by FEM for the infinite beam and finite width plate as in Figure 3.15. Values of $\gamma = -15$ to $+15$ are considered in the inverse Fourier transform.

Some low frequency fluctuations occur in the FEM result. Although an attempt was made to simulate an infinite length using high structural damping near the free end, the FE model is actually finite and the global modes are related to the finite structure. Nevertheless, good agreement is found above about 20 Hz. Because the beam is assumed to be infinite in the Fourier transform method, the peaks and dips of the mobility are only related to dynamic characteristics of the finite width plate. The result in Figure 3.16 can be seen to oscillate around that of the infinite beam and semi-infinite plate (from Figure 3.14).

3.4 Finite beam coupled to finite plate

3.4.1 Motion of finite beam by Fourier series

In the previous section, the motion of the infinite beam coupled to a finite width plate has been described and formulated. As this defines the relationship between the beam and the plate, the response of a finite beam-plate system can be obtained if that relationship is maintained.

Consider the finite coupled beam-plate system shown in Figure 2.2 with sliding at both ends of the beam. The plate edge parallel to the beam is pinned, and the other two plate edges ($x = 0$ and $x = L_x$) are assumed to be sliding.

Then the behaviour of the coupled beam with sliding conditions at its ends can be expressed in terms of cosine orders, as follows,

$$\cos\left(\frac{n\pi x}{L_x}\right),\ n = 0,1,2,3,\cdots \tag{3.51}$$

where L_x is the length of the beam and n is the number of half-cosine waves along the coupled beam. Note that the relationship between the coupled beam and the plate defined in the previous sections is maintained. Thus, the motion of the finite coupled beam with sliding end conditions may be written as a Fourier series

$$\tilde{w}_b(x) = \frac{\tilde{W}_{b,0}}{2} + \sum_{n=1}^{\infty} \tilde{W}_{b,n} \cos(k_{x,n} x) \tag{3.52}$$

where $k_{x,n} = n\pi / L_x$ and $\tilde{W}_{b,n} = \tilde{W}_b(k_{x,n})$ is the n^{th} component of the motion of the coupled beam, which is defined in equation (3.24) for the semi-infinite plate case and equation (3.49) for the finite width plate case. $\tilde{W}_{b,0}/2$ is considered as the value for rigid motion of the beam ($k_x = 0$). The motion of the coupled beam is expressed as a Fourier series possessing only cosine functions due to the particular boundary conditions imposed.

In the same manner, the motion of the plate at each position y can also be written in terms of a Fourier series in the x direction, as follows,

$$\tilde{w}_p(x,y) = \frac{\tilde{W}_{p,0}(y)}{2} + \sum_{n=1}^{\infty} \tilde{W}_{p,n}(y)\cos(k_{x,n}x) \tag{3.53}$$

where $\tilde{W}_{p,n}(y) = \tilde{W}_p(k_{x,n}, y)$ is the n^{th} component of the motion of the plate, which is presented in equation (3.38). Thus the method of the previous section can be used, replacing the Fourier transform by a Fourier series.

3.4.2 Power

In this section expressions are derived for the various powers and energies required to investigate the power balance relationship for the beam-plate coupled structure.

The time-averaged power input due to a point harmonic force is [79]

$$P_{input} = \frac{1}{2}\mathrm{Re}\left\{ \tilde{F}_0 \ \tilde{v}_0^* \right\} = \frac{1}{2}\left| \tilde{F}_0 \right|^2 \mathrm{Re}\left\{ \tilde{Y}_0 \right\} \tag{3.54}$$

where $\tilde{F}_0$ is the point force amplitude, $\tilde{v}_0$ is the velocity response amplitude at $x = 0$, $*$ means complex conjugate and $\tilde{Y}_0$ is the point mobility.

The Fourier series for the harmonic force acting on the plate due to the beam of the coupled structure is

$$\tilde{f}_1(x) = \frac{\tilde{F}_{1,0}}{2} + \sum_{n=1}^{\infty} \tilde{F}_{1,n}\cos(k_{x,n}x), \tag{3.55}$$

where the Fourier transformed force $\tilde{F}_{1,n} = \tilde{F}_1(k_{x,n})$ is defined from equation (3.48) with $k_{x,n} = n\pi/L_x$.

The net power transferred from the beam to the plate can be expressed in terms of the distributed interaction force and responses,

$$P_{b\to p} = \frac{1}{2}\int_0^{L_x} \mathrm{Re}\left\{\tilde{f}_1(x)^* \tilde{v}_b(x)\right\} dx, \tag{3.56}$$

where $\tilde{v}_b(x) = i\omega\tilde{w}_b(x)$ is the velocity response of the coupled beam and L_x is the length of the beam. Substituting equations (3.52) and (3.55) into equation (3.56) gives a simpler form of the net power transferred.

$$P_{b\to p} = \frac{L_x}{4}\mathrm{Re}\left\{ i\omega\left(\tilde{F}_{1,0}^* \tilde{W}_{b,0}/2 + \sum_{n=1}^{\infty} \tilde{F}_{1,n}^* \tilde{W}_{b,n} \right)\right\}. \tag{3.57}$$

Also, the dissipated power is obtained from the strain energy of the corresponding substructure. The dissipated power in the finite beam can be written as [12]

$$P_{b,dis} = \omega\eta_b U_{b,\max} \tag{3.58}$$

where $U_{b,\max}$ is the maximum over a cycle of the strain energy in the beam, given by

$$U_{b,\max} = \frac{D_b}{2}\int_0^{L_x} \left| \frac{d^2\tilde{w}_b(x)}{dx^2} \right|^2 dx. \tag{3.59}$$

The second derivative of $\tilde{w}_b(x)$ can be obtained in terms of the Fourier series as

$$\frac{d^2\tilde{w}_b(x)}{dx^2} = -\sum_{n=1}^{\infty} k_{x,n}^2 \tilde{W}_{b,n} \cos(k_{x,n}x) \tag{3.60}$$

where $\tilde{W}_{b,n} = \tilde{W}_b(k_{x,n})$.

The strain energy U in a plate is given by [70]

$$U = \frac{D_p}{2}\int_0^{L_y}\int_0^{L_x} \left[\left(\frac{\partial^2 w_p}{\partial x^2} \right)^2 + \left(\frac{\partial^2 w_p}{\partial y^2} \right)^2 + 2\nu \frac{\partial^2 w_p}{\partial x^2}\frac{\partial^2 w_p}{\partial y^2} + 2(1-\nu)\left(\frac{\partial^2 w_p}{\partial x \partial y} \right)^2 \right] dxdy, \tag{3.61}$$

where $w_p = w_p(x,y,t)$ is time dependent and therefore, each term in the strain energy can be regarded as a time dependent term. Assuming that each term is either

in or out of phase the maximum strain energy in a cycle can be obtained from twice the time-averaged value of each term in equation (3.61), and is given as [21]

$$U_{p,\max} = \frac{D_p}{2}\int_0^{L_x}\int_0^{L_y}\left[\begin{array}{l}\left|\frac{\partial^2\tilde{w}_p}{\partial x^2}\right|^2 + \left|\frac{\partial^2\tilde{w}_p}{\partial y^2}\right|^2 + 2\nu\,\mathrm{Re}\left\{\left(\frac{\partial^2\tilde{w}_p}{\partial x^2}\right)\left(\frac{\partial^2\tilde{w}_p}{\partial y^2}\right)^*\right\} \\ +2(1-\nu)\left|\frac{\partial^2\tilde{w}_p}{\partial x\partial y}\right|^2\end{array}\right] dydx \tag{3.62}$$

where $\tilde{w}_p = \tilde{w}_p(x,y)$. As the motion of the finite plate $\tilde{w}_p$ is given by equation (3.53), the second derivative of $\tilde{w}_p$ with respect to the variables x and y can be expressed using the Fourier series. Finally, the dissipated power in the finite plate is given by

$$P_{p,dis} = \omega\eta_p U_{p,\max}. \tag{3.63}$$

3.4.3 Results

Numerical results are presented for the finite beam attached to a finite plate shown in Figure 2.2. The dimensions of the structure are as given in Table 2.1.

For an external, unit magnitude, point force applied at $x = 0$ the point mobility is shown in Figure 3.17. In equation (3.52), $n = 145$ is used, which approximately corresponds to the wavenumber $k_x = 230$ rad/m at 1412 Hz, corresponding to the non-dimensional wavenumber $\gamma = 15$. Results are also shown obtained using FEM. The number of elements used in the FE model is 6783 (see Figure 2.9) corresponding to 8 elements per wavelength at the maximum frequency. As seen in the figure, the result obtained by the Fourier series method shows very good agreement with that of FEM. Note that the responses agree well even in the higher frequency region.

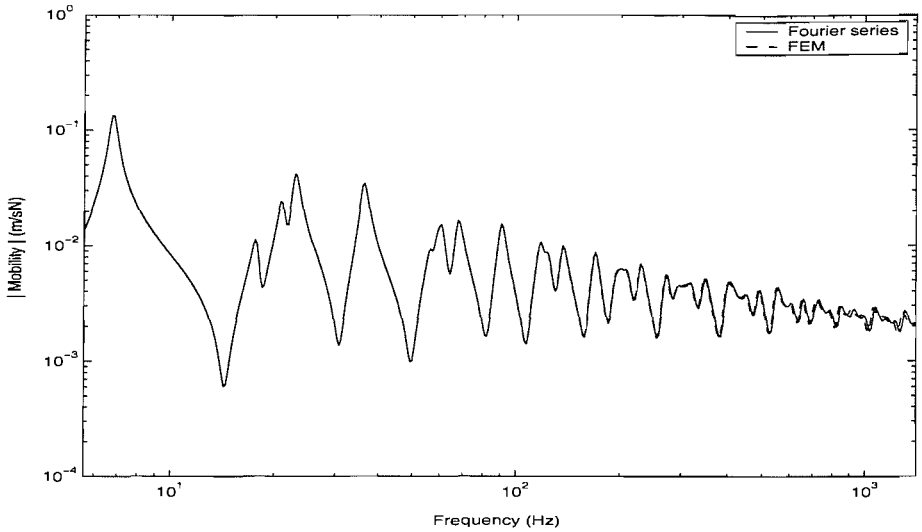

Figure 3.17. Point mobility calculated by different methods for the coupled finite beam-plate structure as in Figure 2.2 (η_p = 0.05 in the plate, η_b = 0.05 in the beam, point force applied at $x = 0$).

In addition to the point mobility comparison, an example of a transfer mobility to an arbitrary point on the plate is shown in Figure 3.18, which also shows good agreement with that of FEM.

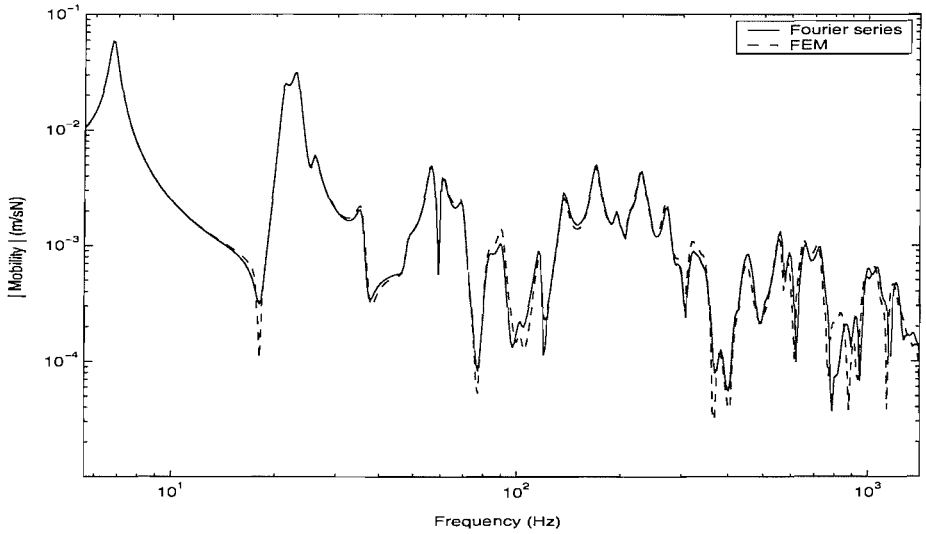

Figure 3.18. Transfer mobility for the plate (at x = 1.50 m and y = 0.49 m) in the coupled finite beam-plate structure as in Figure 2.2 (η_p = 0.05 in the plate, η_b = 0.05 in the beam, point force applied at x = 0).

The total input power and the net power transferred to the plate are compared in Figure 3.19. It is clear that the total power input is greater than the power transferred from the beam to the plate at all frequencies, as expected. Comparing the two powers, one can find that at some frequencies, such as 22.9, 59.8 and 118 Hz, most power is transferred to the plate, while at other frequencies such as 6.7, 36.3 and 90.2 Hz, there is a larger difference between the two powers. This could be explained in terms of the mode shapes of the beam and the plate. Although the modes of the beam and the plate are coupled, nevertheless, at some natural frequencies the mode of the beam is dominant, at other frequencies the mode of the plate is dominant. Therefore, it can be said that when the difference between the two powers is reduced, the mode of the plate is dominant and the plate receives most energy. In that case, the magnitude of the beam motion is relatively small. Conversely, if the difference is large, the magnitude of the beam motion becomes larger than that of the plate. In such a situation, the behaviour of a plate attached to a beam, for example the resonances and anti-resonances of the plate impedance, play an important role. These power-related phenomena will be explained further in Chapter 4 dealing with a wave approach where the plate impedance is discussed.

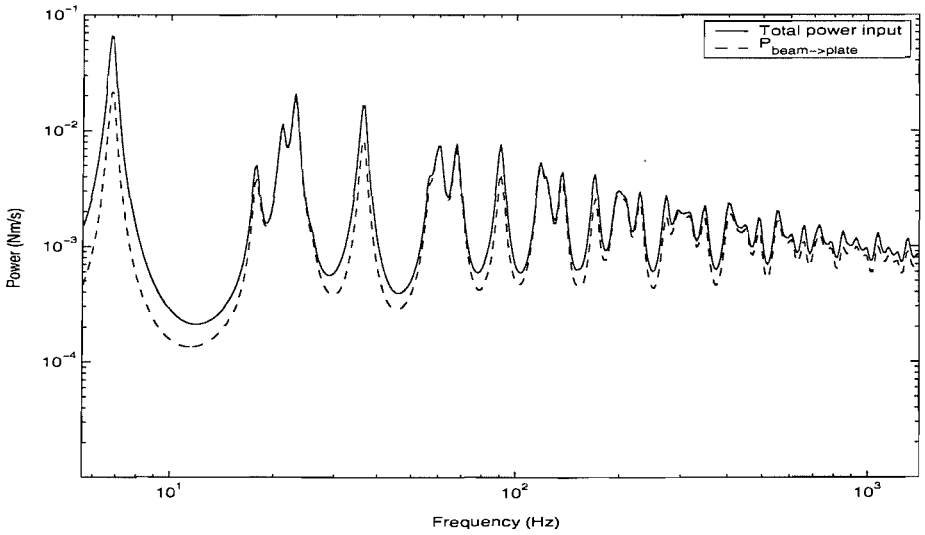

Figure 3.19. Total input power to the coupled structure shown in Figure 2.2 and net power transferred to the plate (η_p = 0.05 in the plate, η_b = 0.05 in the beam, point force applied at $x = 0$).

3.5 Conclusions

In this chapter, the Fourier transform and Fourier series methods are used to analyse the structural behaviour of a coupled beam-plate structure and numerical results are presented and compared with FE analysis.

Firstly, the Fourier transformed motion of the infinite coupled beam is developed when an infinite plate is attached to the beam. From the coupled equations of the motion, the influence of the plate on the beam is identified in the wavenumber domain. The damping effect as well as the mass effect of the plate is identified and explained. It has been shown that the mass effect becomes smaller as frequency increases; the added mass is that within 1/6 of a plate wavelength of the beam. Also, comparing the response of the coupled beam obtained using the Fourier transform, it has been highlighted that the effective damping due to the plate decreases as frequency increases. These phenomena observed here will provide a good reference case in the development of a wave method later incorporating a plate impedance model.

A consistent rule for truncating the sufficiently low level response with respect to the maximum response is used in evaluating the Fourier integral. Using non-dimensional wavenumbers in the range ± 15, the response is truncated at 40 dB below the maximum and the result is accurate to within 0.01%.

To obtain the response of a coupled finite beam and finite width plate, a Fourier series method has been developed and implemented. Then, the corresponding numerical analysis was performed based on the wavenumber range mentioned above. Comparing the numerical results with those of FEM, very good agreement is found.

The developments of the Fourier approach in this chapter can be extended to any system which has a constant cross-section, for example for the analysis of a beam-plate-beam structure. This will be considered further in Chapter 5.

CHAPTER 4
APPROXIMATE WAVE METHOD FOR ANALYSIS OF STIFF ONE-DIMENSIONAL STRUCTURE COUPLED TO FLEXIBLE STRUCTURE

4.1 Introduction

In Chapters 2 and 3, the dynamic characteristics of a coupled structure consisting of a beam and a plate were investigated using a modal approach and a Fourier technique respectively. For the particular boundary conditions considered, these numerical results can be regarded as exact provided that sufficient numbers of modes or Fourier components are included. However, this generally requires large computer resources and computation time. The wave approach proposed by Grice and Pinnington [41] offers a more efficient although approximate method for the analysis of such coupled systems.

In addition, from the viewpoint that the present study concerns the mid frequency analysis, coupling a stiff beam (long wavelength behaviour) and a flexible plate (short wavelength behaviour) by means of a wave approach and analysing their response forms an important aspect of this thesis. In later chapters, the wave method is applied and extended to more complicated systems such as a two-beam and four-beam systems. First, the more basic system consisting of a single beam and a plate is discussed.

The coupled structure considered in this chapter is basically similar to that of Grice and Pinington [41] although a non-symmetrical configuration is considered here with the beam on one edge of the plate, as in previous chapters. Also in [41], the travelling wavenumber of the coupled beam was calculated iteratively, and it was assumed that the nearfield wave in the coupled beam had the same wavenumber as the propagating wave. In this chapter, problems of convergence in the iteration method used for the wavenumber estimation at some frequencies are addressed by

using Muller's method [83]. Also, the nearfield wavenumber is considered separately in the coupled beam. The resulting coupled nearfield wavenumber displays differences from the travelling wavenumber originally determined, but it is shown that using these separate wavenumbers yield a non-physical model.

The ends of the beams are sliding as in previous chapters. However, this boundary condition can be simply changed for a different situation.

Initially, the relationship between the coupled beam wavenumber and the plate wavenumber is presented. The relationship when the nearfield wavenumber is considered separately in the beam is also discussed in Appendix A. The numerical analysis is presented for a pinned condition on the opposite edge of the plate as in the previous chapter. This is based on the numerical evaluation using Muller's method. In Appendix B the influence of the iteration method on the result is reviewed and Muller's method is explained in more detail. The improvement to the results due to its application is shown.

4.2 Infinite beam coupled to semi-infinite plate

4.2.1 Undamped free wave motion

A coupled structure consisting of infinite systems is investigated first. The combined structure consists of a stiffer beam component carrying long-wavelength flexural waves and a flexible plate component carrying short-wavelength flexural waves. Figure 3.1 presented in Chapter 3 shows an infinite beam coupled to the edge of a semi-infinite plate. It is assumed that the ratio of these wavelengths is sufficiently large. It is known that the coupled structure can be analysed in terms of its dispersion relation [41]. It is assumed that the beam is infinitely stiff to torsion along $y = 0$, as in previous chapters.

It should be noted that the following wave approach is only suitable for the case where the stiff beam is excited, so that the excited beam radiates short wavelength waves into the flexible plate. Although wavenumber trace matching can still be used for the plate-excited case in which waves in the plate are incident on the beam at an arbitrary angle, such solutions are not considered here. Thus, in this context the plate is always considered as the 'receiver' in this wave method [41].

Consider first the uncoupled free wave motion of the undamped beam and plate. Thus no external force is applied. Harmonic motion at frequency ω is assumed throughout with a time dependence of $e^{i\omega t}$.

The relevant equations of motion of the beam and plate were presented in equations (3.1) and (3.7) respectively, except that no damping is now considered. A travelling harmonic flexural wave in the infinite beam, uncoupled from the plate, has wavenumber k_b, given by $k_b^4 = (m_b'/D_b)\omega^2$. Nearfield waves also exist with the form $e^{\pm k_b x}$.

When the semi-infinite plate and the infinite beam are joined along the line $y = 0$ a force per unit length $\tilde{f}_1(x)$ acts between them. Equation (3.1) becomes

$$D_b \frac{d^4 \tilde{w}_b}{dx^4} - m_b' \omega^2 \tilde{w}_b = -\tilde{f}_1(x). \tag{4.1}$$

Suppose that the 'free' wave motion of the coupled beam becomes

$$\tilde{w}_b = \tilde{A} e^{-ik_x x} \tag{4.2}$$

for some wavenumber k_x. In Chapter 2, it was shown that the coupled stiff beam dominantly governs the motion of the flexible plate. Thus, by trace wavenumber matching with respect to the coupled beam wavenumber k_x the motion of the plate is given by

$$\tilde{w}_p = (\tilde{B}e^{-ik_y y} + \tilde{C}e^{-k_e y})e^{-ik_x x} \tag{4.3}$$

where $\tilde{B}$ is the amplitude of the wave propagating away from the junction, $\tilde{C}$ is the amplitude of the nearfield wave in the plate which is also generated at the junction, k_y is the trace wavenumber for the propagating wave radiating into the plate normal to the beam and k_e is the trace wavenumber for the nearfield wave in the plate. In the above it is assumed that k_x is real, although as will be seen this is not quite the case.

To obtain the travelling wavenumber k_x in terms of the beam and plate properties, consider the propagating wave solution in the plate $\tilde{w}_p = \tilde{B}e^{-ik_y y}e^{-ik_x x}$. Substituting this into equation (3.7) gives

$$\left[D_p(k_x^4 + 2k_y^2 k_x^2 + k_y^4) - m_p'' \omega^2\right]\tilde{B}e^{-ik_y y}e^{-ik_x x} = 0. \tag{4.4}$$

For non-trivial solutions, the propagating normal trace wavenumber in the plate is found to be

$$k_y = \sqrt{k_p^2 - k_x^2}. \tag{4.5 a}$$

Similarly, letting $\tilde{w}_p = \tilde{C}e^{-k_e y}e^{-ik_x x}$, the normal nearfield wavenumber is

$$k_e = \sqrt{k_p^2 + k_x^2}. \tag{4.5 b}$$

The boundary conditions when a semi-infinite plate is attached at its edge to the beam are:

(i) Continuity equation; equal displacement

$$\tilde{w}_b(x) = \tilde{w}_p(x,0) \tag{4.6}$$

(ii) Sliding condition for the plate; the beam is assumed infinitely stiff to torsion along y=0

$$\left.\frac{\partial \tilde{w}_p}{\partial y}\right|_{y=0} = 0 \tag{4.7}$$

(iii) Force equilibrium condition; the force on the plate is equal and opposite to the force on the beam

$$D_p \frac{\partial}{\partial y}\left(\frac{\partial^2 \tilde{w}_p}{\partial y^2} + (2-\nu)\frac{\partial^2 \tilde{w}_p}{\partial x^2} \right)\Bigg|_{y=0} = \tilde{f}_1(x). \tag{4.8}$$

From the boundary condition (4.6),

$$\tilde{A} = \tilde{B} + \tilde{C}. \tag{4.9}$$

From the boundary condition (4.7),

$$\left[\left(-ik_y \tilde{B} e^{-ik_y y} - k_e \tilde{C} e^{-k_e y} \right) e^{-i\tilde{k}_e x} \right]_{y=0} = 0. \tag{4.10}$$

Therefore, from equations (4.9) and (4.10) the amplitudes of the waves in the plate are given by

$$\tilde{B} = \frac{k_e}{k_e - ik_y}\tilde{A}, \quad \tilde{C} = \frac{-ik_y}{k_e - ik_y}\tilde{A}. \tag{4.11}$$

From the boundary condition (4.8),

$$D_p e^{-ik_x x}\left[ik_y \left\{ k_y^2 + (2-\nu)k_x^2 \right\} \tilde{B} - k_e \left\{ k_e^2 - (2-\nu)k_x^2 \right\} \tilde{C} \right] = \tilde{f}_1(x). \tag{4.12}$$

Substituting for $\tilde{B}$ and $\tilde{C}$ in terms of $\tilde{A}$ gives

$$\left[\frac{ik_y k_e \left\{ k_y^2 + k_e^2 \right\}}{k_e - ik_y} \right] \tilde{A} D_p e^{-ik_x x} = \tilde{f}_1(x). \tag{4.13}$$

Therefore, the plate line impedance presented to the beam for wavenumber k_x can be found. The line impedance is the impedance of the plate per unit length of the beam arising at the coupling junction, which is found from the force per unit length acting on the line junction and a velocity response at the junction, both the force and response being functions of the coordinate x in the form $e^{-ik_x x}$. Therefore, the exact line impedance of the plate is

$$\tilde{Z}'_p = \frac{\tilde{f}_1(x)}{i\omega\tilde{A}e^{-ik_x x}} = \frac{D_p}{\omega}\left[\frac{k_y k_e 2k_p^2}{k_e - ik_y}\right]. \tag{4.14}$$

One can see that the line impedance is independent of the coordinate x. Note that equation (4.14) includes a damping-like term (real part) and also a mass-like imaginary term. Recalling that the plate is undamped, this explains the damping and mass effect of the plate on the coupled beam, which was identified in the wavenumber domain in the Fourier transform method.

Finally, the general dispersion relationship for the coupled structure can be derived from equations (4.1) and (4.14).

$$D_b k_x^4 = m'_b\omega^2 - i\omega\,\tilde{Z}'_p. \tag{4.15}$$

As briefly explained in the first paragraph in this section, an important requirement for this dispersion relationship is that the plate should be more flexible than the beam, so that the plate impedance is smaller than the beam impedance. Note that, although the wavenumber ratio of the plate to the beam is also used as a criterion in this thesis, the small impedance of the plate does not necessarily mean that the plate wavenumber is greater than the beam wavenumber. Provided that the plate impedance is smaller than the beam impedance, it is expected that there are two travelling wave solutions and two nearfield wave solutions to this equation. Note that k_x is not real, due to the damping-like term in $\tilde{Z}'_p$, and also $\tilde{Z}'_p$ is a function of k_x, so that this equation must be solved iteratively. If the plate impedance becomes larger, then the dispersion equation may not converge in an iteration approach and this wave approach may not be usable.

Substituting equations (4.5) and (4.14) into equation (4.15) gives the dispersion equation presented in terms of k_x, k_b and k_p as

$$k_x^4 = k_b^4 + \frac{D_p}{D_b}\sqrt{k_p^2 - k_x^2}\sqrt{k_p^2 + k_x^2}\left(\sqrt{k_p^2 - k_x^2} - i\sqrt{k_p^2 + k_x^2}\right). \tag{4.16}$$

The dispersion equation can be presented in a simpler form if k_p is much larger than k_x. Such an implementation and the explanation of this physical phenomenon follow in section 4.2.4.

4.2.2 Forced response

Once the wavenumber for the coupled structure is evaluated, then the point mobility of the structure can easily be calculated from the equation of the point mobility of an infinite beam. In this section, a semi-infinite beam the end of which is assumed to be sliding is considered because it is more meaningful for comparison with a finite beam structure in the following sections. This differs from the result for an infinite beam by a factor of 2.

Consider a semi-infinite beam located at $0 \le x \le \infty$, and excited at $x = 0$ by a force $\tilde{F}_0$ acting perpendicular to the beam axis. The point mobility can be derived from the general solution of the motion of a beam. In general, the coupled beam may have different wavenumbers for the propagating and nearfield waves. Thus, the corresponding solution of the semi-infinite beam becomes

$$\tilde{w}(x) = \tilde{A}_1 e^{-ik_b x} + \tilde{A}_2 e^{-k_{nf} x}, \tag{4.17}$$

where $\tilde{A}_1$ is the amplitude of propagating wave, $\tilde{A}_2$ is the amplitude of the nearfield wave, k_b is the propagating wavenumber and k_{nf} is the nearfield wavenumber. Note that for an uncoupled beam the nearfield wavenumber is equal to k_b. Since all waves propagate away from the excitation point, waves travelling in the negative x direction waves vanish. Because the slope of the beam end is zero for the sliding boundary condition and the force applied should be the same as the shear force of the beam at $x = 0$, the boundary conditions are

$$\left.\frac{\partial w}{\partial x}\right|_{x=0} = 0,\ D_b \left.\frac{\partial^3 w}{\partial x^3}\right|_{x=0} = \tilde{F}_0 . \qquad (4.18\ \text{a, b})$$

Then the amplitudes $\tilde{A}_1$ and $\tilde{A}_2$ are obtained and the mobility of the semi-infinite beam is

$$\tilde{Y}_b = \frac{i\omega\tilde{w}(x)}{\tilde{F}_0} = \frac{\omega}{D_b(k_b^2 + k_{nf}^2)}\left(\frac{e^{-ik_b x}}{k_b} - i\frac{e^{-k_{nf}x}}{k_{nf}}\right). \qquad (4.19)$$

Because $k_b = k_{nf}$ in an uncoupled semi-infinite beam, the mobility becomes

$$\tilde{Y}_b = \frac{\omega}{2D_b k_b^3}\left(e^{-ik_b x} - ie^{-k_b x}\right) \qquad (4.20)$$

and the point mobility at $x = 0$ is

$$\tilde{Y}_0 = \frac{\omega}{2D_b k_b^3}(1-i). \qquad (4.21)$$

The general relation of equation (4.15) is still valid for the coupled structure consisting of the semi-infinite beam shown in Figure 4.1 and the point mobility for the coupled structure can be calculated from equation (4.19) using the corresponding coupled travelling wavenumber k_x and the nearfield wavenumber k_{nf} of the coupled structure. The travelling and nearfield wavenumbers in a coupled system may be different. Concerning this, further explanations are presented in following sections.

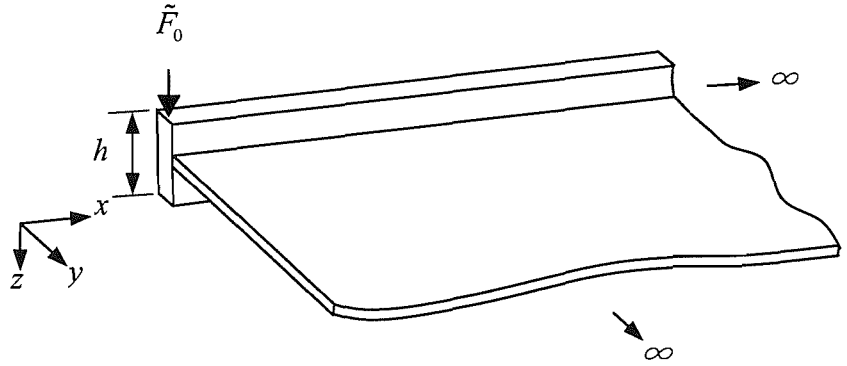

Figure 4.1. A coupled structure consisting of a semi-infinite beam attached to a semi-infinite plate.

4.2.3 Introduction of damping in the beam

The effect of damping in the beam can be introduced to the previous analysis by using a complex bending stiffness $\tilde{D}_b$ which is given in terms of D_b and the structural loss factor of the beam η_b as follows [79].

$$\tilde{D}_b = D_b(1+i\eta_b). \tag{4.22}$$

Provided η_b is small the above analysis remains approximately valid. However it should be realised that the derivation of k_y and k_e by wavenumber matching is strictly only applicable in the undamped case.

4.2.4 Approximation by locally reacting impedance

Note that if $k_p >> k_x$, i.e. the plate wavenumber is much larger than the wavenumber in the coupled beam, then the exact line impedance of the plate, equation (4.14) can be written approximately as

$$\tilde{Z}'_p = \frac{\tilde{f}_1(x)}{i\omega\tilde{A}e^{-ik_x x}} \approx \frac{D_p k_p^3}{\omega}(1+i) = \frac{m''_p\omega}{k_p}(1+i). \tag{4.23}$$

Equation (4.23) is known to be valid if the plate wavenumber is sufficiently larger than the coupled beam wavenumber [41]. Then the impedance of the plate can be considered as the input point impedance of an equivalent beam of infinite length and unit width driven by a point force (the inverse of equation (4.21)). Therefore, the plate is considered as locally reacting. This means that if the beam propagating wavelengths are much longer than those in the plate, then the wave radiates into the plate at an angle which is almost normal to the axis of the beam. Thus, in fact the plate behaves like separate strips. If equation (4.23) is used, k_x^4 can be found directly from equation (4.15) from which the travelling wavenumber and the nearfield wavenumber in the beam can be calculated.

Strictly, the travelling wavenumber k_x and the nearfield wavenumber k_{nf} in the x direction could have different values, but in the present case, since wavenumber trace matching is only based on the propagating wave k_x in the coupled beam, the exact nearfield wavenumber cannot be calculated. By assuming the locally reacting plate impedance, the nearfield wavenumber can be calculated approximately from the roots of k_x^4 in equation (4.15).

If a nearfield wave is present in the beam with no travelling wave, the corresponding plate impedance $\tilde{Z}'_p$ is a function of the nearfield wavenumber in the beam k_{nf}. This leads to different wavenumbers in the plate as described in Appendix A. However, in general, the travelling and nearfield waves are present in the beam together and the corresponding plate impedance should account for both their contributions. Each wave in the beam will 'see' a plate impedance due to the total plate motion. In practice, the travelling wave will dominate the beam response and a reasonable approximation can be obtained by using the plate impedance corresponding to this wave, as given above.

4.2.5 Results

Numerical analysis was performed for the structure shown in Figure 4.1. The relevant material properties of the structure are as listed in Table 2.1 in Chapter 2. The length of the beam L_x and the width of the plate L_y are infinite. It should be emphasised that damping in the beam is considered where necessary, whilst the plate is undamped.

As described in section 4.2.4, if the impedance of a plate can be regarded as locally reacting, the numerical analysis to identify the characteristics of the full structure will be greatly simplified. Before using the simplification, it is necessary to verify whether the assumption is applicable. If the ratio of k_x to k_p is sufficiently small so that the locally reacting impedance is the same as the exact line impedance, it can be said that the locally reacting impedance of the plate is valid.

In Figure 4.2, the relationship between the ratio of the two impedances and k_x / k_p is shown. For $k_x / k_p < 0.5$, the locally reacting impedance is the same as the exact line impedance to within 3 %. The actual ratio k_x / k_p for the structure of Figure 4.1 is shown in Figure 4.3. It has values below 0.5 throughout the frequency range of interest (5.6 Hz to 1412 Hz).

When the actual wavenumbers k_p, k_y and k_e are used in equations (4.14) and (4.23) for the present structure, the locally reacting impedance (equation (4.23)) is a little greater than the exact line impedance (equation (4.14)) by about 3% at 5.6 Hz (maximum error of 3%), which seems negligible. Therefore, the plate can be considered as locally reacting and the general dispersion relation equation (4.15) can be solved using equation (4.23) for the locally reacting impedance of the plate. This assumption is valid for both the infinite plate and a finite plate considered later.

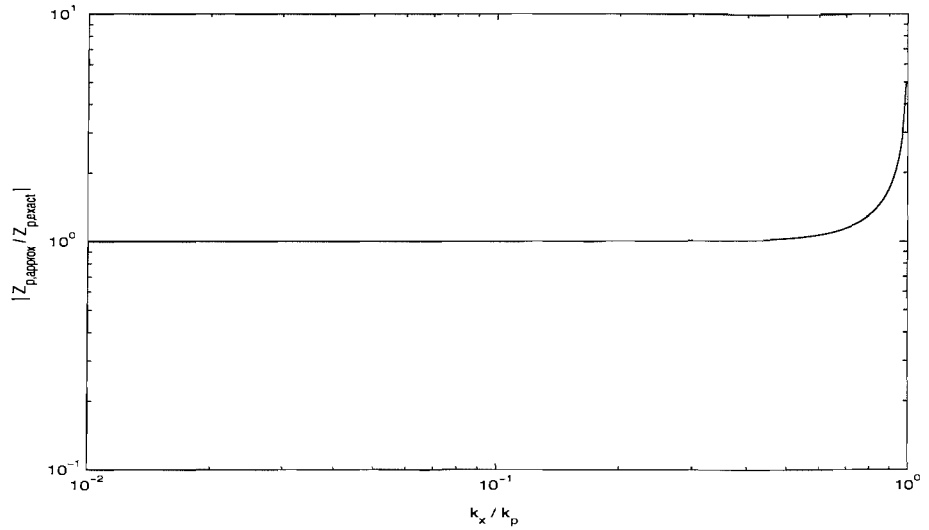

Figure 4.2. Ratio of the locally reacting impedance to the exact line impedance of the semi-infinite plate.

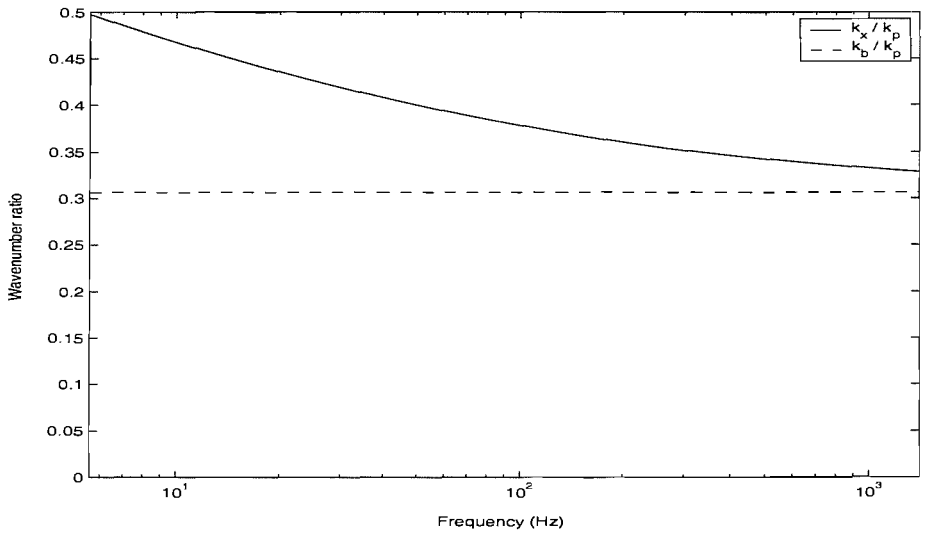

Figure 4.3. Ratio of wavenumbers of the coupled system as in Figure 4.1.

In using the wave method, it is important first to understand the characteristics of the wavenumbers in the structures. The equations related to the wave method start basically from the free or uncoupled wavenumber of a beam or plate. Thus, the coupled beam wavenumber k_x is compared with the free wavenumbers of the semi-infinite beam and the semi-infinite plate in Figure 4.4.

Because the depth of the beam is larger than that of the plate, the wavenumber of the plate is greater than that of beam. The ratio of k_b to k_p is already shown in Figure 4.3 and is constant at 0.306 because both of them are proportional to $\omega^{1/2}$. The coupled wavenumber k_x lies between k_b and k_p. It is greater than k_b due to the presence of the plate impedance in the dispersion equation (4.15). The mass of the plate increases k_x, but its influence is smaller at high frequency because the equivalent mass is m_p''/k_p, see equation (4.23). Because of this, as shown in Figure 4.3, the ratio of k_x to k_p does not have a constant value.

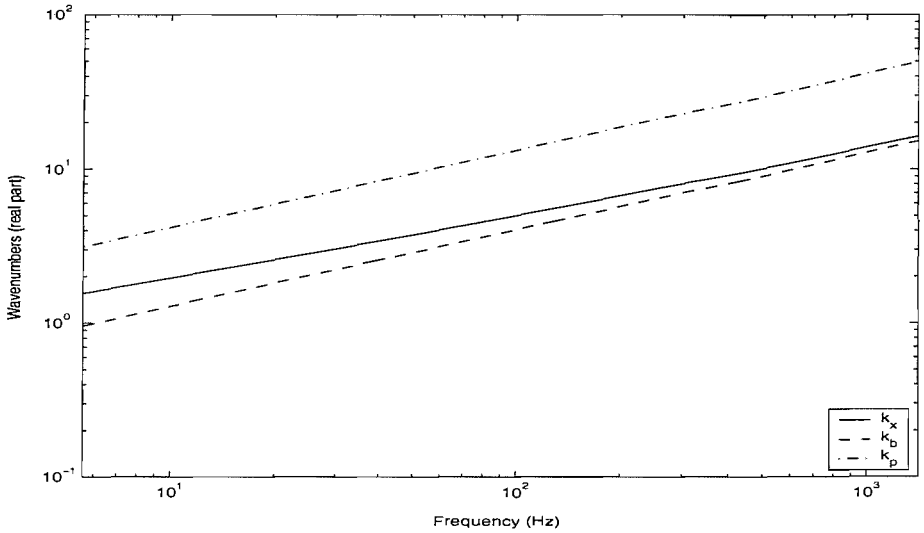

Figure 4.4. Travelling wavenumbers of the coupled beam (k_x), the uncoupled beam (k_b) and the uncoupled plate (k_p). k_x is calculated on the basis of a locally reacting plate.

The imaginary part of the wavenumber is related to the damping of the structure. As mentioned in section 4.2.1, the 'damping' part of the plate impedance makes the coupled wavenumber k_x complex. Physically this means that the plate appears to add damping to the beam although it does so by energy radiation into the plate. Note that the coupled system is assumed to be undamped at this stage. An equivalent loss factor for the beam η can be derived from

$$\eta = -\frac{\mathrm{Im}(k_x^4)}{\mathrm{Re}(k_x^4)} \approx -4\frac{\mathrm{Im}(k_x)}{\mathrm{Re}(k_x)} \tag{4.24}$$

and is presented in Figure 4.5. This shows how the damping falls with increasing frequency. This tendency was previously described by Heckl [64].

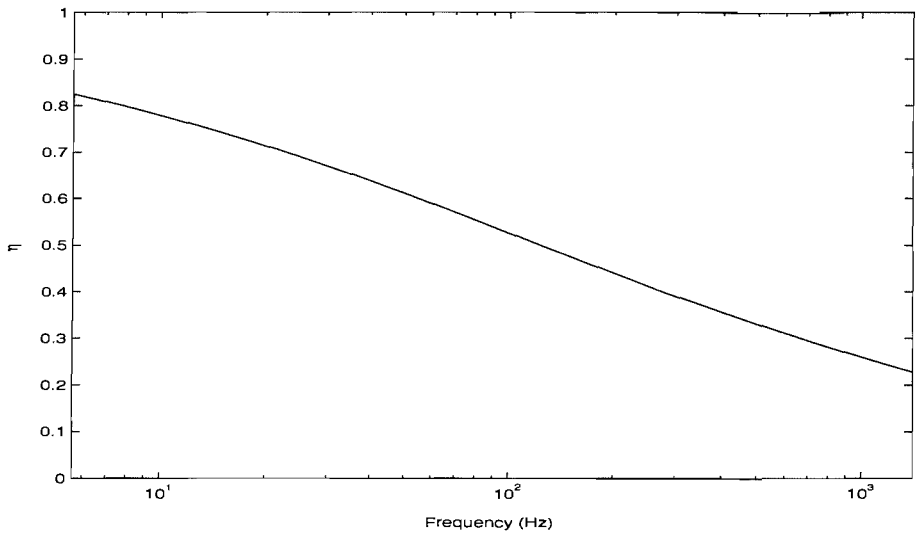

Figure 4.5. Equivalent loss factor η in the coupled structure as in Figure 4.1. k_x is calculated on the basis of the locally reacting plate.

In addition to the damping effect of the plate, it would be interesting to see how the dynamic characteristics change when damping is introduced to the beam. A loss factor equal to 0.05 is introduced into the beam. In Figure 4.6, the imaginary part of the wavenumber k_x is shown from which the damping can be inferred. Although the difference is small, it can be seen that the damping increases, particularly at higher frequencies where the equivalent loss factor from the plate is smaller (see Figure 4.5).

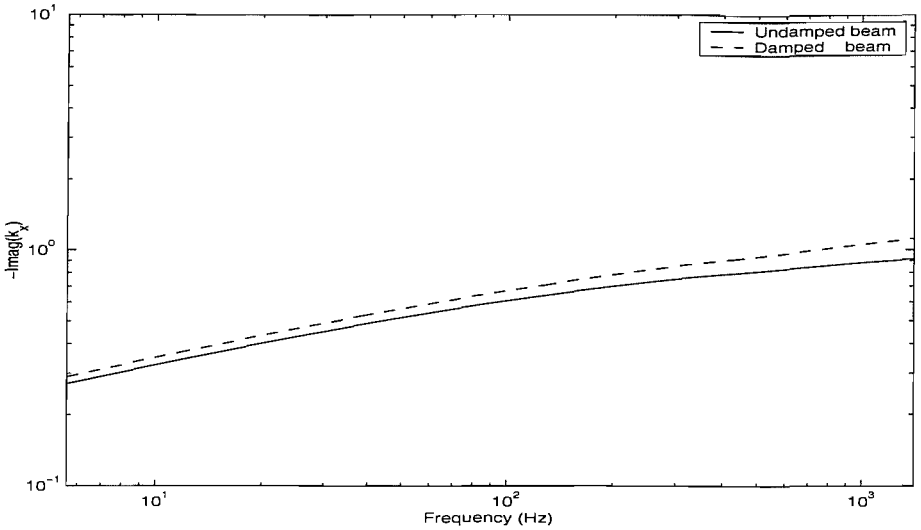

Figure 4.6. Imaginary part of the wavenumber k_x for undamped and damped ($\eta_b = 0.05$) beam coupled to semi-infinite plate.

Figure 4.7 shows the point mobility of the beam-plate system. If damping is included in the beam, the level of the point mobility will be reduced slightly, but as shown in Figure 4.7, the difference between the solid line and the dashed line (lower two lines) in the mobility graph is not distinguishable.

In the phase graph, it can be seen that the dashed line in the upper two lines shows a delayed phase due to the inclusion of the beam damping. The point mobility of the structure consisting of the damped semi-infinite beam and the undamped semi-infinite plate is used later in this chapter for comparison with the results of different finite structures. Figure 4.7 also shows the mobility and its phase of an uncoupled semi-infinite beam with a sliding end. Concerning the effect of damping, the tendency is similar to the coupled beam. A comparison of the mobilities between the coupled beam and the uncoupled beam was already made and discussed in section 3.2.7 (see Figure 3.14) where the mass and damping effect of the plate was explained.

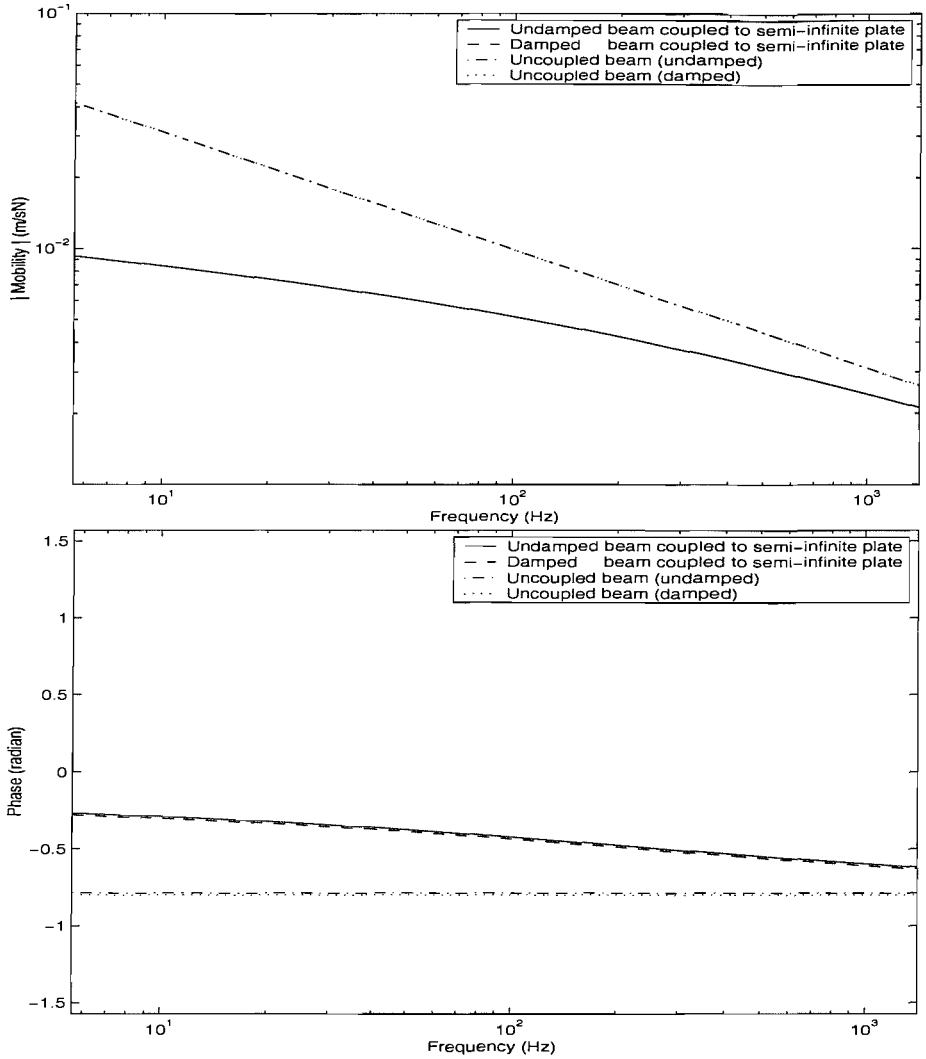

Figure 4.7. Point mobility and phase of the coupled system consisting of the semi-infinite beam and semi-infinite plate as in Figure 4.1 and the uncoupled semi-infinite beam.

Finally, the results from the wave model are compared with those of the Fourier transform method for the case when the beam is damped ($\eta_b = 0.05$) and the plate is undamped. The non-dimensional wavenumber range in the Fourier transform is $\gamma = -15$ to $+15$. A similar result (with a damped plate) based on the Fourier transform was shown in Chapter 3 (see Figure 3.14) except that the beam was assumed to be infinite instead of semi-infinite. Thus for comparison here, twice the magnitude of the point mobility of the Fourier transform method is used (for this, see the explanation with respect to Figure 3.16). The corresponding results

are compared in Figure 4.8. They show good agreement with maximum errors of about 3% and 0.02 radian for the magnitude and phase respectively.

A similar comparison of the uncoupled beam was already presented in section 3.2.5 (see Figure 3.5), in which for the same non-dimensional wavenumber range of $\gamma = \pm 15$ in the Fourier transform the maximum error was about 0.01% with respect to the analytical solution. Thus, here, the response of the Fourier method can be considered as accurate. Recalling that the approximate impedance of the plate was a little larger than the exact impedance, it may be expected that the point mobility level based on the wave method is lower than that of the exact Fourier method in Figure 4.8. However, one can see that the point mobility level is actually a little greater than that of the Fourier method. Thus, in addition to the approximation of the plate impedance, it seems that there is another reason producing such a difference. Indeed, in the wave method, it was assumed that the nearfield wavenumber k_{nf} has the same value as the propagating wavenumber k_x. Thus, the error in Figure 4.8 seems to be related to the substitution of the nearfield wavenumber by the travelling wavenumber in the beam. Concerning this, a further investigation follows in the next section.

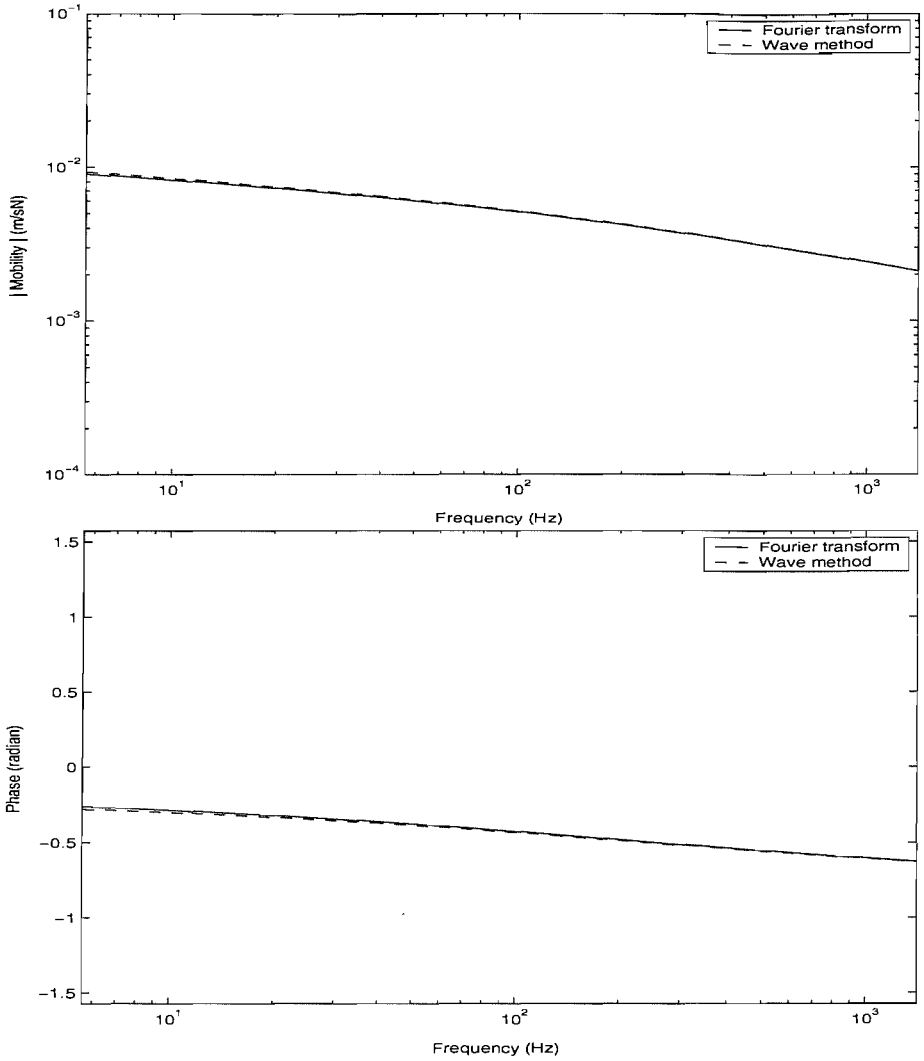

Figure 4.8. Point mobility and phase of the semi-infinite beam coupled to the semi-infinite plate obtained using the wave method and the Fourier transform method (non-dimensional wavenumber range $\gamma = -15$ to $+15$). The beam is damped ($\eta_b = 0.05$) and the plate is undamped.

4.3 Infinite beam coupled to finite width infinitely long plate

4.3.1 Travelling coupled wave for general boundary conditions on plate edge

The impedance of a finite width plate as shown in Figure 3.15 with a general boundary condition at the edge $y = L_y$ can be obtained from a wave approach in the same way. The beam is again assumed to be infinitely stiff to torsion.

Assuming initially that there is no damping in the plate, the response in the infinitely long plate of width L_y joined to an infinitely long beam can be written as

$$\tilde{w}_P = (\tilde{B}e^{-ik_y y} + \tilde{C}e^{-k_e y} + \beta_y \tilde{r}\tilde{B}e^{ik_y y} + \tilde{D}e^{k_e(y-L_y)})e^{-ik_x x} \tag{4.25}$$

where $\beta_y = e^{-ik_y 2L_y}$ represents a phase shift over length $2L_y$, $\tilde{r}$ is the complex reflection coefficient at the edge of the plate $y = L_y$ and $\tilde{D}$ is the amplitude of the nearfield wave which is generated at the opposite edge of the plate. The response of the beam is assumed to be $\tilde{w}_b = \tilde{A}e^{-ik_x x}$ as before.

The boundary conditions when a finite plate is attached at its edge to the beam are the same as for the semi-infinite plate structure. Therefore, from the first boundary condition (4.6),

$$\tilde{A} = \tilde{B} + \tilde{C} + \beta_y \tilde{r}B + \tilde{D}e^{-k_e L_y}. \tag{4.26}$$

From the second boundary condition (4.7),

$$\left[\left(-ik_y \tilde{B}e^{-ik_y y} - k_e \tilde{C}e^{-k_e y} + ik_y \beta_y \tilde{r}\tilde{B}e^{ik_y y} + k_e \tilde{D}e^{k_e(y-L_y)}\right)e^{-i\bar{k}_e x}\right]_{y=0} = 0. \tag{4.27}$$

Because the beam is attached to the edge $y = 0$ of the plate, at sufficiently high frequency it can be assumed that the influence of the nearfield from the opposite edge will be negligible, which means $\tilde{D}e^{-k_e L_y} \approx 0$. Therefore, the approximate amplitudes of the waves in the plate are given by

$$\tilde{C} = \frac{-ik_y(1-\beta_y\tilde{r})}{k_e(1+\beta_y\tilde{r}) - ik_y(1-\beta_y\tilde{r})}\tilde{A},\ \tilde{B} = \frac{k_e}{k_e(1+\beta_y\tilde{r}) - ik_y(1-\beta_y\tilde{r})}\tilde{A}. \tag{4.28}$$

From the force equilibrium boundary condition (4.8),

$$D_p e^{-ik_x x}\left[ik_y\left\{k_y^2 + (2-\nu)k_x^2\right\}(1-\beta_y\tilde{r})\tilde{B} - k_e\left\{k_e^2 - (2-\nu)k_x^2\right\}\tilde{C}\right] = \tilde{f}_1(x). \tag{4.29}$$

Substituting for $\tilde{B}$ and $\tilde{C}$ in terms of $\tilde{A}$ and eliminating k_x gives

$$\left[\frac{ik_y k_e(1-\beta_y\tilde{r})\left\{k_y^2+k_e^2\right\}}{k_e(1+\beta_y\tilde{r})-ik_y(1-\beta_y\tilde{r})}\right]\tilde{A}D_p e^{-ik_x x}=\tilde{f}_1(x). \tag{4.30}$$

from which the line impedance of the plate, which is the impedance per unit length along the beam, is given by

$$\tilde{Z}'_p=\frac{\tilde{f}_1(x)}{i\omega\tilde{A}e^{-ik_x x}}=\frac{D_p}{\omega}\left[\frac{k_y k_e(1-\beta_y\tilde{r})2k_p^2}{k_e(1+\beta_y\tilde{r})-ik_y(1-\beta_y\tilde{r})}\right]. \tag{4.31}$$

4.3.2 Approximate impedance and inclusion of the plate damping

The relationship between the wavenumbers k_p, k_y, k_e and k_x is the same as for the semi-infinite plate structure of section 4.2.1 but should be found iteratively from the dispersion equation similar to equation (4.15). If the plate wavenumber greatly exceeds the beam wavenumber i.e. $k_p >> k_x$, then $k_y \approx k_p$, $k_e \approx k_p$ and the line impedance of the plate equation (4.31) can be expressed in the simpler form

$$\tilde{Z}'_p \approx \frac{D_p 2k_p^3}{\omega}\left[\frac{1-\beta_y\tilde{r}}{(1+\beta_y\tilde{r})-i(1-\beta_y\tilde{r})}\right] \tag{4.32}$$

where $\tilde{r}$ depends on the boundary conditions at $y=L_y$. For a pinned condition, the reflection coefficient $\tilde{r}$ becomes –1 while for a sliding condition $\tilde{r}=+1$. $\tilde{Z}'_p$ in equation (4.32) has the appearance of a locally reacting impedance as in section 4.2.4. However, although equation (4.32) no longer contains k_y, k_e etc., explicitly, the factor β_y still retains a dependence on k_y. It is therefore not a completely locally reacting impedance. Nevertheless, it is still a good approximation of the plate impedance.

If hysteretic damping is introduced into the plate, the plate stiffness becomes $\tilde{D}_p = D_p(1+i\eta_p)$ and the wavenumber of the damped plate becomes $\tilde{k}_p \approx k_p(1-i\eta_p/4)$ assuming $\eta_p \ll 1$. Now, equation (4.32) can be modified as follows to include damping terms.

$$\tilde{Z}'_p = \frac{\tilde{F}(x)}{i\omega \tilde{A} e^{-i\tilde{k}_x x}} \approx \frac{\tilde{D}_p 2\tilde{k}_p^3}{\omega}\left[\frac{1-\tilde{\beta}_y \tilde{r}}{(1+\tilde{\beta}_y \tilde{r})-i(1-\tilde{\beta}_y \tilde{r})}\right] \tag{4.33}$$

where $\tilde{\beta}_y = e^{-i\tilde{k}_y 2L_y}$ is the propagating wave attenuation coefficient of the plate, which represents attenuation as well as phase shift over the distance.

4.3.3 Solution for coupled wavenumber

The general dispersion relationship for the infinite beam attached to the finite plate can be derived from equations (4.1) and (4.33), and has the same form as equation (4.15).

$$D_b k_x^4 = m'_b \omega^2 - i\omega \tilde{Z}'_p. \tag{4.34}$$

One can see that k_x is not real, due to the impedance term $\tilde{Z}'_p$. If $\tilde{Z}'_p = 0$, which means the beam becomes uncoupled from the plate, then equation (4.34) has four roots $\tilde{k}_x$ (actually k_b). However, because the approximate impedance term $\tilde{Z}'_p$ which includes $\tilde{\beta}_y = e^{-i\tilde{k}_y 2L_y}$ depends on $\tilde{k}_x$, the equation becomes more complicated and it might be possible that there are more than four roots. Nevertheless, concerning the present case when the plate is flexible compared with the beam, there are only two propagating wave solutions (k_x) and two nearfield wave solutions (k_{nf}) to equation (4.34) that are close to k_b, the corresponding solutions for $\tilde{Z}'_p = 0$. Note that the general equation and the approximate impedance should be solved iteratively as $\tilde{Z}'_p$ depends on k_x.

Again, travelling and the nearfield wavenumbers could be calculated separately, but as mentioned in section 4.2.4, the theoretical development is based on the travelling wave in a coupled beam. Therefore, the nearfield wavenumber k_{nf} is assumed to have the same value as the propagating k_x wave based on the

approximate impedance and the general dispersion relation. This simplification is advantageous in understanding dynamic behaviour of the coupled structure as seen in the results of the following section.

4.3.4 Results

Computer simulations were carried out based on the above theory. Figure 4.9 shows the coupled structure considered, consisting of a semi-infinite beam and a plate which has finite width L_y. For the plate both damped and undamped cases are considered but the beam has damping for both cases. The opposite edge of the plate parallel to the beam is pinned.

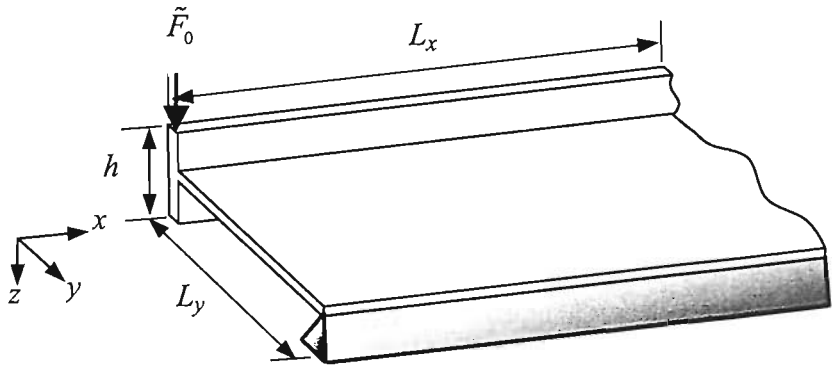

Figure 4.9. A coupled structure consisting of a semi-infinite beam attached to a finite plate with a pinned edge.

Material properties and dimensions considered are as given in Table 2.1 except the length of the beam L_x which is infinite. A point force was applied at the beam end ($x = 0$) which is assumed to be sliding.

As emphasised in section 4.3.3, the wavenumber should be found iteratively. However, the numerical results do not converge using a simple iteration at some specific frequencies, for example mostly near peaks and dips of the coupled wavenumber k_x. To overcome this problem, Muller's method [83] which can find

complex roots is introduced. Then, the coupled beam wavenumber k_x, and thus the corresponding plate wavenumber such as k_y, can be calculated using this method (see Appendix B for the use of Muller's method for the estimation of coupled wavenumbers).

Muller's approach is now used to find the corresponding wavenumbers of the coupled system in which the plate is undamped. Firstly, the impedance of the undamped plate calculated from equation (4.32) is shown in Figure 4.10. It is expected that the resonances (dips) tend to 0 but this is truncated by the frequency resolution. Concerning anti-resonances (peaks), these peaks are related to the selection of roots in Muller's method. It was assumed that there are usually four roots in the dispersion equation, so that only one root in the fourth quadrant of the complex domain can be used. However, at some frequencies where the plate impedance increases, two roots simultaneously exist in the fourth quadrant of the complex domain contours (see Figure B.4). Thus, for the application of this wave method, it is necessary to choose one root and this results in discontinuities when wavenumbers found are presented as a function of frequency.

Roots found in the fourth quadrant of the complex domain contours are shown in Figure 4.11, where it can be seen that there are two roots, for example at 25 Hz. The thick line in the same figure represents the selected wavenumbers to be used in the wave method. Thus, such selection of wavenumbers gives discontinuities and consequently, the plate impedance also shows discontinuities, which determines the peaks of the impedance as in Figure 4.10.

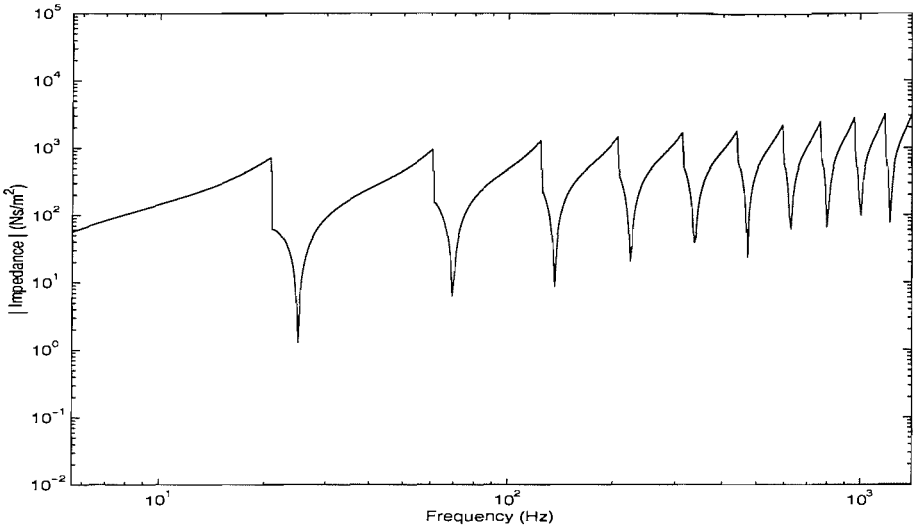

Figure 4.10. Locally reacting impedance of the undamped finite plate.

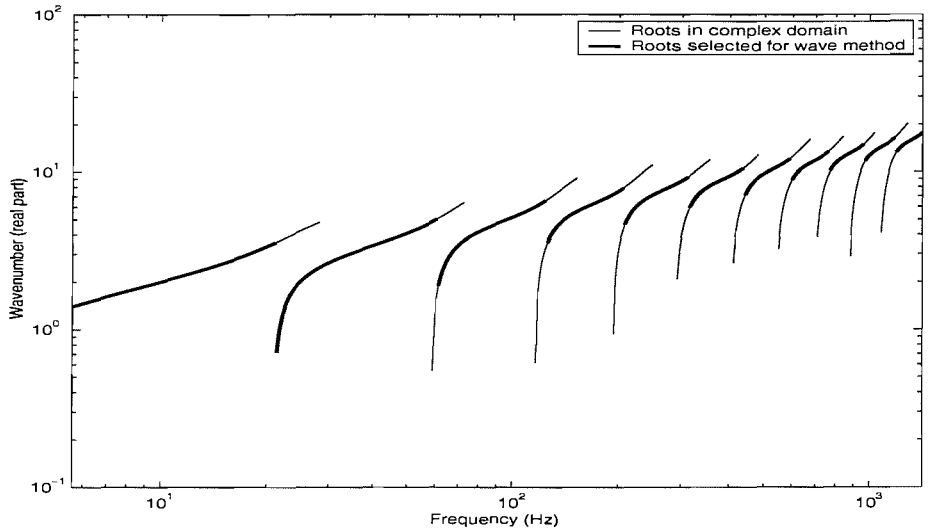

Figure 4.11. Wavenumbers found in the fourth quadrant of the complex domain contours in Muller's method and selected wavenumbers to be used in the wave method.

Figure 4.12 shows the point mobility of the coupled structure. It was calculated using the impedance shown in Figure 4.10 and the general dispersion equation, when the semi-infinite beam of the structure has a damping loss factor 0.05. Also shown is the corresponding characteristic mobility from Figure 4.7 (dashed line). It can be seen that the trend of the point mobility follows the characteristic mobility well.

Because a semi-infinite beam has no resonances or anti-resonances, the dynamic characteristics of the coupled structure will be determined by the characteristics of the finite width plate. It is important to notice that the peaks in Figure 4.10 and the dips in Figure 4.12 occur at the same frequencies. The peaks in the impedance correspond to the anti-resonances, and at these anti-resonance frequencies of the plate the point mobility level of the coupled structure is minimized. A further explanation follows later for the damped plate. The resonances of the coupled structure do not occur at the same frequency as the resonances of the plate strips due to the mass of the beam.

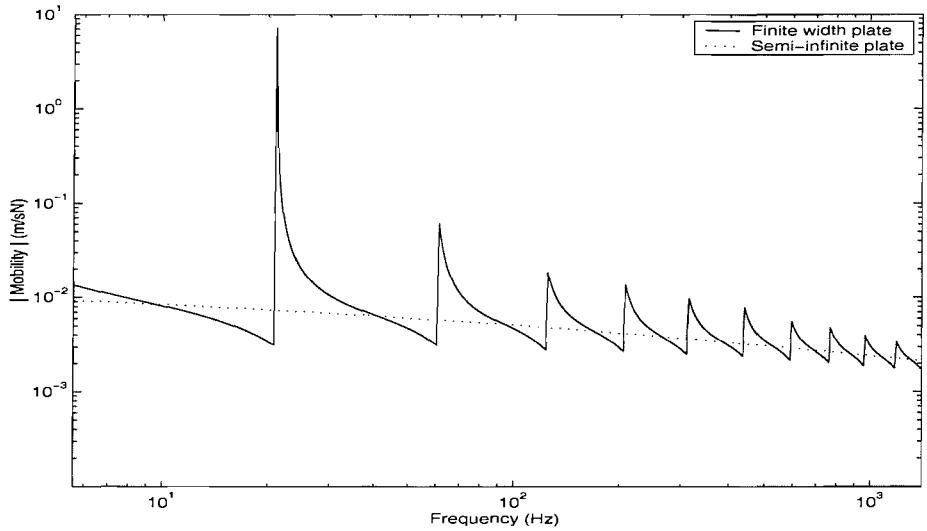

Figure 4.12. Point mobilities of the coupled structures as in Figures 4.9 and 4.1 (undamped plate, $\eta_b = 0.05$ in the beam, point force applied at $x = 0$).

The dynamic characteristics of the same structure are investigated when the damping is added to the plate. First, the propagating wavenumber k_y and the nearfield wavenumber k_e along with k_x (thin solid line) of the coupled finite plate system are compared in Figure 4.13. Also to enable comparison, the free plate wavenumber k_p, the uncoupled beam wavenumber k_b and the coupled beam wavenumber k_x (thick solid line) based on the semi-infinite plate are shown, which can be used as asymptotic representations. As k_p is much larger than k_x, the difference between

k_p, k_y, and k_e is small. This means that k_p can be used in the calculation of the plate impedance instead of k_y and k_e (see equations (4.31) and (4.33)).

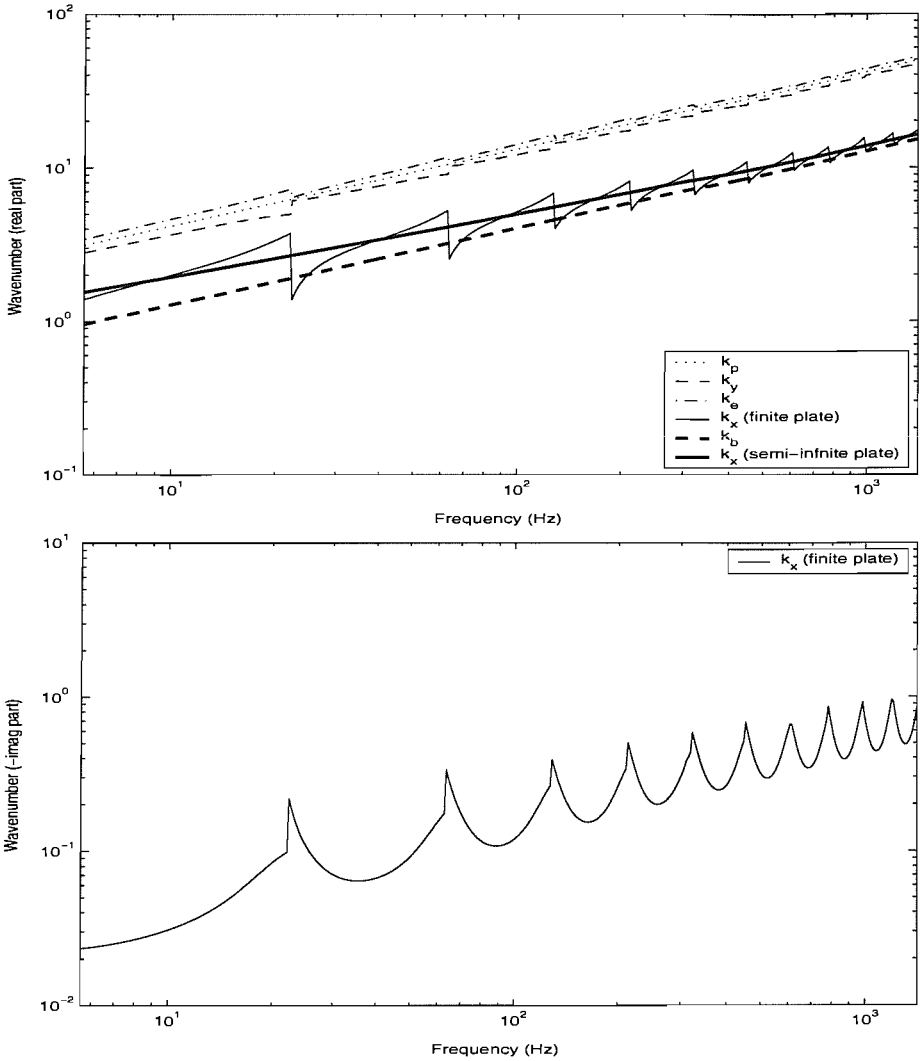

Figure 4.13. Wavenumbers of the coupled structure consisting of the semi-infinite beam and the finite plate as in Figure 4.9. Thick line is corresponding result for a semi-infinite plate.

The coupled beam wavenumber k_x based on the finite plate (thin solid line) shows peaks and dips because of the impedance of the finite width plate attached to the beam. At the resonances of the plate the impedance $\tilde{Z}'_p$ is small (see Figure 4.15 below) and the wavenumber k_x is close to k_b. At the anti-resonances k_x is increased considerably.

The imaginary part of the coupled wavenumber k_x based on the finite plate is also shown in Figure 4.13. As mentioned in section 4.2.5, the imaginary part is related to the damping of the structure. When the imaginary part of the coupled wavenumber is divided by the real part, it is possible to infer an equivalent loss factor. This ratio is shown in Figure 4.14.

For comparison, the approximate line impedance of the damped plate is shown in Figure 4.15, calculated using equation (4.33). Comparing Figures 4.14 and 4.15, it is clear that the equivalent loss factor is maximum at anti-resonance frequencies of the plate (peak in the plate impedance).

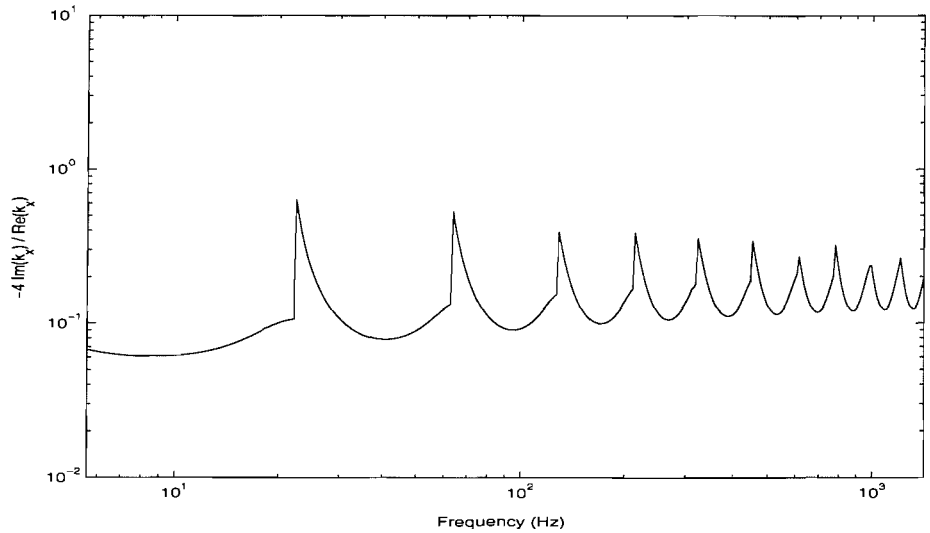

Figure 4.14. Equivalent loss factor η of the wavenumber $\tilde{k}_x$ of the coupled system due to the finite width plate (η_p = 0.05 in the plate).

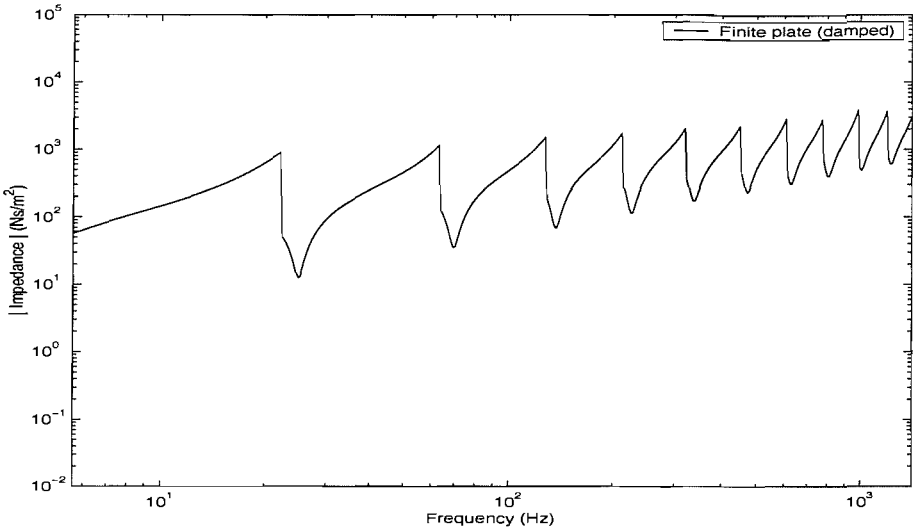

Figure 4.15. Approximate line impedance of the finite width plate (η_p = 0.05 in the plate).

The corresponding point mobility of the coupled structure is shown in Figure 4.16. Similar to the undamped plate, the anti-resonance frequencies of the plate, such as 22.1, 62.7, 126.7 Hz, coincide with the dips of the point mobility of the coupled structure. Therefore, the motion of the coupled beam is reduced at anti-resonances of the plate. This phenomenon is referred to as a 'blocking effect' [41]. Comparing Figures 4.12 and 4.16, it can be seen that the damping of the plate has an obvious influence on the drive point mobility of the beam, especially reducing the peaks.

The point mobility is also compared with predictions using the Fourier method which can be regarded as exact (a non-dimensional wavenumber range of $\gamma = \pm 15$ was used). The general tendency is in good agreement. However, there are frequency shifts in the peaks and dips. The two assumptions made in the wave method may be the possible reasons. The first one is that the plate impedance is approximate. As the dips of the mobility are due to the blocking effect of the plate one may assume that the frequency shift of the dips is related to the approximate plate impedance. The second may be related to the nearfield wavenumber assumption. The peak frequency and level are apparently related to the nearfield wave as well as the travelling wave at the excitation point. Recalling that the nearfield wavenumber is assumed to have the same value of the travelling wavenumber, such an assumption may cause this difference in the point mobility.

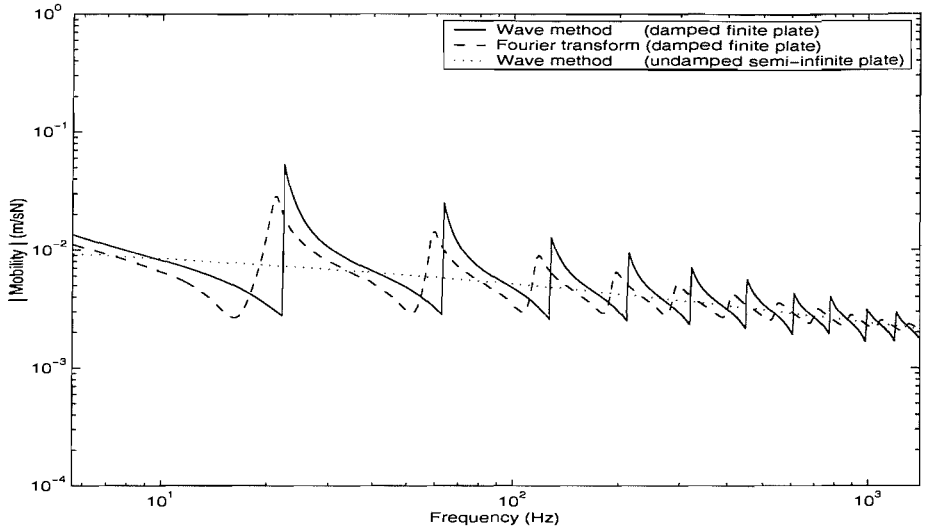

Figure 4.16. Point mobilities of the coupled structures as in Figures 4.9 and 4.1 (η_p = 0.05 in the damped plate, η_b = 0.05 in the beam, point force applied at x = 0.0 m).

Comparison of transfer mobilities may be useful as the nearfield wavenumber contribution will be reduced. They are compared between the two methods in Figure 4.17, for a response point located at $x = 2.0\,\mathrm{m}$ along the semi-infinite beam. Firstly, one can see that the frequency corresponding to the blocking effect is very similar in the two methods, although there is still a small difference at low frequencies due to the approximate impedance (recall that the error of the approximate impedance is maximum at 5.6 Hz). Thus, the assumption of the plate impedance appears not to have a large effect. Then, concerning the peak frequencies, they are also in good agreement especially at high frequencies. Thus, the difference found in the point mobility comparison seems to be more related to the nearfield wavenumber assumption. Thus, in the following section the nearfield wavenumber is considered separately and the limitation of such an approach is examined.

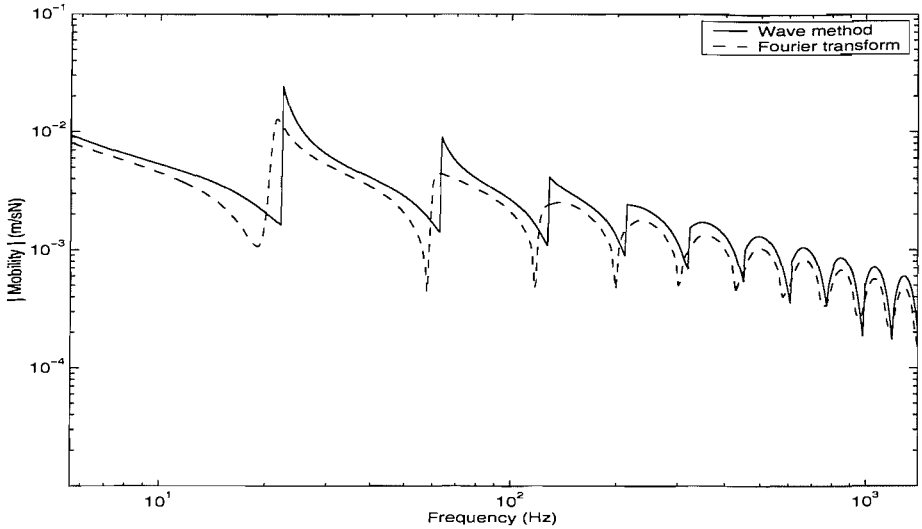

Figure 4.17. Transfer mobilities of the coupled structure as in Figures 4.9 and 4.1 (η_p = 0.05 in the plate, η_b = 0.05 in the beam, point force applied at x = 0.0 m, response at x = 2.0 m).

4.4 Finite beam coupled to finite rectangular plate

4.4.1 Beam response for the coupled system

The general relationship (equation (4.34)) of the coupled system comprising an infinite beam and a plate of finite width can be extended to the structure which is finite in length as shown in Figure 2.2 (thus a rectangular plate), where it is assumed that the beam has a sliding boundary at both ends. Note that the plate behaves strip-like as the plate wavenumber is assumed to be much larger than the beam wavenumber and strictly in the wave model there are no boundary conditions applied at the plate edges normal to the beam. However, as discussed in Chapter 2, the motion of the flexible plate is governed by the stiff beam. Thus, it is expected that the boundary conditions of the plate edges normal to the beam are also close to the sliding conditions.

The general solution for the motion of the finite beam at frequency ω is

$$\tilde{w} = \tilde{A}_1 e^{-i\tilde{k}_x x} + \tilde{A}_2 e^{-\tilde{k}_{nf} x} + \tilde{A}_3 e^{i\tilde{k}_x x} + \tilde{A}_4 e^{\tilde{k}_{nf} x} \tag{4.35}$$

where $\tilde{A}_1$ and $\tilde{A}_3$ are the amplitudes of travelling waves, $\tilde{A}_2$ and $\tilde{A}_4$ are the amplitudes of the nearfield waves, $\tilde{k}_x$ and $\tilde{k}_{nf}$ are the complex travelling wavenumber and nearfield wavenumber respectively, as determined previously. These may be different at this stage.

If the beam has length L_x with an external point force $\tilde{F}_0$ applied at one end $x = 0$, and has sliding boundary conditions at both ends, the boundary conditions can be written in a matrix form,

$$\begin{bmatrix} -ik_x & -k_{nf} & ik_x & k_{nf} \\ ik_x^3 & -k_{nf}^3 & -ik_x^3 & k_{nf}^3 \\ -ik_x e^{-i\tilde{k}_x L_x} & -k_{nf} e^{-\tilde{k}_{nf} L_x} & ik_x e^{i\tilde{k}_x L_x} & k_{nf} e^{\tilde{k}_{nf} L_x} \\ ik_x^3 e^{-i\tilde{k}_x L_x} & -k_{nf}^3 e^{-\tilde{k}_{nf} L_x} & -ik_x^3 e^{i\tilde{k}_x L_x} & k_{nf}^3 e^{\tilde{k}_{nf} L_x} \end{bmatrix} \begin{Bmatrix} \tilde{A}_1 \\ \tilde{A}_2 \\ \tilde{A}_3 \\ \tilde{A}_4 \end{Bmatrix} = \begin{Bmatrix} 0 \\ \tilde{F}_0 / \tilde{D}_b \\ 0 \\ 0 \end{Bmatrix}. \tag{4.36}$$

Having solved this for the amplitudes $\tilde{A}_i$, the transfer mobility from the excitation point $x = 0$ to the response at an arbitrary position x on the beam can be calculated from the relationship between the force and velocity,

$$\tilde{Y}_b(x) = \frac{i\omega\tilde{w}(x)}{\tilde{F}_0} = \frac{\omega}{\tilde{D}_b} \frac{\tilde{A}_1 e^{-i\tilde{k}_x x} + \tilde{A}_2 e^{-\tilde{k}_{nf} x} + \tilde{A}_3 e^{i\tilde{k}_x x} + \tilde{A}_4 e^{\tilde{k}_{nf} x}}{\tilde{k}_x^3 \tilde{A}_1 + i\tilde{k}_{nf}^3 \tilde{A}_2 - \tilde{k}_x^3 \tilde{A}_3 - i\tilde{k}_{nf}^3 \tilde{A}_4}. \tag{4.37}$$

4.4.2 Plate response for the coupled system

The response of the plate for a travelling wave in the beam is as given in equation (4.25), and by obtaining the coefficients in the equation, the response can be determined. The coefficients will be calculated from equations (4.6) – (4.8) which describe the boundary conditions.

The plate response is calculated from consideration of each beam wave and the corresponding plate impedance. By adding the four different responses of the plate generated by the four different waves in the beam, which are a forward travelling wave (k_x+), backward wave (k_x-), forward nearfield wave ($k_{nf}+$) and backward nearfield wave ($k_{nf}-$), the plate response can be obtained.

4.5. Results for finite beam coupled to finite rectangular plate

In this section some numerical results are given for the coupled finite structure. The dimensions are the same as shown in Table 2.1. The length of the beam is 2.0 m (L_x = 2.0 m) and loss factors of the subsystems are 0.05. The plate edge parallel to the beam is considered to be pinned. Results are compared with those obtained by the Fourier method discussed in Chapter 3 with the non-dimensional wavenumber range of $\gamma = \pm 15$.

4.5.1 Mobilities

The point mobility of the coupled structure is shown in Figure 4.18 along with the corresponding result of the Fourier method. The non-dimensional wavenumber range used is $\gamma = -15$ to $\gamma = +15$. Also shown is the characteristic mobility of a coupled structure consisting of a semi-infinite beam and a plate of semi-infinite length and width located in $x \geq 0$, $y \geq 0$ (dotted line). Comparing the result from the wave analysis with that from the Fourier method, they agree reasonably well even at low frequencies although they differ in detail. The characteristic mobility passes through the centre of these results, as expected.

Some small sharp troughs in the analytical point mobility, for example at 22.1, 62.7 and 126.6 Hz coincide exactly with the anti-resonances of the finite width plate calculated on the basis of the travelling wavenumber $\tilde{k}_x$ (Figure 4.15).

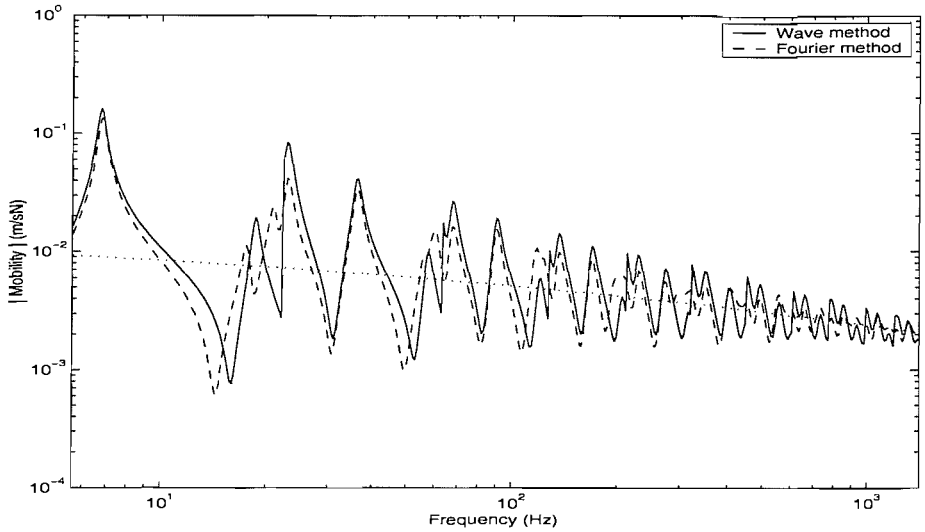

Figure 4.18. Point mobility of the coupled structure as in Figure 2.2 (η_p = 0.05 in the plate, η_b = 0.05 in the beam, point force applied at x = 0). Dotted line indicates characteristic mobility of a structure consisting of a semi-infinite beam and plate of a semi-infinite length and width.

By calculating $\tilde{k}_{nf}$ separately, the influence on the point mobility is shown in Figure 4.19. In some regions, such as the first trough near 14.1 Hz in the analysis, the result based on using $\tilde{k}_x$ throughout in equation (4.35) appears to give better agreement with that of the Fourier method than the result including a separate value for $\tilde{k}_{nf}$. In general, although there are some differences in the level of the peaks and troughs, this change seems to have only a small influence on the response of the structure. It can be assumed that $\tilde{k}_{nf}$ does not significantly affect the behaviour of the whole structure because the nearfield wave is limited to the excited region or the ends of the beam.

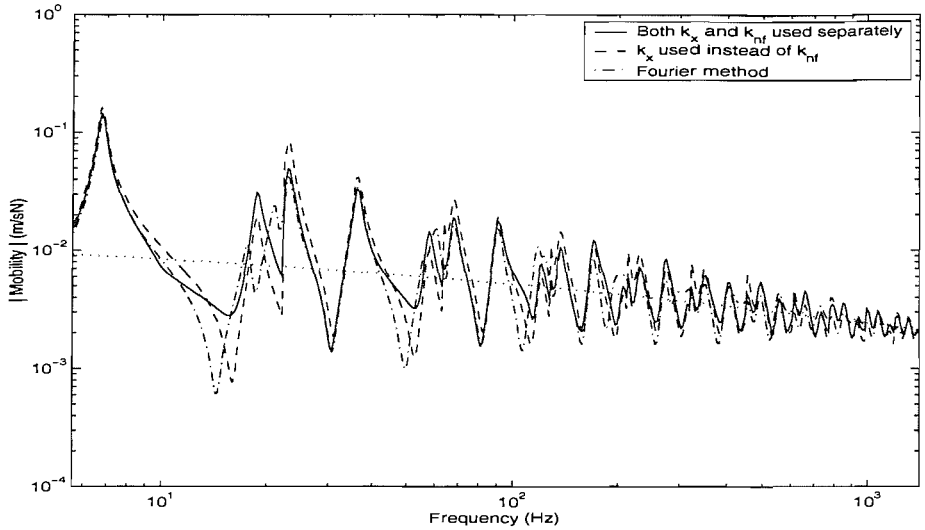

Figure 4.19. Point mobility of the coupled structure as in Figure 2.2 (η_p = 0.05 in the plate, η_b = 0.05 in the beam, point force applied at x = 0). Dotted line indicates characteristic mobility.

In Figures 4.20 and 4.21, examples of the plate response are shown. These are obtained from the sum of the results provided by the forward and backward travelling and nearfield waves as mentioned in section 4.4.2, although, in fact, the values of $\tilde{k}_x$ is used throughout in equation (4.35). Generally the level of the response agrees quite well with the Fourier method and the positions of the troughs in the response agree well even in the high frequency region for both figures. Note that no boundary conditions were applied at the plate edges normal to the beam in the wave model, whilst the sliding conditions were considered in the Fourier method. Thus, the assumption that the strip-like plate motion is close to that of the plate in the sliding conditions seems valid.

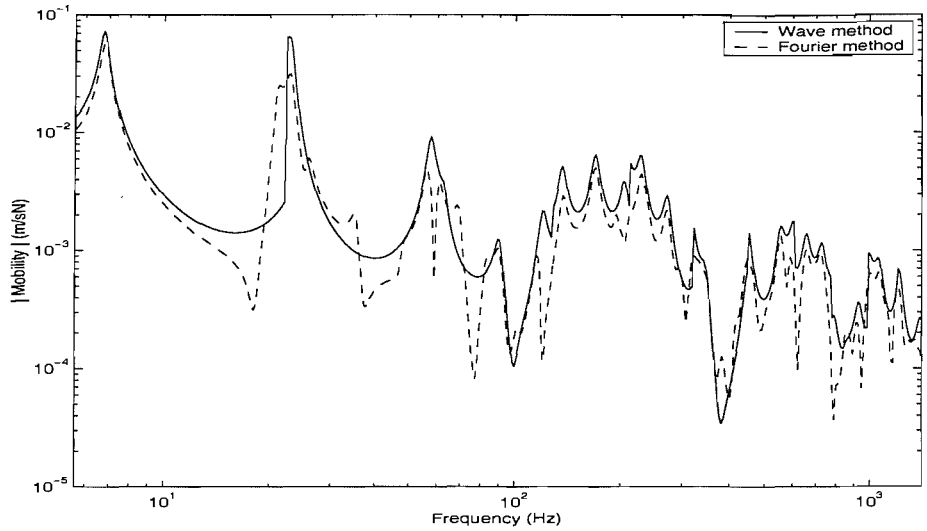

Figure 4.20. Transfer mobility for the plate (at x = 1.50 m and y = 0.49 m) in the coupled structure as in Figure 2.2 (η_p = 0.05 in the plate, η_b = 0.05 in the beam, point force applied at x = 0).

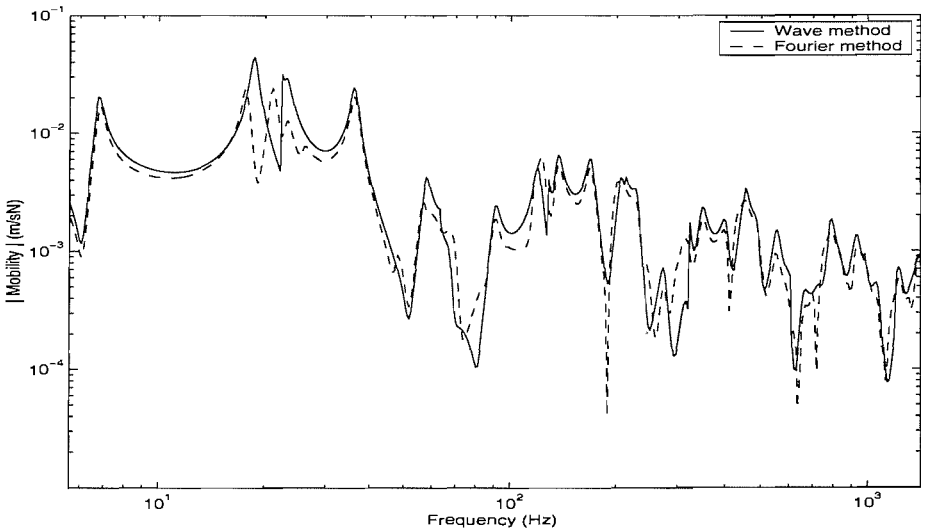

Figure 4.21. Transfer mobility for the plate (at x = 0.89 m and y = 0.45 m) in the coupled structure as in Figure 2.2 (η_p = 0.05 in the plate, η_b = 0.05 in the beam, point force applied at x = 0).

4.5.2 Power balance

Before discussing the power balance relationship of the wave model, the power results based on the wave method are briefly compared with those obtained from the Fourier method, which were presented in section 3.4.3. Total power input is shown in Figure 4.22. It can be seen that they are generally in good agreement between the two methods.

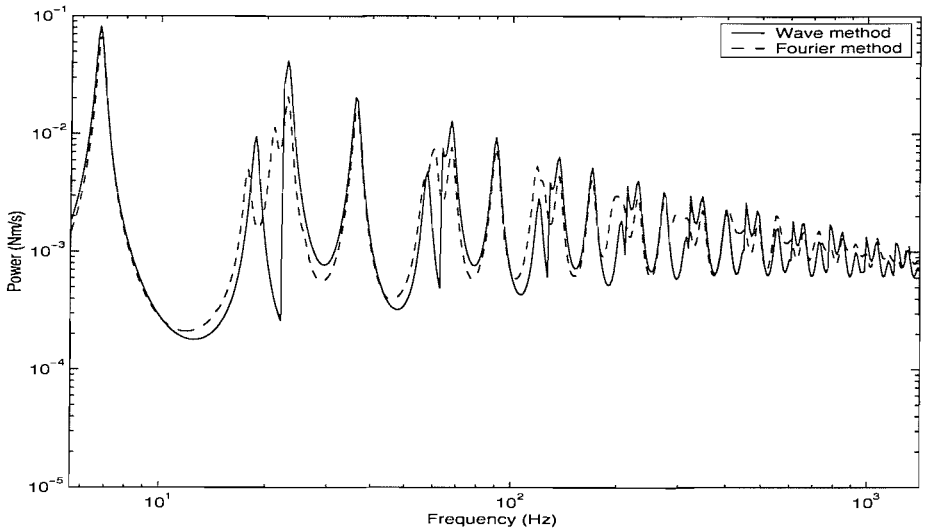

Figure 4.22. Total input power inserted to the coupled structure shown in Figure 2.2 (η_p = 0.05 in the plate, η_b = 0.05 in the beam, point force applied at x = 0) based on the wave method and the Fourier series method.

Also, the power transferred to the plate is shown in Figure 4.23. Although the results of the two methods have the same tendency, it seems that the difference tends to increase especially at some troughs such as 12 Hz and 46 Hz. At these frequencies, the use of the strip model for the plate appears inappropriate, which may increase the difference between the wave and Fourier methods. A further discussion follows in terms of the power ratio below.

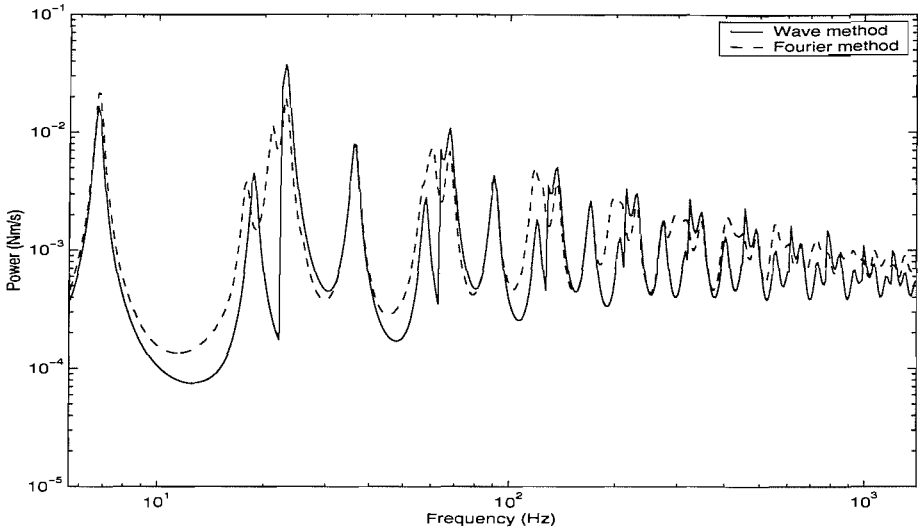

Figure 4.23. Net power transferred to the plate of the coupled structure shown in Figure 2.2 (η_p = 0.05 in the plate, η_b = 0.05 in the beam, point force applied at x = 0) based on the wave method and the Fourier series method.

The power balance relationship of the wave model is now investigated. In Figure 4.24, the total input power and the net power transferred to the plate are compared for the model in which the travelling wavenumber k_x is used for both the travelling and nearfield waves. It is clear that the power is maximum at the resonances of the coupled structure (see Figure 4.18). Comparing the two powers, at peaks just above the anti-resonances of the plate using the travelling wavenumber k_x, the plate receives most energy such as at the peaks at 22.9, 63.5 and 128 Hz. Here the total input power and the net power transferred to the plate have almost the same values. The magnitude of the beam motion becomes larger than that of the plate at other peaks such as at 6.7, 18.7, 35.9 and 91.3 Hz, and then the difference between the two powers is larger. The ratio of the power transferred to the plate to the total input power is shown in Figure 4.25. This has maxima close to 1 at the peaks of the plate impedance (see Figure 4.15) i.e. the anti-resonances of the plate using the plate.

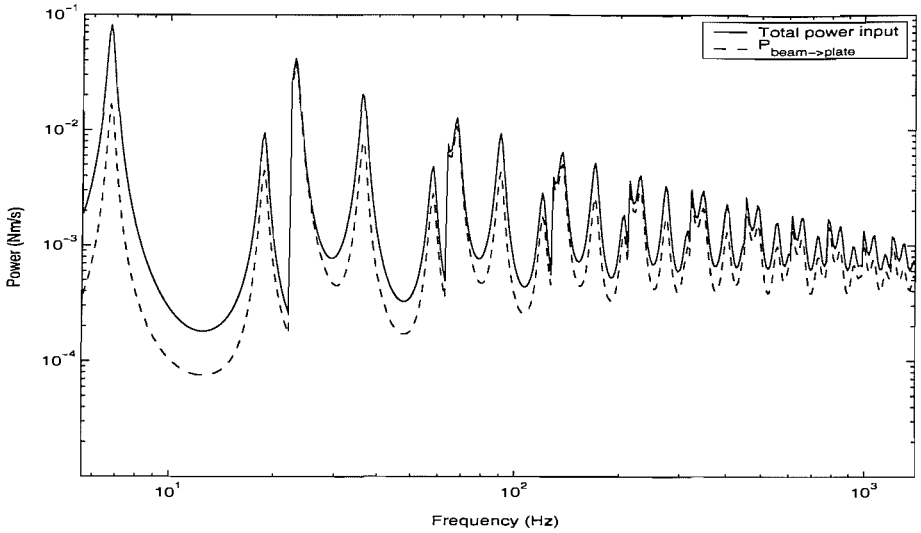

Figure 4.24. Total input power inserted to the coupled structure shown in Figure 2.2 (η_p = 0.05 in the plate, η_b = 0.05 in the beam, point force applied at x = 0) and net power transferred to the plate. Wave method is used.

The difference of the power transfer between the wave and Fourier methods mentioned above may be seen clearly in terms of the power ratio. Although the difference is reduced at the anti-resonance frequencies, it seems that the power transfer based on the wave method is generally smaller than that based on the Fourier method. This is because the wave method assumes that the plate is strip-like. A further explanation follows in the next figure.

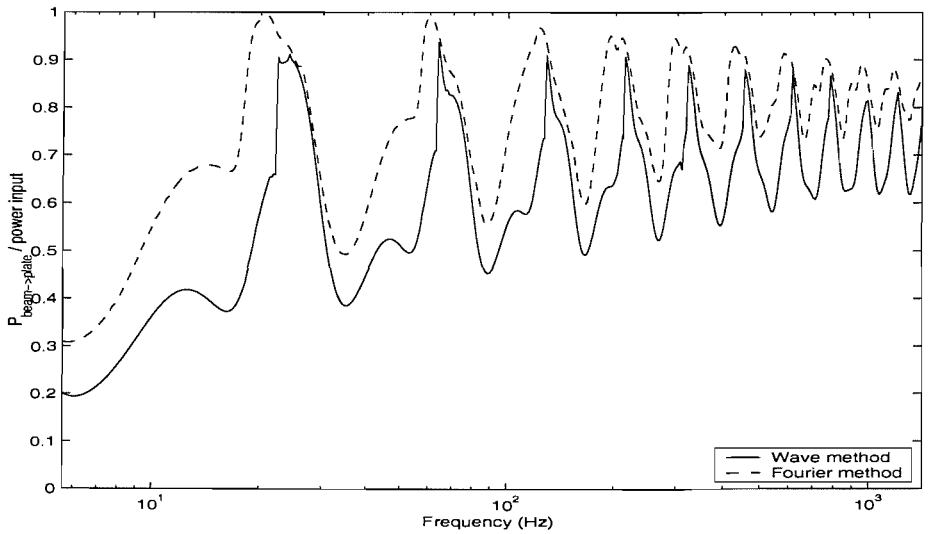

Figure 4.25. Ratio of the power transferred to plate to the total input power shown in Figure 4.24.

The power balance for the beam was checked and it was found that the sum of the power transferred to the plate and the power dissipated by the beam is equal to the total power input to the combined structure with a mean error of 0.3% due to numerical integration.

For the plate the power balance is investigated. Note that, as the plate behaves like strips the strain energy is obtained approximately by using the sum of the strain energy of the strips. The power dissipated by the plate is calculated using equation (3.63) where the damping loss factor $\eta_p = 0.05$ is considered. The corresponding result is shown in Figure 4.26. One can see that the power dissipated in the plate is larger than the power transfer at the junction and it seems that energy conservation is violated. However, in fact this is also related to the motion of the plate. That is, as the plate behaves strip-like in the y direction, the power dissipation in the x direction cannot actually be taken into account in this wave method. Thus, as seen in the figure, if the damping loss factor η_p is used the power dissipated by the plate tends to be larger and the power relationship does not hold.

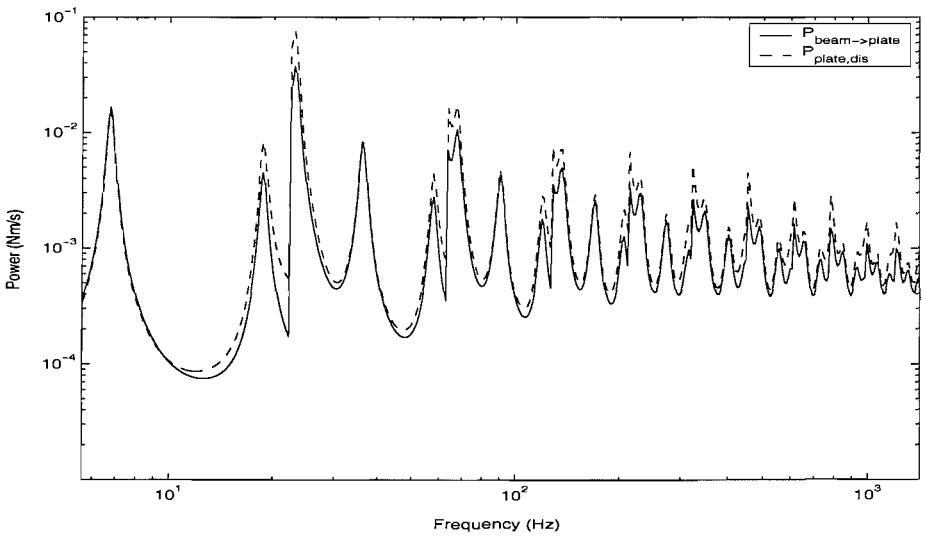

Figure 4.26. Comparison of power balance for the plate in the coupled structure shown in Figure 2.2 (η_p = 0.05 in the plate, η_b = 0.05 in the beam, point force applied at x = 0 of beam).

However, if the equivalent loss factor calculated from the wavenumber $\tilde{k}_y$ is used for the plate (thus $\eta_{k_y} \approx -4\,\mathrm{Im}(\tilde{k}_y)/\mathrm{Re}(\tilde{k}_y)$), it is found that the power balance relationship holds. The corresponding equivalent loss factor of the wavenumber $\tilde{k}_y$ is shown in Figure 4.27. This equivalent loss factor is smaller than damping loss factor of the plate. Comparing this with Figure 4.14, one can see that the frequencies at troughs coincide with the peaks of the equivalent loss factor of the wavenumber $\tilde{k}_x$. Using this equivalent loss factor η_{k_y} the power dissipated in the plate was obtained and it is found that the difference between the power transfer and the power dissipation is only 3% on average.

Since the beam dissipated power and the power transfer $P_{b\to p}$ add to give the input power, and $P_{b\to p}$ does not require adjustment to the loss factor, it seems more reliable to use $P_{b\to p}$ than $P_{p,dis}$.

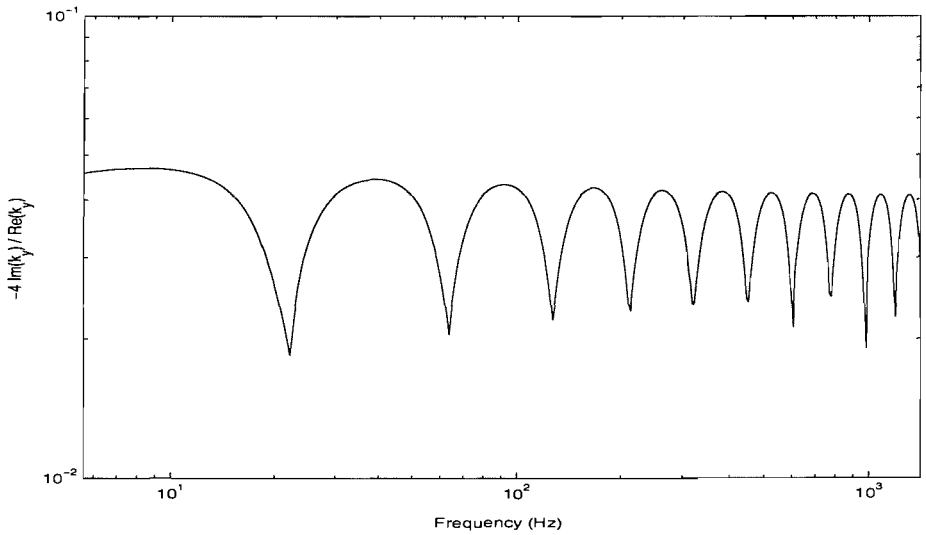

Figure 4.27. Equivalent loss factor η_{k_y} of the wavenumber $\tilde{k}_y$ of the coupled system due to the finite width plate (η_p = 0.05 in the plate).

Although the power balance relationship holds using the equivalent loss factor of the wavenumber in the y direction, it is clear that the power dissipated in the plate is underestimated as only power dissipation in the y direction is considered.

Meanwhile, because of such an underestimate of the power dissipated in the plate, it is expected that the power dissipated in the beam may be overestimated, as long as the power input level remains similar. This will be shown in the next chapter dealing with two-beam-plate systems.

4.5.3 Discussion

Note that the discussion above is based on the case when the travelling wavenumber $\tilde{k}_x$ is substituted for the nearfield wavenumber $\tilde{k}_{nf}$ in equation (4.35) and corresponding plate wavenumbers are considered. If the travelling wavenumber $\tilde{k}_x$ and the nearfield wavenumber $\tilde{k}_{nf}$ are determined separately from their corresponding plate impedances, although the power transferred to the plate is expected to be the same as the power dissipated by the plate, it is found that they do not agree. The dissipated power obtained from the sum of the plate responses for each of the different waves in the coupled beam generally shows a lower level than the net power transferred to the plate [84]. Therefore, it seems that the behaviour of the plate cannot be separately considered in terms of the different waves of the beam, and a simple sum of the separate responses seems to be in error.

In summary, if the travelling wavenumber $\tilde{k}_x$ is used throughout in the equation of motion of the beam, the power balance holds. However, it seems that the calculation of the plate response based on the separation of the coupled wavenumber has some limitation regarding energy conservation. As the influence on the response due to the separation of the nearfield wavenumber seems small, in further studies dealing with the wave method, it is assumed that the nearfield wavenumber has the same value as the travelling wavenumber.

4.6 Conclusions

The vibrational characteristics of a structure consisting of a beam possessing small wavenumbers and a plate possessing large wavenumbers has been calculated by means of the wave method. The structure is non-symmetric unlike the symmetric structure considered by Grice and Pinnington [41].

The general relationship between the coupled beam wavenumber and the plate wavenumber has been derived when the travelling and nearfield wavenumbers in the coupled beam are separately considered, and the corresponding plate impedance has been explained. This shows that the impedance equation has the same form regardless of wave types but the numerical values for the impedance are changed. Although the wavenumbers are basically obtained using an iteration method, the non-convergence of the wavenumber in the iteration procedure at certain frequencies has been explained. As an alternative numerical approach, it has been shown that Muller's method can be applied to obtain the complex coupled wavenumber based on the dispersion equation.

The wavenumbers are obtained by assuming a plate impedance based on the travelling wavenumber in the beam. This is reasonable approximation where the motion of the beam is dominated by the travelling wave but gives poor results in frequency regions where both waves have a high decay.

It was shown that, for the present structure, the exact line impedance could be replaced by a simplified approximate impedance. This means that the line impedance of the plate can be considered as the input point impedance of the corresponding beam (thus strip) driven by a point force. To allow such simplification in the wave method, the wavenumber of the free plate should be at least about twice as large as that of the coupled beam, which is satisfied for the case considered in this chapter for the frequency range considered.

It was shown that the plate behaves like added damping as well as mass when coupled to the beam. The ratio of the imaginary part to the real part of the coupled wavenumber shows that the equivalent loss factor falls with increasing frequency, as shown by Heckl [64]. The plate introduces a blocking effect to the beam. When the travelling wave is present in the beam, the equivalent loss factor of the beam is maximum at the anti-resonance of the finite plate, and thus the mobility level of the coupled structure is minimized. This is because the plate reduces the motion of the beam at this frequency.

The total input power injected to the structure consisting of a finite beam and a finite plate was compared with the power transferred to the plate. The power transferred to the plate was obtained from the approximate impedance of the plate, which behaves like separate strips. In such a case, it seems that the power dissipated in the plate is underestimated because of the strip-like motion of the plate. From the ratio of the power transferred to the plate to the total input power, it was seen that the greatest proportion of power is transferred to the plate at specific frequencies which coincide with the anti-resonance frequencies of the plate. This corresponds to the blocking effect.

It should be noted that the results mentioned above are based on some assumptions. Firstly, coupled wavenumbers are calculated based on wavenumber trace matching which only strictly applies when structures have no damping. For application of the wavenumber trace matching in damped structures, it is assumed that the loss factor of the spine is very small and the spine wavenumber is much smaller than the receiver wavenumber. Secondly, the approximate impedance of the plate is adopted. This is satisfactory only when the free plate wavenumber is about twice as large as the coupled beam wavenumber.

A violation of energy conservation occurs if the plate responses are calculated in terms of separate beam wave types, the beam wavenumbers also being calculated independently from the corresponding plate impedances. However if all wavenumbers are determined from the same impedance, so that the same

wavenumber k_x is used for travelling and nearfield waves, no violation of energy conservation occurs.

CHAPTER 5
TWO PARALLEL BEAMS COUPLED TO A PLATE

5.1 Introduction

The various methods developed in the previous chapters have been applied to obtain the response of a coupled system consisting of a single beam and a plate. An aim of this thesis is to deal with more complicated systems such as two beams or four beams coupled to a plate. As a step towards investigation of a framed structure of four beams surrounding a plate, the previous analyses are extended here to apply to a structure consisting of two identical beams connected by a rectangular plate.

The Fourier method developed can readily be extended to the case where two beams are attached to a finite width plate, using continuity and force equilibrium conditions. From the relevant equations it will be seen that this method can also be used where these beams are dissimilar. The limits required for convergence found previously in Chapter 3 are again used in this chapter.

The applicability of the wave method as an approximate method for a single beam-plate coupled system was shown in Chapter 4. A further study is carried out here to find a wave solution for a symmetric beam-plate-beam system. By symmetry, this structure can be assembled from solutions of a plate of half the width attached to one beam for which the opposite edge of the plate parallel to the beam is either pinned or sliding. The synthesis procedure is described and some numerical results are shown. In the wave approach, the wavenumbers are found using the plate impedance corresponding to the travelling wave in the beam as this is expected to dominate the response.

The results of the Fourier method are firstly compared and validated against those obtained using the modal method extended from Chapter 2. Then, results based on the Fourier method and the wave method are presented and some comments are

given on comparisons between the two methods, indicating their advantages and disadvantages. Although the same boundary conditions are considered for comparison between the methods, strictly, the strip-like plate assumed in the wave model has no boundary conditions on the plate edges normal to the beam.

5.2 Fourier technique for analysis of beam-plate-beam systems

5.2.1 Coupling between infinitely long structures

In Chapter 3 the Fourier transform and Fourier series techniques were introduced to analyse a coupled system consisting of a single beam and plate. In a similar way, the Fourier method can be applied to a structure comprising two beams. The waveguide structure consisting of two infinite beams and an infinitely long finite width plate are shown in Figure 5.1 along with their force relationships. It is arranged that their neutral axis lies in the centre of the beams. Harmonic motion at frequency ω is assumed. It is again assumed for simplicity that the beams are infinitely stiff to torsion along $y=0$ and $y=L_y$. In later chapters, a four-beam coupled system is studied. Thus, for consistency, the driven beam is named 'beam 1' and the opposite beam is named 'beam 3'.

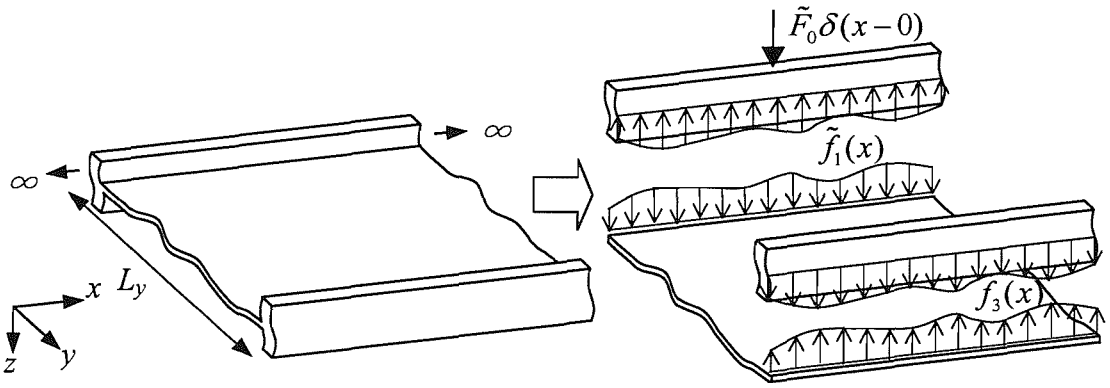

Figure 5.1. A coupled structure consisting of infinite two beams attached to an infinitely long finite width plate and force relationship between them.

When the plate and beam 1 are joined along the line $y=0$, a force per unit length $\tilde{f}_1(x)$ acts between them as shown in Figure 5.1. It is assumed that the external point force is acting on the beam at $x=0$ (beam 1). The force is defined by $\tilde{F}_0\delta(x-0)$. Now considering all forces related to beam 1, the motion of this beam with damping becomes

$$\tilde{D}_{b1}\frac{d^4\tilde{w}_{b1}(x)}{dx^4}-m'_{b1}\omega^2\tilde{w}_{b1}(x)=\tilde{F}_0\delta(x-0)-\tilde{f}_1(x) \tag{5.1}$$

where subscript $b1$ stands for beam 1, $\tilde{D}_{b1}$ is its complex bending stiffness and m'_{b1} is its mass per unit length. In the same manner, the equation of motion for the other beam (beam 3) is

$$\tilde{D}_{b3}\frac{d^4\tilde{w}_{b3}(x)}{dx^4}-m'_{b3}\omega^2\tilde{w}_{b3}(x)=\tilde{f}_3(x)\,. \tag{5.2}$$

Therefore, taking the spatial Fourier transform of equations (5.1) and (5.2) gives respectively

$$\tilde{D}_{b1}k_x^4\tilde{W}_{b1}(k_x)-m'_{b1}\omega^2\tilde{W}_{b1}(k_x)=\tilde{F}_0-\tilde{F}_1(k_x), \tag{5.3}$$

$$\tilde{D}_{b3}k_x^4\tilde{W}_{b3}(k_x)-m'_{b3}\omega^2\tilde{W}_{b3}(k_x)=\tilde{F}_3(k_x)\,. \tag{5.4}$$

where $\tilde{F}_1(k_x)$ and $\tilde{F}_3(k_x)$ are the Fourier transforms of $\tilde{f}_1(x)$ and $\tilde{f}_3(x)$ respectively.

The equation of motion of the free plate with damping and the corresponding Fourier transform are the same as shown in equations (3.7) and (3.10) in section 3.2.1.

Assuming a solution for the harmonic wave in the plate $w_p(y)=\tilde{B}e^{k_y y}$, the wavenumber relationship can be determined as in section 3.2.1. The waves in the plate propagating or decaying away from the junction of beam 1 and the plate are

shown in equation (3.14). If $|k_x| < |\tilde{k}_p|$, then wavenumber $\tilde{k}_{y1}$ is considered as a travelling wave, and $\tilde{k}_{y2}$ is considered as a nearfield wave. Conversely, if $|k_x| > |\tilde{k}_p|$, then all of them behave as nearfield waves.

Consequently the motion of the plate can be written as

$$\tilde{W}_p(k_x, y) = \tilde{B}_1 e^{\tilde{k}_{y1} y} + \tilde{B}_2 e^{\tilde{k}_{y2} y} + \tilde{B}_3 e^{\tilde{k}_{y3} y} + \tilde{B}_4 e^{\tilde{k}_{y4} y} \tag{5.5}$$

where $\tilde{k}_{y1}$ and $\tilde{k}_{y2}$ are calculated in equations (3.14), $\tilde{k}_{y3} = -\tilde{k}_{y1}$ and $\tilde{k}_{y4} = -\tilde{k}_{y2}$.

Based on the wavenumbers obtained, the response of the beams and the plate can be identified. This procedure starts initially from the boundary conditions. All boundary conditions related to the beams and plate are as follows.

(i) Continuity equation for beam 1 and beam 3; equal displacement to the plate at junctions $y = 0$ and $y = L_y$ respectively,

(ii) Sliding condition; the beams are assumed infinitely stiff to torsion along $y = 0$ and $y = L_y$.

In a similar manner as presented in section 3.2.2 the relationship of the displacements with respect to the beam and plate can be found. By introducing a matrix form, it can be written simply as

$$\begin{Bmatrix} \tilde{W}_{b1}(k_x) \\ \tilde{W}_{b3}(k_x) \\ 0 \\ 0 \end{Bmatrix} = \begin{bmatrix} 1 & 1 & 1 & 1 \\ e^{\tilde{k}_{y1}L_y} & e^{\tilde{k}_{y2}L_y} & e^{\tilde{k}_{y3}L_y} & e^{\tilde{k}_{y4}L_y} \\ \tilde{k}_{y1} & \tilde{k}_{y2} & \tilde{k}_{y3} & \tilde{k}_{y4} \\ \tilde{k}_{y1}e^{\tilde{k}_{y1}L_y} & \tilde{k}_{y2}e^{\tilde{k}_{y2}L_y} & \tilde{k}_{y3}e^{\tilde{k}_{y3}L_y} & \tilde{k}_{y4}e^{\tilde{k}_{y4}L_y} \end{bmatrix} \begin{Bmatrix} \tilde{B}_1 \\ \tilde{B}_2 \\ \tilde{B}_3 \\ \tilde{B}_4 \end{Bmatrix}. \tag{5.6}$$

(iii) Force equilibrium condition; the forces on the plate are equal and opposite to the respective forces on the beams

$$\begin{Bmatrix} \tilde{F}_1(k_x) \\ \tilde{F}_3(k_x) \end{Bmatrix} = \begin{bmatrix} \tilde{D}_p\tilde{k}_{y1}^3 & \tilde{D}_p\tilde{k}_{y2}^3 & \tilde{D}_p\tilde{k}_{y3}^3 & \tilde{D}_p\tilde{k}_{y4}^3 \\ \tilde{D}_p\tilde{k}_{y1}^3 e^{\tilde{k}_{y1}L_y} & \tilde{D}_p\tilde{k}_{y2}^3 e^{\tilde{k}_{y2}L_y} & \tilde{D}_p\tilde{k}_{y3}^3 e^{\tilde{k}_{y3}L_y} & \tilde{D}_p\tilde{k}_{y4}^3 e^{\tilde{k}_{y4}L_y} \end{bmatrix} \begin{Bmatrix} \tilde{B}_1 \\ \tilde{B}_2 \\ \tilde{B}_3 \\ \tilde{B}_4 \end{Bmatrix}. \tag{5.7}$$

Substituting equation (5.6) into equation (5.7) gives

$$\begin{Bmatrix} \tilde{F}_1(k_x) \\ \tilde{F}_3(k_x) \end{Bmatrix} = \begin{bmatrix} \tilde{D}_p\tilde{k}_{y1}^3 & \tilde{D}_p\tilde{k}_{y2}^3 & \tilde{D}_p\tilde{k}_{y3}^3 & \tilde{D}_p\tilde{k}_{y4}^3 \\ \tilde{D}_p\tilde{k}_{y1}^3 e^{\tilde{k}_{y1}L_y} & \tilde{D}_p\tilde{k}_{y2}^3 e^{\tilde{k}_{y2}L_y} & \tilde{D}_p\tilde{k}_{y3}^3 e^{\tilde{k}_{y3}L_y} & \tilde{D}_p\tilde{k}_{y4}^3 e^{\tilde{k}_{y4}L_y} \end{bmatrix} \times$$
$$\begin{bmatrix} 1 & 1 & 1 & 1 \\ e^{\tilde{k}_{y1}L_y} & e^{\tilde{k}_{y2}L_y} & e^{\tilde{k}_{y3}L_y} & e^{\tilde{k}_{y4}L_y} \\ \tilde{k}_{y1} & \tilde{k}_{y2} & \tilde{k}_{y3} & \tilde{k}_{y4} \\ \tilde{k}_{y1}e^{\tilde{k}_{y1}L_y} & \tilde{k}_{y2}e^{\tilde{k}_{y2}L_y} & \tilde{k}_{y3}e^{\tilde{k}_{y3}L_y} & \tilde{k}_{y4}e^{\tilde{k}_{y4}L_y} \end{bmatrix}^{-1} \begin{Bmatrix} \tilde{W}_{b1}(k_x) \\ \tilde{W}_{b3}(k_x) \\ 0 \\ 0 \end{Bmatrix}. \tag{5.8}$$

To simplify this equation, new variables σ and τ are introduced.

$$\begin{bmatrix} \sigma_1 & \sigma_2 & \sigma_3 & \sigma_4 \\ \tau_1 & \tau_2 & \tau_3 & \tau_4 \end{bmatrix} = \tilde{D}_p \begin{bmatrix} \tilde{k}_{y1}^3 & \tilde{k}_{y2}^3 & \tilde{k}_{y3}^3 & \tilde{k}_{y4}^3 \\ \tilde{k}_{y1}^3 e^{\tilde{k}_{y1}L_y} & \tilde{k}_{y2}^3 e^{\tilde{k}_{y2}L_y} & \tilde{k}_{y3}^3 e^{\tilde{k}_{y3}L_y} & \tilde{k}_{y4}^3 e^{\tilde{k}_{y4}L_y} \end{bmatrix} \times$$
$$\begin{bmatrix} 1 & 1 & 1 & 1 \\ e^{\tilde{k}_{y1}L_y} & e^{\tilde{k}_{y2}L_y} & e^{\tilde{k}_{y3}L_y} & e^{\tilde{k}_{y4}L_y} \\ \tilde{k}_{y1} & \tilde{k}_{y2} & \tilde{k}_{y3} & \tilde{k}_{y4} \\ \tilde{k}_{y1}e^{\tilde{k}_{y1}L_y} & \tilde{k}_{y2}e^{\tilde{k}_{y2}L_y} & \tilde{k}_{y3}e^{\tilde{k}_{y3}L_y} & \tilde{k}_{y4}e^{\tilde{k}_{y4}L_y} \end{bmatrix}^{-1}. \tag{5.9}$$

Note that σ and τ are related only to the plate properties. The relationship between the forces $\tilde{F}(k_x)$ and the displacements $\tilde{W}_b(k_x)$ can be written simply as

$$\begin{Bmatrix} \tilde{F}_1(k_x) \\ \tilde{F}_3(k_x) \end{Bmatrix} = \begin{bmatrix} \sigma_1 & \sigma_2 \\ \tau_1 & \tau_2 \end{bmatrix} \begin{Bmatrix} \tilde{W}_{b1}(k_x) \\ \tilde{W}_{b3}(k_x) \end{Bmatrix}. \tag{5.10}$$

Substituting equation (5.10) into equations (5.3) and (5.4), gives

$$\begin{bmatrix} \tilde{D}_{b1}k_x^4 - m'_{b1}\omega^2 + \sigma_1 & \sigma_2 \\ -\tau_1 & \tilde{D}_{b3}k_x^4 - m'_{b3}\omega^2 - \tau_2 \end{bmatrix} \begin{Bmatrix} \tilde{W}_{b1}(k_x) \\ \tilde{W}_{b3}(k_x) \end{Bmatrix} = \begin{Bmatrix} \tilde{F}_0 \\ 0 \end{Bmatrix}. \tag{5.11}$$

As $m'_{b1}\omega^2/\tilde{D}_{b1} = \tilde{k}_{b1}^4$ and $m'_{b3}\omega^2/\tilde{D}_{b3} = \tilde{k}_{b3}^4$, equation (5.11) can be written as

$$\begin{bmatrix} k_x^4 - \tilde{k}_{b1}^4 + \sigma_1/\tilde{D}_{b1} & \sigma_2/\tilde{D}_{b1} \\ -\tau_1/\tilde{D}_{b3} & k_x^4 - \tilde{k}_{b3}^4 - \tau_2/\tilde{D}_{b3} \end{bmatrix} \begin{Bmatrix} \tilde{W}_{b1}(k_x) \\ \tilde{W}_{b3}(k_x) \end{Bmatrix} = \begin{Bmatrix} \tilde{F}_0/\tilde{D}_{b1} \\ 0 \end{Bmatrix}. \tag{5.12}$$

Finally, by inverting this equation the response of beam 1 can be expressed as

$$\tilde{W}_{b1}(k_x)=\frac{\tilde{F}_0}{\tilde{D}_{b1}}\frac{k_x^4-\tilde{k}_{b3}^4-\tau_2/\tilde{D}_{b3}}{\left(k_x^4-\tilde{k}_{b1}^4+\sigma_1/\tilde{D}_{b1}\right)\left(k_x^4-\tilde{k}_{b3}^4-\tau_2/\tilde{D}_{b3}\right)+\sigma_2\tau_1/\left(\tilde{D}_{b1}\tilde{D}_{b3}\right)}. \tag{5.13}$$

Accordingly, the response of beam 3 becomes

$$\tilde{W}_{b3}(k_x)=\frac{\tau_1/\tilde{D}_{b3}}{k_x^4-\tilde{k}_{b3}^4-\tau_2/\tilde{D}_{b3}}\tilde{W}_{b1}(k_x). \tag{5.14}$$

The responses $\tilde{w}_{b1}(x)$ and $\tilde{w}_{b2}(x)$ can be obtained from the inverse Fourier transform of these equations according to equation (3.4). Moreover from $\tilde{W}_{b1}(k_x)$ and $\tilde{W}_{b3}(k_x)$, equation (5.6) can be used to find $\tilde{B}_1$, $\tilde{B}_2$, $\tilde{B}_3$ and $\tilde{B}_4$. These can then be substituted into equation (5.5) to give $\tilde{W}_p(k_x,y)$ which can be inverse Fourier transformed to give $\tilde{w}_p(x,y)$ (equation (3.8)).

It should be noted that equations (5.13) and (5.14) allow the beams to be dissimilar. Thus, for example, two beams having different second moments of area or mass per unit length coupled to a plate can be analysed. It is an advantage of the Fourier method in contrast to the wave method in the analysis of two parallel beams coupled to a plate. Two dissimilar beams coupled to a rectangular plate will be investigated in Chapter 7 in connection with an experimental study and validation.

5.2.2 Response of finite two-beam structure

The above theory can be readily applied to the finite coupled structure, shown in Figure 5.2, where the ends of both finite beams are considered to be sliding. The two corresponding edges of the plate are also assumed to be sliding. As before, the beams are assumed to have infinite torsional stiffness.

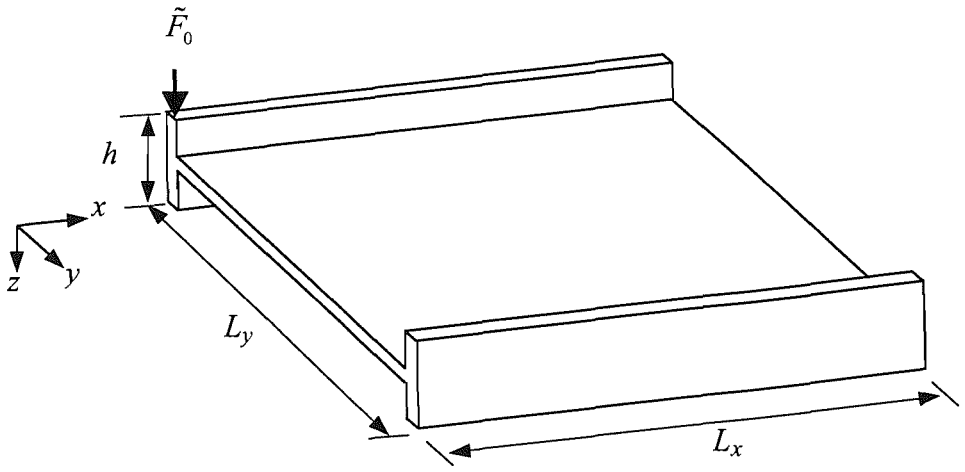

Figure 5.2. A coupled structure consisting of two finite beams attached to a rectangular plate.

As explained in section 3.4.1, the behaviour of the coupled beams with sliding conditions can be described in terms of cosine orders. Therefore, the motions of the coupled beams 1 and 3 are written in the same form as equation (3.52) and the motion of the plate as presented in equation (3.53) in the same section. The solution at each value of wavenumber in the Fourier series is obtained as in the previous section.

5.2.3 Results based on the Fourier technique

Using the Fourier series, the response of the finite beam-plate-beam structure shown in Figure 5.2 is calculated. The width of the plate L_y is 1.5 m and all other material properties and dimensions are the same as given in Table 2.1. Although the mathematical development allows the two beams to have different properties, for the purpose of validation the two beams are here taken to be identical. Structural loss factors of 0.05 are used for the beams and plate.

The Fourier series is truncated at a non-dimensional wavenumber of 15 ($\gamma = k_x/k_b = 15$ at 1412 Hz) as proposed in Chapter 3 which gives a maximum number of Fourier components of 145.

For comparison, a modal model is constructed. In Chapter 2 dealing with the modal method, only a single beam coupled to the rectangular plate was discussed. However, a similar procedure can be applied so that the contribution of the second beam can be incorporated. A two-beam system is discussed later in Chapter 6 where the two-beam system is realised by eleminating two parallel beams in a fully framed system. Thus, the details concerning the two-beam system are not explained at this stage. However, as dicussed in section 2.6.1, the maximum mode number should be chosen for the present application, as the plate width is changed from 0.75 m to 1.50 m. In Chapter 2, the non-dimensional wavenumbers with respect to the plate free wavenumber were chosen to be $\gamma_{p,x} = 0.69$ and $\gamma_{p,y} = 2.25$ (see Table 2.2). These give maximum mode numbers of $M = 21$ and $N = 51$ for the present case. For convenience $M = N = 51$ are used here in the modal model consisting of two beams and a plate.

One may notice at this stage that the Fourier method and the modal method use the same cosine function with the same wavenumber k_x to describe the motion along the x direction. They are presented in equations (3.51) and (2.5) respectively. Thus, the maximum number of components in the Fourier series n and the maximum mode number M have in fact the same physical meaning. That is, if the same value for M and n is used then the response of the structure along the x direction should be identical ignoring the behaviour along the y direction. Thus, for comparison between the two methods strictly it is expected that the same value for M and n should be used, even though the responses may not be identical due to the motion along the y direction. However, note that in this section $M = 51$ and $n = 145$ are used. This is related to the computer resources that are limited in calculation as the modal method deals with a matrix, the size of which is defined by the maximum mode number in the two directions. Meanwhile, in the Fourier

method the motion along the y direction is defined in fact in terms of only four waves for a given wavenumber k_x, which reduces calculation time. Thus, the response based on the Fourier method is likely to be more accurate than that based on the modal method as $n > M$ here.

First, the point mobility at one end of the beam is compared in Figure 5.3. The results show excellent agreement between the Fourier series and the modal method (maximum errors of 0.9%).

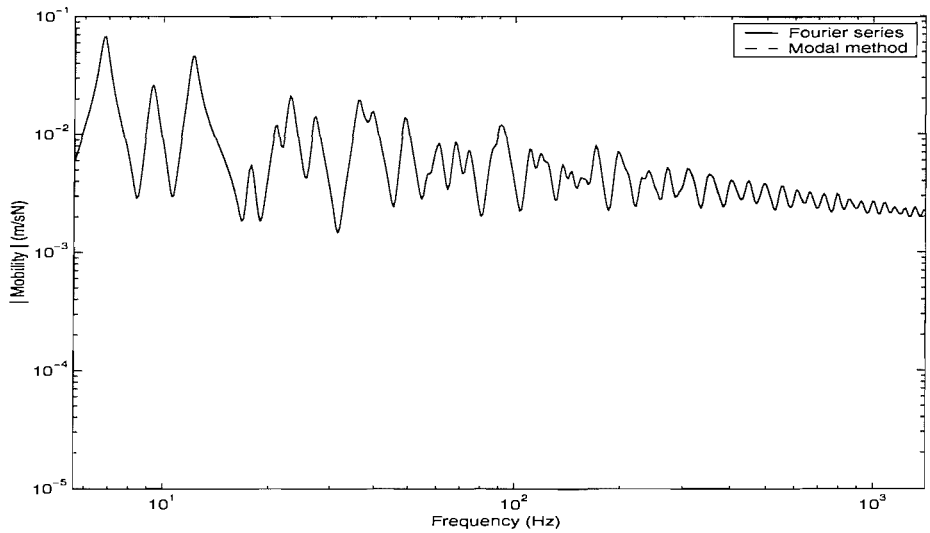

Figure 5.3. Point mobility of the finite beam-plate-beam structure (point force applied at $x = 0$ of beam 1).

Also, the transfer mobilities to points on the plate and beam 3 are shown in Figures 5.4 and 5.5 respectively. They are obtained at points of $x = 1.51$ m and $y = 0.99$ m on the plate and $x = 0$ m on beam 3 when the point force is applied at $x = 0$ of beam 1. Comparing them with those obtained using the modal method, they agree well. Maximum errors of 16% at 820 Hz and 60% at 1150Hz are found in the respective figures which correspond to the deepest trough. They occur due to the numerical integration, so that the average errors for the whole frequency range considered are only 0.09% and 0.3% respectively.

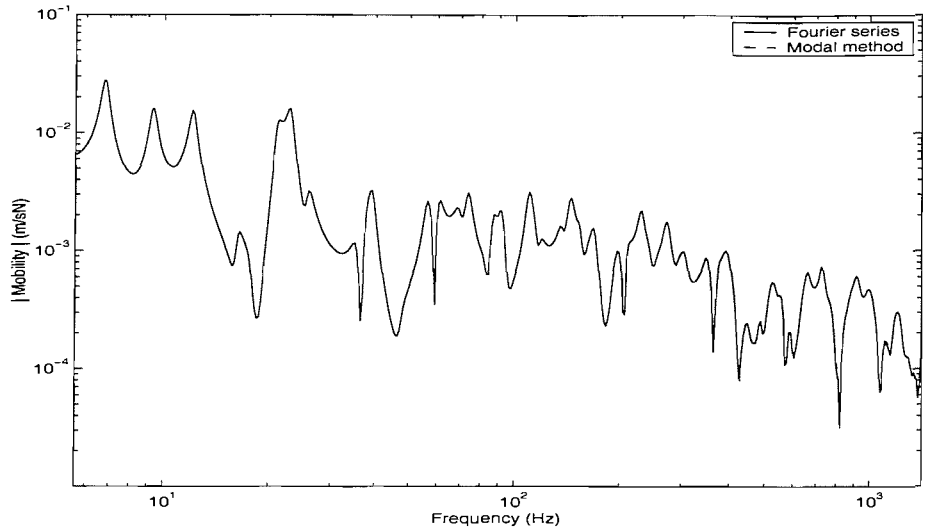

Figure 5.4. Transfer mobility for the finite beam-plate-beam structure to a point on the plate (at $x = 1.51$ m and $y = 0.99$ m, point force applied at $x = 0$ of beam 1).

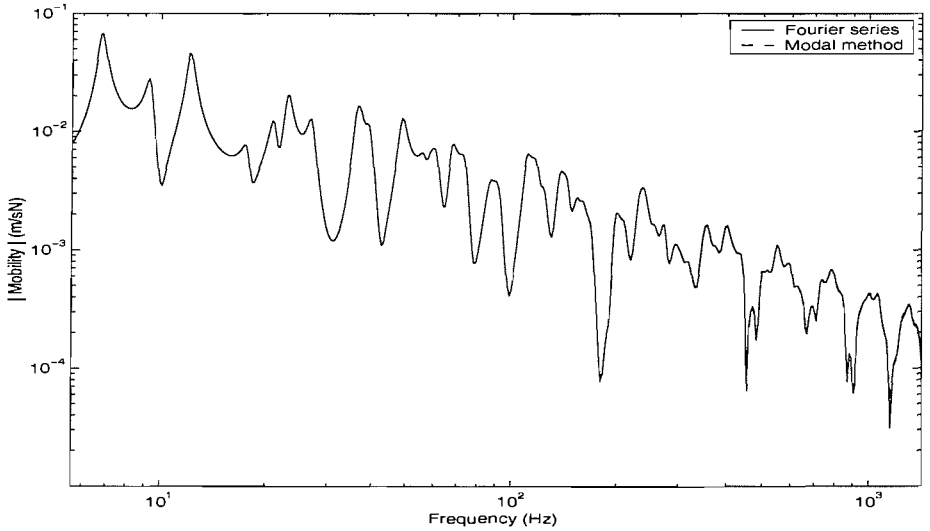

Figure 5.5. Transfer mobility for the finite beam-plate-beam structure to a point on beam 3 (at $x = 0$, point force applied at $x = 0$ of beam 1).

Considering the good agreement between the Fourier and the modal methods, the Fourier method may be regarded as an exact method for obtaining the correct response of the coupled structure such as the beam-plate-beam structure under the boundary conditions.

The various powers are compared with the total power in Figure 5.6. The difference between the two transferred powers corresponds to the dissipated power in the plate (maximum error of 0.001%). Also the net power transferred from the plate to beam 3 is equal to the dissipated power in beam 3 (maximum error of 0.001%). One can see that the power transferred to beam 3 is smaller than that transferred from beam 1 to the plate by more than 10 dB at all but the lowest frequencies, the difference increasing at higher frequencies. Thus, it can be said that the power transferred from beam 1 to the plate is mostly dissipated in the plate. Consequently, it is expected that the power from beam 1 is hardly transferred to beam 3. However, comparing the power dissipated in beams 1 and 3, they are generally similar in level except at higher frequencies. Thus, although most power is dissipated in the plate, it seems that a significant fraction of the power from beam 1 is still transmitted to beam 3.

It may be noted that the plate has a much higher modal density than the beams, so that if the subsytems have similar average modal energy, the plate will have a higher total energy, as here.

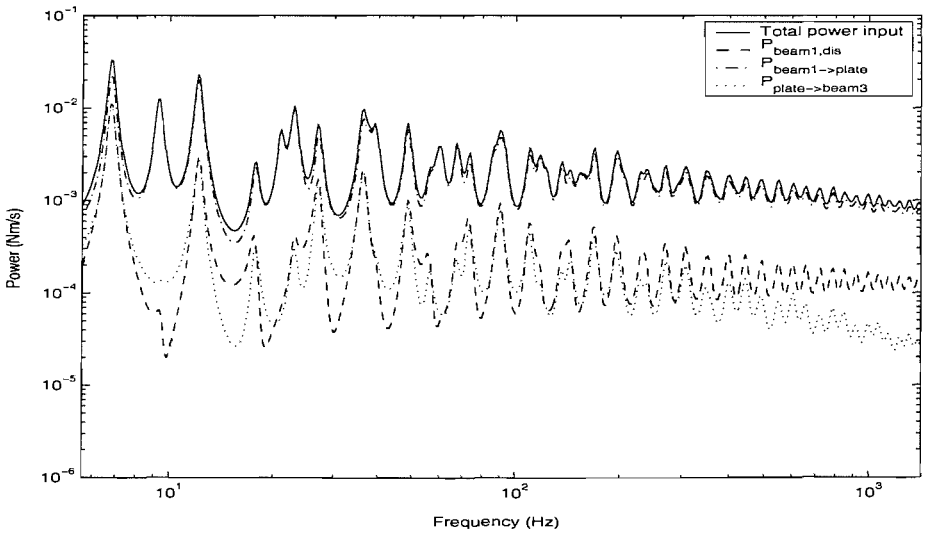

Figure 5.6. Total input power to the coupled structure as in Figure 5.2, the power dissipated in beam 1, the net power transferred to the plate and the net power from the plate to beam 3 (point force applied at x = 0 of beam 1). The two identical beams are considered (beam height = 68 mm).

When two beams with different heights are considered for this (all other dimensions and material properties are not changed), the results are as shown in Figure 5.7. One can see that the difference of the dissipated power between beam 1 and beam 3 is increased compared with Figure 5.6 (thus the power transferred to beam 3 is smaller) even at lower frequencies. The effect is much larger than simply due to the change in impedance and indicates that when the beam wavenumbers are different the transfer through the plate is reduced considerably.

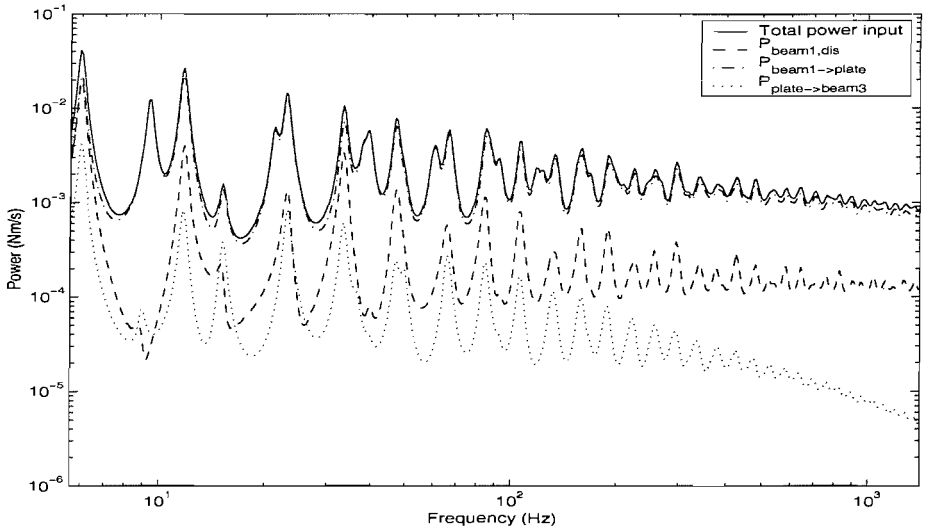

Figure 5.7. Total input power to the coupled structure as in Figure 5.2, the power dissipated in beam 1, the net power transferred to the plate and the net power from the plate to beam 3 (point force applied at $x = 0$ of beam 1). The beam heights of beam 1 and beam 3 are 68 mm and 44 mm respectively.

5.3 Wave method for analysis of a symmetric beam-plate-beam system

The approximate wave method used to model a single beam and plate is extended to find the response of a symmetric beam-plate-beam system. It is assumed that the plate impedances acting upon the two parallel beams are the same. Then, the

approximate plate impedance found in Chapter 4 can be used for such an analysis. As in Chapter 4 this is based on the travelling wave in the beam. A symmetric structure consisting of two identical beams and single rectangular plate is examined as follows.

5.3.1 Synthesis from non-symmetric structure

Consider the coupled structure consisting of two finite beams attached to a rectangular plate as shown in Figure 5.2, where the two beams are identical. A point force is applied at one end of the beam and it is assumed that the ends of the beams are sliding. Note that although the sliding ends are assumed here for comparison with the Fourier method, the boundary conditions in the wave method are arbitrary. For example, the response of the free-free coupled beam can also be found using the similar procedure explained below. Due to the stiffness of the beams, the edges of the plate also effectively have a sliding boundary condition, although no constraints are required. This is because in the present case the plate is assumed to behave like independent strips. All the dimensions are the same as in the previous section and thus, the width of the plate is 1.5 m. For convenience, this is written as $2L_y$.

Now, by symmetry, the wave motion in the plate can be described by a combination of the waves reflected by a pinned condition along the middle line of the plate ($y = L_y$), parallel to the beam, and the waves reflected by a sliding condition along the same line. Such a technique is common in FE analysis [3]. Therefore, the analysis performed previously for the structure consisting of one beam and one plate in Chapter 4 can be used in this analysis. Figure 5.8 shows how the response of the symmetric structure can be synthesized from a combination of the motion of the structure which is symmetric and that which is antisymmetric about the middle line ($y = L_y$) of the plate. In each case half the force amplitude is applied on one side.

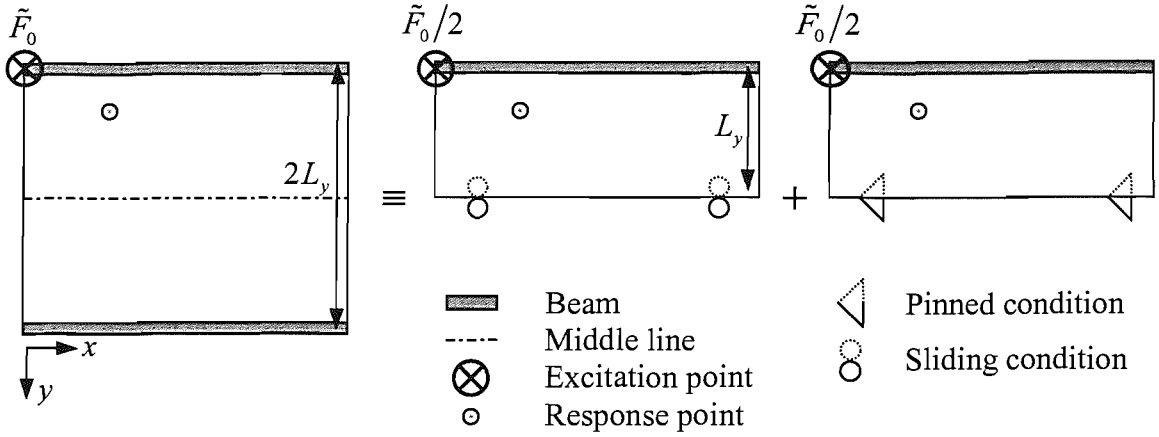

Figure 5.8. Response of a symmetric structure calculated from consideration of the symmetric and antisymmetric motion.

If the point force is applied at the end of beam 1 of the symmetric structure, the response of the upper half ($0 \le y \le L_y$) of the structure can be assumed to be the sum of the antisymmetric response of the structure with a pinned condition and the symmetric response of the same structure with a sliding condition at $y = L_y$. Meanwhile, the response of the lower half ($L_y \le y \le 2L_y$) can be obtained from the difference between the results. In terms of transfer mobilities this gives

$$\tilde{Y}_{sum}(y) = \left[\tilde{Y}_{sld}(y) + \tilde{Y}_{pin}(y)\right]/2 \qquad \text{for } 0 \le y \le L_y, \tag{5.15 a}$$

$$\tilde{Y}_{sum}(y) = \left[\tilde{Y}_{sld}(2L_y - y) - \tilde{Y}_{pin}(2L_y - y)\right]/2 \quad \text{for } L_y < y \le 2L_y \tag{5.15 b}$$

where the subscripts *pin* and *sld* represent the pinned and sliding boundary conditions of the plate edge $y = L_y$ respectively.

The force acting on the plate from the beam can be calculated from the transfer mobility of the beam and the approximate plate impedance for the corresponding boundary condition. For example, the force acting on the plate from beam 1 of the synthesized structure can be expressed in the form

$$\tilde{f}_1(x) = \frac{\tilde{F}_0}{2}\left(Y_{b1,pin}(x)Z'_{p,pin} + Y_{b1,sld}(x)Z'_{p,sld}\right). \tag{5.16}$$

The force acting on the other beam, beam 3, can also be calculated in the same way. No net external force acts on beam 3 as the forces in the two component models cancel. As the response of the beam-plate-beam structure is found from the sum of the antisymmetric and the symmetric responses, only a configuration with identical beams can be modelled using such a synthesis.

While such an approach is commonly used, for example in FEM [3], it should be realised that the coupled wavenumbers in the two component models differ, as they depend on different line impedances. The assembly from symmetric and antisymmetric models, therefore, represents an approximation in the present analysis.

5.3.2 Results based on the wave method

The numerical analysis of the coupled system consisting of two identical beams coupled to a rectangular plate as in Figure 5.2 is carried out in this section. For the wave method, the symmetric and antisymmetric motions of the single beam system are required. In section 4.3.4, numerical calculations were already given for the case when the opposite edge of the plate parallel to the beam is pinned, giving a reflection coefficient $\tilde{r} = -1$. The dynamic behaviour of the same coupled system where the opposite edge is sliding can be realised by simply changing the reflection coefficient to unity ($\tilde{r} = 1$) in equation (4.33). The numerical analysis for such a case is presented in Appendix C, in which the corresponding wavenumbers, plate impedance, point mobility and power relationship are discussed in a similar manner as in section 4.5. From the responses of the single-beam coupled system with the pinned and then with the sliding opposite edge, the response of two identical beams coupled to the rectangular plate can be found. Note that the dimensions of the two-beam system are the same as that discussed in section 5.2, with twice the width of Chapter 4.

Firstly, the point mobility of the combined structure, calculated using equation (5.15), is shown in Figure 5.9. Comparing it with corresponding results from the

Fourier method, generally close agreement is found. The mobility contains dynamic characteristics of both the pinned and sliding systems; for example the peaks at 6.7, 23.2, and 36.4 Hz correspond to the resonance frequencies of the pinned system (see Figure 4.18) and those at 9.7, 27.5, and 40.1 Hz are the resonance frequencies of the sliding system (Figure C.4 in Appendix C). The former modes correspond to anti-symmetric behaviour of the whole structure, and the latter to symmetric behaviour. Also, it can be seen that the plate impedances (Figures 4.15 and C.3) have an influence on the synthesized structure as well. At the anti-resonance frequencies 22.1, 62.7 and 126.7 Hz of the pinned plate and 9.4 and 39.5 Hz of the sliding plate, the point mobility of the combined system has small troughs. Some of the anti-resonances seem to have no influence on the response of the structure, but this is because the response is described by the sum of the two structures with different boundary conditions. For example, the anti-resonance of the sliding structure at 262 Hz does not result in any trough because the response is dominated by the resonance of the pinned structure at 272 Hz.

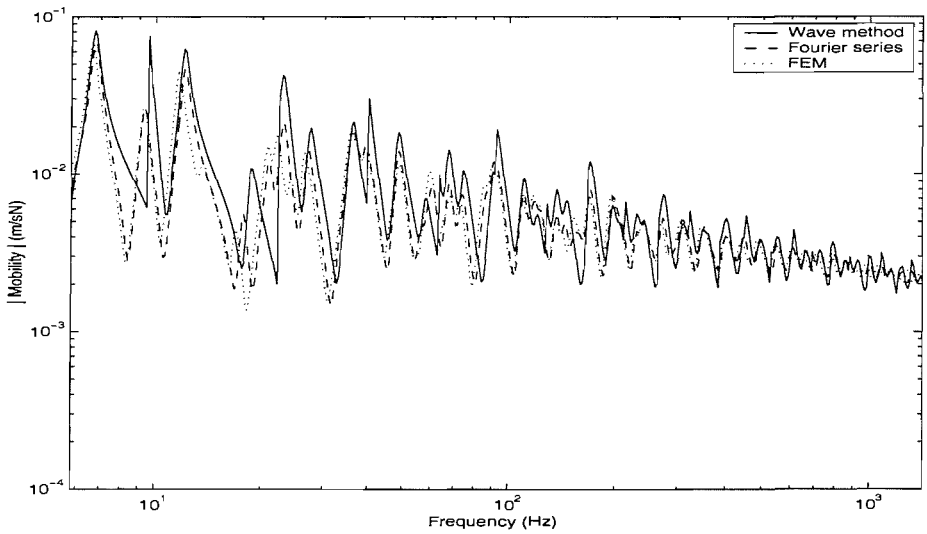

Figure 5.9. Point mobility of the symmetric coupled structure as in Figure 5.2 (point force applied at $x = 0$ of beam 1). The FEM results have free boundaries on the plate at $x = 0$ and $x = L_x$.

The transfer mobilities to a point on the plate are compared in Figure 5.10. They show good agreement between the wave model and the Fourier method. The small

differences at low frequencies may occur because of the approximations of the plate impedance and nearfield wave in the coupled beam.

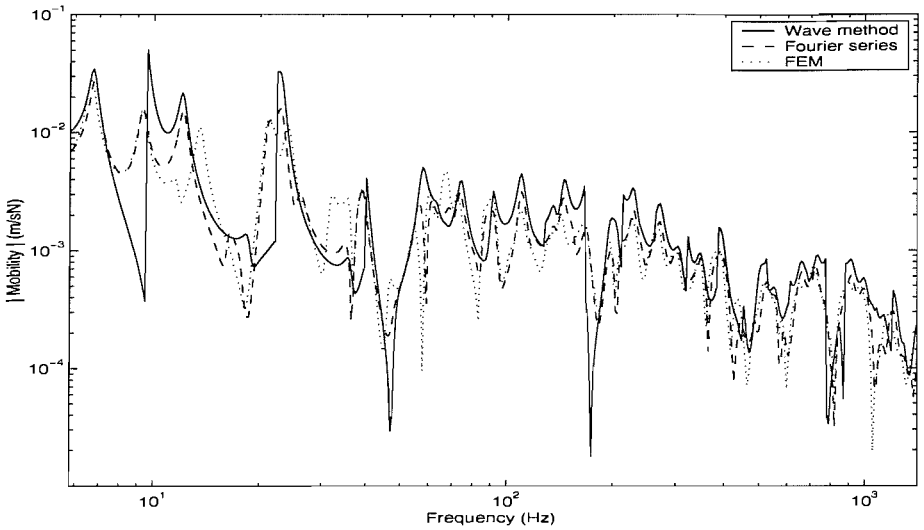

Figure 5.10. Transfer mobility for the plate (at x = 1.51 m and y = 0.99 m) in the coupled structure as in Figure 5.2 (point force applied at x = 0). The FEM results have free boundaries on the plate at $x = 0$ and $x = L_x$.

In both approaches, sliding beam ends are assumed. However, it has been noted that strictly the corresponding plate edges normal to the beam behave in different ways, that is, in the Fourier approach, the edges experience sliding conditions, while in the wave method no boundary conditions are applied. However, as discussed with respect to the modal model in Chapter 2, the motion of the coupled beam has a dominant effect on the plate motion. The comparisons presented above show that the responses are in very good agreement at low frequencies as well as high frequencies, from which it can be said that the effect of differences in the boundary conditions is small, as expected. This can be confirmed by comparing them with the results obtained from FE that are also shown in the same figures. Although the FE model has free boundary condition on those plate edges (the beams still have sliding boundaries), one can see that the differences seem small even at low frequencies.

Figure 5.11 shows the total input power, the power dissipated in beam 1 and the power transferred between the subsystems obtained using the wave method. Due to the fact that response of the system is synthesised using two different plate impedances, the calculated power transferred to beam 3 and the power dissipated by the beam differ by up to 35% (mean error of 0.4% for the whole frequency range considered). Nevertheless, these differences are still relatively small (at most 1.3 dB and 0.02 dB on average) so that the synthesis approach can be used with some caution.

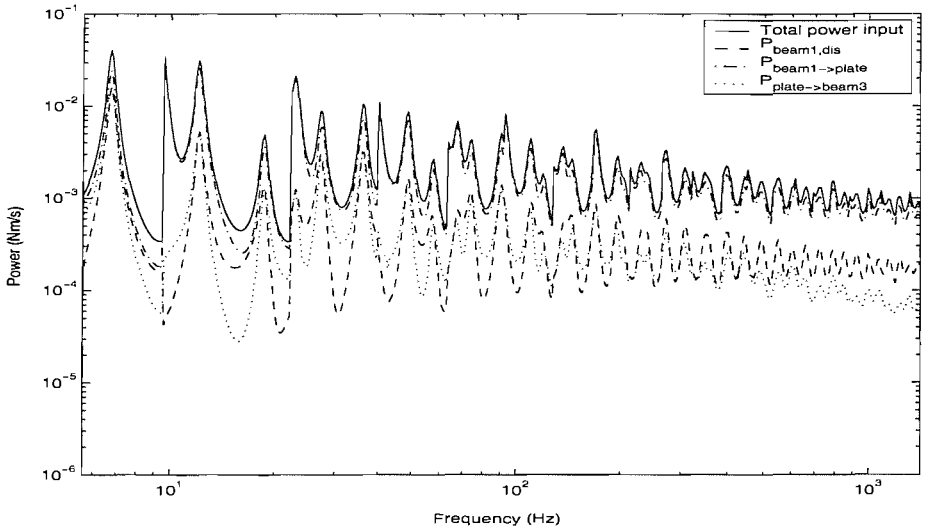

Figure 5.11. Total input power to the symmetric coupled structure as in Figure 5.2, the power dissipated in beam 1 and the power transferred to the plate and to beam 3.

Comparing this result with that for the Fourier method given in Figure 5.6, generally good agreement is found for the power input. However, as mentioned in section 4.5.2, one can see that the power transfer from beam 1 to the plate tends to reduce, whilst the power dissipated in the beams seems to increase as expected. Thus, strictly it seems difficult to predict an exact level of the dissipated or transferred power using this wave method. However, the differences of the power transfer and the power dissipated in beam 1 are small compared with those based on the Fourier method and such a power investigation is still useful to estimate the general power relationship between subsystems. For example, the result discussed in section 5.2.3 that most

power is dissipated in the plate and there is still some power transmission from beam 1 to beam 3 can also be found here from Figure 5.11.

5.4 Conclusions

In this chapter, two parallel beams coupled to a rectangular plate were studied using both the Fourier method and the wave method. As explained in Chapters 3 and 4, the latter is regarded as an approximate method while the former produces an exact response. Their responses were examined and also advantages and disadvantages of the two methods were discussed.

The developments of the Fourier approach show that it is applicable for the analysis of a beam-plate-beam structure. The transfer mobility as well as the point mobility show very good agreement with those from the modal method. The formulation developed can be applied to non-symmetric beam-plate-beam systems and results for this will be examined in connection with the experimental study later.

The wave model was also extended to a beam-plate-beam system. Using a combination of two single beam-plate models comprising pinned and sliding plate opposite edges respectively, an analysis of the symmetric beam-plate-beam structure was synthesised when one of the beams is excited. The response of the synthesized model shows features from both the symmetric and antisymmetric response. Application of this approach is possible for other arbitrary beam boundary conditions, which is not the case for the Fourier method.

The wave method is an approximate approach. However, good agreement is found between the mobilities of the symmetric beam-plate-beam system obtained with the present method and those from the Fourier method. The power balance holds approximately, although the error (1.3 dB at most) is larger than that of the Fourier method, due to the approximation and the synthesis procedure. Strictly, the power transfer to the plate and the power dissipated in the beams differ from the exact

values due to the approximations in the wave method. Nevertheless, such a power investigation seems useful to give an insight of the power relationship between subsystems, as the difference is mostly small.

The Fourier method provides an exact response as long as a sufficient number of Fourier components is included in the Fourier series. The wave method is much more efficient, as its dispersion equation is based on only the free wavenumber of the subsystems. However, the approximation of the plate impedance only results in an approximate response compared with the Fourier method. A discussion of the computational time and computer resources required for the different methods will be presented at the end of Chapter 6 where a more complicated four-beam system is studied.

CHAPTER 6

FULLY FRAMED STRUCTURE

6.1 Introduction

Several numerical methods have been used to investigate the structural behaviour of a coupled structure consisting of beams and a plate. As well as a modal approach and a Fourier approach, a wave technique was introduced and applied to a structure consisting of one or two parallel beams coupled to a rectangular plate in Chapters 4 and 5.

A fully framed structure consisting of four beams surrounding a rectangular plate is an important concern in the present research, as it is a principal configuration considered in many engineering structures, e.g. automotive vehicles, ship hulls, etc. Although the numerical approaches developed previously have produced good results for the vibrational motion in the cases considered, they have rarely been used for the analysis of framed structures consisting of four beams.

It has been shown that the wave approach can be used to obtain an approximate response of a beam-plate coupled structure as long as the system consists of a subsystem (spine) possessing long wavelength waves and a receiver subsystem possessing short wavelength waves. Thus, in principle, this technique can be applied to give an approximate dynamic response for a fully framed structure. It is necessary to have an accurate result for comparison with this approximate wave-based solution. Thus, in this chapter the modal method considered in Chapter 2 is applied to the framed structure. The accuracy of this method is limited only by the number of modes included in the series.

There are a few published studies on a framed structure consisting of four beams and a plate [68, 69] (see section 1.5). Both studies quoted concentrated on predicting the plate behaviour, rather than that of the beam. Also, both papers

assumed that the motion of the ends of each beam is zero. From the point of view that the stiff beams possessing the bending waves radiate short-wavelength bending waves into the plate, the behaviour of the beams is very important [41]. Therefore, the present study, which considers the beam as well as the plate and allows for excitation at the beam ends, differs from the studies described above.

Grice and Pinnington considered a box structure and introduced a so-called spine and receiver [55] (see section 1.4.5). This concept is also considered in the present research. However, here the coupled wavenumber, representing the long wavelength wave including the effect of the plate impedance, is obtained to describe the motion instead of using the finite element model.

This chapter is divided into two main parts. Firstly the modal approach of Chapter 2 is extended to the four-beam-plate system. The number of modes that should be included in the calculation is an important issue in the mode-based analysis. For this, numerical results are shown and compared with those based on the Fourier technique previously investigated in Chapter 5, although the structure consisting of only two beams is used as there is no result previously obtained for the four-beam structure. Then, the dynamic response of the four-beam structure using the modal method is compared with that of the finite element method (FEM).

In the second part, the procedure for obtaining an approximate response using the wave technique is explained. The principal equations, such as the equation of motion of a beam and the expression for the plate impedance, are emphasised and numerical results are shown for comparison of the various techniques. The corresponding equations of motion, based on the wave method for a four beam structure, are presented in Appendix D.

Depending upon the problem and application, the detailed response at individual frequencies is important at low frequencies. However, with increasing frequency the band-averaged response and the variability about a mean value are much more important than narrow band results. The aim of the present study is related to the

dynamic characteristic in the mid and high frequency regions. Thus, results based on the wave method are mostly represented from this point of view. For example, a result such as an octave band average or a confidence interval of a response is just as applicable and useful as narrow-band results. Hence such results are also presented.

The modal and wave methods are applied to a perspex plate 1.0×0.75 m with a thickness of 2 mm, surrounded by beams 22×6 mm. As in previous sections the frequency range selected is 5.6 to 1412 Hz (one-third octave bands 6.3 to 1250 Hz). In this range each beam has between 7 and 9 modes so that the beams can be considered to be in their "low frequency" range. The plate has a modal density of about 0.4 modes per Hz, so that its 10^{th} mode occurs by about 23 Hz and about 500 modes can be expected below 1412 Hz. The modal overlap factor [12, 21] of the plate is greater than unity above about 50 Hz. This, therefore, has "high frequency" behaviour over much of the frequency range considered.

6.2 A modal formulation for the coupled motion of a system of two or four beams attached to a plate

6.2.1 A modal method for the framed structure

The motion of a framed structure consisting of four beams and a rectangular plate, as shown in Figure 6.1, is investigated here. The modal method for a single beam coupled to a rectangular plate involving the modal coupling technique was presented in Chapter 2. Similarly, for the framed structure, its behaviour can be described in terms of mode shapes and the coupling based on the modal coordinates of the plate.

The boundary conditions for the analysis of the framed structure as in Figure 6.1 are similar to those presented in Chapter 2. The beams are assumed infinitely stiff to torsion and correspondingly all edges of the plate are assumed to be sliding,

which significantly reduces the complexity of the analytical and numerical analyses. As in Chapter 2 a separable solution is used for the plate and thus, the beam shape functions along the plate edges in the x and y directions are used as the two sets of functions.

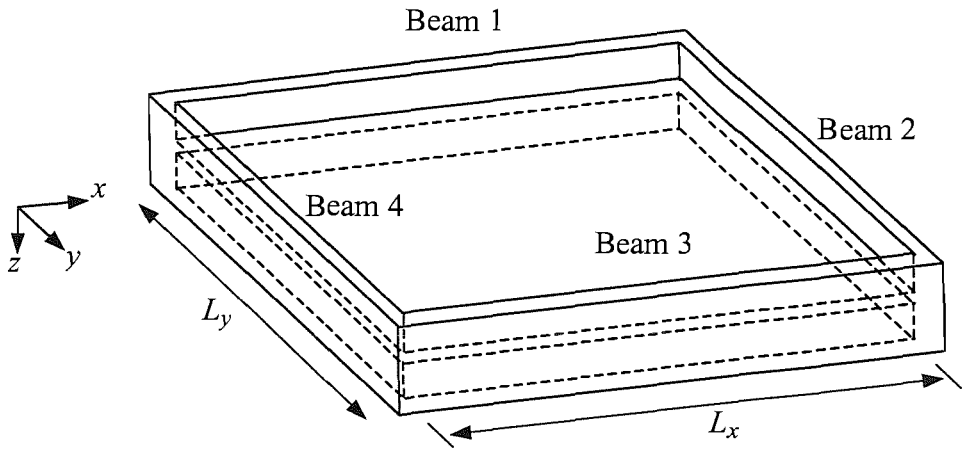

Figure 6.1. The coupled structure consisting of four beams and a rectangular plate.

Similar to section 2.5.2, the flexural motion of the framed structure can first be derived using the mode shapes of the uncoupled plate satisfying the boundary conditions ψ_r and generalised coordinates q_r. They are shown in equation (2.49). The maximum mode number R should be determined for practical use.

The flexural displacement of the beams shown in Figure 6.1 is

$$\begin{aligned} w_{b1}(x,t) &= w_p(x,0,t);\ \ w_{b3}(x,t) = w_p(x,L_y,t) \\ w_{b4}(y,t) &= w_p(0,y,t);\ \ w_{b2}(y,t) = w_p(L_x,y,t) \end{aligned} \tag{6.1}$$

due to continuity at the plate edges.

Writing the equations of motion in terms of the plate modal coordinates, the generalised mass matrix of the coupled structure is found, in a similar way to chapter 2, to be

$$\mathbf{M} = \mathbf{M}_p + \boldsymbol{\beta}_1 \mathbf{M}_{b1} \boldsymbol{\beta}_1^T + \boldsymbol{\beta}_2 \mathbf{M}_{b2} \boldsymbol{\beta}_2^T + \boldsymbol{\beta}_3 \mathbf{M}_{b3} \boldsymbol{\beta}_3^T + \boldsymbol{\beta}_4 \mathbf{M}_{b4} \boldsymbol{\beta}_4^T \tag{6.2}$$

where $\mathbf{M}_p$ is the modal mass matrix of the plate, $\mathbf{M}_{bi}$ is the modal mass matrix of beam i in beam modal coordinates and $\boldsymbol{\beta}_i$ is a transformation matrix from beam to plate modal coordinates. For plate mode r defined in terms of cosine orders m_r and n_r in the x and y directions (see equation (2.14)),

$$\beta_1 = C_k \int_0^{L_x} \phi_{m_r}(x)\phi_{n_r}(0)\phi_k(x)dx = \delta_{m_r k}, \tag{6.3 a}$$

$$\beta_2 = C_l \int_0^{L_y} \phi_{m_r}(L_x)\phi_{n_r}(y)\phi_l(y)dy = \delta_{n_r l}(-1)^{m_r}, \tag{6.3 b}$$

$$\beta_3 = C_k \int_0^{L_x} \phi_{m_r}(x)\phi_{n_r}(L_y)\phi_k(x)dx = \delta_{m_r k}(-1)^{n_r}, \tag{6.3 c}$$

$$\beta_4 = C_l \int_0^{L_y} \phi_{m_r}(0)\phi_{n_r}(y)\phi_l(y)dy = \delta_{n_r l}, \tag{6.3 d}$$

where $\phi_k(x) = \cos(k\pi x/L_x)$, $\phi_l(y) = \cos(l\pi y/L_y)$, $\cos m\pi = (-1)^m$ and

$$C_k = \begin{cases} 1/L_x & \text{for } k = 0 \\ 2/L_x & \text{for } k \geq 1 \end{cases}, \tag{6.4}$$

$$C_l = \begin{cases} 1/L_y & \text{for } l = 0 \\ 2/L_y & \text{for } l \geq 1 \end{cases}. \tag{6.5}$$

The maximum numbers of modes m and k may be chosen to be the same and so may the numbers of modes n and l.

Similarly the generalised stiffness matrix is

$$\mathbf{K} = \mathbf{K}_p + \boldsymbol{\beta}_1\mathbf{K}_{b1}\boldsymbol{\beta}_1^T + \boldsymbol{\beta}_2\mathbf{K}_{b2}\boldsymbol{\beta}_2^T + \boldsymbol{\beta}_3\mathbf{K}_{b3}\boldsymbol{\beta}_3^T + \boldsymbol{\beta}_4\mathbf{K}_{b4}\boldsymbol{\beta}_4^T \tag{6.6}$$

where $\mathbf{K}_p$ is a diagonal matrix with $K_{p,r} = \omega_{p,r}^2 M_{p,r}$ and $K_{bi,m} = \omega_{bi,m}^2 M_{bi,m}$.

The force is applied to beam 1, so, as in Chapter 2 the generalised force in plate modal coordinates is given by

$$\mathbf{F} = \boldsymbol{\beta}_1 \mathbf{F}_{b1} \tag{6.7}$$

where $\mathbf{F}_{b1}$ is the generalised force in beam 1 modal coordinates given by $F_{b1,m} = F_0 \phi_m(x_1)$ with a point force F_0 applied at $x = x_1$ on beam 1. Steady state harmonic motion is assumed and then, introducing the hysteretic damping to the matrix $\tilde{\mathbf{K}}$ results in the generalised coordinates as in equation (2.55). The flexural displacement of the framed structure is determined from the generalised coordinates obtained and the shape functions as in equation (2.49).

6.2.2 Configuration of framed structure

In the following, numerical simulations based on the modal method are presented and configurations of the framed structure to be used are explained. The structure consisting of four beams and a rectangular plate shown in Figure 6.1 is investigated.

The numerical analysis based on the wave method will also be included later in this chapter. An important assumption of the wave method used in this research is that the wavenumber of the free plate k_p should be at least about twice as large as the coupled beam wavenumber k_x (see section 4.2.5). In principle this is not a restriction on the modal approach, but has been adopted so as to be able to consider results produced by the two methods. The material properties and dimensions of the coupled structure are given in Table 6.1. Note that some of the dimensions differ from those used in Chapters 2 – 5, in particular the beam length and height and thickness of the beam and plate. This is for consistency with the dimensions of the framed structure to be used in the experimental study in Chapter 7.

The free wavenumbers of the beam and the plate are compared in Figure 6.2. The corresponding wavenumber ratio is a constant and equal to $k_p/k_b = 3.18$. This is large enough to apply the wave method in the present frequency range of interest (see Figure 4.4).

Table 6.1. Material properties and dimensions of the coupled structure shown in Figure 6.1.

Material	Perspex
Young's modulus, E (GNm^{-2})	4.4
Poisson's ratio, ν	0.38
Density, ρ (kgm^{-3})	1152.0
Beam length, L_x (m)	1.0
Beam thickness, b (mm)	6.0
Plate width, L_y (m)	0.75
Plate thickness, t_p (mm)	2.0
Height of beam, h (mm)	22.0
Damping loss factor of beam, η_b	0.05
Damping loss factor of plate, η_p	0.05

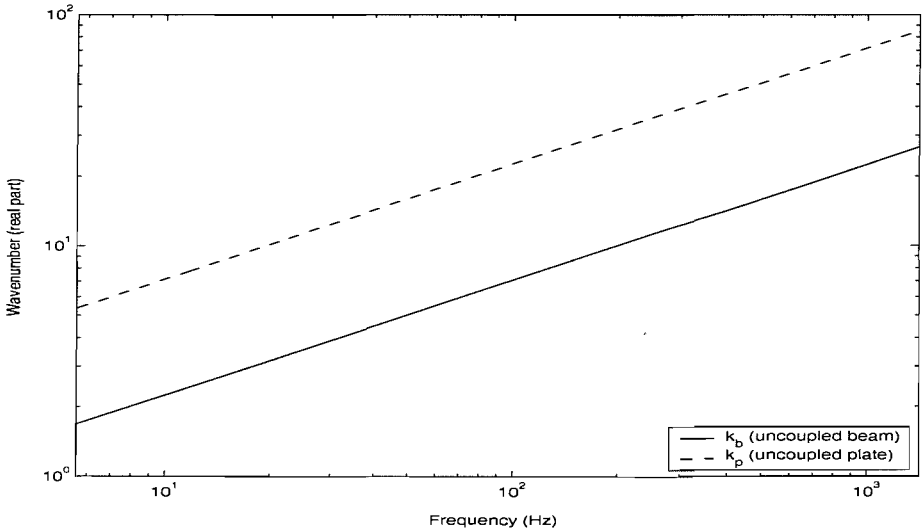

Figure 6.2. Wavenumber comparison of the subsystems.

6.2.3 Test of convergence: two-beam-plate coupled system

The number of modes to be included in the numerical solution for adequate convergence needs to be determined. This was already studied for the single-beam system in Chapter 2, where the response accuracy was compared to the modal

model itself having a large mode number ($M = N = 200$). A similar examination is carried out here for the two-beam-plate coupled system. Unlike the single-beam-plate structure, the difference in response predictions is investigated here using other known numerical analyses. In Chapter 5, the Fourier technique was introduced to find the response of the coupled structure consisting of two beams and a rectangular plate and the results of this technique can be used for comparison. Comparing the difference between two methods, it is expected that the appropriate number of modes necessary for the frequency range of interest (5.6 - 1412 Hz) can be ascertained.

It can be expected that the number of modes required for the two-beam structure can also be used reliably for the equivalent four-beam structure of similar dimensions. The four-beam structure is actually stiffer than the two-beam case suggesting that fewer modes should be required, or conversely that for a given number of modes the accuracy should be better than that of the two-beam case.

The two-beam structure considered is shown in Figure 5.2. All material properties and dimensions are the same as for the four-beam structure (Table 6.1). Also sliding boundary conditions were assumed as described previously. The relevant matrix equations are shown in section 6.2.1. However, as there are no beams along the y direction, the corresponding mass and stiffness beam contributions should be zero.

In the Fourier approach the wavenumber range considered in the calculation is defined in terms of the non-dimensional wavenumber $\gamma = k_x / k_b$ where $k_x = n\pi / L_x$ and n is the number of half-cosine waves along the beam length L_x (see sections 3.2.2 and 3.4.1). Clearly, extending the range for the Fourier transform produces better results. However, it also requires much more computation time and it was shown that a range of $\gamma = \pm 15$ results in less than 0.01% error in the amplitude at 5.6, 100 and 1412 Hz for the present (single beam) coupled structure (see Figure 3.11). Thus, in the present case, a total of 129 Fourier coefficients is used which corresponds to a non-dimensional wavenumber range of $\gamma = \pm 15$ at 1412 Hz.

An external unit force is applied at $x = 0$ of beam 1 as shown in Figure 5.2. To compare the results of the modal method with those of the Fourier technique a spatially averaged kinetic energy estimate of the plate is used as in Chapter 2. To obtain this 20 points are randomly selected on the plate. Assuming the Fourier technique is an exact result for this problem, the difference E_ω is defined by

$$E_\omega = E(\omega) = \left|\langle T_F(\omega)\rangle - \langle T_{MN}(\omega)\rangle\right| / \langle T_F(\omega)\rangle \tag{6.8}$$

where $\langle T_F(\omega)\rangle$ is the space-averaged kinetic energy of the plate based on the Fourier technique and $\langle T_{MN}(\omega)\rangle$ is that with the maximum mode number MN based on the modal method. Then, equation (2.57) can be used to give the error e in dB, which is expressed in terms of the frequency-averaged difference $\overline{E}_\omega$.

First, the space-averaged kinetic energy using the Fourier method is shown in Figure 6.3 in terms of a narrow frequency resolution. The plate has about 500 modes in this frequency range, the modal density being about 0.4.

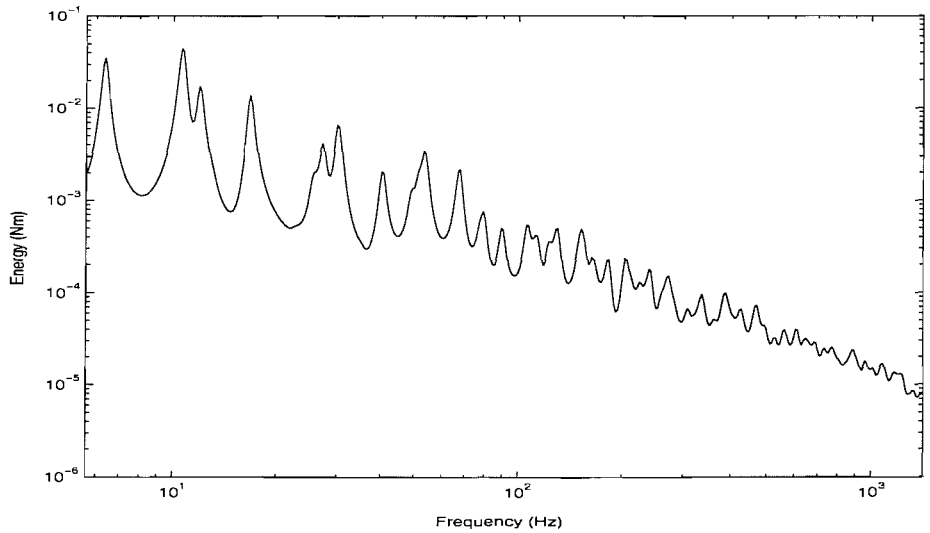

Figure 6.3. Kinetic energy averaged over 20 points of the plate of the coupled system as in Figure 5.2. Excitation at x = 0.0 m, y = 0.0 m (beam left hand end). Maximum component number of n = 128 is used in the Fourier series based on the non-dimensional wavenumber range of $\gamma = \pm 15$ at 1412 Hz.

The decibel difference e between the modal method and Fourier method is evaluated for different values of the maximum mode number in the x direction (M) and the maximum mode number in the y direction (N). The mode numbers were chosen to be at intervals of 2. Similar to section 2.6.1, the error e is considered in various one-third octave bands for the convergence investigation. The bands considered have centre frequencies of 20, 100, 1000 and 1250 Hz.

The error distribution corresponding to the centre frequency of 100 Hz is shown in Figure 6.4. As expected, while the error gradually reduces in the y direction, the reduction in the x direction is rapid at small mode numbers reaching a minimum at $M = 8$. The normalised wavenumber in terms of the beam free wavenumber of the one-third octave centre frequency, corresponding to the trough at $M = 8$, is about 3.

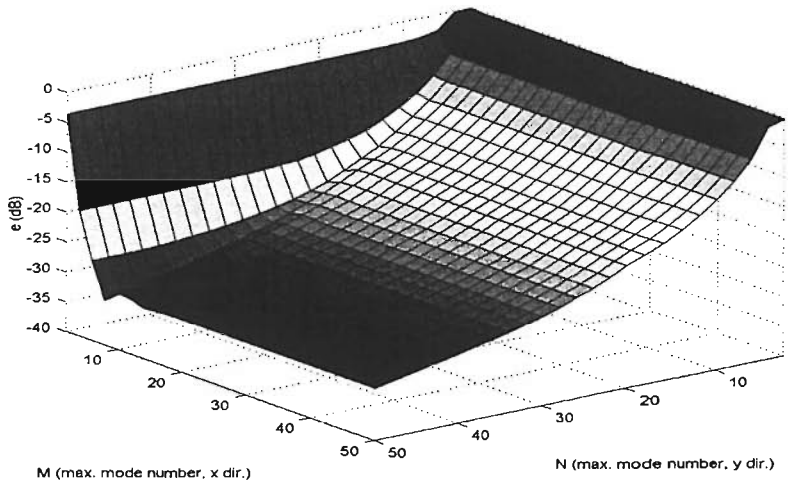

Figure 6.4. Error of the one-third octave band average in the modal method compared to the Fourier technique (f_c = 100 Hz). The results are shown as a function of the maximum mode number.

The error distribution in the one-third octave band with centre frequency of 1 kHz is shown in Figure 6.5. The error is greater for a given maximum mode number due to the shorter wavelengths present at higher frequencies.

A trough occurs at $M = 10$, at which the normalised wavenumber with respect to the free beam wavenumber gives a factor of about 1. The two stiffer beams lying in the x direction have a dominant influence on the motion in this direction, whereas one needs a higher number of sliding modes in the y direction to get a good prediction.

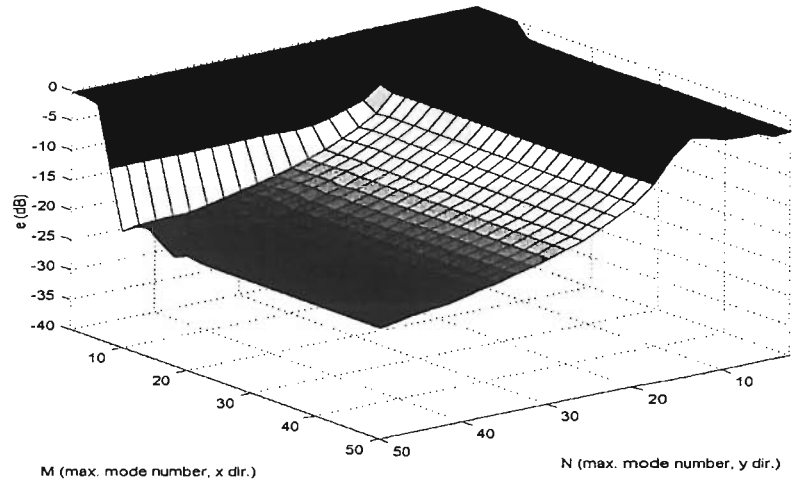

Figure 6.5. Error of the one-third octave band average in the modal method compared to the Fourier technique (f_c = 1 kHz). The results are shown as a function of the maximum mode number.

The non-dimensional wavenumbers $\gamma_{p,x}$ and $\gamma_{p,y}$ introduced in equation (2.58) are also adopted to find the criteria for the convergence less dependent on the frequency range. The error shown in Figure 6.4 is replotted using contours in Figure 6.6 as a function of the non-dimensional wavenumbers. The thick line is shown to indicate the mean error of about –20 dB (= 1%).

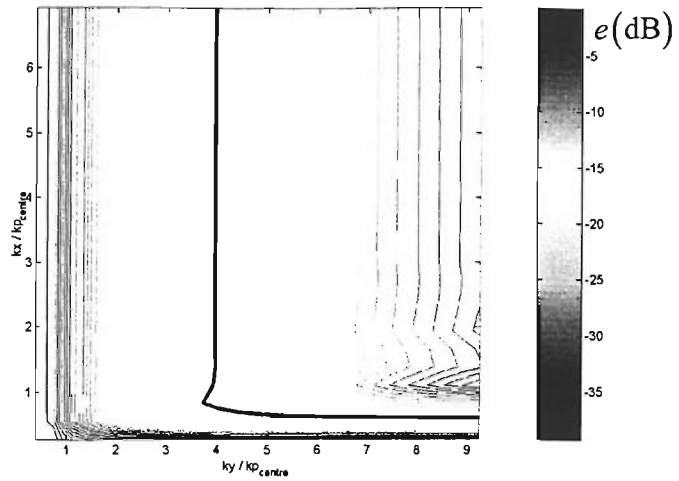

Figure 6.6. Contours of the one-third octave band average error as a function of the non-dimensional wavenumbers in the modal solution (f_c = 100 Hz).

Another example of contours is shown in Figure 6.7, which gives the mean errors at the centre frequency of 1 kHz shown in Figure 6.5. The thick line also indicates the error of about –20 dB.

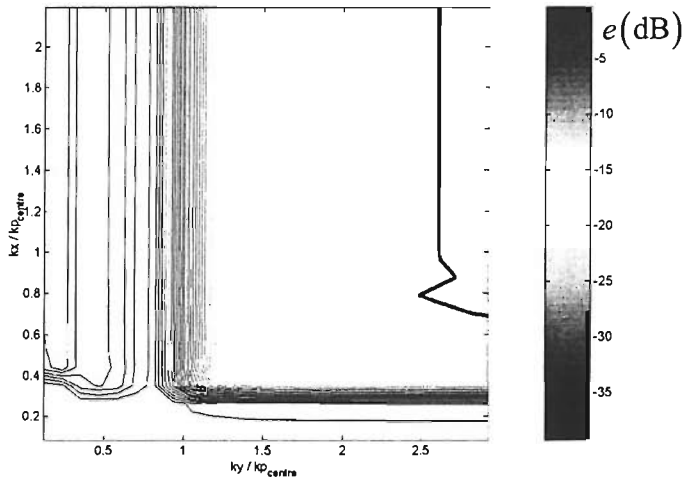

Figure 6.7. Contours of the one-third octave band average error as a function of the non-dimensional wavenumbers in the modal solution (f_c = 1 kHz).

In both Figures 6.6 and 6.7 the mean error of –20 dB occurs at around $\gamma_{p,x} \approx 0.8$ and $\gamma_{p,y} \approx 2-4$. Similar results are found for the centre frequencies of 20 and 1250

Hz. Thus, the introduction of the non-dimensional wavenumber seems useful for this two-beam-plate system as well as for the single beam system to predict the accuracy of the response independent of frequency. As the beam motion governs the plate motion in the x direction parallel with the beam, using the wavenumber ratio of $k_p/k_b = 3.18$ in the present case, a particular non-dimensional wavenumber to give the error of –20 dB is chosen, similar to the single beam situation (see section 2.6.1). The results are summarised in Table 6.2, where the minimum M and N are chosen to give the non-dimensional wavenumbers presented in the table. Selecting $M \times N = 21 \times 50$ results in the mean error of –27.4 dB (0.18 %) for the whole frequency range of 5.6 – 1412 Hz.

Table 6.2. Relationship between the maximum mode number and non-dimensional wavenumber in various one-third octave bands for a mean error of –20 dB.

f_c	$\gamma_{p,x}$	$\gamma_{p,y}$	M	N
20 Hz	0.7	2.2	3	4
100 Hz	1.2	3.9	9	22
1000 Hz	0.8	2.6	19	45
1250 Hz	0.8	2.6	21	50

Subsequently in the present study dealing with the framed structure $M = 50$ and $N = 50$ have been chosen for computations as the computational time is acceptable. These correspond to a maximum plate wavenumber of 2.5 times the free plate wavenumber at the maximum frequency (and eight times that of the beams). It is expected that, for the four-beam coupled structure, the accuracy may increase as two other beams are attached which are stiffer than the plate and hence govern the coupled structural behaviour. Thus, it is expected that if $M \geq 50$ and $N \geq 50$ then the error will be less than 0.18%.

6.2.4 Numerical result of four-beam-plate coupled system

The four-beam structure shown in Figure 6.1 is analysed using the modal procedure represented in section 6.2.1. Firstly the point mobility of the coupled structure is obtained when a harmonic point force of unit magnitude is applied at $x = 0$, $y = 0$, the joint of beams 1 and 4. The response is compared with a finite element (FE) model prediction in Figure 6.8. The beam in the FE model is modelled using Euler-Bernoulli beam elements (400 elements) and the plate with shell elements (9804 elements) corresponding to at least 8 elements per plate free wavelength ($\lambda_p = 0.074$ m at 1412 Hz) and all plate edges and the ends of the beams are also assumed to be in sliding conditions. The result of the modal method shows an excellent agreement with that of the FE model, the latter itself also being an approximate numerical solution.

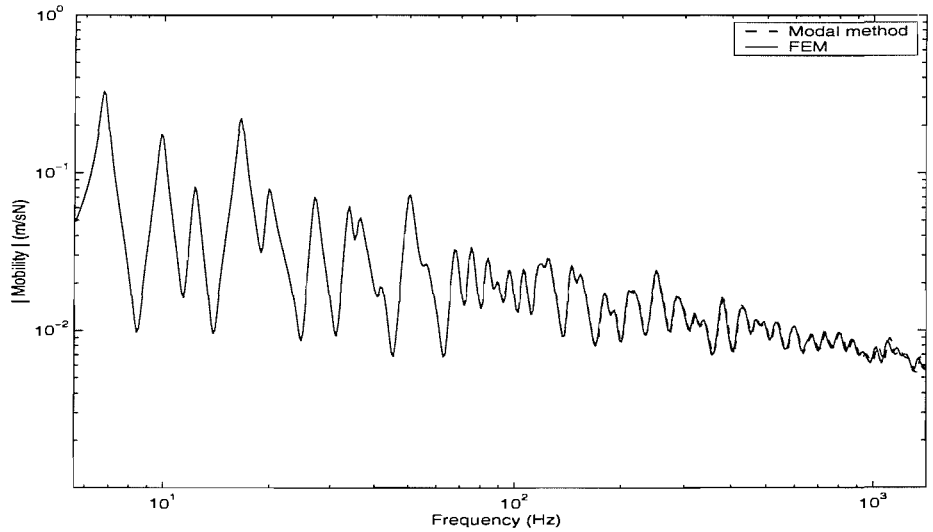

Figure 6.8. Point mobility of four-beam-plate structure obtained using the modal method and the FE method (excitation at $x = 0$).

Also an example of the transfer mobility comparison with FE is shown in Figure 6.9, also giving good agreement.

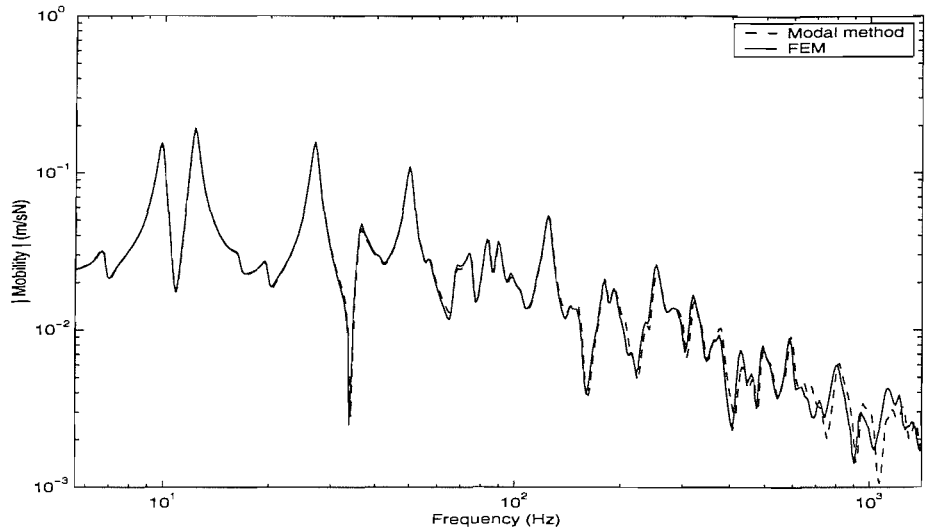

Figure 6.9. Transfer mobility of four-beam-plate structure obtained using the modal method and the FE method (excitation at $x = 0$, response at $x = 0.51, y = 0.51$).

Although the modal method requires significant computational time and resources, it produces excellent responses. These results are used in the following section to compare with a further development of the wave method.

6.3 Analysis of four-beam-plate coupled system using a wave approach

6.3.1 Wave approach

In Chapters 4 and 5, and the previous work of Grice and Pinnington [41], it was shown that a wave approach can conveniently be used for the analysis of a simple coupled structure such as a beam and a plate under certain assumptions. The most important restriction is that the wavenumber of the plate should be at least about twice as large as that of the beam.

The wave method has also been applied to a more complicated system, where a box structure was investigated using the concept of the wave approach, although the spine structure was modelled using the FEM [55].

In this section, the framed structure consisting of four beams and a rectangular plate is investigated. The beams possessing the long wavelength waves are modelled by the wave method instead of the FEM. As in the previous section the beams are assumed to be infinitely stiff in torsion so that the edges of the plate are effectively in sliding. For such boundary conditions on the opposite edges of the plate, the approximate wave impedance of the plate is given by equation (4.33), in which $\tilde{r} = 1$ for a sliding condition.

It should be emphasised that the terminology *width* in the discussion of the wave method is always used to mean the dimension in the direction normal to the beam axis and the *opposite edge* refers to the plate edge parallel to the attached beam whatever the orientation of the beam. Thus, L_y in equation (4.33) is the width of the finite plate between the beam axis lying at $y = 0$ and the opposite edge lying at $y = L_y$. If the plate is infinitely wide so that $L_y = \infty$, then the approximate impedance of the plate is simply presented by equation (4.23).

The general dispersion equation for the built-up structure is given by equation (4.34). Note that, as equation (4.33) includes the plate trace wavenumber $\tilde{k}_y$, an iterative method is required to find the coupled beam wavenumber $\tilde{k}_x$ in solving equations (4.34) and (4.33). Muller's method is used as before to get improved results (see Appendix B). Also, the plate impedance corresponding to the travelling wavenumber in the beam is used. Once the coupled beam wavenumber is found, the motion of the finite beam possessing the coupled wavenumber can be represented by equation (4.35).

6.3.2 Coupled structure consisting of four beams: application of the wave method

If it can be assumed that most of the power due to excitation on the beam is dissipated in the plate and only a small fraction of the power is transferred to other beams, then it may be possible that the framed structure consisting of four beams and the rectangular plate can be represented by a system consisting of the four beams each having the coupled wavenumber due to the plate impedance. Then such a system can be modelled simply using the wave method. The structure physically satisfying the above assumption is realised in Figure 6.10. In the figure, the width of the plates attached to beams 1 and 3 is L_y and for the plates attached to beams 2 and 4 the width is L_x.

As sliding edges are assumed in the framed structure in Figure 6.1, the same sliding boundary conditions are used at the opposite edges for the structure shown in Figure 6.10. This may result in different responses compared with those of the framed structure, as in fact the opposite edges should be attached to other beams. However, if the assumption explained above holds, it is expected that their influence will be reduced and although affecting the individual frequency behaviour this approach might still be useful for the mean response calculation.

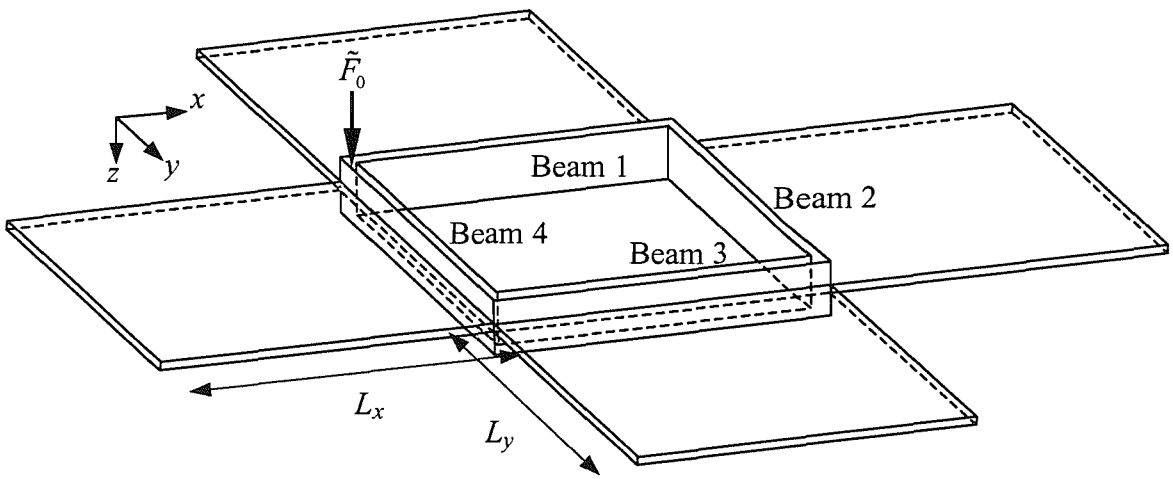

Figure 6.10. Configuration of the coupled structure for the use of the wave method.

The external force is applied at the corner of beam 1 and beam 4. As the coupled beam wavenumber to be used in modelling is based on the assumption that the opposite edges of the plates shown in Figure 6.10 are sliding, equation (4.33) is used in equation (4.34). Also, it is assumed here that beams 1 and 3 are identical with the same (coupled) wavenumber $\tilde{k}_x$ and that beams 2 and 4 are identical with wavenumber $\tilde{k}_y$, although they could be different, as considered in Chapter 7.

The method for obtaining the response using the wave model is similar to that given in Appendix D. This describes a frame of four beams in which no plate is attached to the beams. Thus the beams possess the free beam wavenumber, $\tilde{k}_b$. The boundary conditions of the wave model consisting of four beams are also explained and these are the same as those used in the modal model in section 6.2. In order to model the structure shown in Figure 6.10, only the coupled wavenumber obtained from equation (4.34) needs to be substituted for the uncoupled beam wavenumber in the method of Appendix D.

6.4 Numerical analysis of four-beam-plate coupled system

6.4.1 Mobilities

As explained in the previous section, the wave approach is an approximate method and it is necessary to compare its results with other known methods. In section 6.2, the modal method and its numerical examples were shown for the framed structure and this gives good results. Thus the results based on the wave method are compared here with those of the modal method. The highest modal order used in the modal method is 50 ($M = N = 50$, see section 6.2.3)

The first step in the wave analysis is to determine the wavenumbers of the corresponding subsystems of the coupled structure. Firstly the coupled beam

wavenumbers k_x, k_y and the corresponding uncoupled wavenumbers are shown in Figure 6.11. It can be seen that, although the wavenumbers k_x and k_y follow the same asymptotic line, corresponding to a beam coupled to a semi-infinite plate, their peaks and troughs are different as the plate widths are different.

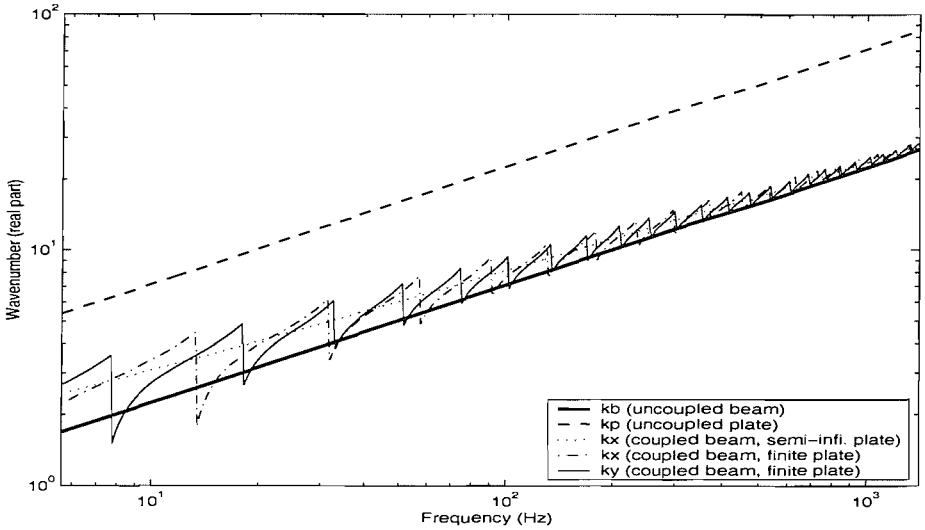

Figure 6.11. The coupled beam wavenumber k_x, k_y and the related wavenumbers.

It is interesting to compare the point mobilities of the two structures of Figures 6.10 and D.1 so the effect of the plate can be understood. They are compared in Figure 6.12, in which the result of the structure from Appendix D is the same as given in Figure D.2. It can be seen that there are many more resonance peaks when the plate is attached, due to the coupling with plate modes. However, one can also see that (i) the average vibrational level significantly decreases and (ii) the height of the peaks and troughs is reduced. This is likely to be because the plate behaves like mass and damping attached to the beam, as explained in Chapter 4.

An asymptotic representation for the point mobility shown in Figure 6.12 may be useful to understand the effect of the plate. The asymptotic line of the point mobility of the framed structure can be obtained by making two adjacent beams semi-infinite in the structures shown in Figures 6.10 and D.1; the other two beams are in fact removed. Thus, for example beams 1 and 4 remain in Figure D.1 if an

external force is applied the joint of those beams. The point mobility of such a system consisting of two semi-infinite beams joined at right angles can be found in the same way as explained in Appendix D, except that amplitudes of the reflected waves in equation (D.1) should be zero. The sliding condition of the joint is not changed. The relevant equation of the point mobility is given by

$$\tilde{Y}_0 = \frac{i\omega\tilde{w}(x=0)}{\tilde{F}_0} = \frac{(1-i)\omega}{4\tilde{D}_b\tilde{k}_b^3} \tag{6.9}$$

where $\tilde{k}_b$ is the beam wavenumber when the system is not coupled to plate. This is the same result as for an infinite beam.

The effect of the semi-infinite plate coupled to the beams can be realised by replacing $\tilde{k}_b$ by the coupled beam wavenumber $\tilde{k}_x$ which is obtained in equations (4.23) and (4.34). In such a situation the two plates coupled to beams 1 and 4 in Figure 6.10 are infinite in their respective width direction. Thus, the semi-infinite plates do not physically surround the joint where the two beams meet. However, as the plate mostly behaves strip-like in the width direction, it is expected that equation (6.9) with $\tilde{k}_x$ obtained from the semi-infinite plate represents the asymptotic point mobility of the four-beam-plate structure.

The asymptotic lines for the point mobilities of the framed structures shown in Figures 6.10 and D.1 are also shown in Figure 6.12. It seems that they represent the general tendency of the corresponding point mobilities very well. It can be seen that the coupled plate reduces the response level because of the added mass effect. This effect however decreases with increasing frequency as the effective mass due to the plate reduces (see also Figures 3.14 and 4.7).

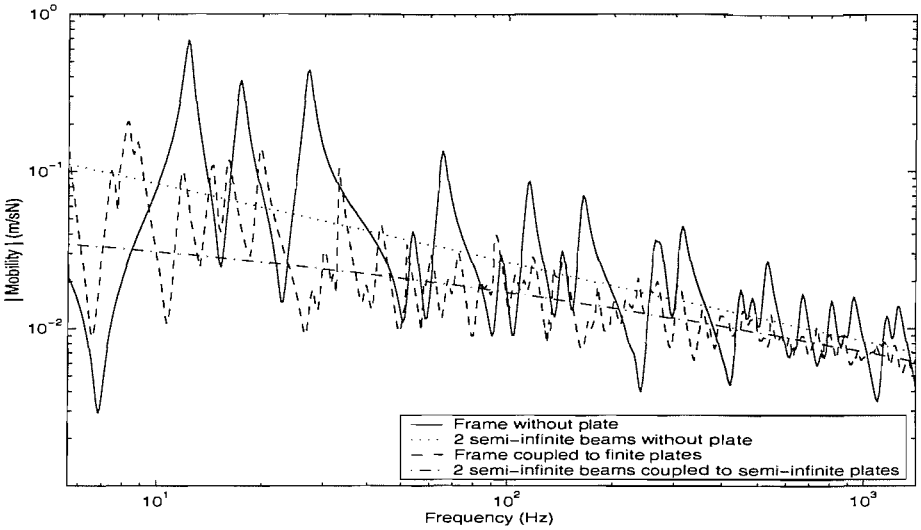

Figure 6.12. Point mobility comparison of the plate-coupled structure as in Figure 6.10 and the structure consisting of only four beams as in Figure D.1 (based on the wave method, excitation at $x = 0$).

The point mobility of the coupled system is compared with that predicted by the modal method in Figure 6.13. It can be seen that the results are in good agreement at high frequencies, although at lower frequencies there are detail differences between the two methods. This will be discussed later.

It is also interesting to compare these point mobilities with that obtained when semi-infinite plates are assumed connected to the beam framework. The semi-infinite plate is realised by letting the width of the plates shown in Figure 6.10 be infinite and the corresponding wavenumber can be found using equation (4.23) instead of equation (4.33) in equation (4.34). This wavenumber is shown in Figure 6.11. One can see that the point mobilities in Figure 6.13 oscillate around the line obtained using the semi-infinite plates. It seems that most of the peaks may occur due to the oscillating finite plate. The damping added to the beams increases when the semi-infinite plate is introduced, resulting in a behaviour of the coupled structure similar to a heavily damped beam. It is known that the attached plate with a short wavelength behaves like a mass and damping on a beam possessing a long wavelength, such an arrangement acting as a fuzzy structure [42, 46].

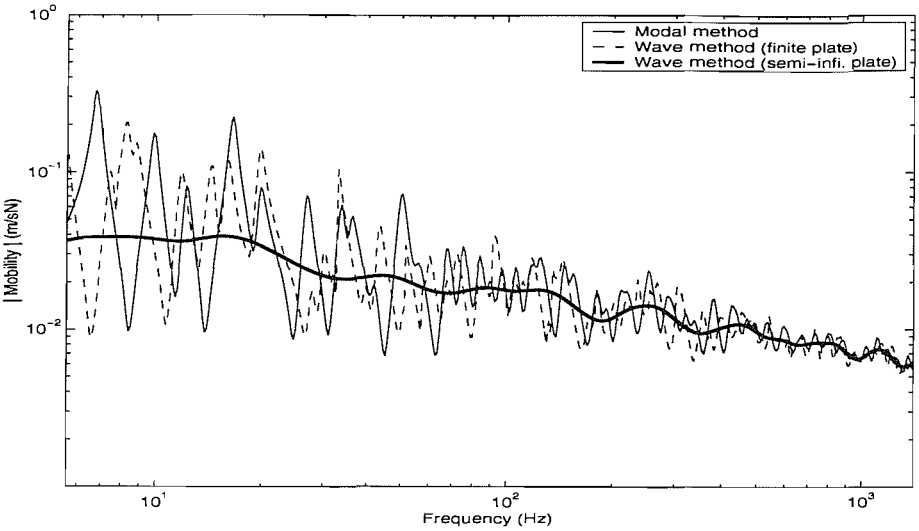

Figure 6.13. Point mobilities of the coupled structure as in Figure 6.10 based on the wave method and the modal method (excitation at $x = 0$).

6.4.2 Power investigation

An investigation of the power transfer in the system is important, as the wave model is based on the assumption that most power is dissipated in the plate. Thus, first, the power transferred from the beams to the plate, equal to the dissipated power in the plate, is investigated. For the wave method the power transferred is the sum over all four attached plates (similarly the plate energy is also found from the sum of the energy of each plate).

Since the exact location of resonance peaks is of less interest than a frequency band average result in a mid-frequency analysis, the power transferred from the four beams to the plate based on the wave and modal methods is compared in terms of one-third octave band averages in Figure 6.14. Although it was expected that the result based on the wave method underestimates, in fact the average values of the two methods agree, especially at high frequencies. The differences below about 60 Hz may occur because of differences in global modes between the structure shown in Figure 6.10, assumed for the wave method, and the framed structure used in the modal method (Figure 6.1). Thus the assumptions used for the wave method do not

appear to be appropriate for calculating the low frequency response and subsequent coupling power.

The average values are also compared with the result where attached semi-infinite plates are considered. Very good agreement can be observed at high frequencies.

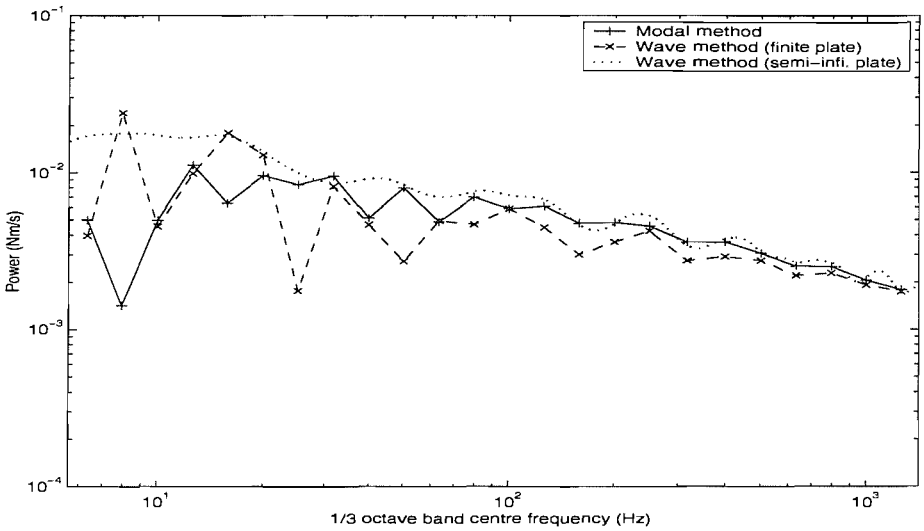

Figure 6.14. Power transfer from four beams to the plate in one-third octave bands (point force is applied at $x = 0$).

The results shown in Figure 6.14 imply that the average power transfer is hardly influenced by changes in the plate width. This is verified here by simply changing the plate width. The width of each plate attached to the beams is doubled. Note that the coupled wavenumbers are also changed. The results are shown in Figure 6.15. As expected, they show close agreement except at low frequencies, even though the width of all plates is changed. Small differences may occur because the larger plate is equivalent to greater damping on the beam.

In addition to the width change, the effect of a boundary condition change is also investigated. The opposite edge of each plate, parallel with each beam is now assumed to be simply supported. This is realised by changing the complex reflection coefficient $\tilde{r}$ in equation (4.33) to -1 and thus the coupled beam wavenumbers $\tilde{k}_x$ and $\tilde{k}_y$ are changed. The numerical result for this situation is also

shown in Figure 6.15, which is in good agreement with others above about 50 Hz. The differences found at low frequencies are clearly due to the different boundary condition considered. Thus, it can be said that the plate width and the boundary condition of the opposite edge far from the beam does not have critical effect on the mean power presentation, at least above about 50 Hz.

It is interesting to recall that the modal overlap factor for the plate is greater than unity above about 50 Hz. Thus, above this frequency the plate may be regarded as a system having high frequency motion, whilst the beams are still in their low frequency region. Consequently, it can be said that in this mid-frequency region of the present system the power transferred to the plate is in good agreement between the modal and wave methods.

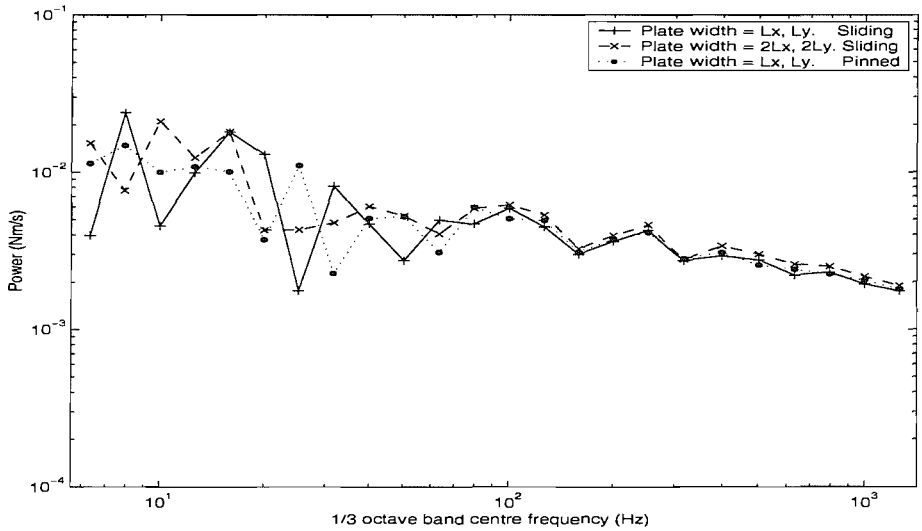

Figure 6.15. Power transfer to plate in one-third octave bands when the plate width and the boundary condition of the plate opposite edges are changed (point force is applied at $x = 0$ of beam 1).

The total power input to the system based on the modal method and the wave method are compared in Figure 6.16 using the one-third octave band average. A very good agreement is found except at low frequencies. Comparing Figures 6.14 and 6.16, one can observe similar tendencies in the difference between two methods, suggesting that the differences in power transfer to the plate are actually due to differences in input mobility.

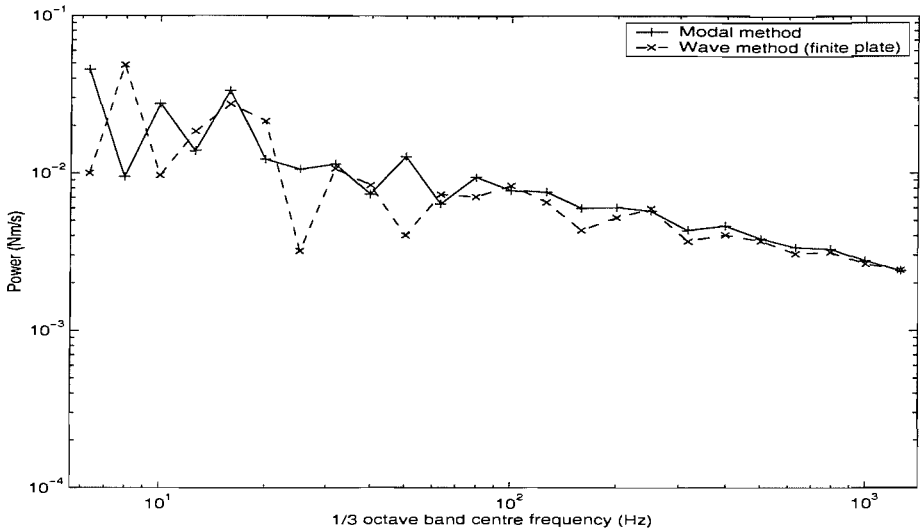

Figure 6.16. Input powers based on the modal method and the wave method in one-third octave bands (point force is applied at $x = 0$ of beam 1).

The power transfer from the four beams to the plate normalised by the input power is shown for the two methods in Figure 6.17.

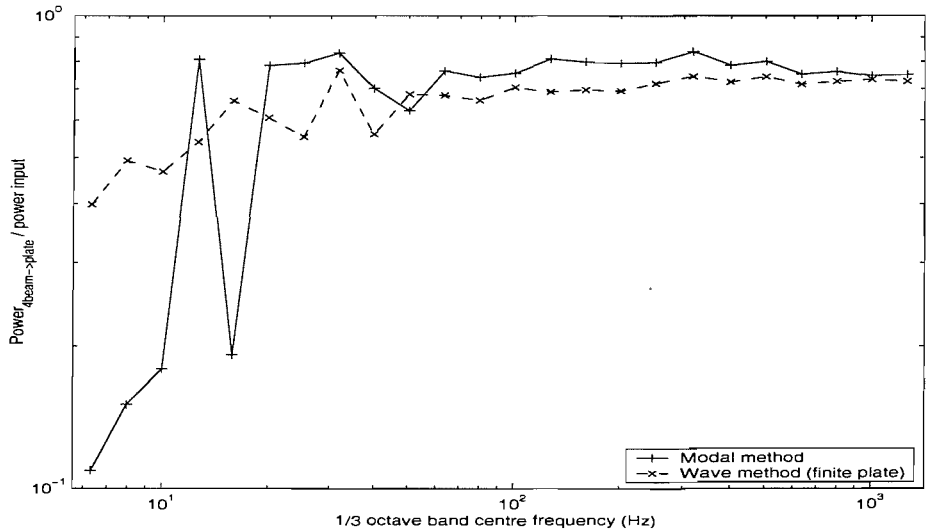

Figure 6.17. Power ratio (of power transfer from the four beams to the plate to the power input) based on the modal method and the wave method in one-third octave band average (point force is applied at $x = 0$ of beam 1).

Even though it is expected that the power transfer of the wave model is an underestimate, it can be seen that the ratios based on the wave method and the

modal method are in reasonable agreement above about 50 Hz. This means that the fully framed structure as in Figure 6.1, can conveniently be analysed for power transfer estimates using the wave method in terms of a mid-frequency analysis. However, it can be seen that the difference is large at low frequencies. This shows that the wave model is not appropriate to represent the motion of the framed structure at these frequencies.

Finally the power dissipated in each subsystem is investigated. It is expected that the dissipated power in each beam is small in comparison with the plate-dissipated power. Also, it is expected that the dissipated powers of each subsystem closely agree between the two methods. The corresponding result is shown in Figure 6.18, which is based on the modal model. One can see that the dissipated power in the plate is larger than the others at least by 10 dB. Thus it can be said that most power is dissipated in the plate. It is interesting to compare the powers dissipated in beams 1 and 4 with those dissipated in beams 2 and 3. Note that the point force was applied at the junction of beams 1 and 4 so that the power is directly transmitted to beams 1 and 4. However, the powers transferred from beam 1 to beam 2 and from beam 4 to beam 3 experience one junction, which may cause some power reflection.

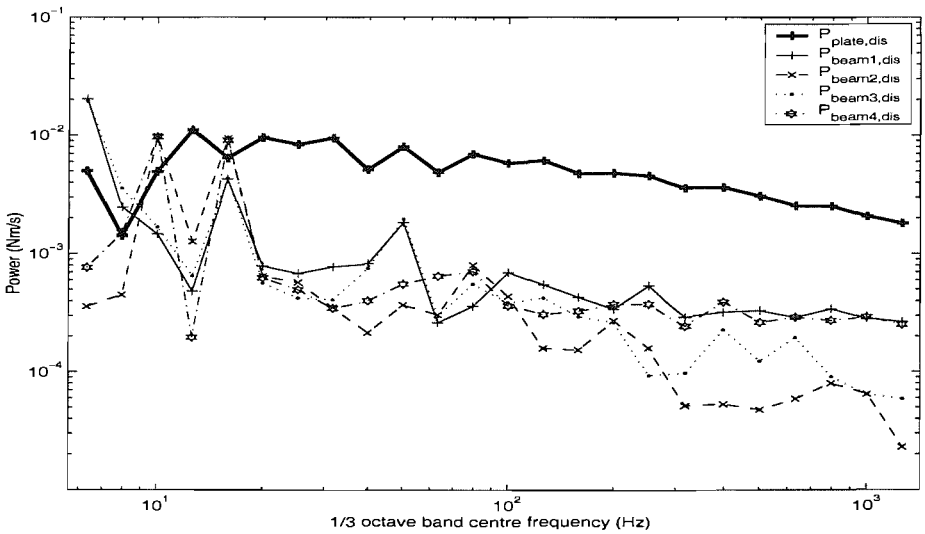

Figure 6.18. Power dissipated in each subsystem in one-third octave bands for the four-beam-plate system. Based on the modal method.

The powers shown in Figure 6.18 are then compared in Figure 6.19 with those found from the wave model. Again, recall that the power transfer to the plate tends to underestimate and the power dissipated in the beam tends to overestimate. Nevertheless, one can see that the levels are in quite good agreement above about 50 Hz and it seems that such an error due to the approximation in the wave method is negligible. The difference mostly occurs in beams 2 and 3. Although it was assumed that most power is dissipated in the plate, some power may be transferred to other beams through the plate in the framed system. However, in the wave model the plate does not physically connect the beams and thus, such power transferred through the plate cannot be described, which results in such a difference. Nevertheless, this difference is relatively small (at most about 5 dB). Consequently, it seems that using the assumption that the power transferred through the plate to other beams can be ignored still gives reasonably good results.

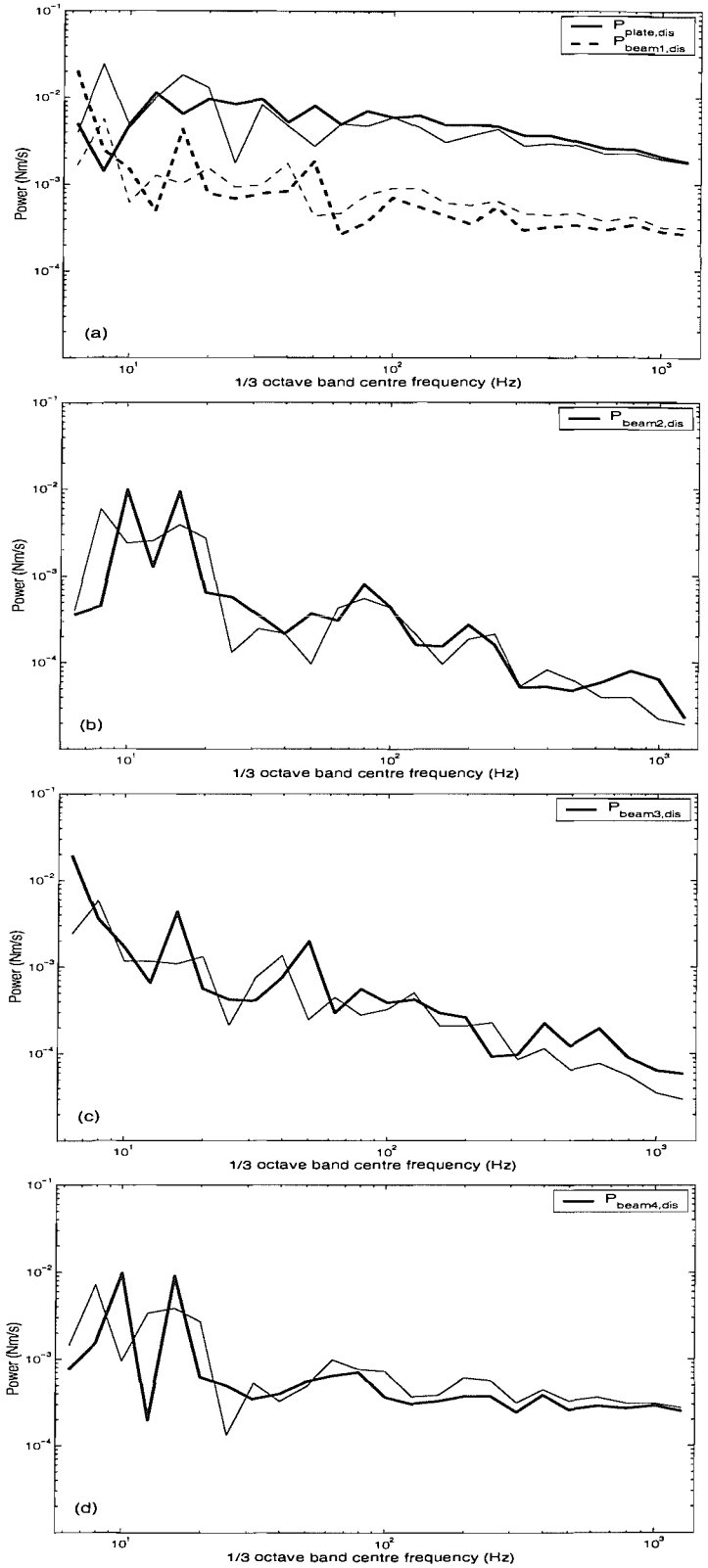

Figure 6.19. Power dissipated in each subsystem in one-third octave bands: comparison between modal method (thick line) and wave method (thin line) for the four-beam-plate system.

6.4.3 Confidence interval for the power transfer

Although good qualitative agreement has been found between the two methods, as seen in Figure 6.14, the magnitude of the fluctuations relative to the average should also be considered. One possible way is to compare the confidence interval of the response so that the distribution of the power in a certain frequency band can be indicated. For this, overlapping octave bands are used at one-third octave band intervals. It is expected that the confidence interval given in terms of octave bands shows smoother results than one-third octave bands. In each octave band 57 frequency data points are used.

The average value of the power is obtained for each octave band, $\overline{P}_{octave}$. Then the power at each frequency is normalised by the octave band average. The normalised power is calculated in dB as follows.

$$P_{dB} = 10\log_{10}\left(P/\overline{P}_{octave}\right) \tag{6.10}$$

where $P = P(\omega)$ is the power in a narrow band.

The 68% confidence interval of the normalised power P_{dB} is obtained explicitly for the results based on the modal method and the wave method. The results for the power transferred to the plate are shown in Figure 6.20. It can be seen that the confidence interval follows the narrow band power very well, although it is not symmetrical with respect to the mean.

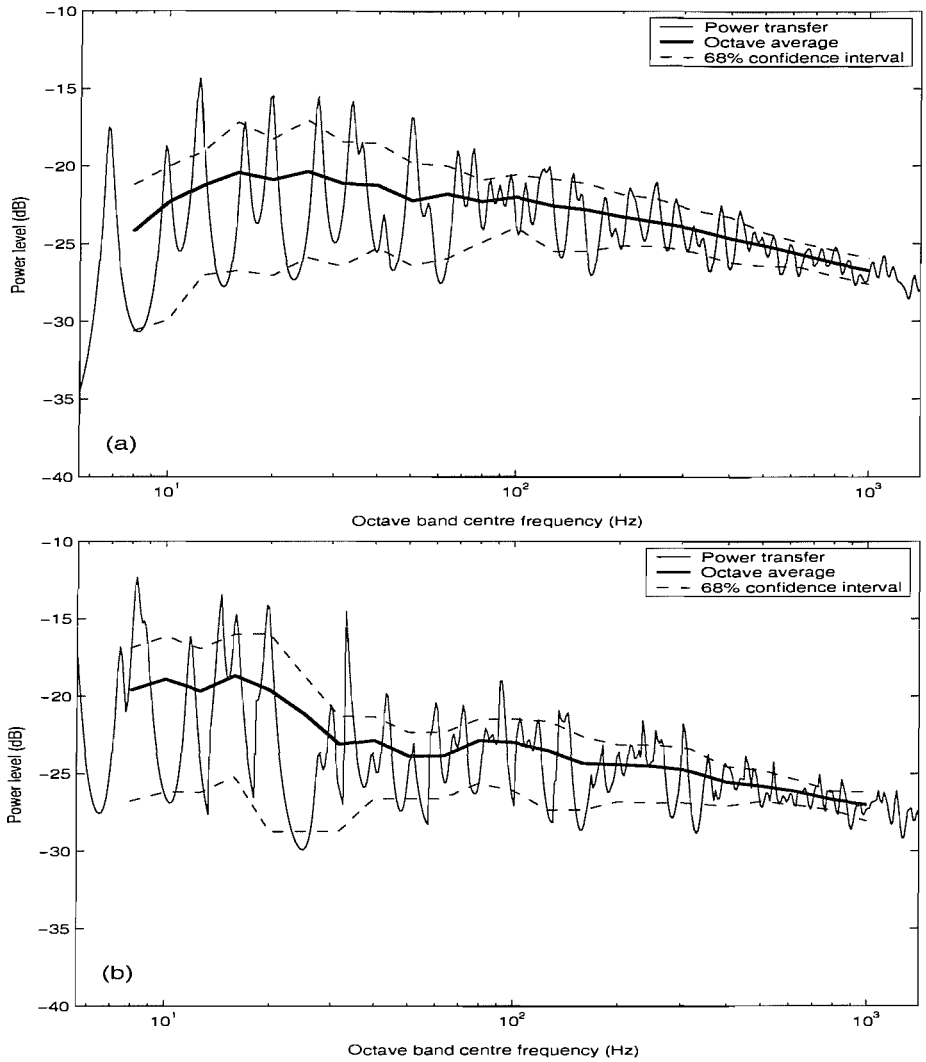

Figure 6.20. Octave band average and 68% confidence interval of the power transferred to the plate; (a) modal method (b) wave method (point force is applied at $x = 0$ of beam 1).

The confidence interval and the octave average shown in Figure 6.20 (a) and (b) are compared simultaneously in Figure 6.21. Comparing the confidence intervals one can see that they show good agreement at most frequencies especially at and above 80 Hz. The differences in the level between the two methods occur mainly because of the difference in the octave band average value; the confidence intervals are mostly similar in width for the two methods.

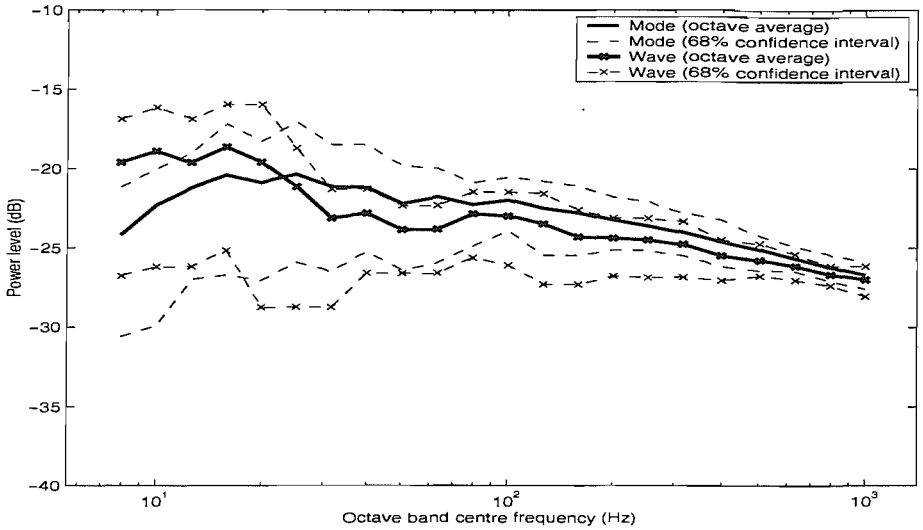

Figure 6.21. Octave band averages and 68 % confidence intervals of the power transferred to the plate based on the modal method and the wave method.

The numerical results indicate that the wave method is useful to obtain the response at mid and high frequencies. For example, the power transfer averaged in one-third octave bands is almost the same as that obtained using the modal method above about 50 Hz, even though it is an approximate result. To interpret this value of frequency, it may be noted that the stiff four-beam structure has only 4 resonance frequencies below 54 Hz (see Figure D.2). The plate has almost 20 modes below 50 Hz and the modal overlap is less than unity below about 50 Hz. Thus in this low frequency region, the wave method is no longer appropriate as a coupling technique of the spine and the receiver structures.

6.4.4 Computation time and computer resources

An important concern in practical applications is related to computer resources and calculation time. An example of a calculation time comparison for the framed structure is shown in Table 6.3. The Fourier method was used for two beams coupled to a rectangular plate, as it is not applicable to the framed system. Although the wave method can predict only approximate responses, it is very advantageous as it requires far less computer resources and time. Also, small

computation time is necessary in the Fourier method because a Fourier series is considered only in the x direction whilst the y direction follows the wave equation. One can see that wave method is the most efficient in terms of calculation time.

Table 6.3. Comparison of computational time (an Intel Pentium 4 computer (CPU 1500 MHz) is used in calculation) for the framed system of four beams and a plate.

	Computation time (min.)	Frequency range of calculation (Hz)	Comments
Modal method	1380	5.6 - 1412	$M = N = 50$
Wave method	0.1	5.6 - 1412	-
Fourier method	0.8	5.6 - 1412	$n = 128$ Two-beam-plate system
FEM	9	0 - 1412	431 modes used

For reference, the computational time required for the FE analysis is also given. In comparing the modal method and FE, it should be noted that the number of modes obtained by FE for the forced response is 431, which is much less than that used in the modal method (2601). Reducing the number of modes in the modal method results in much less computational time. For example, for the present case if 432 modes are considered in the modal method, the computational time significantly decreases to about 10 minutes. In addition, compiled FE code is used in the calculation whereas the other methods are solved by using uncompiled Matlab code.

6.5 Conclusions

A fully framed structure consisting of four beams and a rectangular plate was studied, where both ends of each beam and all the plate edges are assumed to be sliding. The vibrational response of the framed structure was first obtained using the modal method. Then the wave method was applied to the same structure to

obtain an approximate response. The results of the two methods were compared and useful observations and comments given.

The modal method was used to produce an analytical model of the framed structure, the corresponding generalised mass and stiffness matrices of which were found. The dependency of the response on the number of modes included in the calculation was investigated and the maximum mode numbers chosen were used for the modal model, which is considered to give an accurate response for the comparison with the wave model.

Although the modal method gives an accurate result, details such as exact natural frequencies are not of concern in the present study which deals with the mid and high frequencies. Thus an approximate method seems appropriate and the analytical model based on the wave method for the dynamic response of the framed structure was presented. The statistical responses such as one-third octave band averages and a confidence interval of the power were obtained as well as the narrow band response.

In comparison with the modal method it has been shown that the analytical wave model can conveniently be used for the estimation of the vibrational response in the mid and high frequency regions, even though the power transfer and dissipated power found based on the wave method only give an approximate result due to the inherent limitations of this method. For the present framed structure, the wave model gives good estimation above about 50 Hz. Below this frequency band the four-beam frame has only 4 modes and the plate has a modal overlap less than unity.

In the wave model, it is shown that the plate width and the boundary condition of the plate opposite edges are not very critical in obtaining the average power transfer in a certain wider frequency band. However, use of the semi-infinite plates loading the beam framework leads to an over-estimate of the damping of the

framework, although it allows a correct estimate of the power transferred to the plate to be obtained.

The calculation time of the various methods was compared for the framed structure. The wave method offers considerable advantage over the other methods in this respect although it provides an approximate response.

CHAPTER 7

EXPERIMENTAL STUDY OF COUPLED SYSTEMS

7.1 Introduction

Experimental studies have been carried out for the validation of the analytical and numerical models described in previous chapters. Experimental investigations concerning a single-beam-plate system have already been carried out by other researchers [41, 64] and hence in this chapter emphasis is placed on two-beam-plate and framed structures. The results of these are compared with the numerical analyses presented in Chapters 5 and 6.

The structures used in the experiments are made of acrylic (perspex). This is convenient as it is light and various configurations of the experimental structure consisting of stiff and flexible subsystems can easily be made. Also, the structural damping is higher than other materials such as steel. This may be advantageous for numerical predictions, such as in wave methods where convergence might be an issue. Although the nominal material properties of perspex are known [41], more accurate properties including Young's modulus and the structural loss factor were determined experimentally using beam samples.

The effect of a stiff beam on the plate wavenumbers was investigated by estimating the wavenumbers of the coupled plate system using a large set of measured transfer mobilities. The power input obtained experimentally was compared with numerical predictions using various models.

Whereas sliding boundaries were applied in the numerical analyses for convenience, in the experiments the boundaries are free. Consequently comparisons of quantities such as mobilities between models and experiment, particularly in narrow frequency bands, are not entirely appropriate. To overcome this, measured results are expressed in terms of kinetic energies and the ratio of

energies in various subsystems is compared with that obtained from the models. These results are expressed in terms of one-third octave band averages in order to assist comparisons where exact resonance frequencies do not match, and indeed are not of direct interest. The details are explained in the corresponding sections.

7.2 Experimental configurations

7.2.1 Coupled system

Each coupled system consists of a rectangular plate and two or four beams that are made of perspex. In each case the plate has a thickness of 2 mm and dimensions 1.0×0.75 m . Strips of width 6 mm are fixed using a stiff glue above and below the 2 mm plate to form beams which are symmetric about the plate centreline. Four coupled structures denoted C1 – C4 have been studied. The uncoupled plate is named C5. The beam dimensions for the different structures are presented in Table 7.1. These dimensions were measured using a micrometer at three locations on each beam. The averaged dimensions and their maximum tolerances are shown. The numbering of the four beams corresponds to Figure 7.1.

Table 7.1 Nominal dimensions of coupled systems used in measurement.

Sample No.	Type	Beam height and width (mm)					Comments
		h_1	h_2	h_3	h_4	b	
C1	Two-beam	23.7 ± 0.21	-	23.7 ± 0.21	-	6.0 ± 0.07	Two identical beams Beam on the long edge
C2	Two-beam	23.9 ± 0.33	-	14.1 ± 0.34	-	6.1 ± 0.23	Different beam heights Beam on the long edge
C3	Four-beam	23.6 ± 0.86				6.1 ± 0.11	Framed structure Four beams of same height
C4	Four-beam	24.1 ± 0.36	13.3 ± 1.11	13.3 ± 1.11	24.1 ± 0.36	6.0 ± 0.41	Framed structure Adjacent beams of same height
C5	Uncoupled plate (2 mm)	-	-	-	-	-	-

A representative configuration of the coupled structure (here, C3) and the cross-section of the beams are shown in Figure 7.1. The subscript corresponding to each beam is the number as shown in Figure 7.1 and as written in the table. Note that beam 1 is located at the bottom of the plate in this chapter, whereas it has been shown at the top in the figures in previous chapters. Thus, the two-beam coupled systems consist of parallel beams 1 and 3. Note that the dimensions of the subsystems are chosen such that the wavenumber ratio of the free plate wavenumber to the coupled beam wavenumber k_p/k_x is at least about 2. As the coupled beam wavenumber k_x is larger than the free beam wavenumber k_b it is expected that the free wavenumber ratio k_p/k_b should be somewhat larger than 2. For the present system C2, for example, the wavenumber ratios are $k_p/k_{b1} = 3.5$ for beam 1 and $k_p/k_{b3} = 2.7$ for beam 3. Thus, the requirement is met for these structures considered in the experiments.

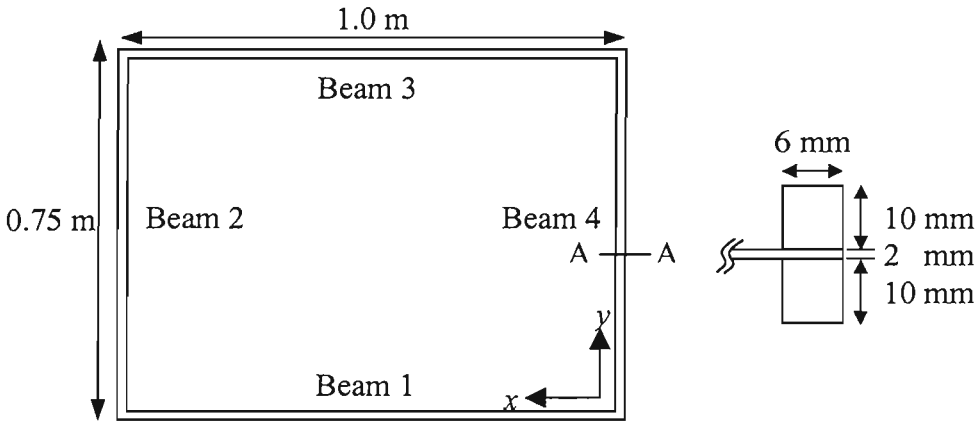

Figure 7.1. Configuration of coupled structure C3 consisting of four beams and a rectangular plate. The structure is shown in the photograph in Figure 7.4.

7.2.2 Beam samples

To determine the basic material properties of the perspex, four beams were prepared which were similar to those used in the coupled specimens (see Table 7.2). Two plate strips, samples U1 and U2, were prepared to obtain Young's

modulus and structural loss factor. Two beams, samples U3 and U4 were made of acrylic blocks of 6.0 mm width glued to the upper and lower faces of a plate strip, as shown in Figure 7.2. These correspond to the beams in the beam-plate systems considered in the previous section. The measured masses per unit length, densities and the nominal dimensions are presented in Table 7.2. A Poisson's ratio of 0.38 is used for the perspex as given in [41]. The procedure to obtain Young's modulus is explained in section 7.4.3.

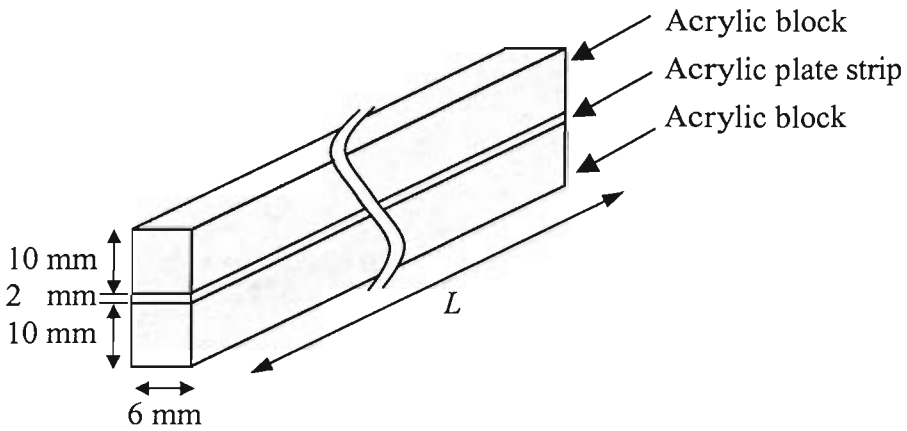

Figure 7.2. Configuration of the beams U3 and U4.

Table 7.2. Nominal dimensions and material properties of subsystems made of acrylic material (perspex).

Sample No.	Type	Size $L \times b \times h$ (mm)	Mass per length, m' $(\mathrm{kg\,m^{-1}})$	Density, ρ $(\mathrm{kg\,m^{-3}})$	Young's modulus, E $(\mathrm{GNm^{-2}})$
U1	Plate strip	600×6.6×2.0	0.0160	1212	4.28
U2	Plate strip	400×6.6×2.0	0.0160	1212	4.58
U3	Beam	1000 × 6.1 (± 0.35) × 22.8 (± 0.13)	0.161	1158	4.96
U4	Beam	1000 × 6.7 (± 0.15) × 14.3 (± 0.57)	0.106	1106	4.76

7.3 Experimental procedure

Two methods are used to measure mobilities. One consists of using an instrumented impact hammer and accelerometers. However, for the coupled systems where a large grid of points is required the use of accelerometers would give excessive measurement times. Furthermore, accelerometers would add mass loading to the thin plate. Instead, a scanning laser vibrometer was used which enables many points to be measured with excitation being provided by a shaker. In this section, the experimental procedure for the coupled structures using the laser vibrometer will be presented. The configuration commonly used throughout all the experiments is described. Additional detail will be mentioned later, as necessary, in the corresponding sections.

The structure to be measured was suspended vertically using nylon cord and an electrodynamic exciter located near the bottom of the structure. The laser vibrometer was positioned to cover all the area of the structure to be measured. The configuration is shown schematically in Figure 7.3 including the test instruments. Details of the instruments are listed in Table 7.3. Figure 7.4 shows a photograph of the experimental configurations, in which the coupled system C3 is suspended and the exciter is attached to beam 1 using a stinger. Beam 1 was located at the bottom of the experimental configuration.

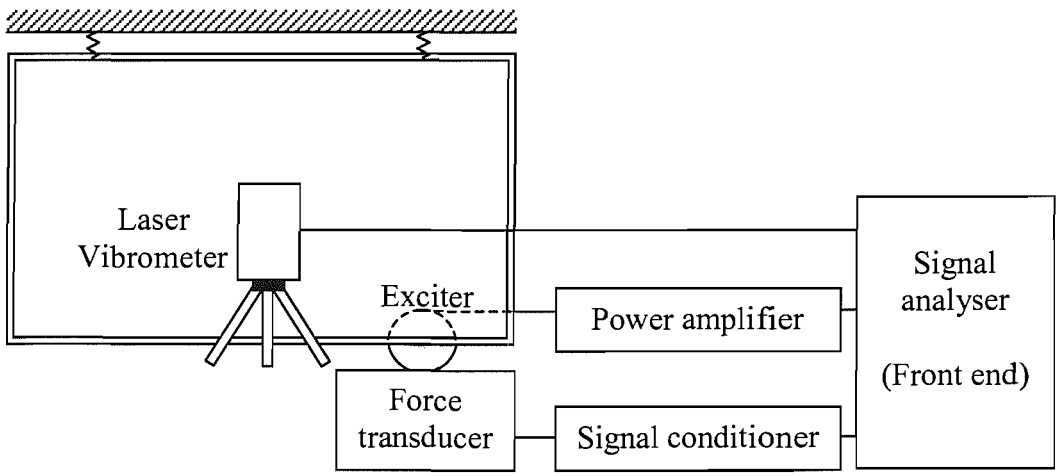

Figure 7.3. Instrumentation used for the measurement using laser vibrometer.

Table 7.3. Equipment used for measurement.

Equipment	Make / Model	Serial Number
Laser vibrometer	Polytec OFV 056	6012264
Front end	Polytec PSV-Z 040H	5015391003
Exciter	LDS V201	69439-5
Force transducer	PCB 208C01	20824
Signal conditioner	PCB 441A42	748
Power amplifier	Ariston AX-910	07000190

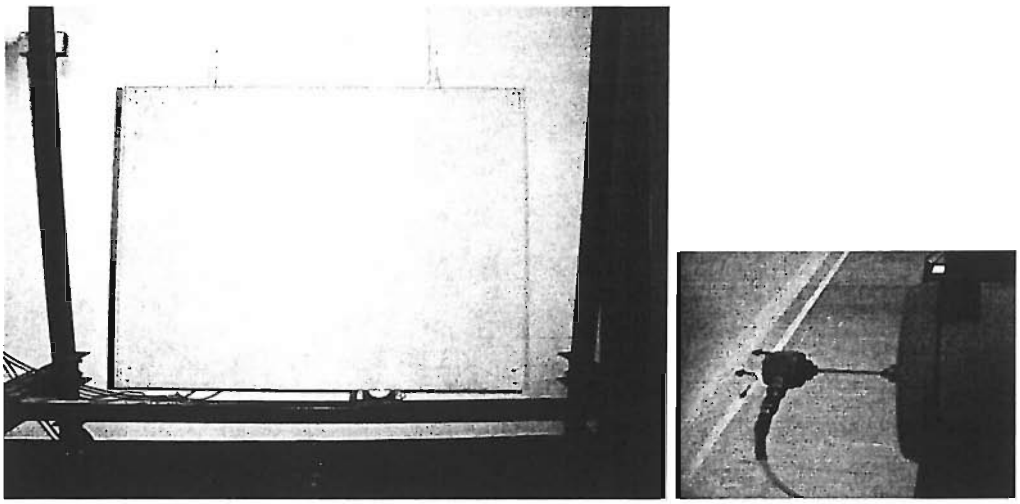

Figure 7.4. Experimental configurations for the measurement of mobilities (four- beam system C3) and the attachment of the exciter.

A pseudo-random force was applied at the centreline of beam 1 using the exciter as seen in Figure 7.4 and the force signal was measured by a force transducer. The exciter was located 0.36 m from the right-hand end of beam 1 (which is designated $x = 0$). This is an arbitrary location chosen part way along beam 1. The corner was avoided as it is shown in Appendix D that the sliding boundary conditions have a greater effect on the input power at the corners.

In most experiments the velocities of each response point were averaged over 20 data samples. However, the mobilities used for calculating the structural loss factor of the uncoupled systems were averaged 100 times for a more accurate response. The frequency range used for the predictions in previous chapters is 5.6 – 1412 Hz and the experiments were conducted to cover at least this range. For example, for the measurement of the mobility to be used in a subsequent energy calculation, the frequency range was 0 – 1.6 kHz and a 2.0 kHz low pass filter was incorporated in the software of the signal analyser (sampling frequency of 8.192 kHz). The frequency resolution was 1 Hz. However, in some cases the frequency range was changed depending upon the subsequent processing and calculations required.

Figure 7.5 shows an example of a measurement of the point mobility which demonstrates an excellent coherence.

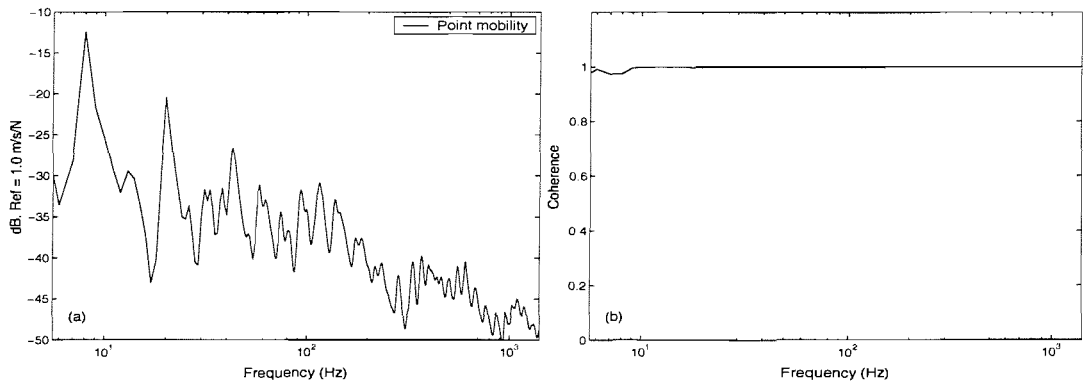

Figure 7.5. An example of point mobility and its coherence function for the two-beam coupled system C1 measured using shaker excitation and laser vibrometer. Force and response at $x = 0.36$ m of beam 1.

7.4 Measurement of material properties

Before considering experiments for the verification of the numerical models, it is necessary to determine some basic material properties of the structures, for example the structural loss factor and Young's modulus, to be used in the

numerical models. The experimental procedure and the corresponding results will be presented.

7.4.1 Measurement

Various methods can be used to determine the damping loss factor, such as the decay rate method [12] and an input mobility technique [41]. However, for a lightly damped system with low modal overlap, a half-power bandwidth technique [85] involving a natural frequency is convenient. Experimental samples U1 – U4 were used for obtaining the structural damping loss factor (DLF) based on the half-power bandwidth technique as they represent the subsystems of the coupled systems. Strictly the DLF of the plate should be obtained from sample C5. However, this is more difficult due to the high modal density of the plate. Thus plate strips U1 and U2 are used. Beams U3 and U4 additionally include the glue layers of the built-up beams. It is therefore interesting to compare their results with U1 and U2.

The experimental procedure was as explained in section 7.3 using the scanning laser vibrometer and exciter. The beams were suspended freely. The point force was applied at 0.25 m from the end of the beam in each case using a pseudo random signal. To obtain better results, separate frequency ranges of 10 – 800 Hz, 300 – 1250 Hz and 1.0 – 1.6 kHz were chosen and the responses were averaged over 100 data samples.

The Young's modulus of each uncoupled system can be found from the natural frequencies of the corresponding systems (the mass is already known). Thus the same experimental results can simply be used for this. Each beam was suspended at the 2 nodal points of the fundamental bending mode, which is important to get an exact Young's modulus (see section 7.4.3). However since motion was perpendicular to the suspension cords, their influence on other modes should be negligible.

7.4.2 Structural loss factor

Once the mobility is obtained, the structural loss factor can be calculated using the half-power bandwidth technique as [85]

$$\eta_n \simeq \frac{\Delta\omega}{\omega_n} \tag{7.1}$$

where ω_n is the n th natural frequency and $\Delta\omega$ is the frequency bandwidth corresponding to –3 dB from the maximum level. An example is given in Figures 7.6 and 7.7. Figure 7.6 shows a transfer mobility of the uncoupled beam U3, the maximum level at the natural frequency at approximately 131 Hz is marked by ◎ in Figure 7.7 with the horizontal line showing 3 dB lower than the maximum level. The DLFs of each uncoupled system were investigated in the same manner and the results obtained are summarised in Table 7.4.

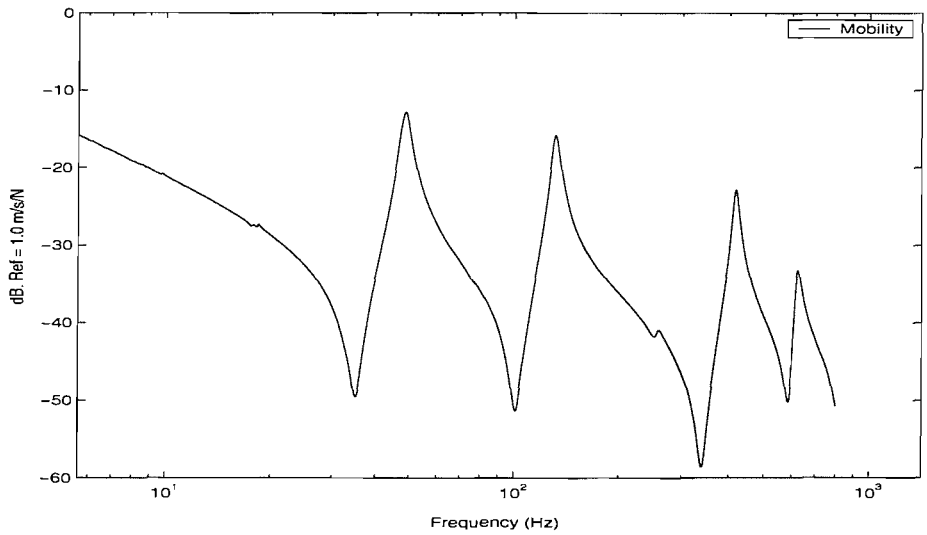

Figure 7.6. Transfer mobility Y of beam U3 for the loss factor estimation. $20\log_{10}(Y/\mathrm{Ref})$ with Ref =1.0 m/s/N. Force at 0.25 m and response at 0.4 m from the end of the beam (beam length L_x = 1.0 m).

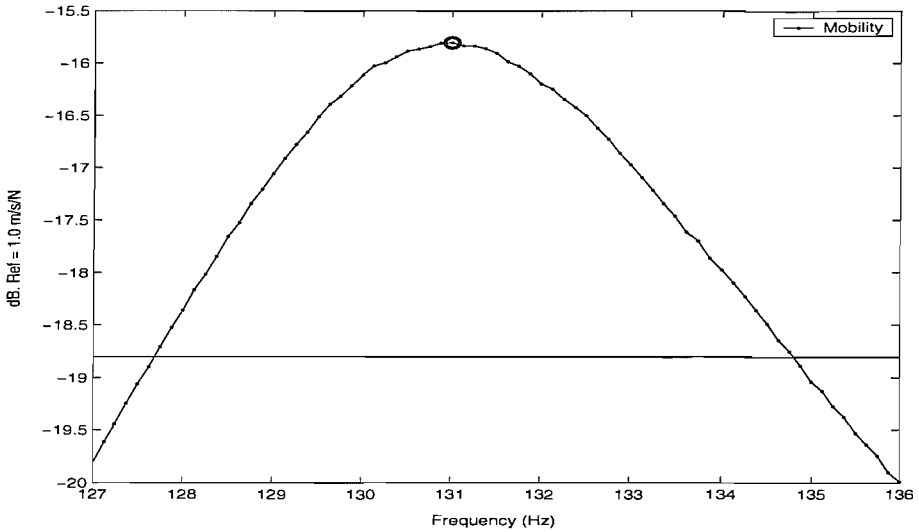

Figure 7.7. Selection of the frequency bandwidth based on half-power bandwidth technique (natural frequency $\simeq$ 131 Hz, beam U3).

Table 7.4. Structural damping loss factor η of uncoupled structures and the corresponding natural frequencies based on the half-power bandwidth method.

U1		U2		U3		U4	
f_n	η_1	f_n	η_2	f_n	η_3	f_n	η_4
56.5	0.062	53.8	0.065	48.5	0.069	30.5	0.075
108	0.056	144	0.053	131	0.055	78.9	0.065
178	0.051	316	0.062	416	0.042	252	0.061
391	0.058	739	0.042	623	0.046	384	0.053
662	0.040	1023	0.043	844	0.043	689	0.044
1013	0.042	1358	0.042	1099	0.041	998	0.040
-	-	-	-	-	-	1338	0.047

It is clear that the loss factors reduce with increasing frequency, in agreement with published results [41, 64]. Although they show a clear tendency in terms of frequency, it is impractical to use these values in calculating frequency-related power quantities. Interpolated values are therefore sought for practical application. A linear regression technique with respect to a logarithmically scaled frequency

($\log(f)$) has generally been used previously [41, 64] for DLFs and this is adopted here. The corresponding formula for the linear regression is given by [86]

$$\eta(f) = a_0 + a_1 \log(f) + e \tag{7.2}$$

where a_0 and a_1 are coefficients representing the intercept and the slope respectively, e is the residual and f is the frequency. The coefficients a_0 and a_1 can be determined to minimise the sum of the squares of the residual. The DLFs and their linear regression results are shown in Figure 7.8. Results for plate strips U1 and U2 are given together in a single regression; similarly for U3 and U4.

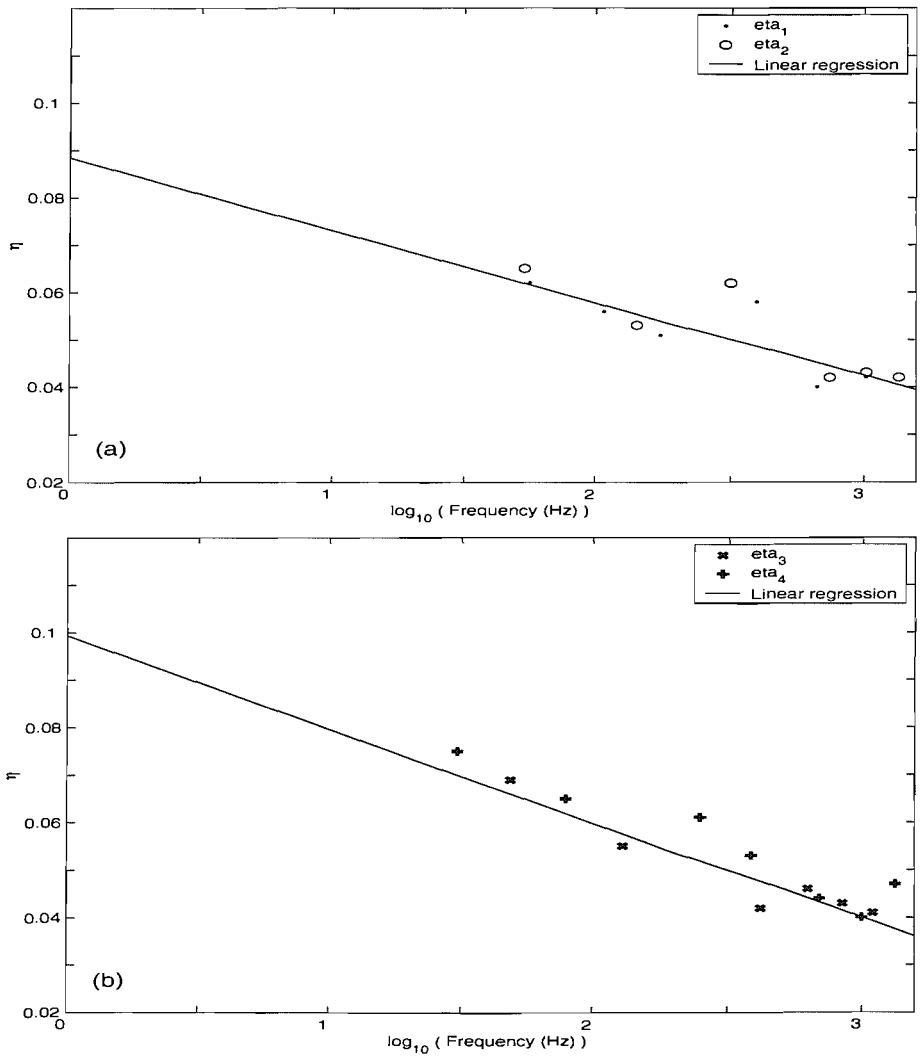

Figure 7.8. Structural loss factors and their linear regression results: (a) samples U1 and U2, (b) samples U3 and U4.

These structural loss factors are compared together in Figure 7.9. It seems that there is no clear difference between them. It may thus be concluded that the glue layers in beams U3 and U4 have negligible effect on the damping.

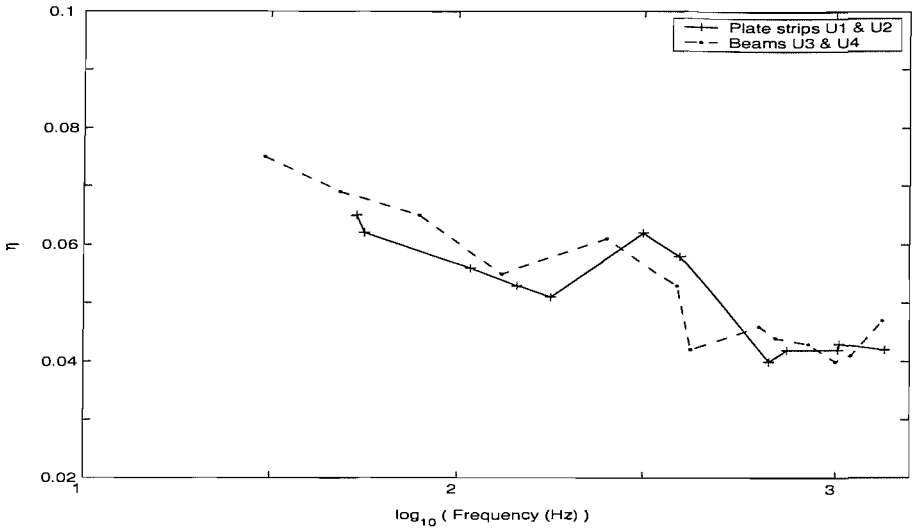

Figure 7.9. Structural loss factors of the uncoupled systems.

7.4.3 Measurement of Young's modulus

Masses and densities were obtained simply from weighing the beam samples. The Young's modulus E of a beam can be found from its bending stiffness, described in terms of frequency and wavenumber as follows.

$$E = D_b / I = \omega^2 m_b' / k_b^4 I \tag{7.3}$$

where D_b is the bending stiffness, ω is frequency, m_b' is mass per unit length of the beam, k_b is the wavenumber corresponding to the frequency ω and $I\left(=bh^3/12\right)$ is the second moment of area of the beam. E is evaluated by determining ω and k_b at resonances of the beam.

In order to reduce the effect of the boundary conditions, each beam was suspended by thin threads at the 2 nodal points in the fundamental bending mode and consequently free-free boundary conditions apply. The flexural wavenumbers

corresponding to the resonances of a uniform free-free beam are known (e.g. [71]). For example, the wavenumber of a mode having 2 nodal points is given by $k_b L_x = 4.730$ where L_x is the length of the beam.

The natural frequencies of the uncoupled beams U1 – U4 were obtained experimentally. For example, for the taller beam U3, the fundamental natural frequency was 48.5 Hz and the bending stiffness can be calculated by

$$E = \frac{D_b}{I} = \frac{m'_b \omega^2}{k_b^4} \frac{12}{bh^3} = 4.96 \times 10^9 \text{ N/m}^2 . \tag{7.4}$$

It should be noted that the plate strips U1 and U2 are very flexible and thus the added mass effect of the force transducer may be large. Thus the natural frequencies of the systems U1 and U2 used to obtain the Young's modulus were found by means of an impact hammer and small accelerometer (PCB 352C22, 0.5 g) instead of the exciter and the force transducer, the detailed procedure for which is not given here. The measured Young's modulus is presented in the earlier Table 7.2. For the Young's modulus of the plate, the average value of the plate strips given in the table is used (= 4.43×10^9 N/m^2). In Chapters 2 – 6 the nominal Young's modulus of $E = 4.40 \times 10^9$ N/m^2 was used.

7.5 Experimental wavenumber estimation

7.5.1 Theoretical background

For the application of the wave method, the plate free wavenumber is required to be more than twice as large as the beam wavenumber. Consequently the wavenumber component k_y radiating into the plate from the beam-plate junction is assumed to be close to the plate free wavenumber k_p allowing the plate to be represented by a local impedance. This important hypothesis needs to be verified. In this section the wavenumbers of a plate-beam system are determined experimentally.

The estimation of the wavenumbers of a two-dimensional structure may begin with equation (7.5) defining the correlation of the measured transfer mobility with a travelling wave $e^{i(\omega t-k_x x-k_y y)}$.

$$\tilde{\Upsilon}(k_x,k_y,\omega)=\int_{x_{\min}}^{x_{\max}}\int_{y_{\min}}^{y_{\max}}\tilde{Y}(x,y,\omega)e^{-ik_x x}e^{-ik_y y}dxdy \tag{7.5}$$

where k_x and k_y are the wavenumber components corresponding to directions x and y, ω is the frequency of interest and $\tilde{Y}$ is the transfer mobility of the two-dimensional system for a fixed force point. The dimensions of the scanned area are defined by $(x_{\max}-x_{\min})\times(y_{\max}-y_{\min})$, which is assumed to be rectangular. Note that the correlation function $\tilde{\Upsilon}$ is a continuous function of the wavenumbers k_x and k_y. Thus, it is expected that this correlation will have a maximum value at a particular wavenumber pair (k_x,k_y) corresponding to the dominant wavenumber at the particular frequency.

For practical reasons, $\tilde{Y}(x,y,\omega)$ is only available at discretely chosen response points. Thus equation (7.5) should be modified for discretely sampled data as [87] and normalised in the same way as the Modal Assurance Coefficient (MAC) such that the value is between 0 and 1.

$$\tilde{\Upsilon}(k_x,k_y,\omega)=\left|\sum_{m=1}^{M}\sum_{n=1}^{N}\tilde{Y}(x_m,y_n,\omega)e^{-ik_x x_m}e^{-ik_y y_n}\right|^2\Bigg/\sum_{m=1}^{M}\sum_{n=1}^{N}\left|\tilde{Y}(x_m,y_n,\omega)\right|^2 MN \tag{7.6}$$

where M and N are the numbers of sampled data points in each direction respectively and x_m and y_n are the sample locations (assuming a rectangular grid).

7.5.2 Measurement considerations

As equation (7.6) involves the sampling locations x_m and y_n as well as the wavenumbers k_x and k_y, it is a spatial domain analysis. Similar to a frequency

domain analysis, the accuracy of the wavenumber obtained is dependent on the sampling resolution and the size of the scanned area. In order to have a better resolution of the wavenumber it is necessary to measure over a larger scanning area. In the present study, the length of the scanning area is chosen as 0.64 m, which covers almost the whole plate in the y direction (see Figure 7.10). From conventional Fourier transform theory the wavenumber resolution might be expected to be restricted by the length of the scan area L_a to be $2\pi/L_a$. A further study to choose the wavenumber resolution was performed and presented in Appendix E. It shows that 63% of the principal wavenumber ($k = 2\pi/L_a \times 0.63$, thus $L_a = 0.63\lambda$) can still be identified. For $L_a = 0.64\,\text{m}$ the corresponding lower wavenumber estimation limit is 6.2 rad/m. Wavenumbers below this may be incorrectly estimated and are affected by the limited scan length.

Another factor influencing the estimation of the wavenumber is the scanning resolution, i.e. spatial aliasing due to spacing of the measurement points. In order to reduce the measuring and post-processing times a reduced frequency range of 5.6 – 500 Hz was selected here. The resolution of the measurement points was chosen to be 2 cm, equal to about 1/6 the wavelength at 500 Hz (which is 0.12 m), which is sufficient to eliminate the spatial aliasing effect in the frequency range 5.6 – 500 Hz.

Figure 7.10 shows the configuration used for the plate wavenumber measurement of the two-beam coupled structure C1 and the scanning area consisting of the measurement points. The number of scanning points was 1089 ($=33\times33$) and the distance from the grid to the closest edge was 0.03 m and 0.025 m in the x and y directions respectively. The point force was applied on the centreline of beam 1 at $x = 0.36$ m from the right-hand end. This is close to the centre of the scanned area. The mobility at each point was obtained by averaging over 20 data samples. The same procedure was applied to the uncoupled plate C5 for comparison.

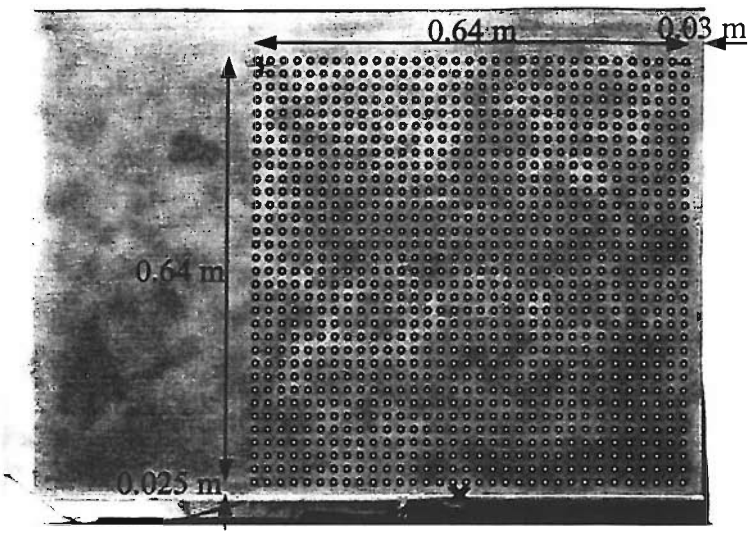

Figure 7.10. Configuration for the wavenumber measurement in two-beam coupled structure C1. The symbol ✖ on beam 1 indicates the excitation point (x = 0.36 m from the right-hand end of beam 1).

7.5.3 Plate wavenumbers

The spatial average of the modulus squared of the mobilities $\left\langle \left|\tilde{Y}\right|^2 \right\rangle$ was first calculated for systems C1 and C5 and shown in Figure 7.11, from which various resonance frequencies can be distinguished.

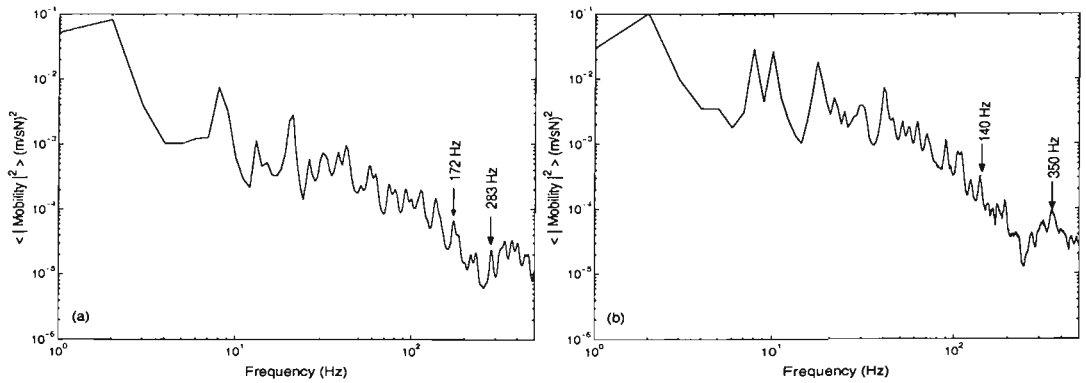

Figure 7.11. Space-averaged mobility amplitude over 1089 measurement points of (a) the two-beam coupled structure C1 (b) the uncoupled plate C5.

The spatial distribution of the plate vibration can be obtained from the transfer mobilities of the 1089 points. The motion at natural frequencies in particular should give a clear behaviour. Figure 7.12 shows two examples in terms of the contours of the amplitudes. These are at the natural frequencies of 172 and 283 Hz of the beam-plate coupled system C1. Two other examples at the natural frequencies of 140 and 350 Hz of the uncoupled plate C5 are shown in Figure 7.13. These frequencies are identified in Figure 7.11.

It can be seen that, in the beam-plate system, the wavelength across the plate is shorter than that along the beam. Node lines in the beam are reflected in the plate response, so that the motion of the plate is governed by the motion of the beam. By contrast the uncoupled plate C5 does not show clear node lines parallel to its edges. The wavelengths in the two directions seem similar.

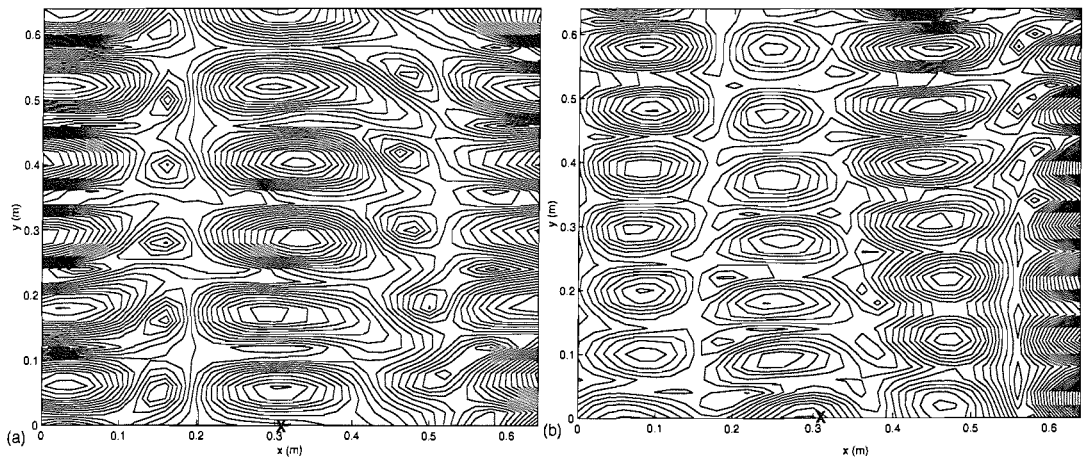

Figure 7.12. Contour of mobility amplitudes (a) at 172 Hz (b) at 283 Hz of the two-beam coupled structure C1. The symbol ✖ on the x axis indicates the excitation point.

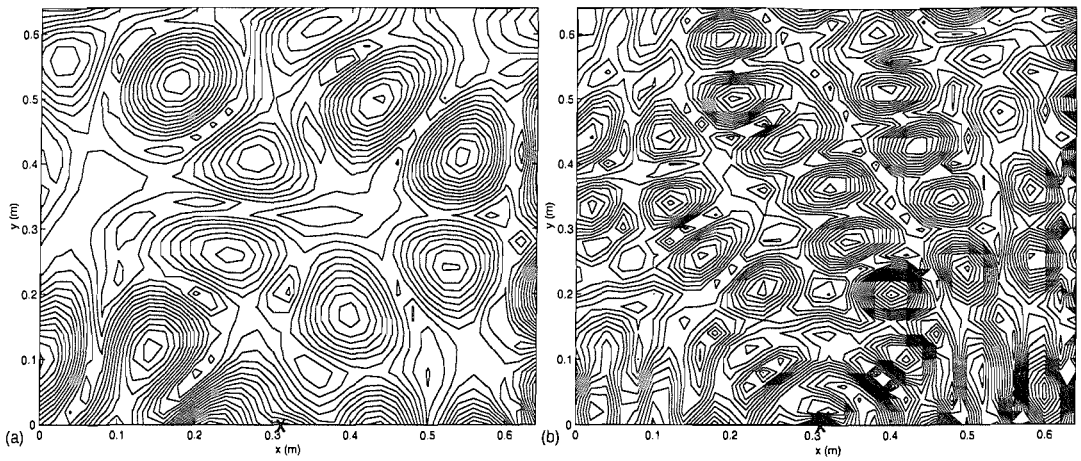

Figure 7.13. Contour of mobility amplitudes (a) at 140 Hz (b) at 350 Hz of the uncoupled plate C5. The symbol ✖ on the x axis indicates the excitation point.

The wavenumber of the system is investigated using equation (7.6). An example of the results of this calculation is shown in Figure 7.14. This gives wavenumber results for the two-beam-plate system C1 at 283 Hz. There are two dominant peaks that are propagating in opposite x directions. The most dominant plate wavenumber is given by $k_x = 17.8$ rad/m and $k_y = -33.4$ rad/m which yield a combined wavenumber $k_p = \sqrt{k_x^2 + k_y^2} = 37.8$ rad/m. A value of 38.5 rad/m for k_p is expected from the numerical model at this frequency. Other peaks correspond to the same wavenumber heading in the opposite x and y directions.

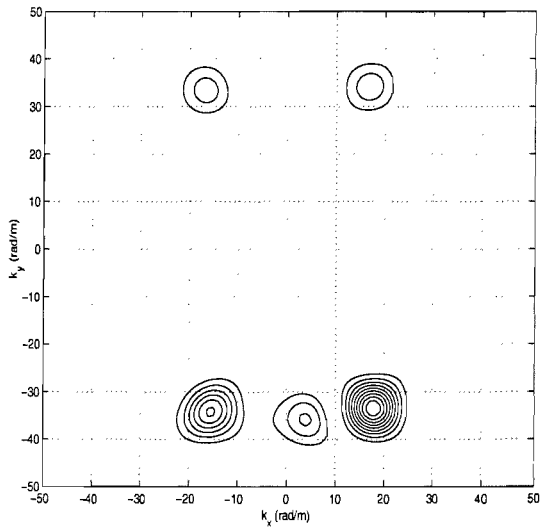

Figure 7.14. Dominant wavenumbers of the two-beam-plate system C1 at 283 Hz.

The same calculation is carried out to obtain the dominant wavenumber of the uncoupled plate C5 where the motion at 140 Hz is investigated. The result is shown in Figure 7.15. Unlike the result of Figure 7.14, it seems that the waves propagate in several directions located on a circle of radius 27 rad/m, which is the free plate wavenumber at this frequency (the expected wavenumber is k_p = 27.1 rad/m). It seems difficult to find a dominating propagation wave in a particular direction.

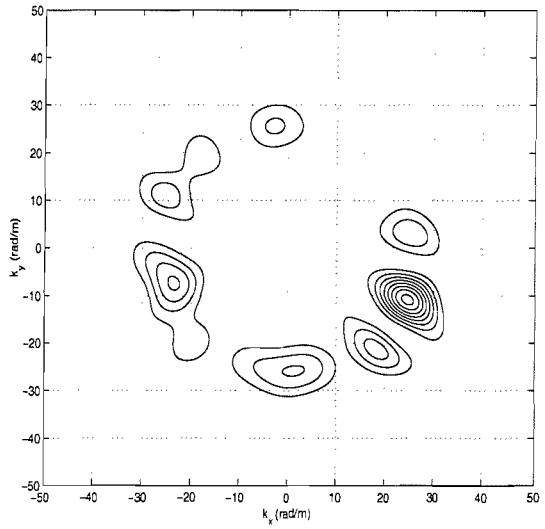

Figure 7.15. Dominant wavenumbers of the uncoupled plate C5 at 140 Hz.

The dominant plate wavenumbers obtained in the frequency range 5.6 – 500 Hz are incorporated into Figure 7.16. The theoretical wavenumber of the uncoupled plate is shown in the same figure for comparison, in which the physical properties are based on the experimental results of section 7.2.1. One can see that the experimental value k_p of the coupled plate is in very good agreement with that of the free plate wavenumber and the theoretical wavenumber represents the experimental ones very well. Greater deviations are found below 20 Hz where the grid is rather small for accurate resolution of the wavenumbers, the details of which follow below.

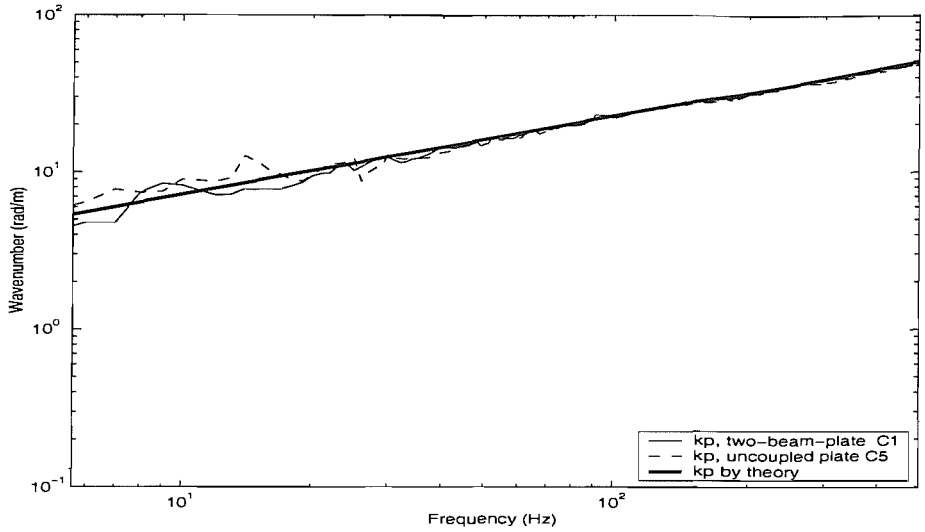

Figure 7.16. Wavenumbers of two-beam-plate system C1 and uncoupled plate C5 with theoretical values for comparison.

In Figure 7.17 the trace wavenumbers k_x and k_y of the coupled plate obtained at each frequency are compared with the theoretical wavenumbers of the uncoupled systems.

Although more than one peak occurs in the correlation at each frequency, as shown for example in Figure 7.14, it is found that the dominant trace wavenumber k_x of the coupled plate mostly follows the uncoupled beam wavenumber k_b above about 100 Hz. As mentioned before, and in Appendix E, the lower limit for resolving the wavenumber in the present situation is about 6.2 rad/m. Thus, if the wavenumber to be estimated is less than this it may not be correctly identified. This approximately corresponds to about 80 Hz for the beam free wavenumber. However, it seems that the wavenumber lower limit influences the wavenumber k_y only at very low frequencies. The plate wavenumber k_p given by the trace wavenumbers k_x and k_y may also be inaccurate only at very low frequencies, as k_x is much smaller than k_y even though k_x is inaccurate below about 100 Hz.

Although there is some limit at low frequencies due to the wavenumber resolution, the results indicate that the behaviour of the plate in the direction of the beam is

dominated by the beam behaviour. On the other hand, the trace wavenumber in the y direction is close to the free plate wavenumber. Consequently, the important hypothesis in the wave method, namely that the wavenumber k_y is approximately equal to the plate wavenumber k_p, can be confirmed from these results.

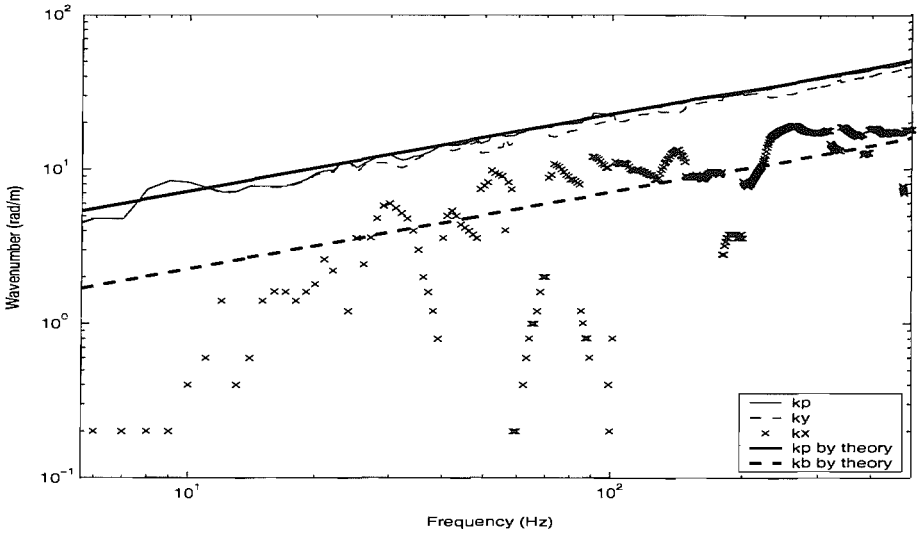

Figure 7.17. Wavenumber comparison of the two-beam-plate system C1.

It should be noted that the estimation method has been performed at each measurement frequency and in certain cases, for example anti-resonances, it might also not be possible to estimate the wavenumbers well.

7.6 Energy and power in the coupled systems

In this section dissipated and transferred powers of the subsystems are evaluated and compared with the corresponding theoretical results.

7.6.1 Measurement

As previously, the point force was applied at $x = 0.36$ m on the centreline of beam 1. Firstly, the point mobility was measured using the laser vibrometer. As it is not feasible to obtain the strain energy of a vibrational system, its kinetic energy is considered, which can be found simply using the vibrational velocity of the structure and its mass.

Measurement points were selected randomly over the plate and the beams of the coupled system, and used to give an estimate of the spatially averaged energy. Figure 7.18 shows 20 points selected over the plate, which were used in the measurement for all coupled systems. For each beam of the coupled structure, 10 points were selected. Although strictly they should be selected on the beams, because of the thin width of the beam ($b = 6$ mm) it was difficult to align the laser beam exactly on the middle of the beam, which results in poor responses. Thus, the laser was aimed to measure along a parallel line less than 1 cm from the beam (thus in fact on the plate). As the motion along this line is mainly dependent on the motion of the beam it is expected that the error will be small (note that the plate wavelength at the maximum frequency (1412 Hz) is about 7.3 cm).

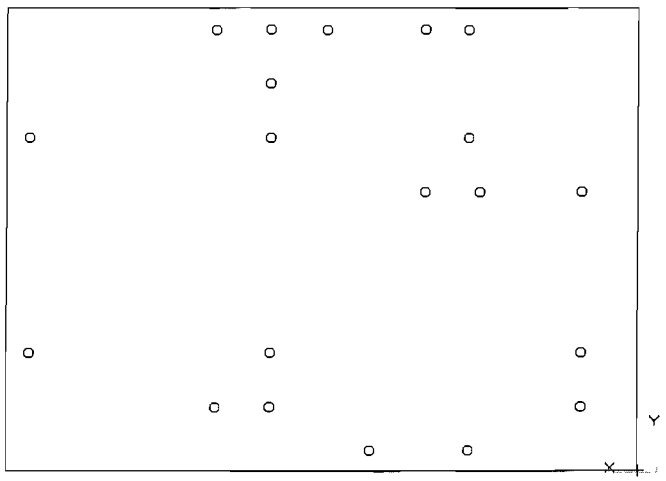

Figure 7.18. Randomly selected measurement points of the plate.

7.6.2 Kinetic energy and power

Assuming that the time-averaged kinetic and strain energies are equal, for a uniform structure if the transfer mobilities of N points are measured, the spatially averaged energy of the subsystem normalised by the mean square force is given by [21]

$$E\Big/\overline{F_0^2} = m\sum_{i=1}^{N}\frac{|\tilde{v}_i|^2}{2N\overline{F_0^2}} = m\left\langle |\tilde{Y}_i|^2 \right\rangle \tag{7.7}$$

where $\left\langle |\tilde{Y}_i|^2 \right\rangle$ is the space-averaged value of $|\tilde{Y}_i|^2$, $\tilde{Y}_i$ is the transfer mobility given by $\tilde{v}_i/\tilde{F}_0$, $\tilde{v}_i$ is the velocity amplitude at the ith point, $\overline{F_0^2}$ is the mean square force at the point force, and m is the total mass of the corresponding subsystem.

The power is also normalised by the mean square force. The power dissipated in the subsystem normalised by the mean square force is given by

$$P_{dis}\Big/\overline{F_0^2} = \omega\eta E\Big/\overline{F_0^2} = \omega\eta m\left\langle |\tilde{Y}_i|^2 \right\rangle \tag{7.8}$$

where ω is the circular frequency and η is the structural loss factor which has been determined in section 7.4.2. Similarly the input power normalised by the mean square force is given by

$$P_{input}\Big/\overline{F_0^2} = \mathrm{Real}\left\{\tilde{Y}_0\right\} \tag{7.9}$$

where $\tilde{Y}_0$ is the input mobility. Thus, energy and power can conveniently be expressed in terms of the mobility and they can be compared with those obtained from the numerical models. In the following sections the energy and power refer to values normalised by the mean square force.

7.6.3 System of two identical beams coupled to a plate: wave method

Firstly, the input power and dissipated power estimates are compared for the two-beam coupled system C1 consisting of two identical beams. The results are shown in Figure 7.19, in which the dissipated power of each subsystem is obtained using equation (7.8). One can see that the estimates of input and dissipated power are approximately equal. The slight differences may occur because: (i) the selected random points only approximately represent the energy (ii) the structural loss factor is also approximate being given by the linear fit to the discrete damping loss factors and (iii) the kinetic and strain energies are not equal, the difference is expected away from the resonances at low frequencies. Nevertheless, they are in good agreement and it can be concluded that the energy obtained using the space-averaged mobility reasonably represents the energy that each subsystem possesses.

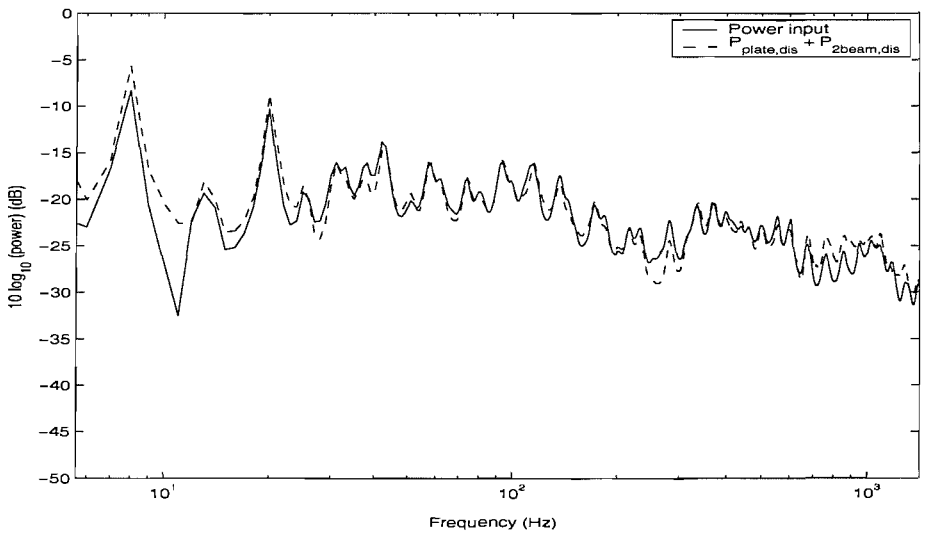

Figure 7.19. Input and dissipated power of the two-beam-plate system C1. Power normalised by the mean square force, dB re 1 W/N^2, experimental results.

The power dissipated in each subsystem is shown in Figure 7.20. One can see that most power is dissipated in the plate as discussed in Chapter 5 dealing with modelling such systems with two parallel beams (see Figures 5.6 and 5.11).

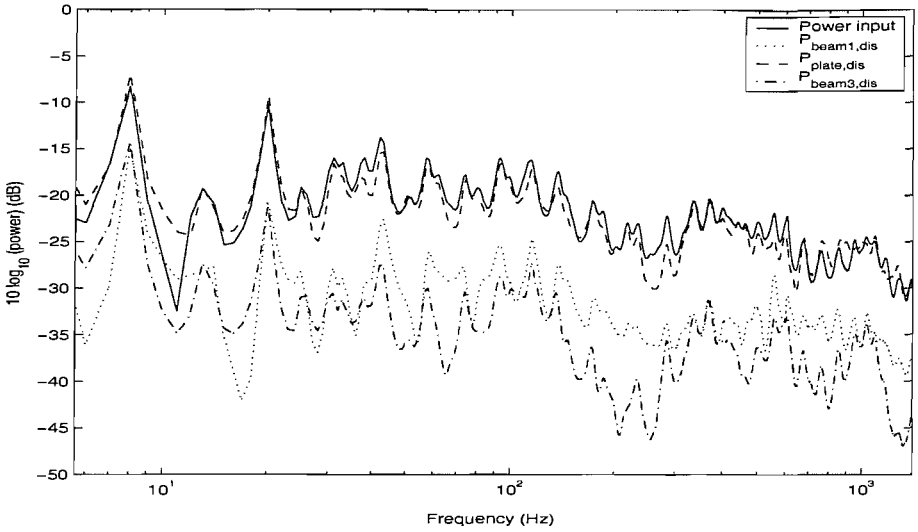

Figure 7.20. Power comparison of the two-beam-plate system C1. Power normalised by the mean square force, dB re 1 W/N^2, experimental results.

The numerical model is now compared with the experimental results. This comparison is made initially in terms of input power. The numerical model considered here is based on the wave method. The system has two identical beams and is constructed using symmetric and anti-symmetric responses as discussed in Chapter 5. Unlike the model in Chapter 5 both ends of the experimental beam are free and the other edges of the plate are also effectively free, which are the same as the experimental situation for the system C1. However in the model the rotation of beams 1 and 3 is constrained, which differs from the experimental situation. The force point is located at $x = 0.36$ m as in the experiment.

The input power shown in Figure 7.19 is compared with that of the wave model in Figure 7.21. They agree very well in the mid-frequencies between about 40 and 300 Hz. The difference at low frequency occurs because of the different boundary conditions as mentioned above.

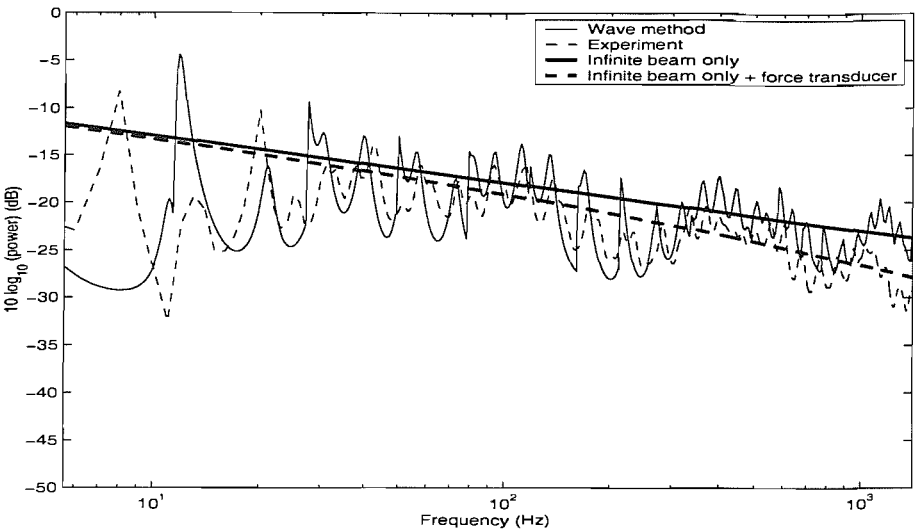

Figure 7.21. Input power for the two-beam-plate system C1: comparison between the wave method model and the experiment.

One can find that there is a general undulating trend. Small peaks and dips are also found on the general trend. These small peaks and dips occur due to the vibrating plate coupled to the beam, as discussed in Chapter 6 (see Figure 6.12). Meanwhile, the general undulation may be related to the excitation point and the corresponding motion of the beam, which may be explained in terms of the motion of the beam. The excitation point ($x = 0.36$ m) coincides with a node of the mode of the uncoupled beam with natural frequency 273 Hz. This is close to the general dip at about 250 Hz. Meanwhile, the uncoupled beam motion at the natural frequency of 450 Hz shows an antinode at the excitation point, which corresponds to the general peak at about 400 Hz. These relationships are summarised in Table 7.5.

Table 7.5. Relationship of the motions between the coupled system C1 and the corresponding uncoupled beam.

Natural frequency (Hz), uncoupled beam	Motion in fundamental bending mode	Motion at excitation point	Corresponding approximate frequency in coupled system C1 (Hz) and peak/dip
273	4 nodal points	node	250 (dip)
450	5 nodal points	antinode	400 (peak)
673	6 nodal points	antinode	590 (peak)
939	7 nodal points	node	830 (dip)
1251	8 nodal points	antinode	1130 (peak)

A level difference is found between the numerical model and the experiment at high frequencies in Figure 7.21. This does not appear to be related to the boundary conditions. Rather, it seems to be related to the mass of the force transducer. This can be confirmed by comparing the impedances of an infinite beam that has the same dimensions as beam 1 and the force transducer. The actual mass of the force transducer that has an effect on the experiment has been measured, and found to be about 62 % of the force transducer mass itself (22.7 g)*. Thus, an effective mass of 14 g is considered for comparison. The impedances of a beam in flexural motion and of a point mass are given by [79]

$$Z_b = 2\rho A c_B (1+i);\ Z_{mass} = i\omega m \tag{7.10}$$

where ρ is the density, $A(=b\times h)$ is the cross-sectional area, $c_B\left(=\sqrt[4]{D_b / m_b'}\sqrt[2]{\omega}\right)$ is the phase velocity of a flexural wave, D_b is the bending stiffness, m_b' is the mass per unit length of the beam, and m is the mass. The calculated impedances are

* The effective mass of each side of the force transducer was measured by attaching it to the exciter through a stinger and measuring the force applied to the free part of the transducer. An accelerometer measured the acceleration allowing the mass of the free part of the transducer to be determined from Newton's second law.

compared in Figure 7.22. It is clear that the mass effect is not negligible at high frequencies.

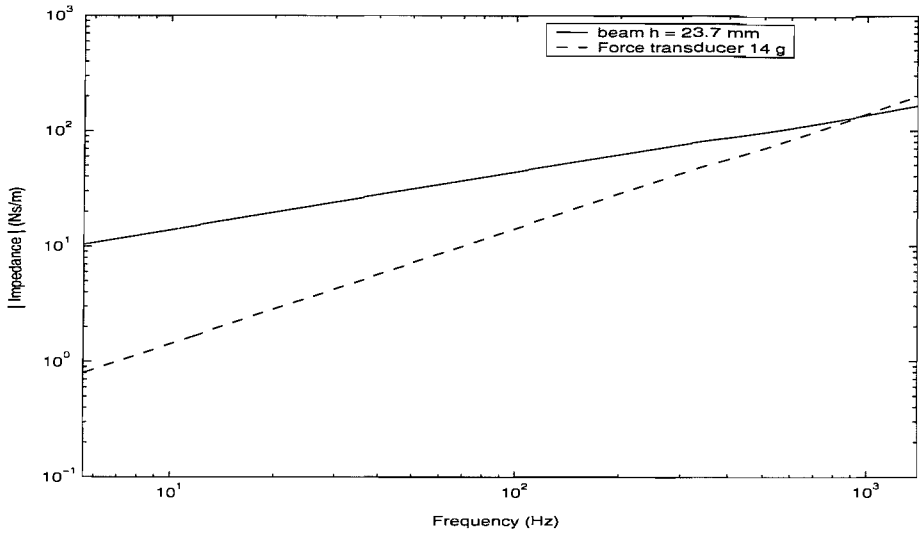

Figure 7.22. Impedance comparison of an infinite beam (h = 23.7 mm) and the mass of the force transducer (mass = 14 g).

The mass effect introduced by the force transducer upon the measurement of the power input to the beam can be calculated by [88]

$$\mathrm{Re}\{Y_{b+mass}\} = \mathrm{Re}\{Z_b\} \Big/ \left[\left(\mathrm{Re}\{Z_b\}\right)^2 + \left(\mathrm{Im}\{Z_b\} + \omega m\right)^2 \right] \tag{7.11}$$

where Y_{b+mass} is the point mobility of the mass-attached beam, which results in the measured power input. The estimated power inputs obtained using the real part of the mobilities, $\mathrm{Re}\{Y_{b+mass}\}$ and $\mathrm{Re}\{Y_b\}$ using the infinite beam are also plotted in Figure 7.21 for comparison. The difference between these lines is similar to that between the wave method and experiment at high frequencies with a difference of 4.2 dB at 1412 Hz. It seems clear that the mass effect reduces the power input level in the experiment. The same phenomena occur for other coupled systems considered later in this chapter.

The input powers shown in Figure 7.21 are replotted in one-third octave bands in Figure 7.23. The calculated power input incorporating the mass of the force transducer is also considered in the same figure, which shows excellent agreement with the experimental result except at low frequencies.

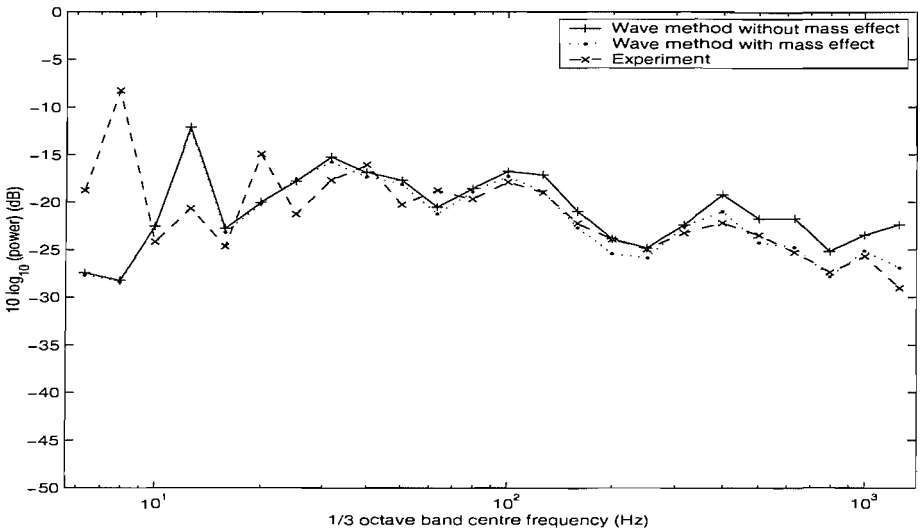

Figure 7.23. Input power in one-third octave bands for the two-beam-plate system C1: comparison between the wave method model and the experiment (dB re 1 W/N^2).

Next, results are compared in terms of the energy ratio between the various subsystems. This has the advantage of reducing the effect of boundary conditions and cancelling out any mass effect of the force transducer. The boundary conditions may influence the general level of the FRF through the whole frequency range, and may also change the natural frequencies, thus peaks and dips. The differences in response level are eliminated by comparing the energy ratios. Differences in the frequency of peaks and dips have less influence if a frequency band average, such as one-third octaves, is used.

The energy ratio between the subsystems at discrete frequencies is shown in Figure 7.24. The upper figure shows the plate energy divided by that of beam 1; the lower figure shows the ratio of the energies of the two beams. Results for the wave method are shown along with the experimental results.

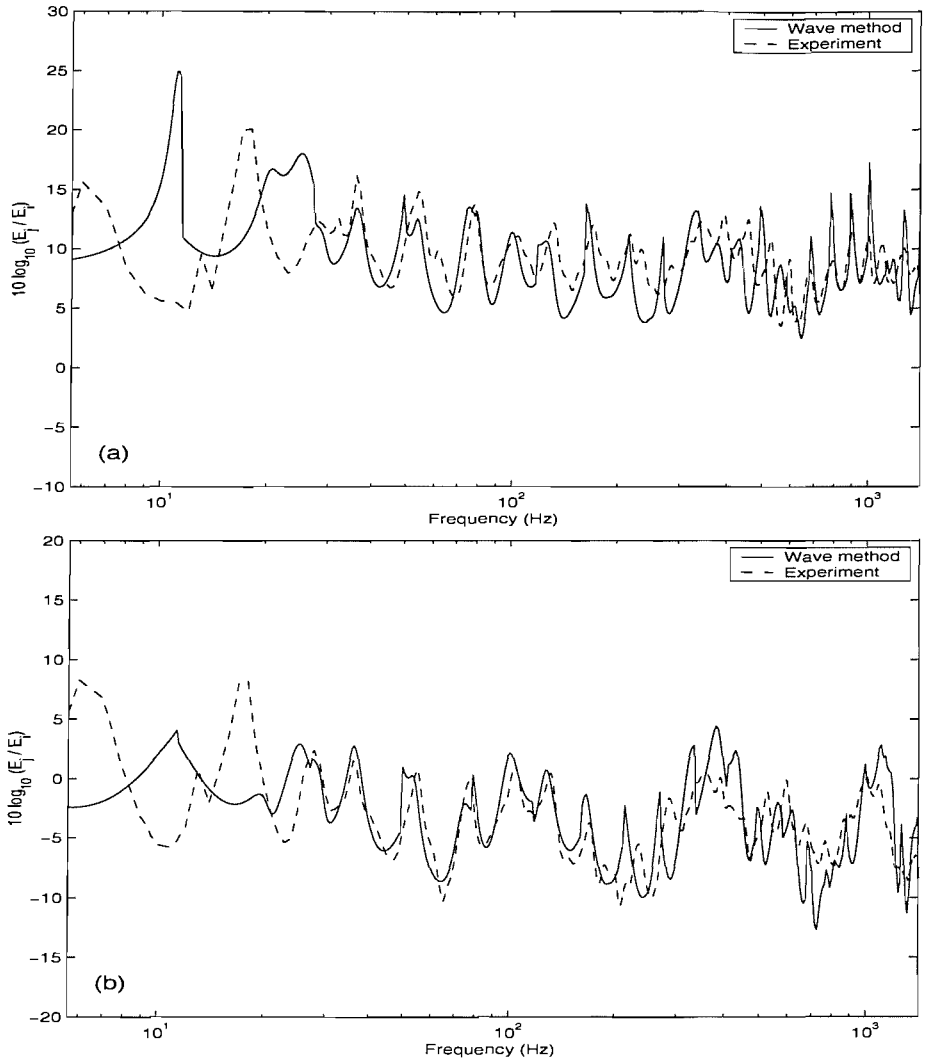

Figure 7.24. Energy ratio of the two-beam-plate system C1. The wave model and experimental results for (a) E_{plate}/E_{beam1}, (b) E_{beam3}/E_{beam1}.

One can see that there is very good agreement between theory and experiment for both cases, even at low frequencies, apart from differences in the exact location of peaks and dips. The difference at very low frequencies may occur because the rotation of the beams is suppressed in the wave model and the approximate plate impedance is used instead of the exact line impedance (see also Chapter 5). Comparing the two figures 7.24 (a) and (b), one can also see that as most of the energy transmitted from the driven beam to the plate is dissipated in the plate connecting the two beams, the energy transferred to the third beam is smaller. Nevertheless it is on average only about 5 dB less than that of the driven beam.

Although the figures above show excellent agreement even at low frequencies, it is of interest to re-evaluate the energy ratio in terms of a one-third octave band average. This is obtained by firstly calculating the one-third octave band energy of each subsystem and then their ratio. The results are shown in Figure 7.25. From these results, the numerical wave model is seen to represent the experimental situation well and can be used for the frequency average response prediction of such a structure.

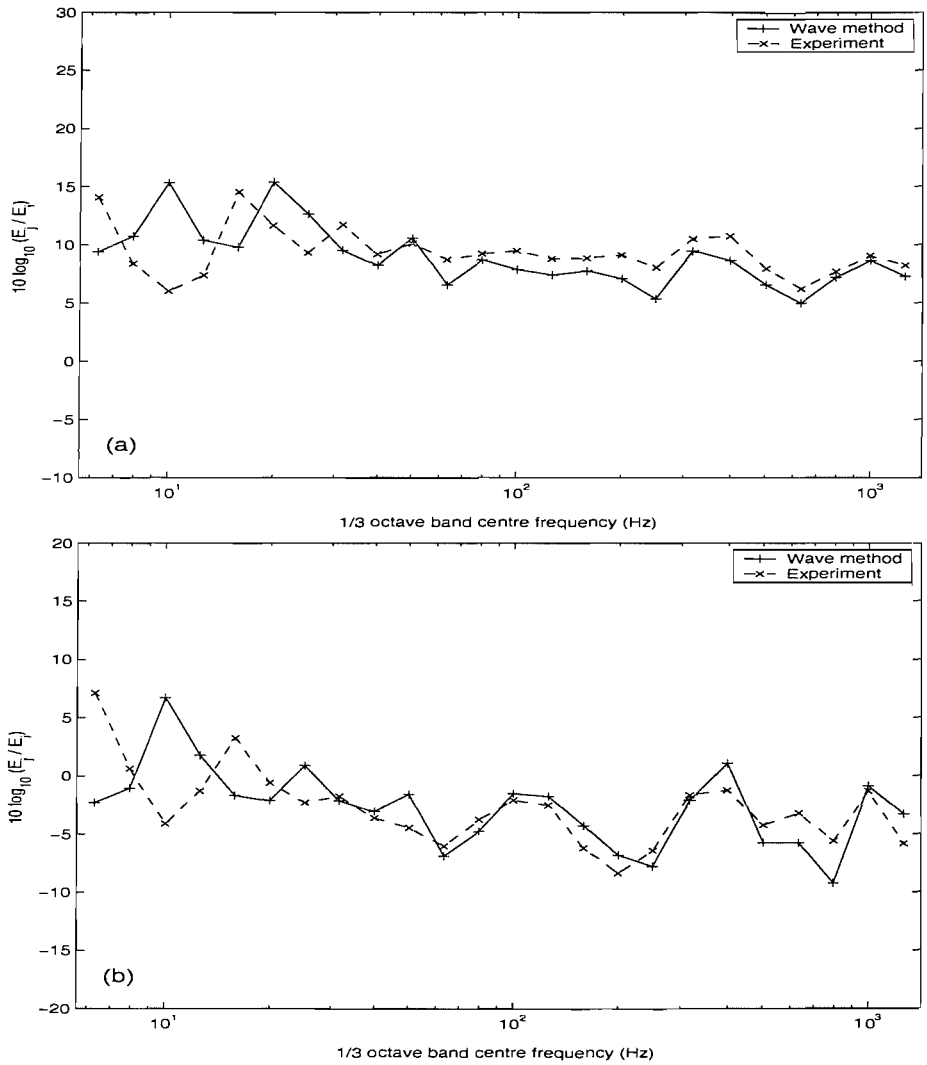

Figure 7.25. Energy ratio in one-third octave bands for the two-beam-plate system C1. The wave method and experimental results for (a) energy ratio E_{plate}/E_{beam1}, (b) energy ratio E_{beam3}/E_{beam1}.

7.6.4 System of two identical beams coupled to a plate: Fourier method

The same system C1 is now investigated using the numerical model based on the Fourier transform technique. Note that in the Fourier method, both ends of the two beams and the all edges of the plate are sliding. Thus the boundary conditions of the beam ends and the two edges normal to the beams are different from those in the experiment. The numerical model based on the Fourier method and the experimental results are compared. The effect of the different boundary conditions may also be identified by comparing the numerical results of the wave model from the previous section and the Fourier method.

Firstly, the input powers are compared in Figure 7.26. Differences occur at low frequencies because of differences in the boundary conditions. At high frequencies the effect of added mass can be seen as explained in the previous section. In the mid-frequencies between 50 and 500 Hz, however, they show reasonably good agreement. Comparing this with Figure 7.21 for the wave model, one can see that the differences are slightly greater, which may be due to the different boundary conditions (see below).

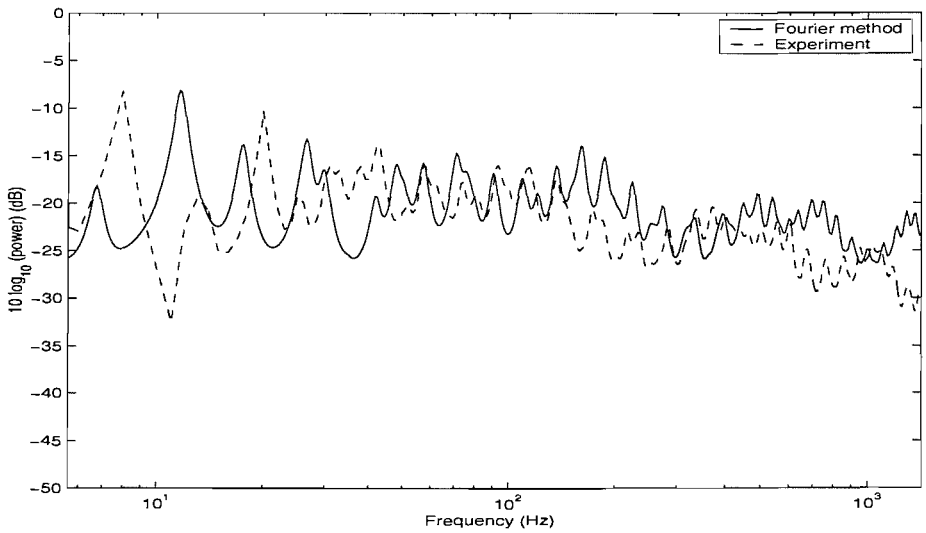

Figure 7.26. Input power of the two-beam-plate system C1: comparison between the Fourier method model and the experiment.

The power input in one-third octave bands is shown in Figure 7.27. Comparing this with Figure 7.23 the differences are greater although the result of the Fourier method is still in quite good agreement with that of the experiment. The boundary effect seems clearer and this is probably related to the motion of the beam. One can find that there is a consistent frequency shift in the general trend especially above 100 Hz. It seems for example that the dip of 250 Hz in the experiment moves to 315 Hz in the numerical result. The frequency shift may be explained in terms of different boundary conditions (sliding and free) and corresponding motion of an uncoupled beam.

Consider the uncoupled beam having the same beam properties. If the beam ends are sliding, then there is a natural frequency of the beam at 356.1 Hz where the beam has 4 nodal points in its bending mode ($k_b = 4\pi$). The most similar experimental motion having 4 nodal points occurs at 273 Hz in the beam where the beam ends are free (although strictly the two motions are different especially at the ends of the beam). The frequency shift occurs by about a factor of 1.30 ($=356.1/273$) for these similar modes, which is similar to the shift seen in Figure 7.27. Frequency shifts in the other peaks and dips shown in Figure 7.27 may also be explained in a similar way.

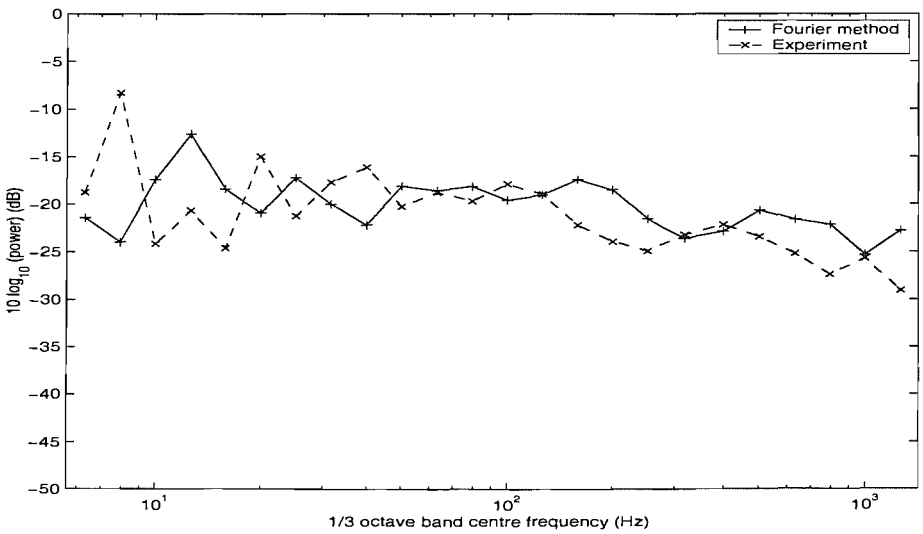

Figure 7.27. Input power in one-third octave bands for the two-beam-plate system C1: comparison between the Fourier method model and the experiment.

The energy ratio is compared in the same manner as in the previous section. Figure 7.28 shows the one-third octave band averages of the energy ratios between the subsystems for both the Fourier method and the experiment. It can be seen that the numerical model replicates the experimental situation well, especially the energy ratio between the driven beam (beam 1) and the plate.

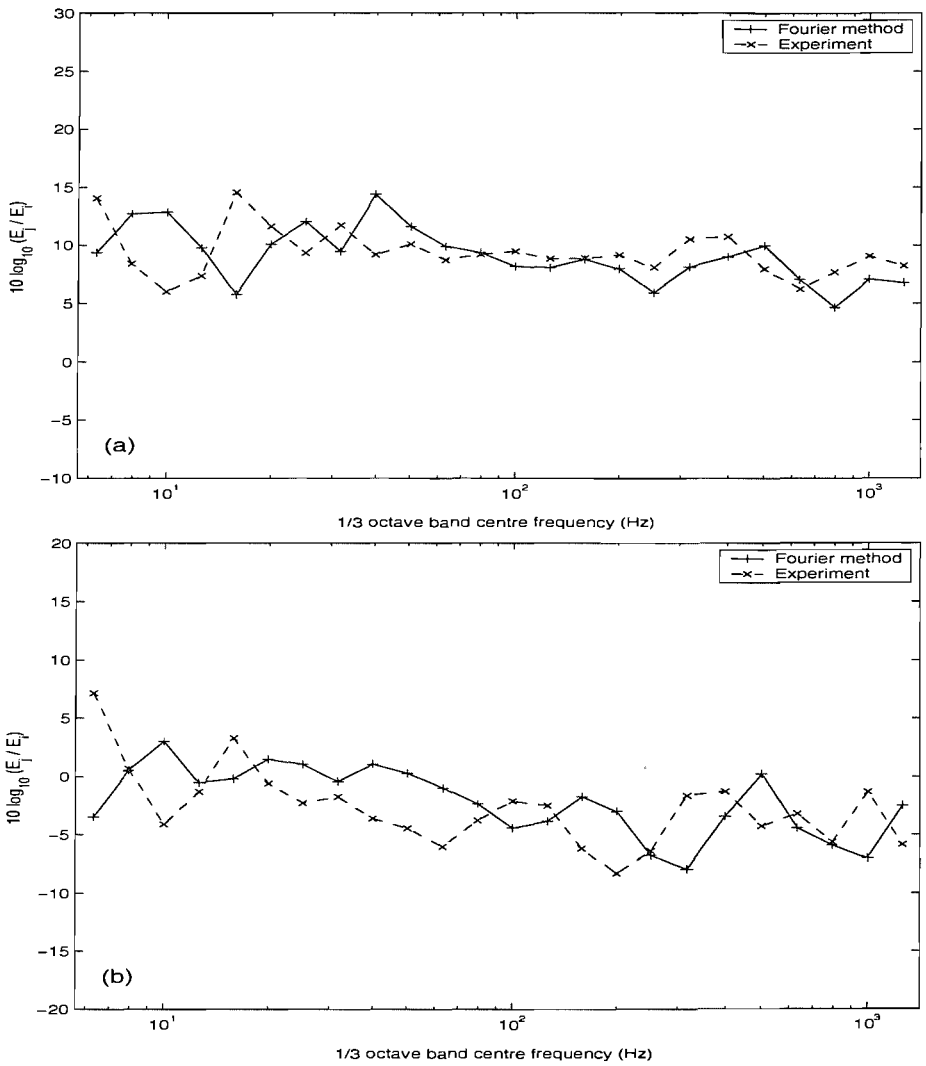

Figure 7.28. Energy ratio in one-third octave bands for the two-beam-plate system C1. The Fourier method and experimental results for (a) energy ratio E_{plate}/E_{beam1}, (b) energy ratio E_{beam3}/E_{beam1}.

7.6.5 System of two dissimilar beams coupled to a plate

As the wave model considered in Chapter 5 is not appropriate to describe the system consisting of two dissimilar beams, here the results are compared only with the numerical model based on the Fourier transform technique. While both ends of the two beams are sliding and all edges of the plate are also in sliding in the numerical model, experimentally the ends of the beams and the plate edges are free.

The measured input power and the total dissipated power of all subsystems are shown in Figure 7.29, showing good agreement.

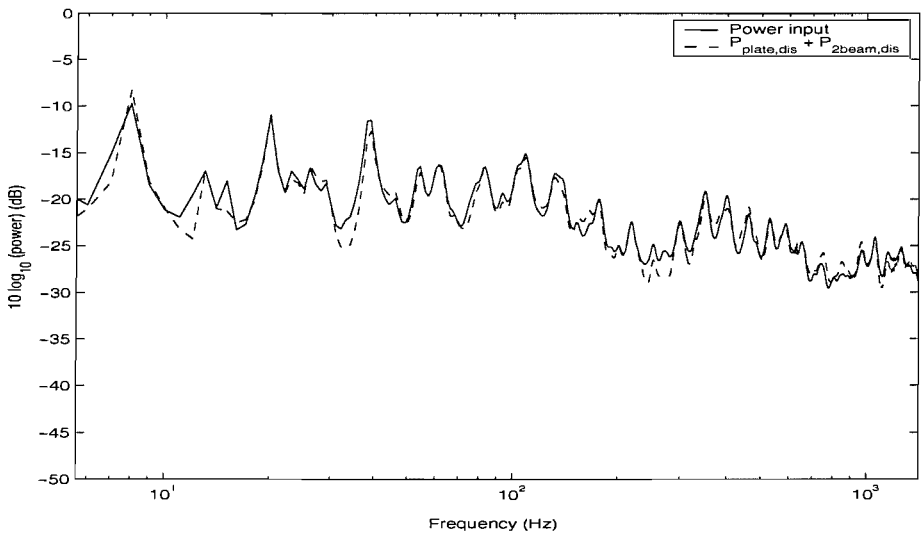

Figure 7.29. Input and dissipated power of the two-beam-plate system C2. Power normalised by the mean square force, dB re 1 W/N^2, experimental results.

The numerical input power is compared with that obtained experimentally in Figures 7.30 and 7.31. The same tendency is found as in the previous section. That is, detail differences are found at low frequencies due to the different boundary conditions and at high frequencies the mass of the force transducer introduces a consistent difference.

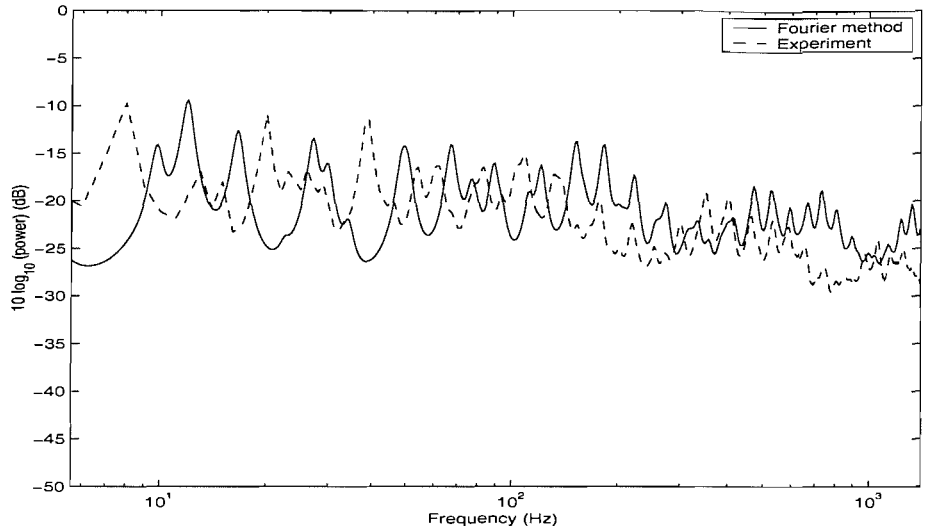

Figure 7.30. Input power of the two-beam-plate system C2: comparison between the Fourier method and the experiment.

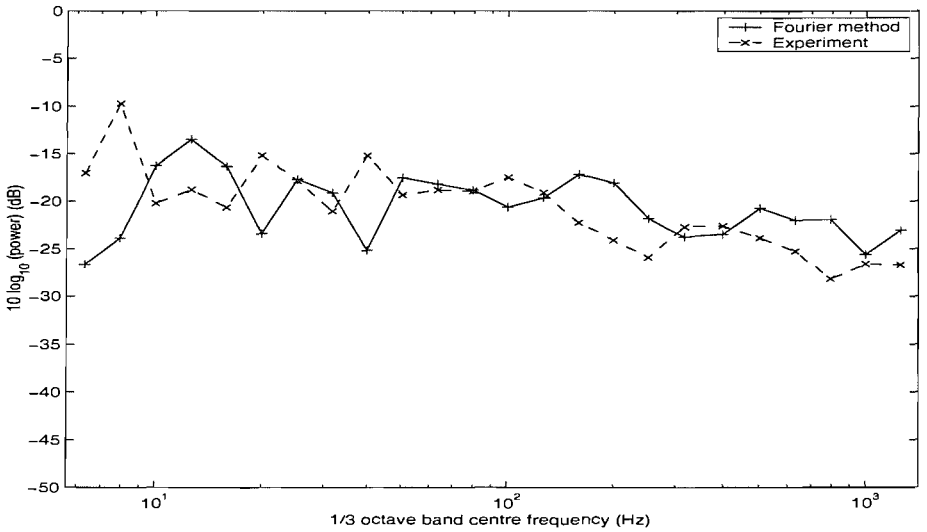

Figure 7.31. Input power in one-third octave bands for the two-beam-plate system C2: comparison between the Fourier method and the experiment.

The energy ratios between the driven beam (beam 1) and the energy-receiving subsystems (beam 3 and the plate) are calculated in terms of one-third octave band averages for both the numerical model and the experiment, and are shown in Figure 7.32. Detail differences are found at low frequency, largely due to the different boundary conditions of the beam-ends and also probably the plate edges attached to the beams.

The energy ratio between the driven beam and the plate is in very good agreement above about 50 Hz, which may be considered as the mid-frequency region in this present structure consisting of stiffer beams and a flexible plate (see also section 6.4.2). The results for the plate are similar to those found for two identical beams in the previous section. However the energy of beam 3 is much less in the present case of dissimilar beams, particularly at high frequencies (compare with Figure 7.28). The numerical results drop lower than the experimental results (although it should be recalled that the latter are measured on the plate adjacent to the beam).

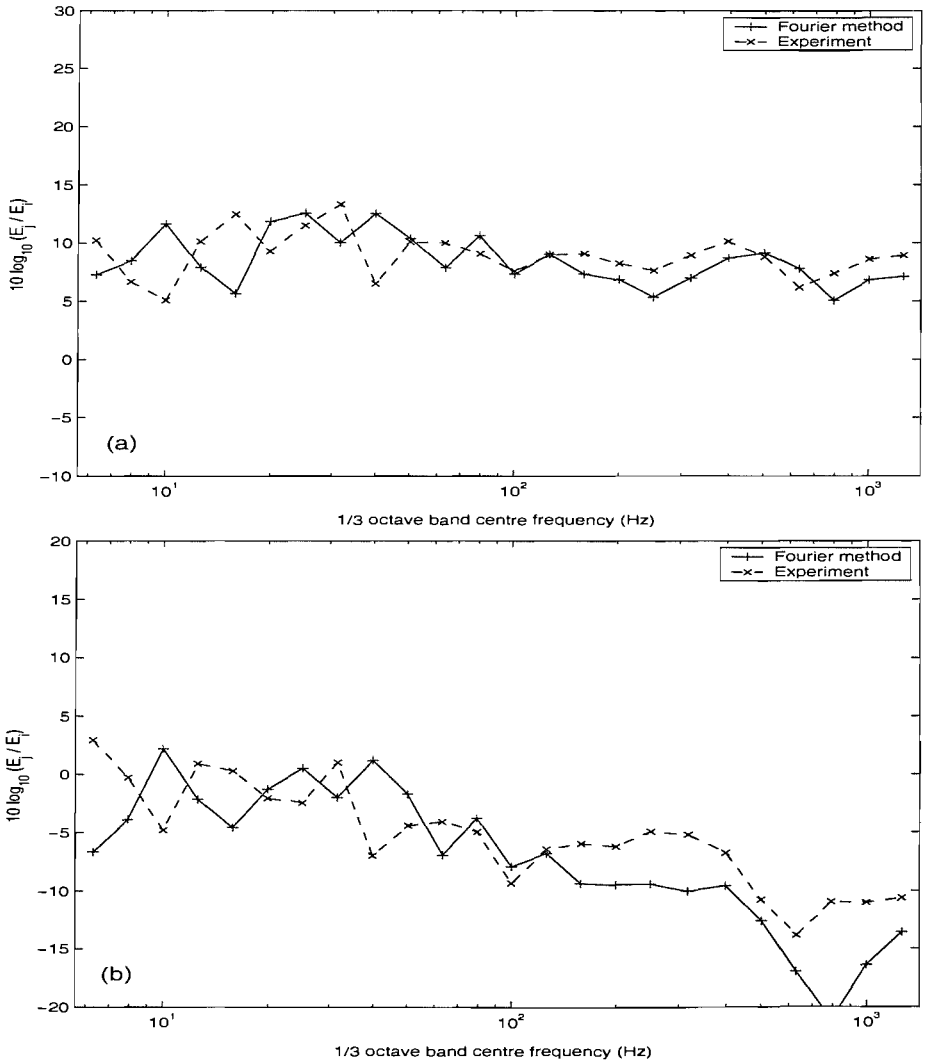

Figure 7.32. Energy ratio using one-third octave band energy of the two-beam-plate system C2. Numerical model based on Fourier method: (a) E_{plate}/E_{beam1}, (b) E_{beam3}/E_{beam1}.

Comparisons based on the energy ratio are very useful to verify a numerical model for the mid and high frequency analysis even though the boundary conditions are different from those in the experiment. Also the comparison shows the usefulness of the strategy of adopting sliding boundary conditions in the mid and high frequency analyses. The same technique is applied to a more complex system consisting of four beams and a rectangular plate in the following sections.

7.6.6 Fully framed structure consisting of similar beams

This section deals with coupled structure C3, a system consisting of a rectangular plate surrounded by four identical beams. The framed structure was studied in Chapter 6 where the modal method was used to obtain an exact response and the wave method an approximate response. Their responses are compared here with the experimental results.

In the modal model a maximum number of 50 modes is used for each direction x and y. It should be noted that the numerical model based on the modal method is constructed using sliding boundary conditions on the beam ends and plate edges. Sliding boundary conditions are also applied to the ends of each beam in the wave model as beam torsion is suppressed. Moreover in the wave method, the plate does not connect the beams and the wave model is represented by four plates attached to the individual beams. This is different from the wave model considered in section 7.6.3 which uses the symmetric and anti-symmetric responses and in which consequently the plate does connect the two beams.

In Figure 7.33 the measured input power of coupled system C3 is compared with the sum of the dissipated power of each subsystem, the plate and beams 1 – 4. One can see that good agreement is found for this system.

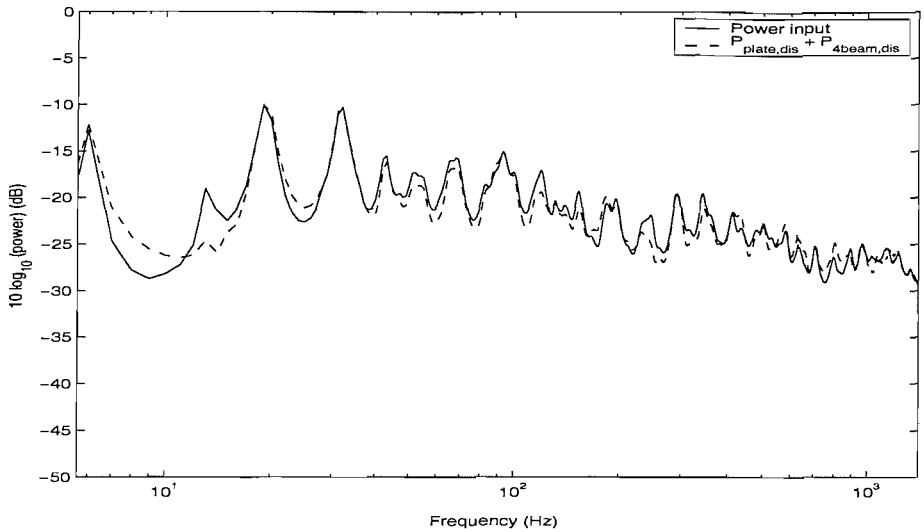

Figure 7.33. Input and dissipated power of four-beam-plate system C3. Power normalised by the mean square force, dB re 1 W/N^2, experimental results.

By comparing the power dissipated in each subsystem, the energy transferred between subsystems can be identified. The measured dissipated power in each subsystem is shown in Figure 7.34. It is clear that, as before, most energy is dissipated in the plate, with the driven beam power greater than the others above 30 Hz.

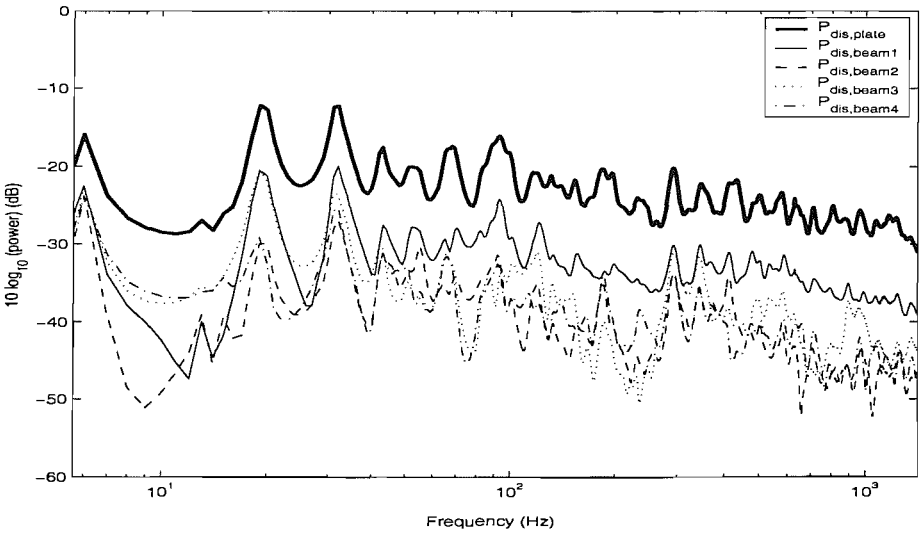

Figure 7.34. Power comparison of the four-beam-plate system C3, experimental results.

The input power shown in Figure 7.33 is now compared by means of one-third octave band averages with those calculated based on the modal method and the wave method, as shown in Figure 7.35. The results of the modal model and the

wave model show close agreement with each other except at low frequencies. These numerical results are in good agreement with the experiment at least in the mid-frequency region between 40 and 300 Hz. A reason for the difference between the numerical result and the experiment at high frequencies is the added mass of the force transducer, as explained previously. If the mass effect is included in the numerical model, the power difference between the numerical model and the experiment in one-third octave bands is at most 3 dB above about 40 Hz.

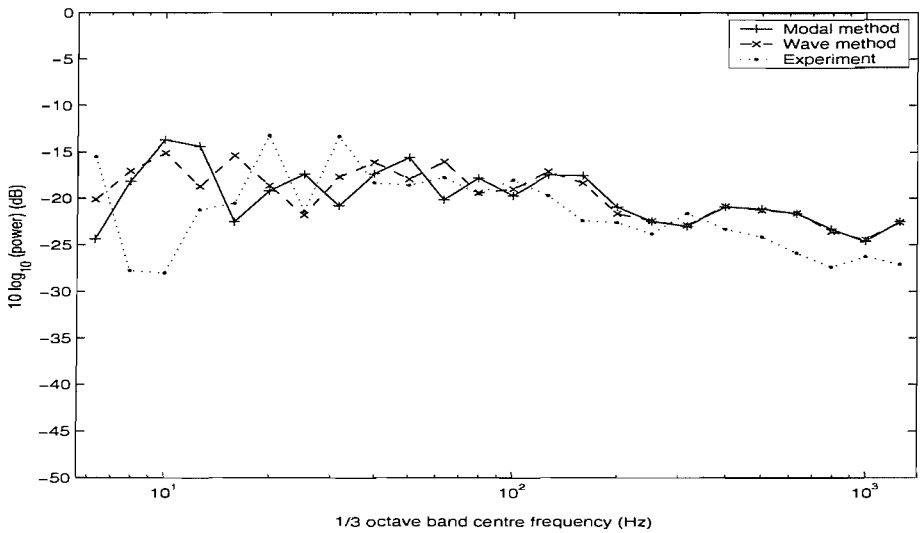

Figure 7.35. Input power in one-third octave bands for the four-beam-plate system C3: comparison between the numerical models and the experiment.

Figure 7.36 shows the energy ratios in one-third octave band form from the experimental results and the two theoretical models. In the wave method the approximate plate energy of the framed structure can be found from the sum of the energies of the four plates (see section 6.4.2). For the energy ratio of the plate relative to the driven beam (beam 1), above about 40 Hz both predicted and experimental results agree very well, within about 3 dB. For other cases, except for beam 3, the maximum difference is less than about 5 dB in the mid and high frequency regions, even though the wave method is known to provide an approximate response. In the experiments and Fourier method, beam 3 has a similar energy to beams 2 and 4 whereas in the wave method it is up to 10 dB lower. A reason for the large difference for beam 3 is due to the modelling

assumption in the wave method. That is, the plate in the wave model does not connect the two beams (beam 1 and beam 3) and thus the energy transfer through the plate between the two beams cannot be realised in such a model. Thus, this implies that, in the description of the beam energy, the power flow through the plate is mostly important to the opposite beam (beam 3) rather than to the other beams. Note that the configuration considered here differs from the earlier chapter in that the force is located on one beam away from a corner. For such a case it seems that the power flow through the beams experiences more power reflection, as there are always two corners between the forcing point and beam 3.

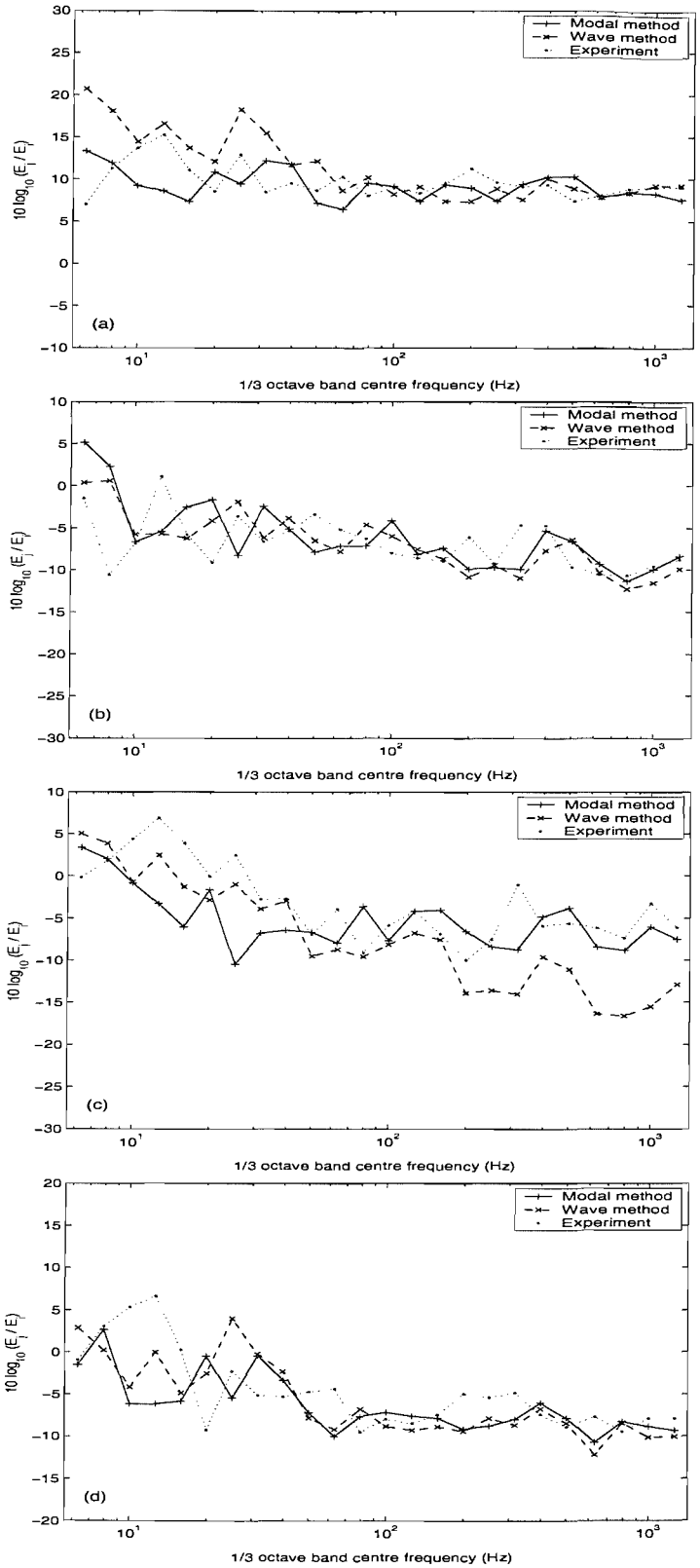

Figure 7.36. Energy ratio in one-third octave bands of four-beam-plate system C3, for the numerical models and the experiment: (a) E_{plate}/E_{beam1} , (b) E_{beam2}/E_{beam1} , (c) E_{beam3}/E_{beam1} , (d) E_{beam4}/E_{beam1} .

7.6.7 Fully framed structure consisting of dissimilar beams

Finally the same investigation was carried out for the coupled system C4, which consists of four beams and a rectangular plate. Adjacent beams 1 and 4 are 24.1 mm high and beams 2 and 3 are 13.3 mm high (see Figure 7.1). Figure 7.37 compares input and dissipated power estimates showing good agreement. The individual dissipated powers are not shown here as they show the same tendency as in section 7.6.6.

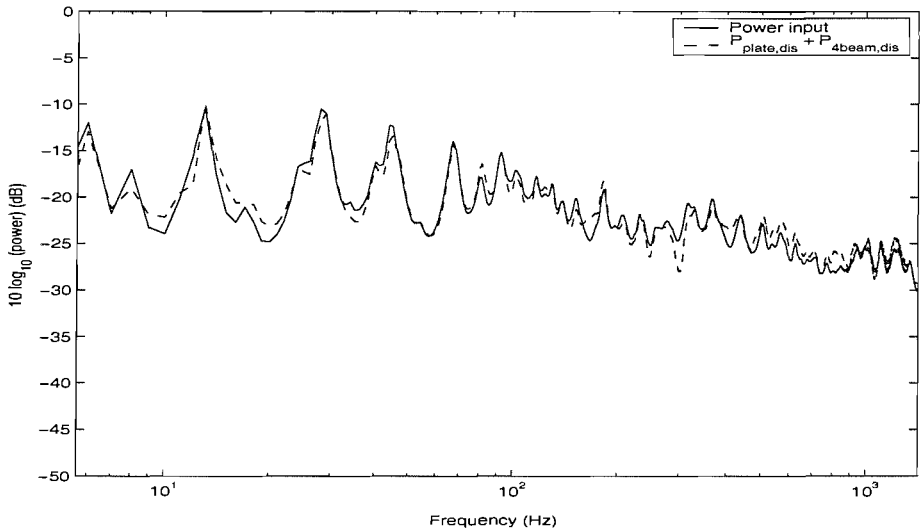

Figure 7.37. Input and dissipated power of the four-beam-plate system C4.

The numerical input powers of the modal method and the wave method are compared with that of the experiment in Figure 7.38. These results show the same tendencies as those for system C3, see Figure 7.35. As in the previous section, the three results are similar, which shows the suitability of the numerical models.

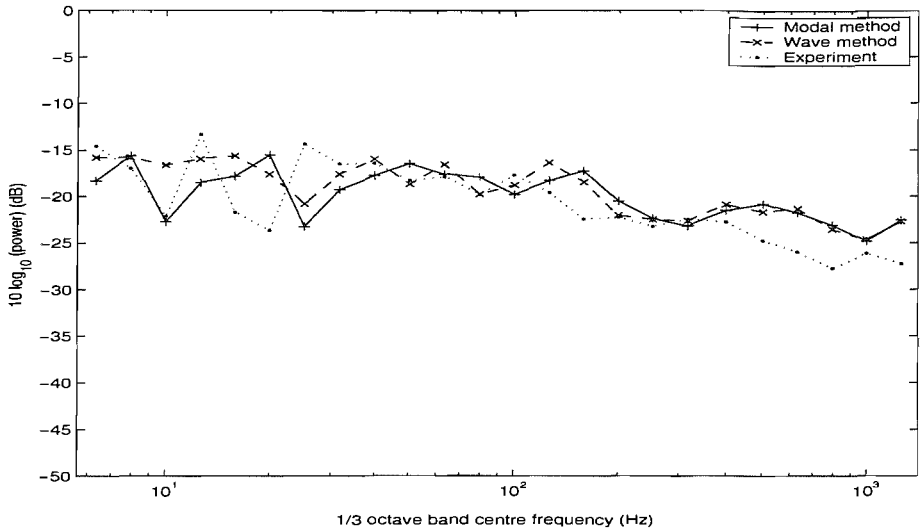

Figure 7.38. Input power in one-third octave bands for the four-beam-plate system C4: comparison between the numerical models and the experiment.

The one-third octave band energy ratios predicted by the modal and wave models are compared with the experimental results in Figure 7.39, which provides further interesting results. The modal model gives close agreement to the experimental results for all cases. The wave model shows reasonable agreement above about 40 Hz for the energy ratio between the stiffer beams and the plate. However, it is found that the difference in the energy of beam 3 increases and also there is difference in beam 2 compared with the case where all the beams were identical. In both cases the wave model gives lower energies than for identical beams, whereas the modal method gives similar results to previously.

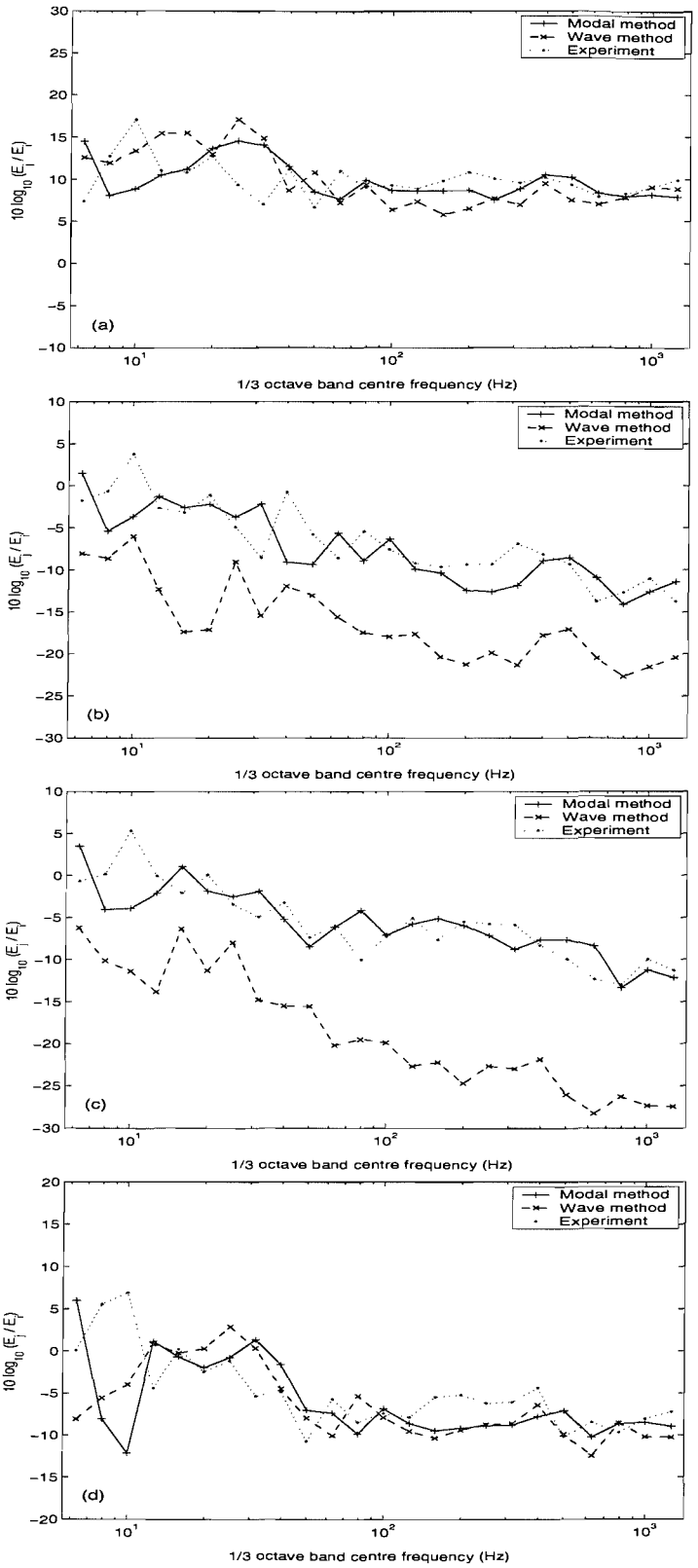

Figure 7.39. Energy ratio in one-third octave bands of the four-beam-plate system C4 for the numerical models and the experiment: (a) E_{plate}/E_{beam1}, (b) E_{beam2}/E_{beam1}, (c) E_{beam3}/E_{beam1}, (d) E_{beam4}/E_{beam1}.

This appears to be due to the fact that the wave model does not physically connect these beams to the excited beam through the plate. Beams 2 and 3 are 13.3 mm high which is less than of beams 1 and 4 (24.1 mm). Power flow from the driven beam to the opposite beam 3, for example, appears to be dominated by power flow through the plate and the wave model cannot reproduce this effect. This implies that the wave model gives better results for a system consisting of much stiffer beams and a more flexible plate. In this case it is known that power transfer through the plate is not so important. If one is solely interested in the driven beam or plate response then Figures 7.36 and 7.39 show that either prediction method could be used as the trends and average levels are in good agreement.

It is interesting to compare the experimental results of systems C2 and C4 which both have dissimilar beams opposite the excitation point. While beams 1 and 3 are connected by other beams as well as the plate in system C4, they are connected only by the plate in system C2. Nevertheless, comparing Figures 7.32 (b) and 7.39 (c), one can find that the energy ratios are at similar levels. Thus, this helps to confirm that the power is hardly transferred to beam 3 through the beams and most of the power is transferred through the plate.

7.7 Conclusions

Experimental studies dealing with various built-up structures consisting of beams attached to a rectangular plate and the comparison with the numerical models provide some important conclusions.

(a) Although the boundary conditions in the numerical models are different from the experimental configuration, comparison of the power input shows the suitability of the models based on the Fourier technique, the modal method and the wave method for mid-frequency analysis, especially when frequency-band averaged results are considered.

(b) By studying the energy ratios it is possible to investigate the energy relationship between subsystems in the built-up structures. The results show that, apart from differences in the narrow-band results at low frequencies, the effect of the boundary conditions is not significant in terms of energy ratios.

(c) In addition, even though the wave model gives only an approximate response, it can be used to predict the behaviour of the two-identical-beam coupled system and the framed structure consisting of four identical beams. Comparison of the numerical and the experimental results shows that the beam-plate coupled system consisting of stiffer beams results in a better estimation in the wave method. When the beams are less stiff they are more influenced by coupling through the plate which has been ignored in this method.

(d) From measurements with a scanning laser vibrometer, the wavenumber of the coupled system consisting of two beams and plate has been identified. It is shown that the wavenumber component in the plate normal to the beam is almost identical to the plate free wavenumber and the trace wavenumber parallel to the beam is dominated by the stiffer beam structure and its wavenumber.

CHAPTER 8

CONCLUSIONS

8.1 Introduction

The mid-frequency region is generally defined the region where neither a deterministic method such as Finite Element Analysis (FEA) nor a probabilistic method such as Statistical Energy Analysis (SEA) can be used reliably. As seen in Chapter 1, there have been many efforts to find a solution for such a frequency region. However, it is also true that most of them remain applied to simpler situations, for example, a system comprising a single beam and a single plate and more research is necessary so that a general tool for mid-frequency analysis can be used practically.

The object of this thesis is to deal with more complicated systems through reasonable approaches and the corresponding results are mainly concentrated on the mid and high frequencies. For this, various analytical and numerical approaches have been examined. The uncoupled beams considered contain only about 10 modes below 1412 Hz. Thus, their behaviour can be regarded as a low frequency motion in the present frequency range (5.6 – 1412 Hz). Meanwhile, the plate considered has about 500 modes in the same frequency range so that it shows high frequency characteristics with a modal overlap greater than unity above 50 Hz (see Chapter 6). The mid-frequency region is thus defined in this thesis, in a narrow sense, as a certain frequency region associated with the coupling of stiff beams and a flexible plate where the beams are in their 'low frequency' region and the plate in its 'high frequency' region. For realisation of these two important objectives, i.e. the consideration of more complicated systems and the coupling of stiff beams and a flexible plate, a coupled system consisting of several beams and a plate is a principal system examined in the thesis.

In particular, a beam-plate-beam coupled structure was analysed based on a Fourier technique. A wave method provides an approximate response of such a structure. A modal method was applied to find the vibrational motion of a framed structure consisting of four beams and a rectangular plate. The approximate wave method was then used to find a reasonable response of the same system, at least in the mid-frequency region. The response obtained using such approaches was firstly evaluated using FEA and then compared with those obtained experimentally. Wavenumbers were also identified from the experiment and shown to satisfy the assumption on which the approximate wave method is based.

8.2 Summaries and conclusions

8.2.1 Analytical methods

FEM and SEA are the most important tools to predict the dynamic response of structural and acoustical systems and are found widely in industrial use; some examples were presented in Chapter 1. Research intended to overcome the limitations of these methods was also reviewed. These previous studies show that more research is still necessary and this thesis provides a contribution to this area.

Among the different kinds of approach in use to analyse the dynamic behaviour of a system, the methods based on a Fourier transform/series and modal coupling are considered in this thesis. These are also used to provide a reference for comparison with the approximate wave method that is developed. These methods have been applied previously to a simple beam and a simple plate. These Fourier and modal methods are also extended here to find the response of more complicated systems.

Firstly, a modal coupling technique was presented in Chapter 2 and applied to a single stiff beam and a rectangular plate. Assuming the plate edges are in sliding conditions, the vibrational response of the coupled system can be found in a relatively simple form using separation of variables. It was shown that the

behaviour of the plate in the beam direction is mostly governed by the stiff beam. This implies that the coupled plate motion can be analysed by means of trace wavenumber matching involving the coupled beam wavenumber in the wave approach.

In Chapter 3, the Fourier method clearly showed the nature of the interaction between the beam and plate in the single-beam coupled system. The fact that the flexible plate acts as an equivalent mass and damping to the beam was shown in the wavenumber domain.

The procedures presented in Chapters 2 and 3 can also be extended to more complex systems. Also, they can be used as a basis for comparison with the approximate wave method. They provide an exact result for the present boundary conditions, apart from the need for an infinite number of modes or Fourier components. Convergence was examined to minimise computational time and computer resources. The criteria determined from the convergence study were utilised in the analysis of more complicated systems.

8.2.2 Approximate wave method

As an approximate approach, a wave method was studied. The wave method, originally proposed by Grice and Pinnington [41] to analyse a symmetric single beam-plate system, was applied to a non-symmetric single beam-plate system. While in the Fourier method the whole range of real values for the coupled beam wavenumber are included in the integral, in the wave approach the coupled beam free wavenumber is calculated based on wavenumber trace matching.

Under the important hypothesis that the coupled beam wavenumber is sufficiently smaller than the plate free wavenumber, it was shown that the exact line impedance for the plate could be substituted by the approximate impedance where the plate trace wavenumbers are assumed to be equal to the plate free wavenumber. This

physically means that the plate can be regarded as many strips along the beam. The damping and mass effect of the coupled plate observed in the Fourier method was analytically explained in terms of the wave approach.

The wave method presented by Grice and Pinnington [41] was enhanced to obtain an improved response. A simple iteration method to find roots in the wave dispersion equation did not converge at certain frequencies. It was shown that introducing Muller's method to identify roots in the complex domain could solve such a problem. Strictly, the travelling and nearfield 'free' wavenumbers in the coupled beam should be different if present separately. Separation of the two wavenumbers was attempted. The corresponding numerical results using these two wavenumbers simultaneously showed violation of the energy conservation between the transferred and dissipated powers in the plate. This could be overcome by using the plate impedance corresponding to the travelling wave when finding the nearfield wavenumber, which yields identical wavenumbers. By using this approach, an approximate system is obtained for which the power balance holds. As the plate behaves like strips, the power in the direction normal to the beam is only taken into account for the dissipated power in the plate. Consequently, the plate-dissipated power is an underestimate. Nevertheless, it was shown that the wave method is still a good approximate approach. A similar approach was also adopted later in the analysis of more complicated systems involving two or four beams.

8.2.3 Analysis of two-beam coupled systems

For analysis of a coupled system consisting of two parallel beams and a plate, the exact Fourier and approximate wave methods were considered. The response of the finite beam-plate-beam system can be found using a simple cosine function in the Fourier series if the opposite two edges of the plate (and the corresponding beam ends) are sliding. The relevant equations show that this method is advantageous as it can be used for a system consisting of two dissimilar beams.

By synthesising symmetric and antisymmetric motions of a single beam-plate system with half the width, the wave method can be used to find the response of a symmetric beam-plate-beam system. If plate impedances acting upon the two beams are assumed to be the same, then the plate impedance and coupled beam wavenumber for the non-symmetric single beam-plate system can be utilised without modification. Although strictly they may be different, a power balance investigation shows the difference to be small. Such a synthesis technique based on the wave model can also be used when the boundary conditions of the beam ends are different, for example, when free-free conditions are considered.

Mobilities and powers were examined based on the Fourier and wave methods. The Fourier method is regarded as an exact method for the present boundary conditions and used as a reference. The symmetric-antisymmetric wave model seems useful in dealing with a symmetric beam-plate-beam system. Although a power investigation of the wave model shows that the power transfer and dissipated power in the coupled system are only approximate, the numerical results show that it can provide a reasonable estimate of the dynamic response at mid-frequencies as well as high frequencies.

The energy ratios and the input power of the numerical models were compared with those obtained experimentally. The ratio of subsystem energies was introduced to reduce the effect of the different boundary conditions between the numerical model and the experiment. It was shown that the Fourier and wave methods replicate the experimental results very well. In the Fourier model, although the results show a small frequency shift in the general peaks and dips compared with the experiments, they can be explained in terms of the different boundary conditions. The general levels are in good agreement. The experiment also shows that the Fourier model can be applied reliably to the coupled system involving two dissimilar beams. The wave model can consider arbitrary boundary conditions with respect to the beam ends and such a frequency shift does not occur in comparison with the experiment. Thus, although the wave model was constituted

based on the approximate plate impedance, the narrow band response as well as the one-third octave band averages are in very good agreement with experiments at mid and high frequencies.

The most important hypothesis in the wave method is that the coupled beam wavenumber should be sufficiently smaller than the plate free wavenumber, so that the plate free wavenumber is almost equal to the trace wavenumber in the direction normal to the beam. This was verified experimentally by estimating the coupled plate wavenumber using a scanning laser vibrometer and a correlation technique. The estimation also shows that the plate motion is predominantly governed by the stiff beam. This was numerically predicted in a convergence study using the modal model consisting of two beams and a plate.

8.2.4 Analysis of four-beam coupled systems

By assuming sliding boundary conditions at the edges of the rectangular plate the motion of a coupled system consisting of four beams surrounding the plate could be obtained relatively simply using the modal method. Although the sliding condition is not a necessary condition in the modal method, it reduces the complexity in its application due to the possibility of separation of the variables in the plate and the fact that plate and beam mode shapes are equal. Strictly, although such boundary conditions are different from the experiment, the differences introduced are not very significant at least in dealing with mid and high frequency regions.

While the modal method gives an exact result as long as a sufficient number of modes are included, the wave method predicts only an approximate response. By assuming most of the power due to an excitation is dissipated in the plate the framed system can be modelled as a system consisting of four beams, each attached to a separate plate. The response in terms of one-third octave band averages showed that this plate-decoupled wave model gives reasonable results compared

with the modal model at least above 50 Hz; the region below this corresponds to the first 3 beam modes and the region where the modal overlap of the plate is less than unity.

In such a wave model, the dimensions and the boundary condition of the four plates were assumed to be the same as the original plate surrounded by four beams. Thus, the opposite edge parallel to the beam is assumed sliding. However, it is not a necessary condition for the modelling and even if a pinned condition or a different width is considered, the average response shows little difference in the mid and high frequency regions. Assuming semi-infinite plates (thus, an infinite width in the direction normal to the beam), however, results in an overestimate in the damping effect on the beam.

The wave model under such assumptions and the modal model were then compared with experiments. Although the boundary conditions of the analytical wave and modal models, i.e. the beam ends sliding and beams infinitely stiff in torsion, are different from those in the experiment, the input power comparison in terms of one-third octave band averages shows the suitability of the numerical models for the mid-frequency analysis. Especially in the wave model, although the inherent limitation that the plate does not connect the beams directly results in differences in the input power at low frequencies, in general it does not affect the results at mid and high frequencies. The energy ratio between subsystems based on one-third octave bands also shows the validity of the wave and modal models as the numerical and experimental results are generally in close agreement. While the modal model shows good agreement in comparison of the subsystem energy ratio, in the wave model there is a difference for the beam furthest from the excitation. This is because in the wave model the plate does not connect the beams.

The comparison with the experiment shows that the plate-decoupled wave model can predict the averaged response of four beam cases well at least in mid and high frequency regions. For example, the power inputs in one-third octave bands agree within 5 dB above about 50 Hz between the numerical four-beam model and the

experiment, even though a frequency shift occurs due to the different boundary conditions. Recall that the motion of the stiff beams is considered to be in their low frequency range while the plate shows high frequency behaviour. Thus, the estimation discussed above shows that the wave-based coupling of such subsystems having low and high frequency characteristics can provide a reasonable response in the mid-frequency region.

An advantage of the wave method is highlighted in terms of computation time and computer resources. Although the wave method can predict only an approximate response it requires far less computer resources and time. For example, for the present case of the framed system, it was shown that the wave method requires only about 1% of the computational time compared with a commercial FE program, despite using uncompiled code.

8.3 Recommended future research

In this section some suggestions for further research are highlighted.

8.3.1 Separation of plate impedances based on travelling and nearfield waves

In the wave method developed in this thesis, the plate impedance obtained based on the travelling wave in the coupled beam is used. This reasonably describes the motion of a beam-plate coupled system as the beam motion is dominated by the travelling wave. Nevertheless, strictly it is expected that the plate impedance depends on the nearfield wave as well as the travelling wave. The nearfield wave effect becomes larger near an excitation point or beam ends. Consequently, the response of the coupled beam might be represented in terms of the two wavenumbers, i.e. the travelling and the nearfield wavenumbers. In this thesis, a separation of the wavenumbers present in the coupled beam was sought and resulted in the violation of energy conservation. The physical system should obey the energy conservation. Thus, further study on the plate impedances dependent on

both the travelling and nearfield waves and the consequent motion of the beam-plate coupled system seems necessary.

8.3.2 Experimental identification of plate wavenumbers in a framed structure

In this thesis, the wavenumber of the plate in a coupled system comprising two identical beams was experimentally identified, from which it is found that the wavenumber in the beam direction is dominated by the beam wavenumber. It might be more complicated if the beams are dissimilar and it is necessary to investigate the plate wavenumber in such a case.

The plate wavenumbers in a framed structure with similar beams seem more interesting as it is expected that they may be related to the beam wavenumber as well as the plate wavenumber. Furthermore, if dissimilar beams are considered in the framed structure, the plate motion will be far more complex. Thus, the wavenumber identification of the coupled plate of various systems is an important topic for future study.

8.3.3 Curved panel and beam structure

In Chapter 1, it was stated that a main structure to be studied, four beams coupled to a plate, is principally important as such a structure can be found in automotive, marine and aerospace applications. For example, the floor and roof of a car are basically framed structures. The roof, however, usually consists of a doubly curved plate. Similarly aircraft consist of framed singly curved plates. In wave approaches in previous studies [41, 54, 55], the plate curvature is not included. Therefore, this could be considered using a wave approach.

8.3.4 Consideration of damping material attached to a plate

Another important area of study involves damping materials. Most important noise-control strategies are based on the use of damping materials, especially for high frequencies. However, their efficiency to control power flow between components such as plates and beams is hardly considered in general, which is important for weight and cost reduction.

In the wave approach, the plate is assumed to be strip-like. Thus, the damping treatment in this direction seems relatively easy and the power transfer between subsystems can be investigated in terms of the partially damped plate. Consequently, it is expected that the optimal location and appropriate material property of the damping treatment may be decided by using the locally damped plate.

8.3.5 Study of joint area in a beam-plate system

It seems especially difficult to understand the behaviour of the joint area of such a structure consisting of beams and a plate. Although the motion of such a framed structure was studied, for example, by Yang and Gupta [69] and Takabatake and Nagareda [68], there were no specific investigations on the joint area. Ohtsuki and Ellyin [89] studied the joint of a framed structure where the structure only consists of beams without a plate. In this thesis, the framed beam-plate system was analysed by assuming the four decoupled plates attached to each beam. Although the general response such as mobilities and powers shows the validity of this assumption at mid and high frequency regions, it is not so clear that the assumption can be acceptable in the joint area as it is expected that the response is more complicated due to the presence of nearfield waves. Thus, an investigation of the joint area of a beam-plate coupled structure seems useful for a future study.

8.3.6 Introduction of an arbitrary configuration in the wave method

It can be said that the structures investigated in this thesis are more complicated than those of previous studies discussed in Chapter 1, as they include systems with two or four beams. Nevertheless, these structures are based on the rectangular plate system. It is of interest to include more general configurations e.g. non-rectangular plates. Such a coupled system may be realised using a similar approach proposed in Chapter 6. Also, FE may be used to model the beams, while the impedance acting on the beam is considered analytically. Grice and Pinington [55] proposed a similar approach. However, their coupled structure, a box structure, was still based on the rectangular configuration and there is considerable scope for further investigation.

REFERENCES

[1] F. Fahy 2001 *Foundations of Engineering Acoustics*. London: Academic Press.

[2] D. A. Bies and C. H. Hansen 1996 *Engineering Noise Control*. London: E & FN Spon; 2nd edition

[3] M. Petyt 1990 *Introduction to finite element vibration analysis*. Cambridge: Cambridge University Press.

[4] O. C. Zienkiewicz and R. L. Taylor 1989 *The Finite Element Method: Basic Concepts and Linear Applications*. London: McGraw Hill; 3rd edition.

[5] S. H. Sung and D. J. Nefske 2001 *SAE Technical papers* 2001-01-1402. Assessment of a vehicle concept finite-element model for predicting structural vibration.

[6] S. K. Jung, J. K. Suh and J. U. Lee 2004 *Korea MSC Users conference.* Evaluation and improvement of vibration and noise in a full vehicle based on CAE (in Korean).

[7] M. J. Moeller, R. S. Thomas, H. Maruvada, N. S. Chandra and M. Zebrowski 2000 *Proceedings of 2nd Automotive Worldwide Conference.* An assessment of a FEA NVH CAE body model for design capability.

[8] J. W. Yoo, J. K. Suh, S. H. Lim, J. U. Lee and M. K. Seo 2000 *Proceedings of 2nd Automotive Worldwide Conference.* Analysis and Correlation for Body Attachment Stiffness in BIW.

[9] W. Han and M. Petyt 1996 *Computers and Structures* **61**, 705-712. Linear vibration analysis of laminated rectangular plates using the hierarchical finite element method – I. Free vibration analysis.

[10] P. Riebero 2001 *Journal of Sound and Vibration* **246**, 225-244. Hierarchical finite element analyses of geometrically non-linear vibration of beams and plane frames.

[11] M. S. Kompella and R. J. Bernhard 1993 *Proceedings of SAE noise and vibration Conference.* Measurement of the statistical variation of structural-acoustic characteristics of automotive vehicles.

[12] R. H. Lyon and R. G. DeJong 1995 *Theory and Application of Statistical Energy Analysis*. Boston: Butterworth-Heinemann.

[13] R. G. White and J. G. Walker (eds) 1982 *Noise and Vibration,* Chapter 7. Ellis Horwood.

[14] R. J. M. Craik 1996 *Sound Transmission through Buildings using Statistical Energy Analysis*. Aldershot: Gower Publishing.

[15] ESDU 99009. An introduction to Statistical Energy Analysis.

[16] C. B. Burroughs, R. W. Fischer and F. R. Kern 1997 *Journal of Acoustical Society of America* **101**, 1779-1789. An introduction to statistical energy analysis.

[17] F. J. Fahy 1994 *Philosophical Transactions of the Royal Society of London* A346 431-447. Statistical energy analysis: a critical overview.

[18] B. R. Mace and J. Rosenberg 1995 *Proceedings of Inter-Noise '95* 1271-1274. Energy flow between two coupled plate: finite element and statistical energy analyses.

[19] B. R. Mace 1992 *Journal of Sound and Vibration* **154**, 289-319. Power flow between two continuous one-dimensional subsystems: a wave solution.

[20] R. G. DeJong 1997 in *Proceedings of IUTAM symposium on Statistical Energy Analysis*, 71-82. An approach to the Statistical Energy Analysis of strongly coupled systems.

[21] W. S. Park 2003 *Ph.D. Thesis, University of Southampton.* The sources of variability in statistical energy analysis coupling of two rectangular plates.

[22] P. W. Smith Jr. 1979 *Journal of Acoustical Society of America*, **65**, 695-698. Statistical models of coupled dynamical systems and the transition from weak to strong coupling.

[23] V. Jayachandran and M. W. Bonilha 2003 *Journal of Acoustical Society of America*, **113**, 1448-61454. A hybrid SEA/modal technique for modelling structural-acoustic interior noise in rotorcraft.

[24] G. Fraser 1998 *Ph.D. Thesis, Heriot-Watt University.* Structure-borne sound in motor vehicles using Statistical Energy Analysis.

[25] T. Yamazaki, M. Kamata and S. Ohno 2003 *10th International Congress of Sound and Vibration, Stockholm, Sweden,* 1179-1183. SEA model of automotive vehicle body-in-white based on modal density estimation.

[26] E. C. N. Wester and B. R. Mace 1996 *Journal of Sound and Vibration* **193,** 793-822. Statistical energy analysis of two edge-coupled rectangular plate: ensemble averages.

[27] F. J. Fahy and A. D. Mohammed 1992 *Journal of Sound and Vibration* **158,** 45-67. A study of uncertainty in applications of SEA to coupled beam and plate systems, part 1: computational experiment.

[28] D. J. Nefske and S. H. Sung 1989 *Journal of Vibration, Acoustics, Stress, and Reliability in Design* **111,** 94-106. Power flow finite element analysis of dynamic systems: basic theory and application to beams.

[29] J. C. Wohlever and R. J. Bernhard 1992 *Journal of Sound and Vibration* **153,** 1-19. Mechanical energy flow models of rods and beams.

[30] O. M. Bouthier and R. J. Bernhard 1995 *Journal of Sound and Vibration* **182,** 129-147. Simple models of energy flow in vibrating membranes.

[31] S.-H. Seo, S.-Y. Hong and H.-G. Kil 2003 *Journal of Sound and Vibration* **259**, 1109-1129. Power flow analysis of reinforced beam-plate coupled structures.

[32] R. S. Langley 1995, *Journal of Sound and Vibration* **182,** 637-657. On the vibrational conductivity approach to high frequency dynamics for two-dimensional structural components.

[33] N. Vlahopoulos, L. O. Garza-Rios, and C. Mollo 1999, *Journal of Ship Research* **43**, 143-156. Numerical implementation, validation, and marine applications of an energy finite element formulation.

[34] N. Vlahopoulos, X. Zhao and T. Allen. 1999 *Journal of Sound and Vibration* **220**, 135-154. An approach for evaluating power transfer coefficients for spot-welded joints in an energy finite element formulation.

[35] B. R. Mace and P. J. Shorter 2000 *Journal of Sound and Vibration* **233**, 369-389. Energy flow models from finite element analysis.

[36] M. P. Castanier, Y.-C. Tan and C. Pierre 2001 *AIAA Journal* **39**, 1182-1187. Characteristic constraint modes for component mode synthesis.

[37] Y.-C. Tan, M. P. Castanier and C. Pierre 2001 *Proceedings of the 19th International Modal Analysis Conference, Kissimmee, USA,* **2**, 1070-1076. Efficient reduced order modelling of low to mid-frequency vibration and power flow in complex structure.

[38] B. R. Mace and P. J. Shorter 2001 *Journal of Sound and Vibration* **242**, 793-811. A local modal/perturbational method for estimating frequency response statistics of built-up structures with uncertain properties.

[39] C. Soize and S. Mziou 2004 *AIAA Journal* **41**, 1113-1118. Dynamic substructuring in the medium-frquency range.

[40] C. T. Hugin 1997 *Journal of Sound and Vibration* **203**, 563-580. A physical description of the response of coupled beams.

[41] R. M. Grice and R. J. Pinnington 1999 *Journal of Sound and Vibration* **230**, 825-849. A method for the vibrational analysis of built-up structures, part 1: Introduction and analytical analysis of the plate-stiffened beam.

[42] C. Soize 1993 *Journal of the Acoustical Society of America* **94**, 849-865. A model and numerical method in the medium frequency range for vibroacoustic predictions using the theory of structural fuzzy.

[43] C. E. Ruckman and D. Feit 1995 *15th International Congress on Acoustics.* Fuzzy structures analysis: a simple example.

[44] G. Coupry and C. Soize 1984 *Journal of Sound and Vibration* **96**, 261-273. Hydroelasticity and the field radiated by a slender body into an unbounded fluid.

[45] C. Soize and K. Bjaoui 2000 *Journal of the Acoustical Society of America* **107**, 2011-2020. Estimation of fuzzy parameters for continuous junctions.

[46] M. Strasberg and D. Feit 1996 *Journal of the Acoustical Society of America* **99**, 335-344. Vibration damping of large structures induced by attached small resonant structures.

[47] L. Ji, B. R. Mace and R. J. Pinnington 2003 *Journal of Sound and Vibration* **265**, 387-399. A power mode approach to estimating vibrational power transmission by multiple sources.

[48] L. Ji, B. R. Mace and R. J. Pinnington 2003 *Journal of Sound and Vibration* **268**, 525-542. Estimation of power transmission to a flexible receiver from a stiff source using a power mode approach.

[49] L. Ji, B. R. Mace and R. J. Pinnington *Journal of Sound and Vibration*. A mode-based approach for the mid-frequency vibration analysis of coupled long- and short-wavelength structures (in press).

[50] R. S. Langley and P. Bremner 1999 *Journal of Acoustical Society of America* **105**, 1657-1671. A hybrid method for the vibration analysis of complex structural-acoustic systems.

[51] R. S. Langley, P. J. Shorter and V. Cotoni 2005 *Proceedings of Novem 2005*. A hybrid FE-SEA method for the analysis of complex vibro-acoustic systems.

[52] N. Vlahopoulos and X. Zhao 1999 *AIAA Journal* **37**, 1495-1505. Basic development of hybrid finite element method for mid-frequency structural vibrations.

[53] X. Zhao and N. Vlahopoulos 2004 *Journal of Sound and Vibration* **269**, 135-164. A basic hybrid finite element formulation for mid-frequency analysis of beams connected at an arbitrary angle.

[54] R. M. Grice and R. J. Pinnington 1999 *Journal of Sound and Vibration* **230**, 851-875. A method for the vibrational analysis of built-up structures, part 2: Analysis of the plate-stiffened beam using a combination of finite element analysis and analytical impedances.

[55] R. M. Grice and R. J. Pinnington 2002 *Journal of Sound and Vibration* **249**, 499-527. Analysis of the flexural vibration of a thin-plate box using a combination of finite element analysis and analytical impedance.

[56] L. Ji and B. R. Mace and R. J. Pinnington 2003 *Journal of Sound and Vibration* **274**, 547-565. A hybrid/Fourier Transform approach to estimating the vibration of beam-stiffened plates systems.

[57] R. S. Langley 1992 *Journal of Sound and Vibration* **159**, 483-502. A wave intensity technique for the analysis of high frequency vibrations.

[58] R. S. Langley 1994 *Journal of Sound and Vibration* **169**, 297-317. Elastic Wave Transmission Coefficients and Coupling Loss Factors for Structural Junctions Between Curved Panels.

[59] R. J. M. Craik, J. A. Steel and D. I. Evans 1991 *Journal of Sound and Vibration* **144**, 95-107. Statistical energy analysis of structure-borne sound transmission at low frequencies.

[60] A. D. Mohammed 1990 *Ph.D. Thesis, University of Southampton.* A study of uncertainty in applications of Statistical Energy Analysis.

[61] K. Shankar and A. J. Keane 1995 *Journal of Sound and Vibration* **185**, 867-890. Energy flow predictions in a structure of rigidly joined beams using receptance theory.

[62] K. Shankar and A. J. Keane 1997 *Journal of Sound and Vibration* **201**, 491-513. Vibrational energy flow analysis using a substructure approach: The application of receptance theory to FEA and SEA.

[63] R. R. Craig and M. C. C. Bampton 1968 *AIAA Journal* **6**, 1313-1319. Coupling of substructures for dynamic analysis.

[64] M. Heckl 1961 *Journal of the Acoustical Society of America* **33**, 640-651. Wave propagation on beam-plate systems.

[65] S. Jianxin, A. T. Moorhouse and B. M. Gibbs 1995 *Journal of Sound and Vibration* **185**, 737-741. Towards a practical characterization for structure-borne sound sources based on mobility techniques.

[66] J. M. Cuschieri 1990 *Journal of Acoustical Society of America* **87**, 1159-1165. Structural power-flow analysis using a mobility approach of an L-shaped plate.

[67] E. Savin 2002 *AIAA Journal* **40**, 1876-1884. Mid-frequency vibrations of a complex structure: Experiments and comparison with numerical simulation.

[68] H. Takabatake and Y. Nagareda 1999 *Computers and Structures* **70**, 129-139. A simplified analysis of elastic plates with edge beams.

[69] J. Yang and A. Gupta 2002 *Journal of Sound and Vibration* **253**, 373-388. Ritz vector approach for static and dynamic analysis of plates with edge beams.

[70] G. B. Warburton 1976 *The Dynamical Behaviour of Structures.* Oxford: Pergamon Press; second edition.

[71] S. S. Rao 1995 *Mechanical vibrations.* Addison-Wesley Publishing Company; third edition.

[72] M. L. James, G. M. Smith, J. C. Wolford and P. W. Whaley 1989 *Vibration of mechanical and structural systems: with microcomputer applications*. New York: Harper and Row Inc.

[73] W. L. Thomson 1972 *Theory of Vibration with Applications*. New Jersey: Prentice-Hall.

[74] L. Meirovich 1986 *Elements of Vibration Analysis*. New York: McGraw-Hill; 2nd edition.

[75] R. Szilard 1974 *Theory and Analysis of Plates*: *Classical and Numerical methods*. New Jersey: Prentice-Hall.

[76] R. E. D. Bishop and D. C. Johnson 1960 *Mechanics of Vibration*. London: The Cambridge University Press.

[77] S. P. Timoshenko and S. Woinowsky-Krieger 1959 *Theory of Plates and Shells*, New York: McGraw-Hill; second edition.

[78] E. Kreyszig 1983 *Advanced Engineering Mathematics*. New York: John Wiley & Sons; fifth edition.

[79] L. Cremer, M. Heckl and E. E. Ungar 1988 *Structure-borne Sound*. Berlin: Springer Verlag; 2nd edition.

[80] G. L. Lamb, Jr 1961 *Journal of Acoustical Society of America* **33**, 628-633. Input impedance of a beam coupled to a plate.

[81] The Math Works, Inc. 2001, *MATLAB Function Reference Volume 3: P – Z* (*on line version*).

[82] R. W. Ramirez 1985 *The FFT Fundamentals and Concepts*. New Jersey: Prentice-Hall.

[83] C. F. Gerald 1977 *Applied Numerical Analysis*, San Luis Obispo.

[84] J. W. Yoo, D. J. Thompson and N. S. Ferguson 2003 *ISVR Memorandom No*: **905**. Structural analysis of a symmetric structure consisting of two beams and a plate based on a wave approach.

[85] D. J. Ewins 2000 *Modal Testing: Theory, Practice and Application*. Baldock: Research studies press; second edition.

[86] S. C. Chapra and R. P. Canale 1989 *Numerical Methods for Engineers*. McGraw-Hill; second edition.

[87] A. N. Thite and N. S. Ferguson 2004 *ISVR Memorandom No*: **937**. Wavenumber estimation: further study of the correlation technique and use of SVD to improve propagation direction resolution.

[88] D. J. Thompson 2001 *Lecture Notes on Noise and Vibration control. MSc. Sound and Vibration Studies*, ISVR, University of Southampton.

[89] A. Ohtsuki and F. Ellyin 2000 *Thin-walled structure* **38**, 79-91. Large deformation analysis of a square frame with rigid joints.

APPENDIX A.
NEARFIELD WAVENUMBER OF COUPLED BEAM

A.1 Theoretical derivation

The dispersion relationship of coupled systems was derived in sections 4.3.2 and 4.3.3, in which the nearfield wavenumber is obtained based on the travelling wave assumption. As seen in section 4.3.4, substituting the travelling wavenumber for the nearfield wavenumber gives an advantage to understand physical phenomena of the structural coupling. However, strictly the two wavenumbers cannot be considered equal. Thus, the nearfield wavenumber is taken into account in this appendix.

Consider first the coupled system consisting of an infinite beam and an infinitely long finite width plate as in section 4.3.1 (see the structure shown in Figure 3.15). A wavenumber relationship can similarly be developed when the nearfield wavenumber in the beam is considered. Suppose that the nearfield wave motion of the beam is represented by

$$\tilde{w}_b = \tilde{A}' e^{-k_{nf} x} . \tag{A.1}$$

where k_{nf} is the nearfield wavenumber in the coupled beam.

Then the motion of the plate with no damping is given by

$$\tilde{w}_P = (\tilde{B}' e^{-ik'_y y} + \tilde{C}' e^{-k'_e y} + \beta'_y \tilde{r} \tilde{B}' e^{ik'_y y} + \tilde{D}' e^{k'_e (y - L_y)}) e^{-k_{nf} x} \tag{A.2}$$

where $\tilde{B}'$ is the amplitude of the travelling wave, $\tilde{C}'$ is the amplitude of the nearfield wave in the plate, $\tilde{D}'$ is the amplitude of the nearfield wave which is generated at the opposite edge of the plate, k'_y is the trace wavenumber for the

travelling wave radiating into the plate normal to the beam, k_e' is the trace wavenumber for the nearfield wave in the plate and $\beta_y' = e^{-ik_y' 2L_y}$ represents a phase shift over length $2L_y$. The dash is used to distinguish them from the case when the travelling beam wavenumber is considered.

Now consider the travelling wave solution in the plate $\tilde{w}_p = \tilde{B}' e^{-ik_y' y} e^{-k_{nf} x}$ to obtain the nearfield wavenumber k_{nf}. Substituting this into equation (3.7) describing motion of the plate results in

$$\{D_p(k_{nf}^4 - 2k_y'^2 k_{nf}^2 + k_y'^4) - m_p'' \omega^2\} \tilde{B}' e^{-ik_y' y} e^{-k_{nf} x} = 0. \qquad \text{(A.3)}$$

For non-trivial solutions $k_{nf}^4 - 2k_y'^2 k_{nf}^2 + k_y'^4 - k_p^4 = 0$. Therefore, the propagating normal trace wavenumber in the plate is

$$k_y' = \sqrt{k_p^2 + k_{nf}^2}. \qquad \text{(A.4 a)}$$

Similarly, letting $\tilde{w}_p = \tilde{C}' e^{-k_e' y} e^{-k_{nf} x}$, then the nearfield plate wavenumber is

$$k_e' = \sqrt{k_p^2 - k_{nf}^2}. \qquad \text{(A.4 b)}$$

They are found by solving the dispersion equation similar to equation (4.34) using k_{nf} instead of k_x. These differ from the results k_y and k_e found for a travelling wave k_x in the beam.

The procedure to obtain the plate impedance when the beam nearfield wavenumber is considered is similar to the case when the travelling wavenumber is considered (see section 4.3.1). All of the equations are the same except equation (4.29), the force equilibrium condition, which is

$$D_p e^{-k_{nf} x} \left[ik_y' \left\{ k_y'^2 - (2-\nu) k_{nf}^2 \right\} (1 - \beta_y \tilde{r}) \tilde{B}' - k_e' \left\{ k_e'^2 + (2-\nu) k_{nf}^2 \right\} \tilde{C}' \right] = \tilde{f}_1(x). \qquad \text{(A.5)}$$

Once k_{nf} has been eliminated from this equation, the equation for the impedance is the same as equation (4.31). Note that even though the equation is not changed, a different value will be calculated because the impedance includes k'_y, k'_e and the phase shift β'_y which is a function of k'_y, all of which differ from the values corresponding to a travelling wave k_x. The introduction of damping on the plate and the approximation of the impedance follow the same procedure as explained for the case of the travelling wavenumber in section 4.3.2.

A.2 Wavenumbers

The nearfield wavenumber k_{nf} in the coupled beam and its corresponding wavenumbers in the finite plate are shown in Figure A.1. The uncoupled beam wavenumber k_b and coupled beam wavenumber k_x using the semi-infinite plate are shown for comparison. One can see that k_{nf} based on the finite plate follows well the asymptotic line k_x.

The corresponding results for the travelling wavenumber are already shown in Figure 4.13. Comparing Figures A.1 and 4.13 show how the plate wavenumbers are changed due to the travelling and nearfield wavenumbers of the beam. It can be seen that the travelling and nearfield waves of the plate in the y direction can be approximated by the free wavenumber of the plate in both cases.

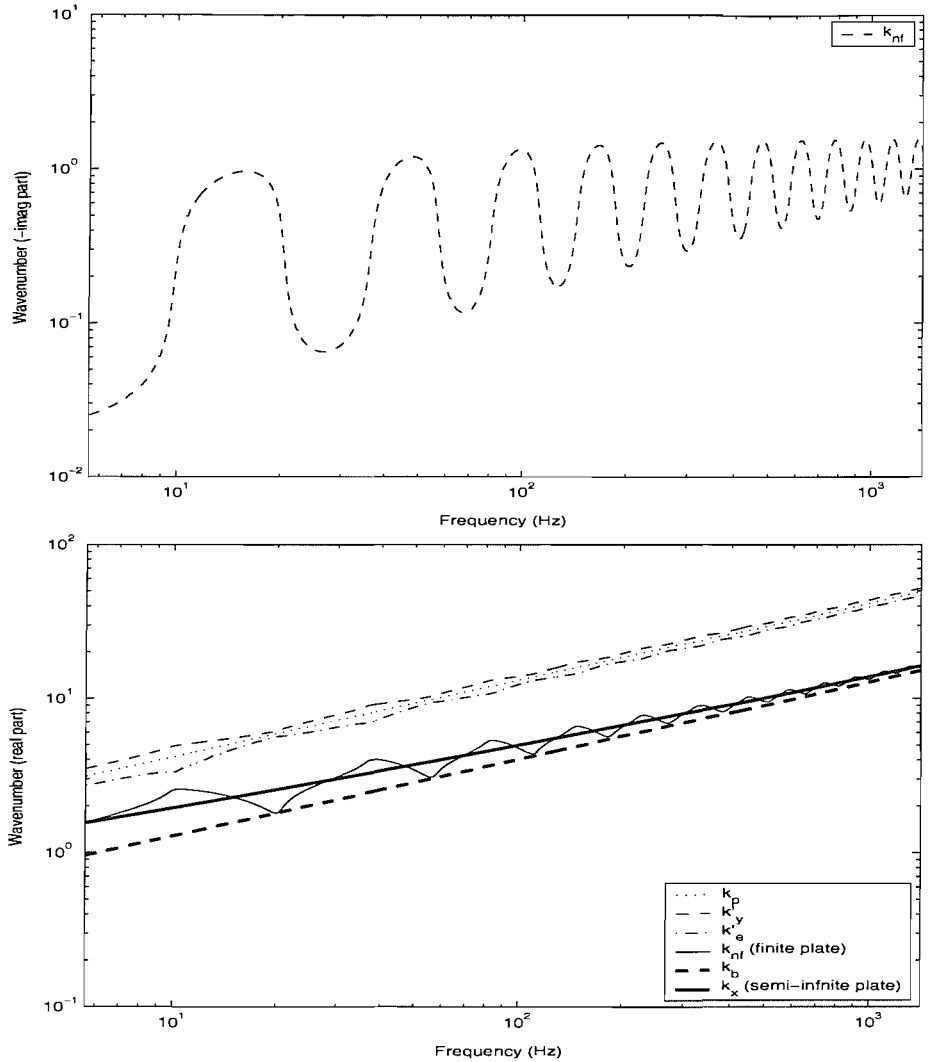

Figure A.1. Comparison of the nearfield wavenumber of the beam and the corresponding wavenumbers of the plate of the coupled structure as in Figure 2.2 ($\eta_p = 0.05$ in the plate, $\eta_b = 0.05$ in the beam).

In Figure A.2, a comparison is given of the imaginary parts of the travelling wavenumber and nearfield wavenumber in the coupled beam as well as the corresponding real parts.

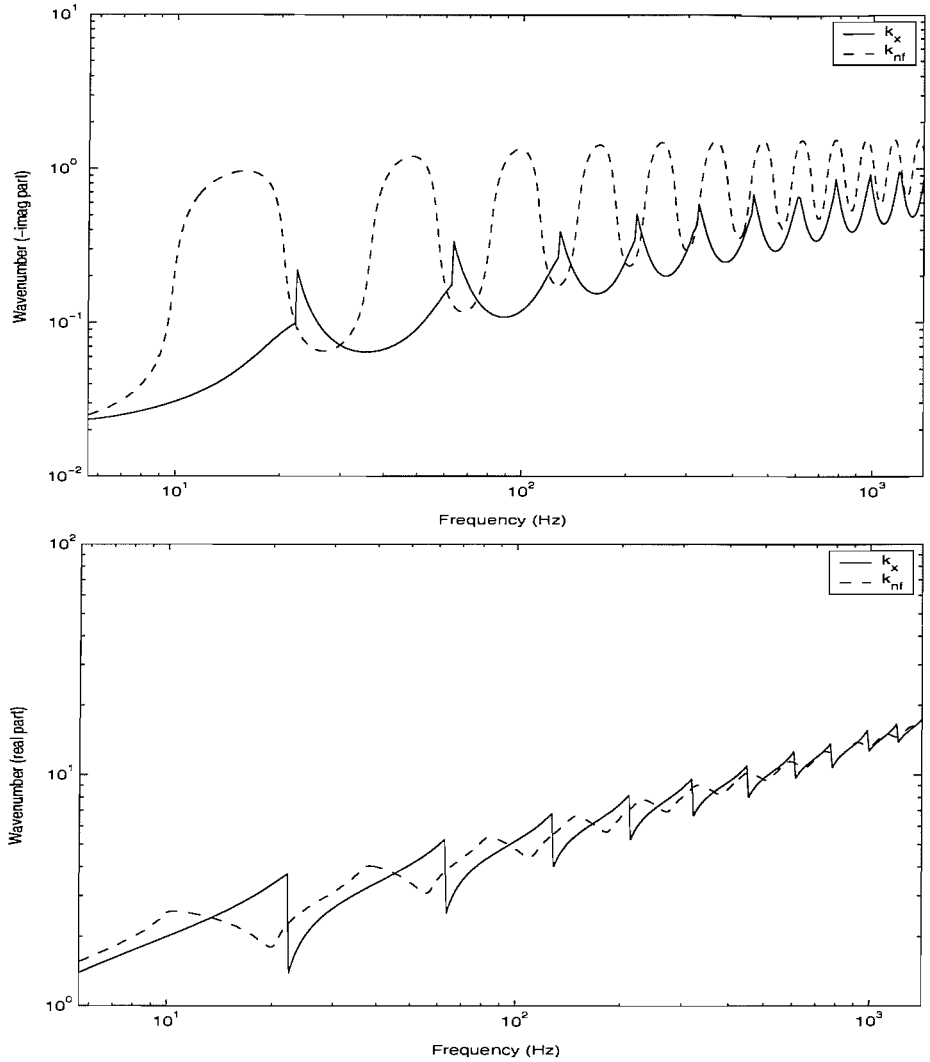

Figure A.2. Comparison of the beam travelling and the nearfield wavenumber in the coupled structure consisting of the finite beam and the finite plate as in Figure 2.2 ($\eta_p = 0.05$ in the plate, $\eta_b = 0.05$ in the beam).

These wavenumbers are related to the plate impedance and, for example, at the peaks of k_x the plate exhibits an anti-resonance (see also Figure A.4). In the same way the nearfield wave number k_{nf} depends on the corresponding impedance of the plate which has peaks at different frequencies. At the peaks of the imaginary part of k_x the plate has a considerable damping effect on the beam.

Approximate equivalent loss factors are shown in Figure A.3, determined according to equation (4.24). Note that at the anti-resonances of the plate, the damping is large so that the small damping approximation no longer holds.

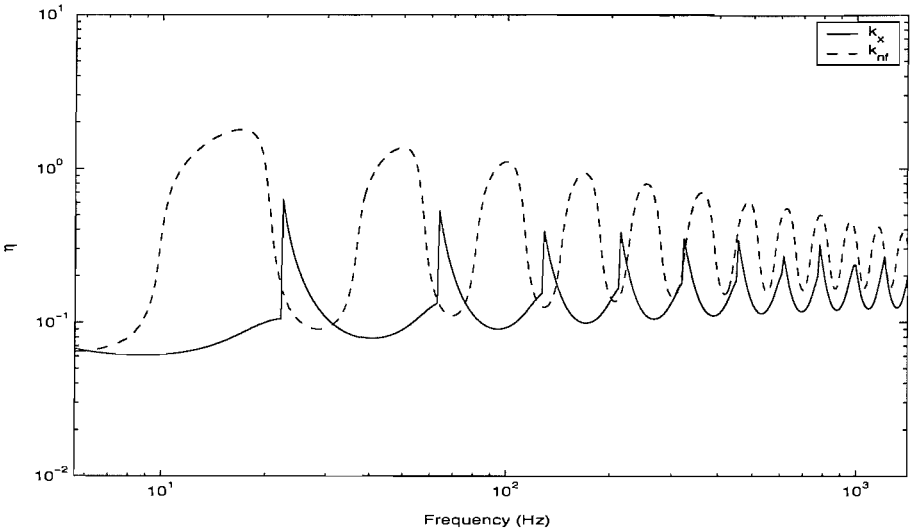

Figure A.3. Equivalent loss factors of the travelling and the nearfield wavenumbers in the coupled beam.

A.3 Impedance

In Figure A.4, the approximate line impedances (see equation (4.33)) of the finite width plate with damping are shown when $\tilde{k}_x$ and $\tilde{k}_{nf}$ are considered respectively. As mentioned before, although the impedance equation (4.33) is unaltered, the figure shows how the values of the impedances are changed when $\tilde{k}_x$ or $\tilde{k}_{nf}$ is considered. The peaks in the impedance correspond to the plate anti-resonances, and comparing Figures A.3 and A.4, it is clear that the equivalent loss factor is maximum around these frequencies.

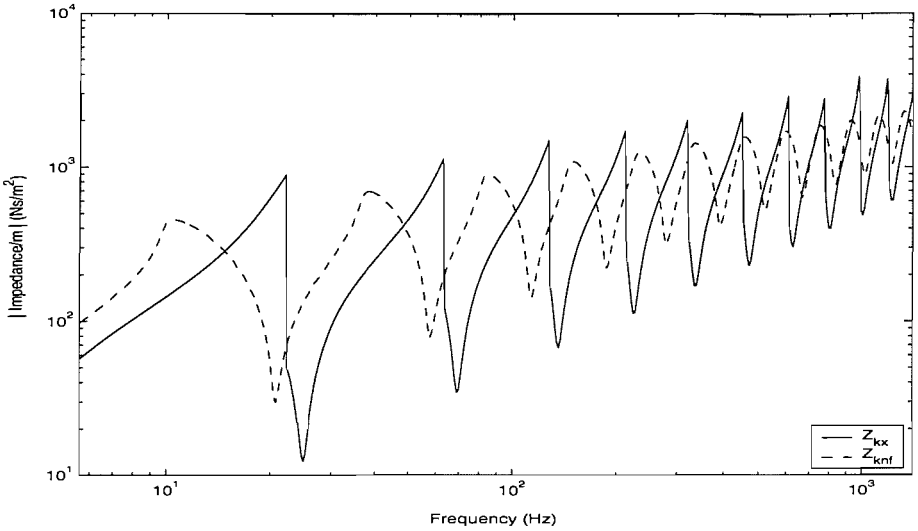

Figure A.4. Approximate line impedance of the finite width plate as in Figure 2.2 ($\eta_p = 0.05$) for the travelling $\tilde{k}_x$ and nearfield $\tilde{k}_{nf}$ wavenumbers in the beam.

APPENDIX B.

USE OF MULLER'S METHOD FOR THE ESTIMATION OF COUPLED WAVENUMBERS

If the coupled wavenumber k_x of a beam-plate system is calculated iteratively, erratic fluctuations are observed in the plate impedance at some frequencies. In this appendix, the iteration procedure is explained briefly and a numerical procedure is described to eliminate these fluctuations.

Consider a finite width damped plate and an infinite beam as shown in Figure 3.15. Corresponding dimensions are the same as those shown in Table 2.1. A pinned boundary condition along the opposite edge parallel to the beam is considered and the beam is also assumed to be infinitely stiff in torsion.

The coupled travelling wavenumber k_x could be obtained iteratively using the dispersion equation for the coupled beam which is given in section 4.3.3.

$$D_b k_x^4 = m_b' \omega^2 - i\omega \tilde{Z}_p' \tag{B.1}$$

where D_b is the bending stiffness of the beam, m_b' is mass per unit length of the beam, ω is frequency and $\tilde{Z}_p'$ is the approximate impedance of the plate. An initial value for k_x can be obtained if the semi-infinite plate is assumed, and then the travelling trace wavenumber k_y of the finite plate can be obtained from the trace wavenumber relationship

$$k_y = \sqrt{k_p^2 - k_x^2} \tag{B.2}$$

where k_p is uncoupled wavenumber of the plate. Using the approximate plate impedance corresponding to this value of k_y an improved estimate for the wavenumber k_x is calculated and this procedure is repeated. At most frequencies

the wavenumbers converge after a small number of iterations (for the present case a maximum of 19 iterations are used). Nevertheless, it has been discovered that erratic behaviour occurs when the coupled wavenumber k_x does not converge during the iteration procedure. Figure B.1 and Figure B.2 illustrate this effect for the case of a damped plate. Figure B.1 shows the result after 18 iterations and Figure B.2 shows that after 19 iterations. For further iterations these results are repeated. Large differences can be seen around 20 Hz, 60 Hz, 130 Hz and 450 Hz.

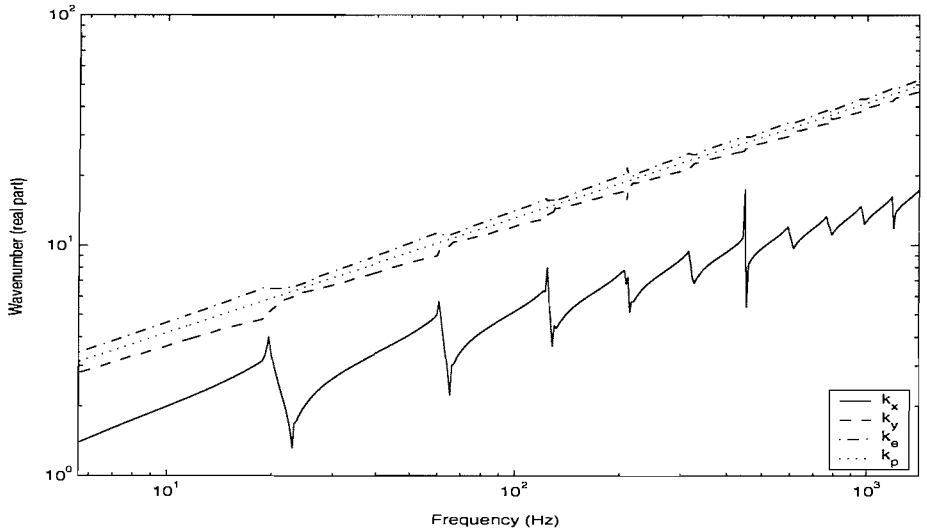

Figure B.1. Comparison of the wavenumber of the coupled structure consisting of an infinite beam and a finite width plate ($\eta_p = 0.05$ in the plate). 18 iterations.

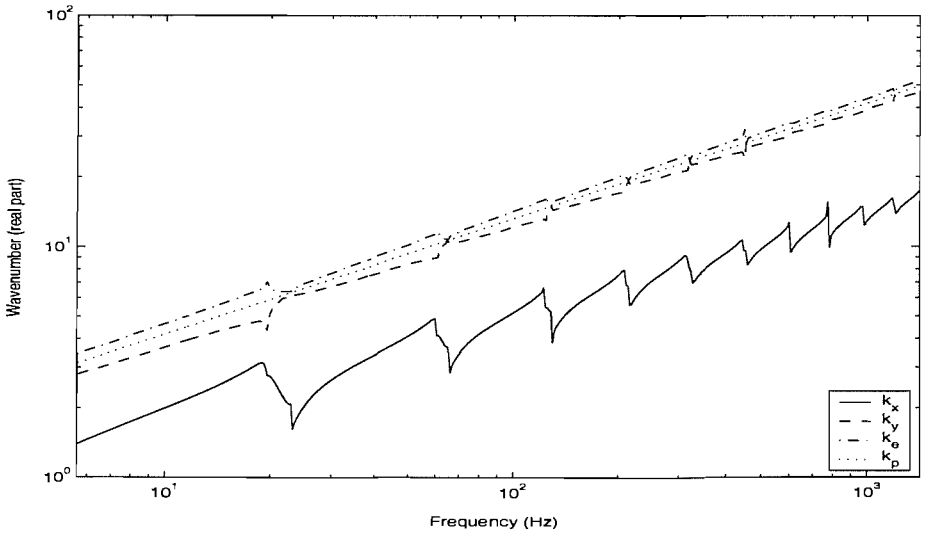

Figure B.2. Comparison of the wavenumber of the coupled structure consisting of the infinite beam and the finite width plate ($\eta_p = 0.05$ in the plate). 19 iterations.

In the figures above, k_p represents the free wavenumber of the plate, k_y the travelling wavenumber perpendicular to the beam, k_e the nearfield wavenumber of the plate in this direction and k_x the coupled wavenumber of the beam. It can be seen that at the first peak near 20 Hz the results do not converge during the iteration. This corresponds to the first anti-resonance of the plate. In this region it can be seen that k_y becomes smaller and k_x become large (Figure B.2). Because the wavenumbers k_x and k_y are related through equation (B.2), the region in which the wavenumbers do not converge occurs when k_y, the wavenumber across the plate, becomes small and k_x, the corresponding travelling wavenumber along the beam becomes large. Therefore, it seems that the iterative method used is not appropriate for some frequency regions, particularly near the peaks in the dispersion curves.

The solution to this problem can start from the dispersion equation (B.1). Because the attached plate impedance $\tilde{Z}'_p$ is a function of the wavenumber $\tilde{k}_x$ the equation can be rewritten as

$$f(\tilde{k}_x) = \tilde{D}_b \tilde{k}_x^4 - m'_b \omega^2 + i\omega\, \tilde{Z}'_p = 0\,. \tag{B.3}$$

As explained in section 4.3.3, it can be assumed that there are four roots close to the uncoupled beam wavenumber $\tilde{k}_b$ and normally two of them represent propagating waves and two nearfield waves. From the complex domain plot, these four roots can be identified. One example for this is shown in Figure B.3. Contours in the figure represent equal values of the function $\left|f(\tilde{k}_x)\right|$ given in equation (B.3) and the four circles in the figure represent roots where $\left|f(\tilde{k}_x)\right| = 0$ (the circles near $\mathrm{Re}(\tilde{k}_x) \approx \pm 5.8$ correspond to peaks and are not roots). Comparing this figure with Figure B.2, it can be said that the root near $\mathrm{Re}(\tilde{k}_x) \approx 3.6$ is the correct value of the travelling wavenumber for the present case.

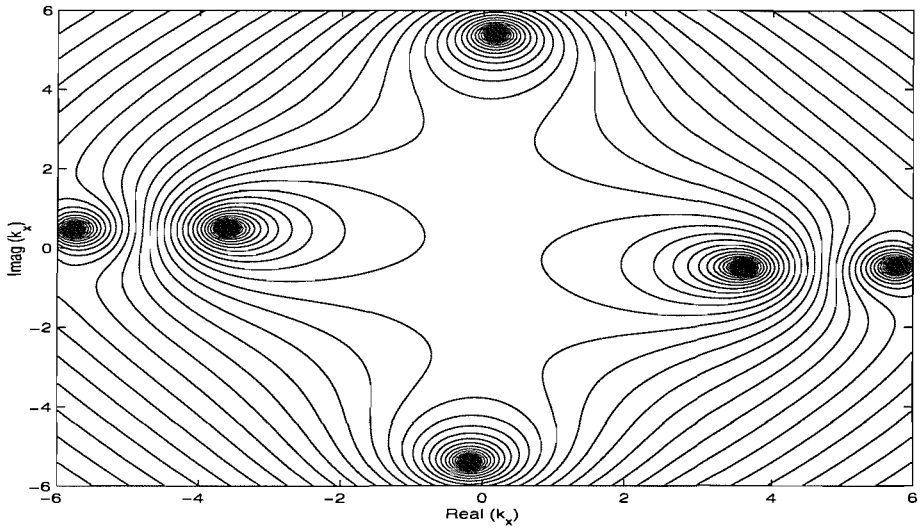

Figure B.3. Complex domain contours (right quadrants) and the roots at 125.1 Hz.

Now, based on these complex domain contours and an appropriate numerical method, the wavenumber $\tilde{k}_x$ can be obtained by calculating the root of this equation. Specifically to obtain such a complex root, Muller's method [83] is a good approach. This method uses a quadratic equation which fits through three points in the vicinity of a root and the proper zero of the equation is used as the estimate of the root. This process is repeated using the set of three points nearest the root being evaluated.

The first three initial values are selected at the complex domain contours such as Figure B.4, basically by trial and error. From the contours the root can be inferred approximately. For example, at 23.7 Hz near the first plate anti-resonance in Figure B.2, the root is expected to exist at the centre of the circles in the fourth quadrant in the contours of Figure B.4. One can see that there are two roots near $\mathrm{Re}(\tilde{k}_x) \approx 1.5$ and 4.9 (the circle near 3.9 corresponds to peak). Thus, although it was assumed that there is only one root in each quadrant in the dispersion equation this is not the case. It is necessary to choose an appropriate root so that it can be used in the wave method, and here the root closer to that found from the dispersion equation is basically chosen. As presented in section 4.3.4, this method for root selection results in wavenumber discontinuity when presented as a function of frequency (see Figure 4.11).

From Figure B.2, it can be inferred that the real part of $\tilde{k}_x$ is smaller than 2 for this case and the root in the lower quadrant is expected to be the centre of circle near $\mathrm{Re}(\tilde{k}_x) \approx 1.5$ in Figure B.4. Therefore, the three initial values are selected by trial and error near this circle. The arrows in Figure B.5 show the procedure converging to find the root near $\mathrm{Re}(\tilde{k}_x) \approx 1.5$ from initial values.

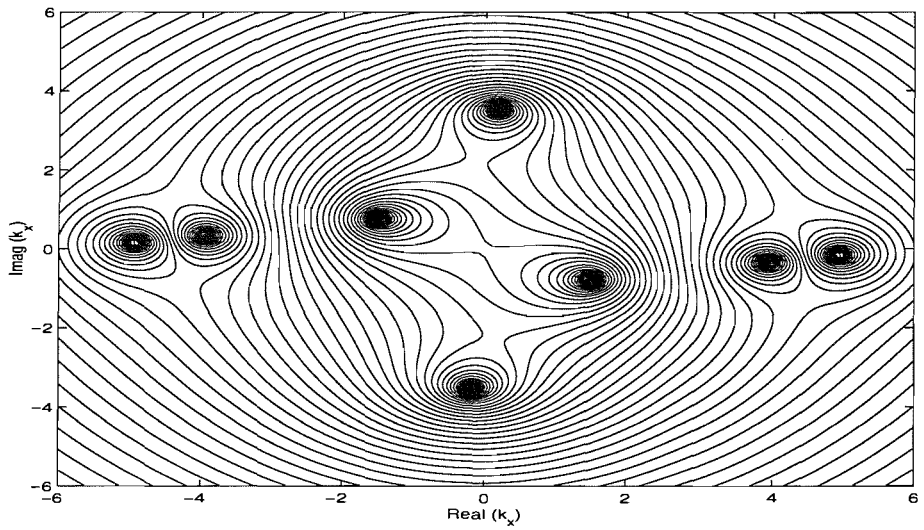

Figure B.4. Complex domain contours and the roots at 23.7 Hz.

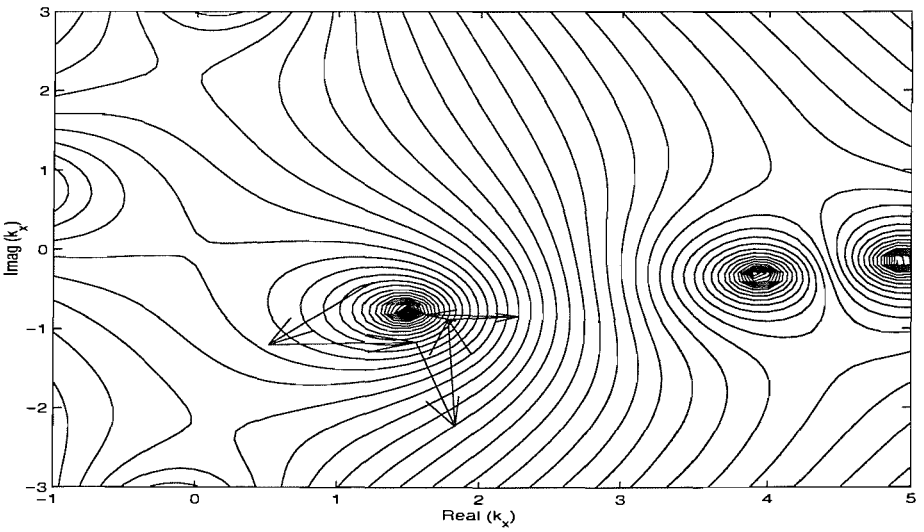

Figure B.5. Root-tracing calculated by Muller's method in the complex domain (23.7 Hz).

As can be seen from Figures B.1 and B.2, during the standard iteration the frequencies at which the wavenumber does not converge can be identified. If the calculated real part of the wavenumber shows more than 0.1 % difference between the results of the 18^{th} and 19^{th} iterations, then that wavenumber is regarded as a wavenumber which does not converge for which Muller's method is then used. The criterion 0.1 % was chosen by trial and error. For example, if 1 % is chosen then the number of calculations required using Muller's method can be reduced but results are not as good. Conversely, if 0.01% is chosen then more calculation is necessary but the results show little improvement. On the basis of the 0.1 % criterion, 66 individual frequencies which do not converge are found and Muller's method is applied to obtain the exact root for the system. Newly calculated wavenumbers $\tilde{k}_x$ and the corresponding plate wavenumbers are shown in Figure B.6, from which it can be seen that the erratic behaviour has been eliminated. The approximate plate impedance, which depends on $\tilde{k}_x$, does not show any erratic fluctuation either, as seen in Figure B.7. It is these results that are used in the thesis.

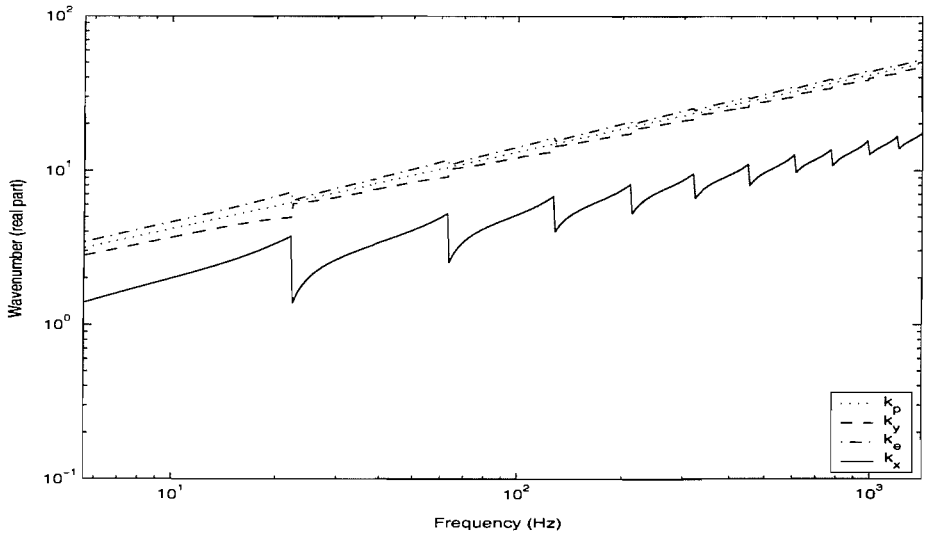

Figure B.6. Comparison of the travelling wavenumber k_x of the coupled structure as in Figure 4.9 ($\eta_p = 0.05$ in the plate) with the plate wavenumbers k_p, k_y, and k_e after using Muller's method.

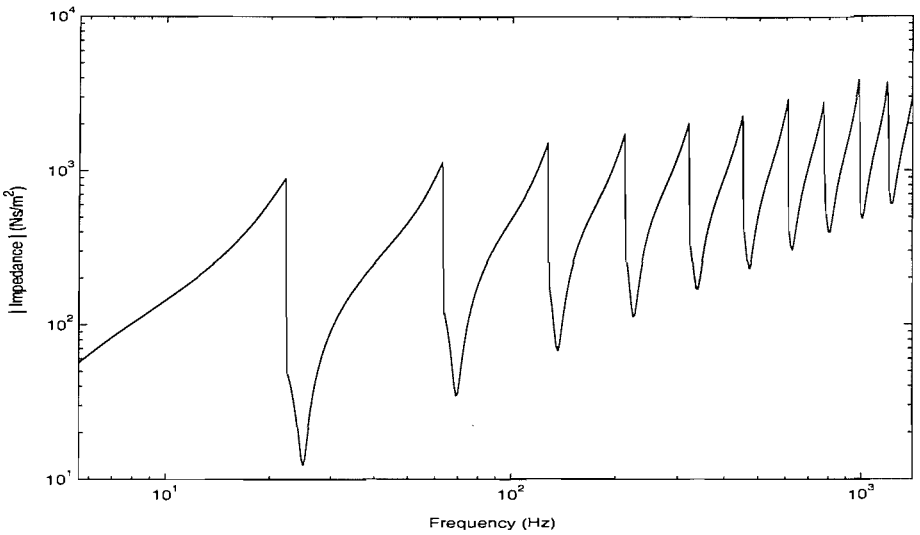

Figure B.7. Approximate impedance of the finite plate ($\eta_p = 0.05$ in the plate) after using Muller's method.

APPENDIX C.
NUMERICAL ANALYSIS OF A SINGLE BEAM COUPLED TO A RECTANGULAR PLATE WITH OPPOSITE EDGE SLIDING

In section 4.3.4, a single beam coupled to a plate was investigated where the plate edge parallel and opposite to the beam is pinned. The same investigation is carried out in this appendix, only the boundary condition is changed from pinned to sliding which means $\tilde{r} = +1$ in equation (4.33). The impedance corresponding to the travelling wavenumber is used to find all wavenumbers.

The basic physical phenomena, for example the relationship between the wavenumbers and the plate impedance and the damping effect of the plate at its anti-resonances, are the same as those found in section 4.3.4. Therefore, only the values of, for example, the resonance frequencies and the anti-resonance frequencies in the impedance will be changed due to the change of the reflection coefficient. Nevertheless, it is important to include the responses of the structure for a sliding plate condition, because this structural analysis is used in the analysis of the structure consisting of two beams which is discussed in section 5.3. The numerical results are presented in the same manner as in section 4.3.4.

C.1 Wavenumbers

Calculating the approximate plate impedance (equation (4.33)) and the dispersion equation (equation (4.34)) the coupled beam wavenumber and the corresponding plate wavenumbers can be found. Muller's method is again used. Figure C.1 shows the wavenumber in the coupled beam and the corresponding wavenumber in the plate. They show that the assumption of the approximate impedance is still valid for

the sliding boundary condition, as $\left|\tilde{k}_x\right| \ll k_p$. Also, it can be seen that the coupled beam wavenumber k_x based on the semi-infinite plate forms the overall trend of k_x based on the finite plate.

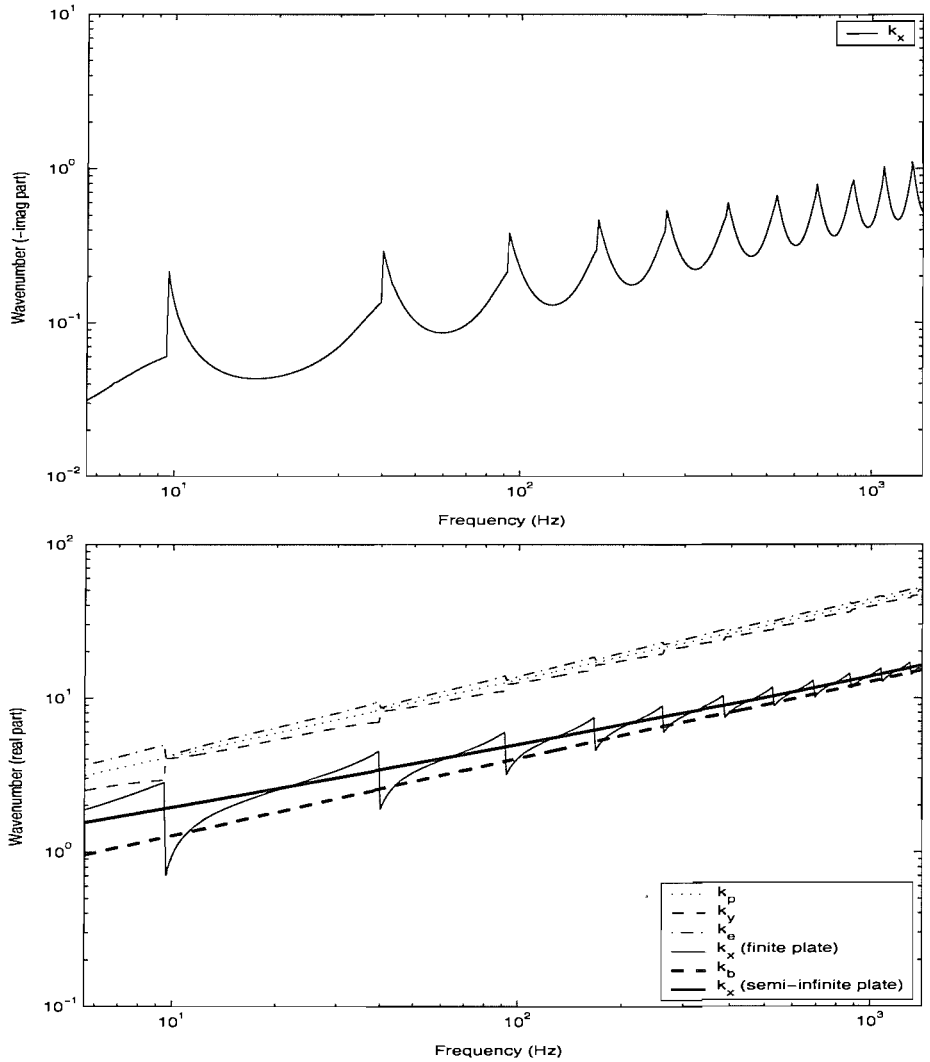

Figure C.1. Comparison of the travelling wavenumber of the beam and the corresponding wavenumbers of the plate of the coupled structure as in Figure 2.2 with a sliding condition on the edge opposite to the beam ($\eta_p = 0.05$ in the plate, $\eta_b = 0.05$ in the beam).

The approximate equivalent loss factor obtained using equation (4.24) is shown in Figure C.2. One can see that the damping effect decreases with increasing frequency as explained in section 4.2.5.

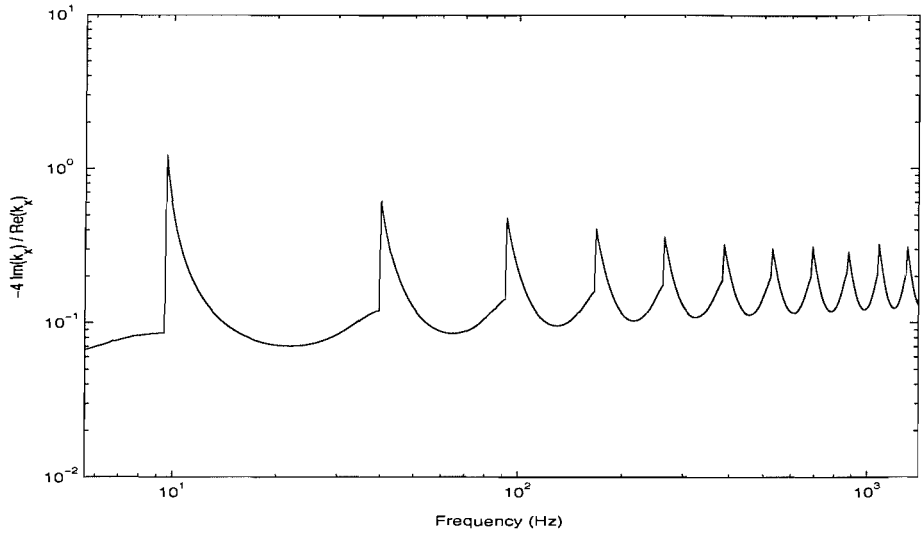

Figure C.2. Equivalent loss factor in the coupled system as in Figure 2.2 with sliding opposite edge.

C.2 Impedance and mobilities

The approximate impedance of the finite plate with damping is shown in Figure C.3. Anti-resonance frequencies in the impedance due to the travelling wavenumber k_x, for example at 9.4, 39.5, 91.3 and 165 Hz, coincide with the frequencies of the peaks in Figures C.1 and C.2.

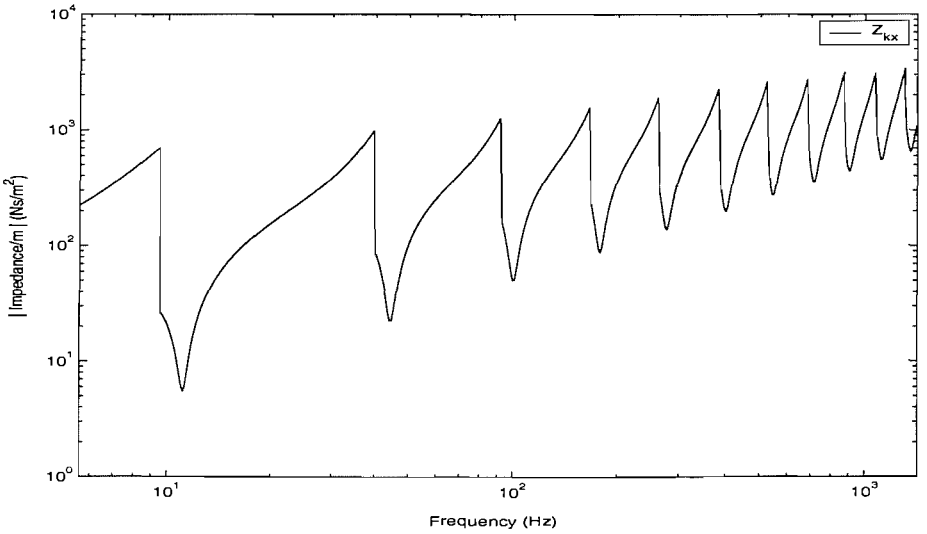

Figure C.3. Approximate impedance of the finite plate as in Figure 2.2 with a sliding condition on the edge opposite to the beam ($\eta_p = 0.05$ in the plate).

The point mobility of the coupled structure for this configuration is shown in Figure C.4. The peaks in the plate impedance result in small troughs in the overall point mobility. The result from the analysis and that from the modal method agree well at low frequencies and their levels at high frequencies are similar on average.

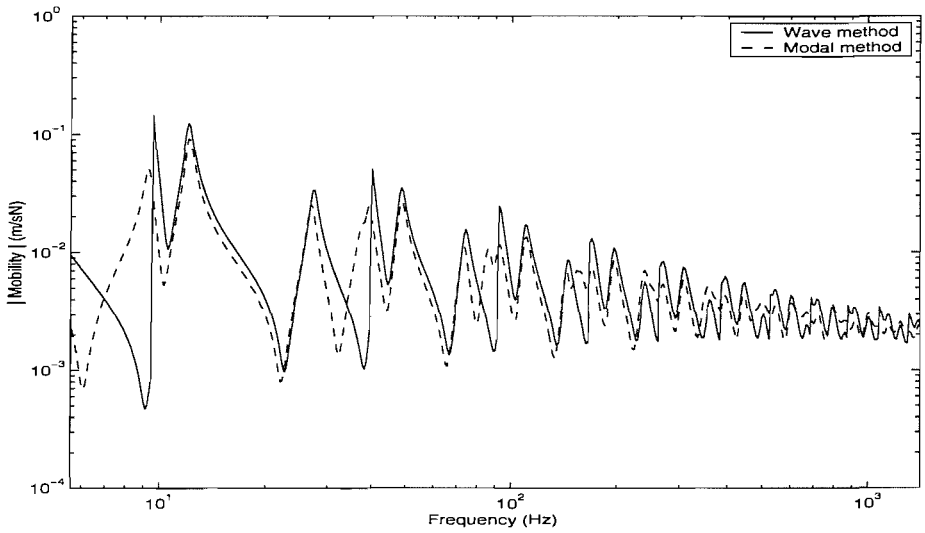

Figure C.4. Point mobility of the coupled structure with the sliding condition ($\eta_p = 0.05$ in the plate, $\eta_b = 0.05$ in the beam, point force applied at $x = 0$). Maximum mode numbers of $M = N = 26$ are used in the modal method (see section 2.6.1).

C.3 Power relationship

The relationship between the input power and the power transferred to the plate and their ratio are shown in Figures C.5 and C.6 respectively. As explained for the pinned structure case, at the anti-resonance frequencies of the plate, such as 9.4, 39.5, 91.3 and 165 Hz, most power is transferred to the plate. These frequencies again coincide with the peaks of the equivalent loss factor based on the travelling wavenumber k_x shown in Figure C.2.

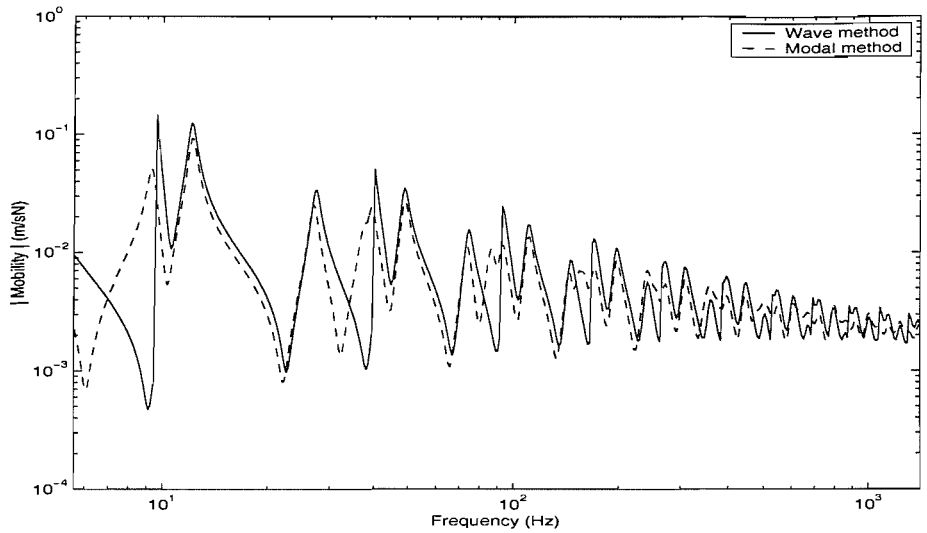

Figure C.5. Comparison of input and transferred powers in the coupled structure for the sliding edge condition ($\eta_p = 0.05$, $\eta_b = 0.05$, point force applied at $x = 0$).

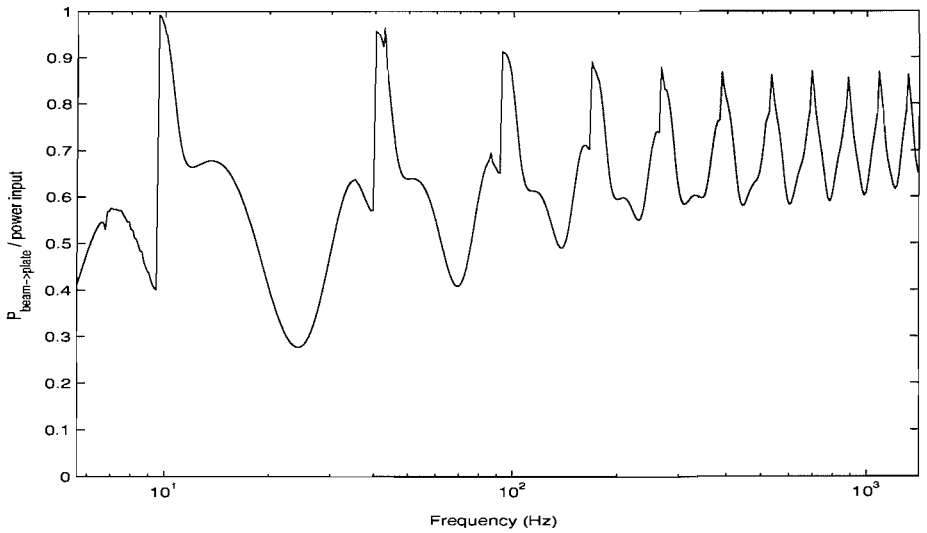

Figure C.6. Ratio of the power transferred to plate to the total input power shown in Figure C.5.

APPENDIX D.
WAVE MODEL OF A FRAME CONSISTING OF FOUR BEAMS

D.1 Equations of motion

A rectangular frame structure consisting of four identical cross-section beams is considered, as shown in Figure D.1. This is solved using a wave approach. Each beam carries free waves with wavenumber $\tilde{k}_b^4 = m_b'/\tilde{D}_b\,\omega^2$ in harmonic motion at frequency ω. An external force is applied at the corner of beams 1 and 4. Each beam is assumed infinitely stiff to torsion. Damping is introduced through a complex bending stiffness $\tilde{D}_b$.

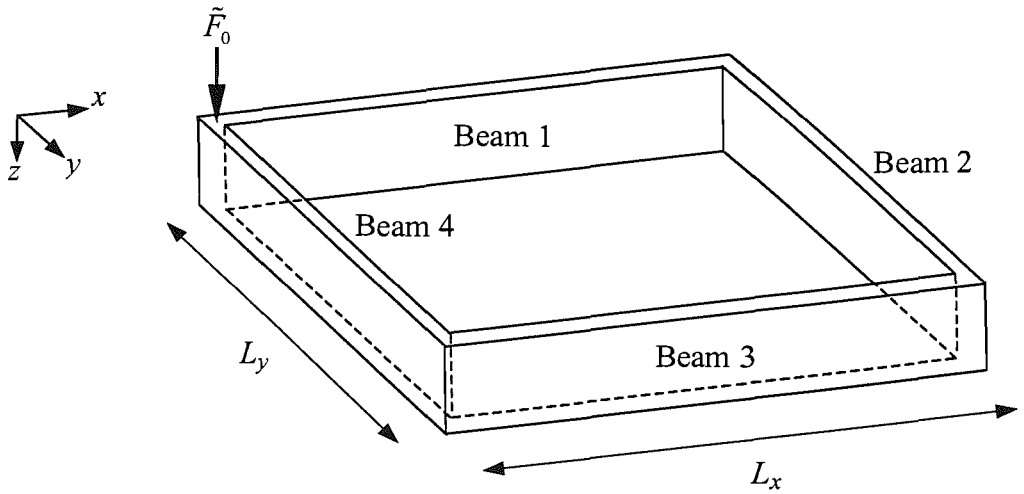

Figure D.1. The wave model consisting of four beams.

The boundary conditions for the four-beam structure as in Figure D.1 are:

(i) Continuity equation; equal displacement at corners

(ii) No rotation at the ends of the beams

(iii) Force equilibrium at the corners

The displacement of each beam can be given by an equation of the following form, shown for example for beam 1

$$\tilde{w}_1(x) = \tilde{A}_1 e^{-i\tilde{k}_b x} + \tilde{B}_1 e^{-\tilde{k}_b x} + \tilde{C}_1 e^{i\tilde{k}_b x} + \tilde{D}_1 e^{\tilde{k}_b x} \tag{D.1}$$

where the subscripts of the equation mean they belong to beam 1. Then, from the first boundary condition, at the corner of beam 1 and beam 2

$$\tilde{A}_1 e^{-i\tilde{k}_b L_x} + \tilde{B}_1 e^{-\tilde{k}_b L_x} + \tilde{C}_1 e^{i\tilde{k}_b L_x} + \tilde{D}_1 e^{\tilde{k}_b L_x} - \tilde{A}_2 - \tilde{B}_2 - \tilde{C}_2 - \tilde{D}_2 = 0. \tag{D.2}$$

The same boundary condition for beam 2 and beam 3 gives

$$\begin{aligned} &\tilde{A}_2 e^{-i\tilde{k}_b L_y} + \tilde{B}_2 e^{-\tilde{k}_b L_y} + \tilde{C}_2 e^{i\tilde{k}_b L_y} + \tilde{D}_2 e^{\tilde{k}_b L_y} \\ &-\tilde{A}_3 e^{-i\tilde{k}_b L_x} - \tilde{B}_3 e^{-\tilde{k}_b L_x} - \tilde{C}_3 e^{i\tilde{k}_b L_x} - \tilde{D}_3 e^{\tilde{k}_b L_x} = 0. \end{aligned} \tag{D.3}$$

For beam 3 and beam 4,

$$\tilde{A}_4 e^{-i\tilde{k}_b L_y} + \tilde{B}_4 e^{-\tilde{k}_b L_y} + \tilde{C}_4 e^{i\tilde{k}_b L_y} + \tilde{D}_4 e^{\tilde{k}_b L_y} - \tilde{A}_3 - \tilde{B}_3 - \tilde{C}_3 - \tilde{D}_3 = 0. \tag{D.4}$$

For beam 1 and beam 4,

$$\tilde{A}_1 + \tilde{B}_1 + \tilde{C}_1 + \tilde{D}_1 - \tilde{A}_4 - \tilde{B}_4 - \tilde{C}_4 - \tilde{D}_4 = 0. \tag{D.5}$$

The condition of no rotation is applied to the ends of the beam, the relevant equation of which for beam 1 is

$$\frac{d\tilde{w}_1(x)}{dx} = -i\tilde{k}_b \tilde{A}_1 e^{-i\tilde{k}_b x} - \tilde{k}_b \tilde{B}_1 e^{-\tilde{k}_b x} + i\tilde{k}_b \tilde{C}_1 e^{i\tilde{k}_b x} + \tilde{k}_b \tilde{D}_1 e^{\tilde{k}_b x} = 0. \tag{D.6}$$

Thus, the two equations given by boundary condition (ii) for beam 1 are

$$-i\tilde{k}_b \tilde{A}_1 - \tilde{k}_b \tilde{B}_1 + i\tilde{k}_b \tilde{C}_1 + \tilde{k}_b \tilde{D}_1 = 0 \tag{D.7}$$

and

$$-i\tilde{k}_b \tilde{A}_1 e^{-i\tilde{k}_b L_x} - \tilde{k}_b \tilde{B}_1 e^{-\tilde{k}_b L_x} + i\tilde{k}_b \tilde{C}_1 e^{i\tilde{k}_b L_x} + \tilde{k}_b \tilde{D}_1 e^{\tilde{k}_b L_x} = 0. \tag{D.8}$$

For beam 2,

$$-i\tilde{k}_b\tilde{A}_2 - \tilde{k}_b\tilde{B}_2 + i\tilde{k}_b\tilde{C}_2 + \tilde{k}_b\tilde{D}_2 = 0 \tag{D.9}$$

and

$$-i\tilde{k}_b\tilde{A}_2 e^{-i\tilde{k}_b L_y} - \tilde{k}_b\tilde{B}_2 e^{-\tilde{k}_b L_y} + i\tilde{k}_b\tilde{C}_2 e^{i\tilde{k}_b L_y} + \tilde{k}_b\tilde{D}_2 e^{\tilde{k}_b L_y} = 0. \tag{D.10}$$

For beam 3,

$$-i\tilde{k}_b\tilde{A}_3 - \tilde{k}_b\tilde{B}_3 + i\tilde{k}_b\tilde{C}_3 + \tilde{k}_b\tilde{D}_3 = 0 \tag{D.11}$$

and

$$-i\tilde{k}_b\tilde{A}_3 e^{-i\tilde{k}_b L_x} - \tilde{k}_b\tilde{B}_3 e^{-\tilde{k}_b L_x} + i\tilde{k}_b\tilde{C}_3 e^{i\tilde{k}_b L_x} + \tilde{k}_b\tilde{D}_3 e^{\tilde{k}_b L_x} = 0. \tag{D.12}$$

For beam 4,

$$-i\tilde{k}_b\tilde{A}_4 - \tilde{k}_b\tilde{B}_4 + i\tilde{k}_b\tilde{C}_4 + \tilde{k}_b\tilde{D}_4 = 0 \tag{D.13}$$

and

$$-i\tilde{k}_b\tilde{A}_4 e^{-i\tilde{k}_b L_y} - \tilde{k}_b\tilde{B}_4 e^{-\tilde{k}_b L_y} + i\tilde{k}_b\tilde{C}_4 e^{i\tilde{k}_b L_y} + \tilde{k}_b\tilde{D}_4 e^{\tilde{k}_b L_y} = 0. \tag{D.14}$$

The shear force acting on beam 1 is given by

$$\tilde{F}_1 = -\tilde{D}_b \frac{d^3\tilde{w}_1(x)}{dx^3} = -\tilde{D}_b\left(i\tilde{k}_b^3\tilde{A}_1 e^{-i\tilde{k}_b x} - \tilde{k}_b^3\tilde{B}_1 e^{-\tilde{k}_b x} - i\tilde{k}_b^3\tilde{C}_1 e^{i\tilde{k}_b x} + \tilde{k}_b^3\tilde{D}_1 e^{\tilde{k}_b x}\right). \tag{D.15}$$

where $\tilde{D}_b$ is the bending stiffness of the beam. As the force equilibrium holds at the corner where two beams join, the corresponding boundary equation can be found. For beam 1 and beam 2 the equation is

$$\begin{aligned}&\left(i\tilde{k}_b^3\tilde{A}_1 e^{-i\tilde{k}_b L_x} - \tilde{k}_b^3\tilde{B}_1 e^{-\tilde{k}_b L_x} - i\tilde{k}_b^3\tilde{C}_1 e^{i\tilde{k}_b L_x} + \tilde{k}_b^3\tilde{D}_1 e^{\tilde{k}_b L_x}\right)\\ &-\left(i\tilde{k}_b^3\tilde{A}_2 - \tilde{k}_b^3\tilde{B}_2 - i\tilde{k}_b^3\tilde{C}_2 + \tilde{k}_b^3\tilde{D}_2\right) = 0.\end{aligned} \tag{D.16}$$

For beams 2 and 3, it is

$$\left(i\tilde{k}_b^3\tilde{A}_2e^{-i\tilde{k}_bL_y}-\tilde{k}_b^3\tilde{B}_2e^{-\tilde{k}_bL_y}-i\tilde{k}_b^3\tilde{C}_2e^{i\tilde{k}_bL_y}+\tilde{k}_b^3\tilde{D}_2e^{\tilde{k}_bL_y}\right)$$
$$+\left(i\tilde{k}_b^3\tilde{A}_3e^{-i\tilde{k}_bL_x}-\tilde{k}_b^3\tilde{B}_3e^{-\tilde{k}_bL_x}-i\tilde{k}_b^3\tilde{C}_3e^{i\tilde{k}_bL_x}+\tilde{k}_b^3\tilde{D}_3e^{\tilde{k}_bL_x}\right)=0. \quad \text{(D.17)}$$

For beams 3 and 4,

$$\left(i\tilde{k}_b^3\tilde{A}_4e^{-i\tilde{k}_bL_y}-\tilde{k}_b^3\tilde{B}_4e^{-\tilde{k}_bL_y}-i\tilde{k}_b^3\tilde{C}_4e^{i\tilde{k}_bL_y}+\tilde{k}_b^3\tilde{D}_4e^{\tilde{k}_bL_y}\right)$$
$$-\left(i\tilde{k}_b^3\tilde{A}_3-\tilde{k}_b^3\tilde{B}_3-i\tilde{k}_b^3\tilde{C}_3+\tilde{k}_b^3\tilde{D}_3\right)=0 \quad \text{(D.18)}$$

For beams 4 and 1, the external force applied at the corner should be included in the equilibrium condition. Thus the corresponding equation is

$$\left(i\tilde{k}_b^3\tilde{A}_1-\tilde{k}_b^3\tilde{B}_1-i\tilde{k}_b^3\tilde{C}_1+\tilde{k}_b^3\tilde{D}_1\right)+\left(i\tilde{k}_b^3\tilde{A}_4-\tilde{k}_b^3\tilde{B}_4-i\tilde{k}_b^3\tilde{C}_4+\tilde{k}_b^3\tilde{D}_4\right)=\tilde{F}_0/\tilde{D}_b \quad \text{(D.19)}$$

Then, equations (D.2) - (D.5), (D.7) - (D.14) and (D.16) - (D.19) can be written into a matrix form.

$$\mathbf{F}=\mathbf{K}\mathbf{u} \quad \text{(D.20)}$$

where the force vector, $\mathbf{F}$ is

$$\mathbf{F}=\left[0\quad 0\quad 0\quad 0\quad 0\quad 0\quad 0\quad 0\quad 0\quad 0\quad 0\quad 0\quad 0\quad 0\quad 0\quad 0\quad \tilde{F}_0/\tilde{D}_b\right]^T, \quad \text{(D.21)}$$

the displacement vector is

$$\mathbf{u}=\left[\tilde{A}_1\quad \tilde{B}_1\quad \tilde{C}_1\quad \tilde{D}_1\quad \tilde{A}_2\quad \tilde{B}_2\quad \tilde{C}_2\quad \tilde{D}_2\quad \tilde{A}_3\quad \tilde{B}_3\quad \tilde{C}_3\quad \tilde{D}_3\quad \tilde{A}_4\quad \tilde{B}_4\quad \tilde{C}_4\quad \tilde{D}_4\right]^T \quad \text{(D.22)}$$

and $\mathbf{K}$ is given by

$$
\mathbf{K} = \begin{bmatrix}
e^{-i\tilde{k}_h l_x} & e^{-\tilde{k}_h l_x} & e^{i\tilde{k}_h l_x} & e^{\tilde{k}_h l_x} & -1 & -1 & -1 & -1 & 0 & 0 & 0 & 0 & 0 & 0 & 0 & 0 \\
0 & 0 & 0 & 0 & e^{-i\tilde{k}_h l_y} & e^{-\tilde{k}_h l_y} & e^{i\tilde{k}_h l_y} & e^{\tilde{k}_h l_y} & -e^{-i\tilde{k}_h l_x} & -e^{-\tilde{k}_h l_x} & -e^{i\tilde{k}_h l_y} & -e^{\tilde{k}_h l_x} & 0 & 0 & 0 & 0 \\
0 & 0 & 0 & 0 & 0 & 0 & 0 & 0 & -1 & -1 & -1 & -1 & e^{-i\tilde{k}_h l_y} & e^{-\tilde{k}_h l_y} & e^{i\tilde{k}_h l_y} & e^{\tilde{k}_h l_y} \\
1 & 1 & 1 & 1 & 0 & 0 & 0 & 0 & 0 & 0 & 0 & 0 & -1 & -1 & -1 & -1 \\
-i\tilde{k}_h & -\tilde{k}_h & i\tilde{k}_h & \tilde{k}_h & 0 & 0 & 0 & 0 & 0 & 0 & 0 & 0 & 0 & 0 & 0 & 0 \\
-i\tilde{k}_h e^{-i\tilde{k}_h l_x} & -\tilde{k}_h e^{-\tilde{k}_h l_x} & i\tilde{k}_h e^{i\tilde{k}_h l_x} & \tilde{k}_h e^{\tilde{k}_h l_x} & 0 & 0 & 0 & 0 & 0 & 0 & 0 & 0 & 0 & 0 & 0 & 0 \\
0 & 0 & 0 & 0 & -i\tilde{k}_h & -\tilde{k}_h & i\tilde{k}_h & \tilde{k}_h & 0 & 0 & 0 & 0 & 0 & 0 & 0 & 0 \\
0 & 0 & 0 & 0 & -i\tilde{k}_h e^{-i\tilde{k}_h l_y} & -\tilde{k}_h e^{-\tilde{k}_h l_y} & i\tilde{k}_h e^{i\tilde{k}_h l_y} & \tilde{k}_h e^{\tilde{k}_h l_y} & 0 & 0 & 0 & 0 & 0 & 0 & 0 & 0 \\
0 & 0 & 0 & 0 & 0 & 0 & 0 & 0 & -i\tilde{k}_h & -\tilde{k}_h & i\tilde{k}_h & \tilde{k}_h & 0 & 0 & 0 & 0 \\
0 & 0 & 0 & 0 & 0 & 0 & 0 & 0 & -i\tilde{k}_h e^{-i\tilde{k}_h l_x} & -\tilde{k}_h e^{-\tilde{k}_h l_x} & i\tilde{k}_h e^{i\tilde{k}_h l_x} & \tilde{k}_h e^{\tilde{k}_h l_x} & 0 & 0 & 0 & 0 \\
0 & 0 & 0 & 0 & 0 & 0 & 0 & 0 & 0 & 0 & 0 & 0 & -i\tilde{k}_h & -\tilde{k}_h & i\tilde{k}_h & \tilde{k}_h \\
0 & 0 & 0 & 0 & 0 & 0 & 0 & 0 & 0 & 0 & 0 & 0 & -i\tilde{k}_h e^{-i\tilde{k}_h l_y} & -\tilde{k}_h e^{-\tilde{k}_h l_y} & i\tilde{k}_h e^{i\tilde{k}_h l_y} & \tilde{k}_h e^{\tilde{k}_h l_y} \\
i\tilde{k}_h^3 e^{-i\tilde{k}_h l_x} & -\tilde{k}_h^3 e^{-\tilde{k}_h l_x} & -i\tilde{k}_h^3 e^{i\tilde{k}_h l_x} & \tilde{k}_h^3 e^{\tilde{k}_h l_x} & -i\tilde{k}_h^3 & \tilde{k}_h^3 & i\tilde{k}_h^3 & -\tilde{k}_h^3 & 0 & 0 & 0 & 0 & 0 & 0 & 0 & 0 \\
0 & 0 & 0 & 0 & i\tilde{k}_h^3 e^{-i\tilde{k}_h l_y} & -\tilde{k}_h^3 e^{-\tilde{k}_h l_y} & -i\tilde{k}_h^3 e^{i\tilde{k}_h l_y} & \tilde{k}_h^3 e^{\tilde{k}_h l_y} & i\tilde{k}_h^3 e^{-i\tilde{k}_h l_x} & -\tilde{k}_h^3 e^{-\tilde{k}_h l_x} & -i\tilde{k}_h^3 e^{i\tilde{k}_h l_x} & \tilde{k}_h^3 e^{\tilde{k}_h l_x} & 0 & 0 & 0 & 0 \\
0 & 0 & 0 & 0 & 0 & 0 & 0 & 0 & -i\tilde{k}_h^3 & \tilde{k}_h^3 & i\tilde{k}_h^3 & -\tilde{k}_h^3 & i\tilde{k}_h^3 e^{-i\tilde{k}_h l_y} & -\tilde{k}_h^3 e^{-\tilde{k}_h l_y} & -i\tilde{k}_h^3 e^{i\tilde{k}_h l_y} & \tilde{k}_h^3 e^{\tilde{k}_h l_y} \\
i\tilde{k}_h^3 & -\tilde{k}_h^3 & -i\tilde{k}_h^3 & \tilde{k}_h^3 & 0 & 0 & 0 & 0 & 0 & 0 & 0 & 0 & i\tilde{k}_h^3 & -\tilde{k}_h^3 & -i\tilde{k}_h^3 & \tilde{k}_h^3
\end{bmatrix}. \tag{D.23}
$$

The displacement of any beam of the coupled structure shown in Figure D.1 can be found from

$$\mathbf{u} = \mathbf{K}^{-1}\mathbf{F} \tag{D.24}$$

allowing $w_i(x)$ to be found from equation (D.1).

D.2 Numerical results

As an example, the point mobility of the structure shown in Figure D.1 is given in Figure D.2. The relevant dimensions and properties of the structure are the same as listed in Table 6.1 except that no plate is attached to the beams. The result is compared with that of FE and they are not distinguishable (maximum error of 0.6%). As in section 6.2.4, the beam are represented by Euler-Bernoulli beam elements (400 elements), constrained to prevent rotation with sliding conditions at the corners.

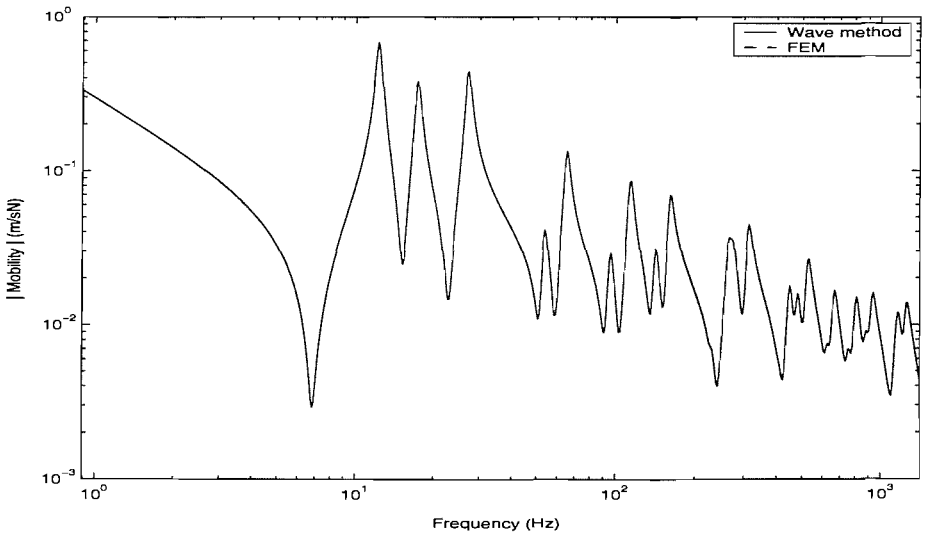

Figure D.2. Point mobility comparison between the wave model and the FE (excitation at $x = 0$ and $y = 0$).

The effect of the torsional stiffness of the rectangular frame structure as in Figure D.1 is identified here. In the FE model the torsional stiffness can simply be realised by releasing the rotational Degree of Freedom (DOF).

Consequently, the sliding boundary condition for the ends of the beam is no longer applied. The results are compared in Table D.1 and Figure D.3. Table D.1 shows the Modal Assurance Criterion value (MAC, [85]), which shows the spatial correlation between the mode shapes obtained with and without the rotational constraint. The table shows the modes below 100 Hz of the system without sliding conditions, which are compared with the rotationally constrained modes. A MAC value equal to unity means that the two modes considered are identical. By allowing the torsional motion of the beams, the natural frequencies of the framed structure occur at lower frequencies than when restrained. For example, it can be seen that the sliding constraint mode at 26.9 Hz is similar to a mode for the system without the sliding constraints occurring at 10.4 Hz. The unconstrained system has three rigid body modes, whereas with the sliding constraints there is only one*. Constraining the beam rotation results in the modes corresponding to 12.2 and 17.3 Hz shown in Table D.1. These modes correspond to a half cosine motion on two opposite beams and rigid motion of the other two beams. Thus, they are rather closer to the rigid modes than other dynamic modes of the system without constraints. So, comparing the dynamic modes of the two systems, although the natural frequencies are significantly changed by the different boundary conditions, the mode shapes are not very different.

* Here, translational rigid modes in x and y directions and a rotational rigid mode with respect to z direction are not included as the FE model is made for comparison with the wave model.

Table D.1. Modal Assurance Criterion between the mode shapes with sliding constraints and without sliding constraints (a zero corresponds to a MAC value of less than 1.0×10^{-3}).

		Modes without sliding constraints (Hz)								
		0	0	0	10.4	24.2	37.8	53.1	63.1	96.9
Modes with sliding constraints (Hz)	0	0.61	0.32	0.07	0	0	0	0	0	0
	12.2	0.38	0.48	0.13	0	0	0	0	0	0
	17.3	0	0.19	0.80	0	0	0	0	0	0
	26.9	0	0	0	0.99	0	0	0	0	0
	53.3	0	0	0	0	0.96	0	0	0.01	0
	64.8	0	0	0	0	0	0.97	0	0	0
	95.0	0	0	0	0	0	0	0.96	0	0
	113	0	0	0	0	0.01	0	0	0.95	0
	142	0	0	0	0	0	0	0	0	0.95

The point mobilities are compared in Figure D.3 where the point force is applied at the joint of beams 1 and 4 as in Figure D.1. It can be seen that allowing the torsional motion of the beam increases the response level as the framed structure becomes more flexible. Especially, at high frequencies, the sliding boundary condition at the excitation point results in a reduction by a factor of 2 in the average level of the point mobility of the framed structure compared with the less constrained case. At very low frequency the difference is larger due to the effect of rotation of the frame on the effective mass.

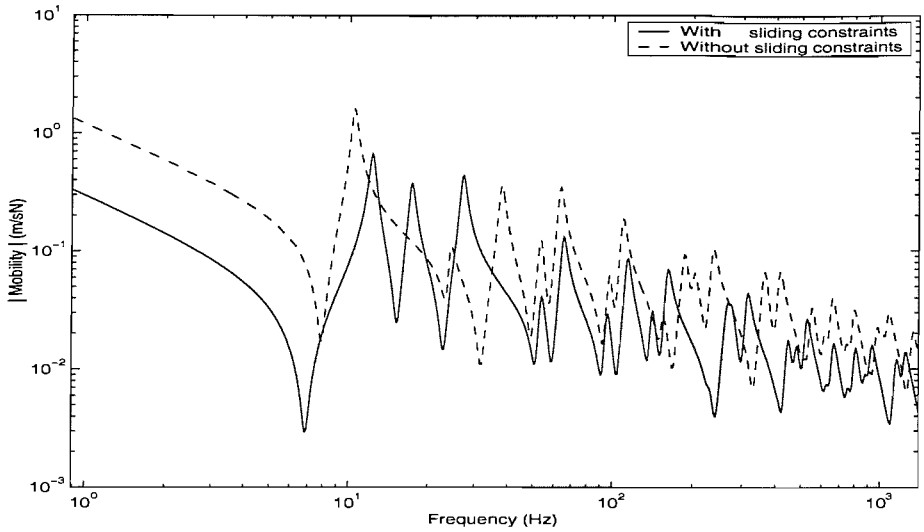

Figure D.3. Point mobility comparison to identify the effect of the rotational constraints on the beam frame structure using FE (excitation at $x = 0$ and $y = 0$).

It is expected that such level differences reduce if the excitation point is moved away from the junction, as the constraint effect reduces. An example is shown in Figure D.4 where the excitation point is located at the middle of beam 1 ($x = 0.5$ m). One can see that the level difference is reduced and, in fact, the general level seems similar except at very low frequencies. However, because the excitation point is located at the mid-point of beam 1, some resonance modes are not identified. Thus, in Figure D.4 only 3 modes are found below 100 Hz for the case without sliding conditions (6 modes found in Figure D.3). Consequently, one may need to choose an appropriate excitation point for the framed structure, so that the two aspects, i.e. the level difference and mode identification, should be considered. In the experimental study in this thesis, an excitation point of 0.36 m from the junction is selected.

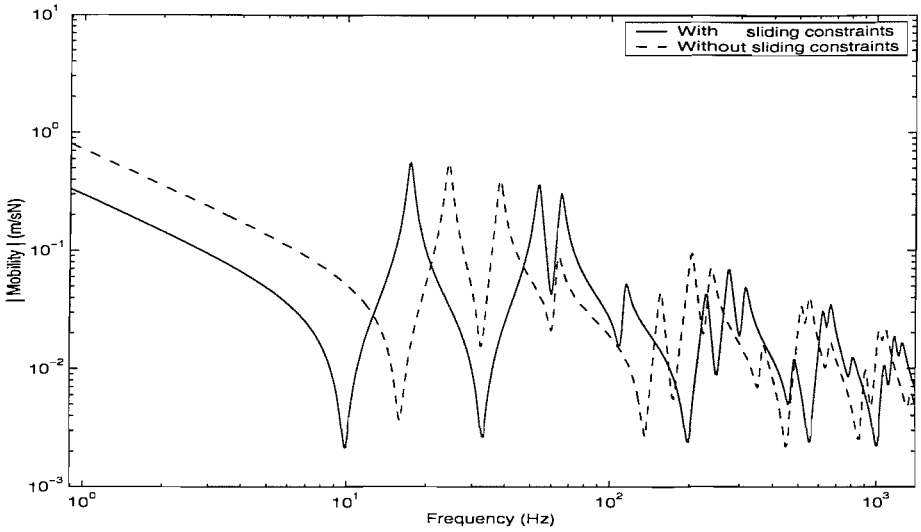

Figure D.4. Point mobility comparison to identify the effect of the rotational constraints on the beam frame structure using FE (excitation at $x = 0.50$ and $y = 0$).

APPENDIX E. WAVENUMBER CONVERGENCE

In the wavenumber estimation from measured data using the spatial Fourier transform of equation (7.6), a larger scanning area gives a better wavenumber resolution. However, as shown in Figure 7.10 the practical area is limited and thus the wavenumber resolution is restricted by this. Although, in the conventional Fourier transform theory the resolution is defined by $2\pi/L_a$ with measuring length L_a, in this appendix an adoptable wavenumber lower limit is investigated.

Various techniques can be used for this. Here the configuration presented in section 7.5.2 is used. A single line of length $L_a = 0.64$ m consisting of 33 points is considered, which is one of the 33 lines forming the scanning area as in Figure 7.10. For convenience this is called beam A and is shown in Figure E.1. Then a sinusoidal motion of the beam A is considered, from which the corresponding wavenumber is estimated.

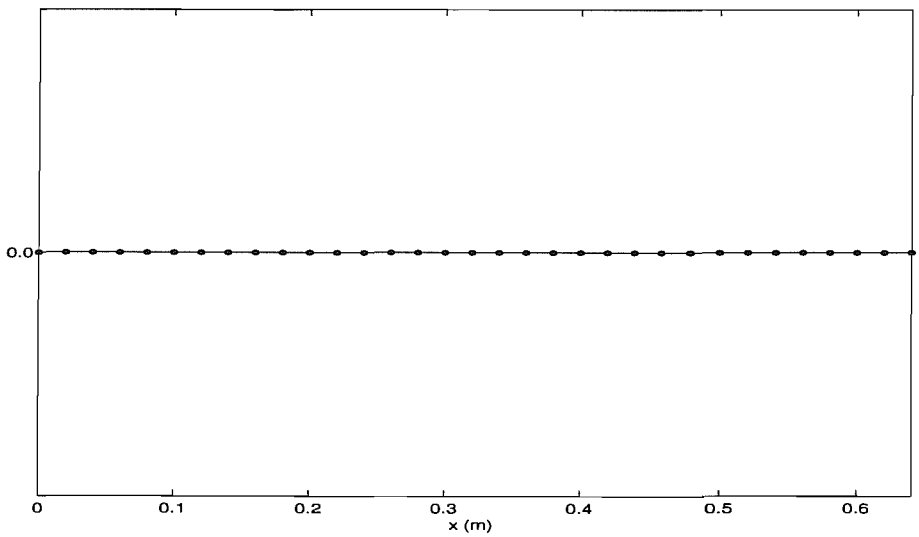

Figure E.1. Beam A consisting of 33 nodes. Length $L_a = 0.64$ m and interval $\Delta x = 0.02$ m.

The representative sinusoidal motion is shown in Figure E.2 (a) where the wavelength is 0.64 m (principal wavelength $\lambda = 0.64$ m) and thus a factor of L_a/λ

is equal to unity ($L_a/\lambda = 1.0$). This is exactly one cycle of a sine function. To evaluate convergence of the wavenumber obtained by equation (7.6) the wavelength for beam A is varied between half and twice the principal wavelength, which seems a reasonable range to investigate the convergence. Correspondingly the factor of L_a/λ is changed from 2 to 0.5. The convergence is shown in terms of L_a/λ. Figure E.2 (b) shows the sinusoidal motion having a factor of $L_a/\lambda = 0.64$.

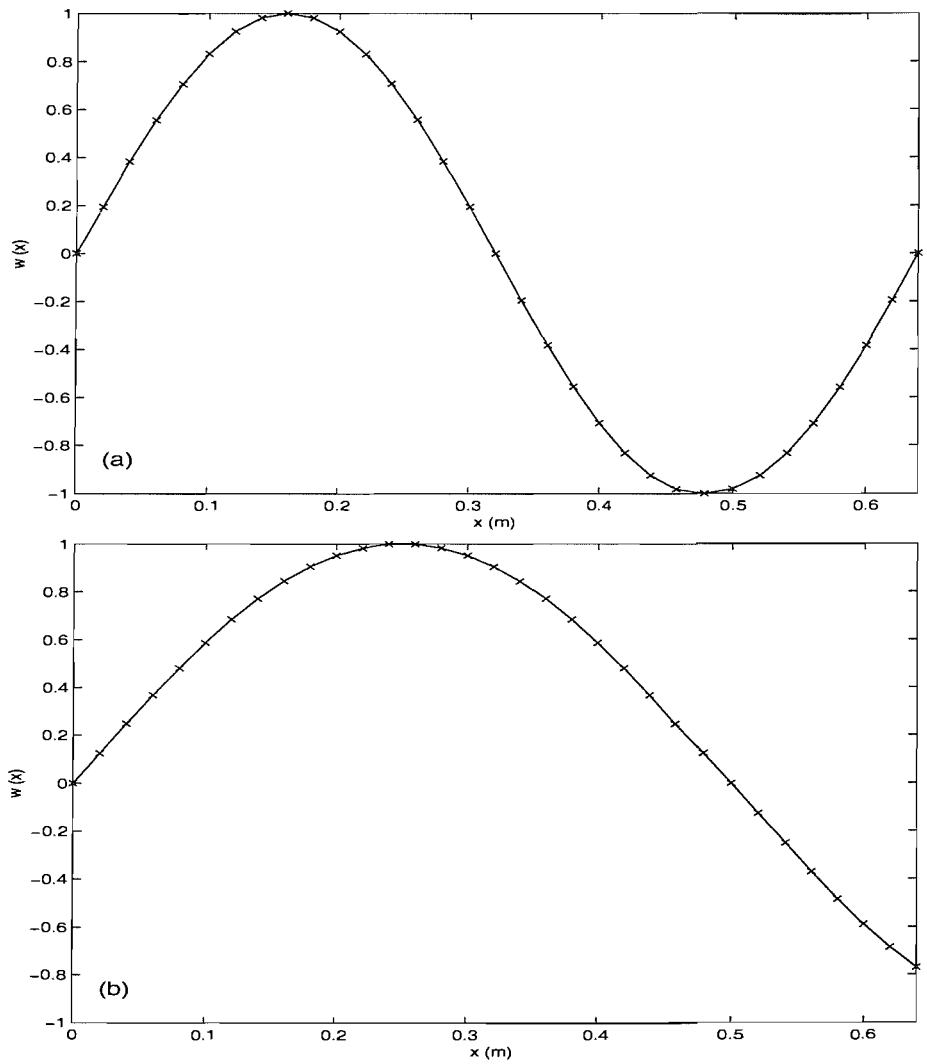

Figure E.2. Motion of the beam A described as a sine function: (a) $L_a/\lambda = 1$, (b) $L_a/\lambda = 0.64$.

To consider various motions, phase changes of 0, $\pi/4$ and $\pi/2$ in the sinusoidal motion are also considered. Figure E.3 shows an example of the motion that has a single cycle with a phase change of $\pi/4$.

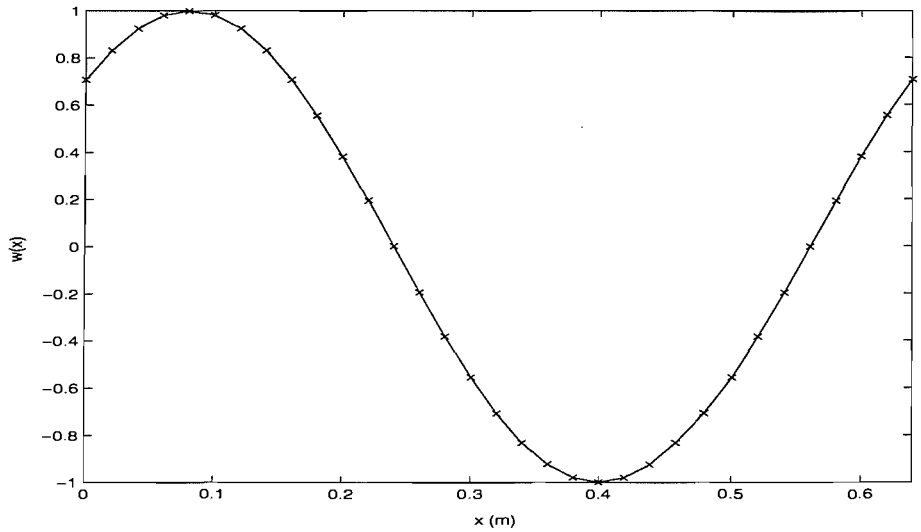

Figure E.3. Motion of the beam A. L_a/λ = 1, phase change of π/4.

Wavenumber estimates are found using equation (7.6) and various displacement motions mentioned above. L_a/λ is varied in steps of 0.02 between 0.5 and 2.0. Calculation examples at factors of L_a/λ being equal to 0.64 and 1.0 with the phase change of 0 are shown in Figure E.4 where the correlation function of equation (7.6) was used (thus normalised value). They give $k_{estimate} = 8.2$ rad/m for the motion of L_a/λ = 1.0 and $k_{estimate} = 5.7$ rad/m for the motion of L_a/λ = 0.64. The corresponding exact wavenumbers are $k_{exact} = 9.8$ rad/m and $k_{exact} = 6.3$ rad/m respectively.

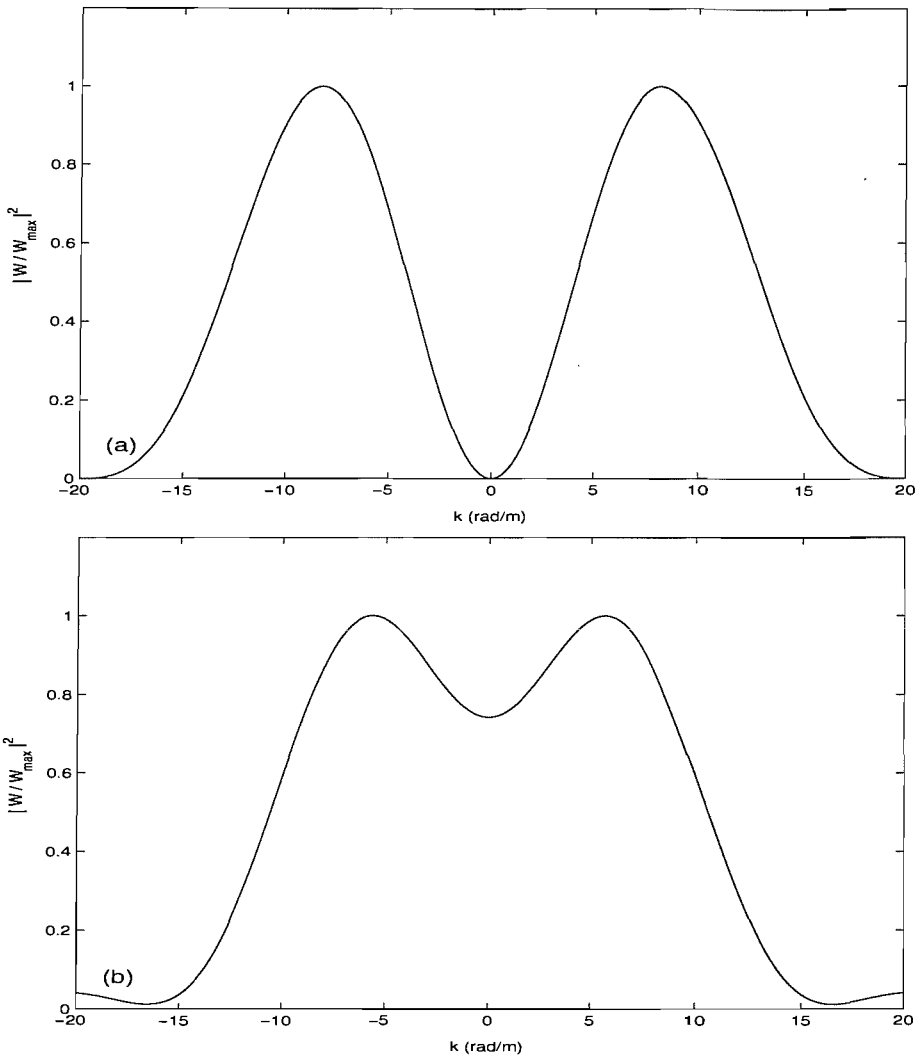

Figure E.4. Dominant wavenumber of the beam A: (a) $L_a/\lambda = 1$ and phase change of 0, (b) $L_a/\lambda = 0.64$ and phase change of 0. The results are shown based on equation (7.6).

The estimates and the exact wavenumbers are compared in terms of L_a/λ. Firstly, the comparison is presented in Figure E.5 where the phase change of 0 is considered. Even when the motion consists of a full sine function ($\lambda = 0.64$ m, $L_a/\lambda = 1$) it can be seen that the estimated wavenumber shows an error of 16 % as the calculation uses only limited discrete data. However, the estimates converge with increasing L_a/λ as expected. The minimum number of L_a/λ to produce a reasonable estimate of the exact wavenumber occurs at $L_a/\lambda = 0.63$ (error of 16%). In such a case the corresponding wavenumber lower limit can be found as $k = 2\pi/\lambda \approx 6.2$ rad/m from $L_a/\lambda = 0.63$ (equivalent to $kL_a = 2\pi \times 0.63$).

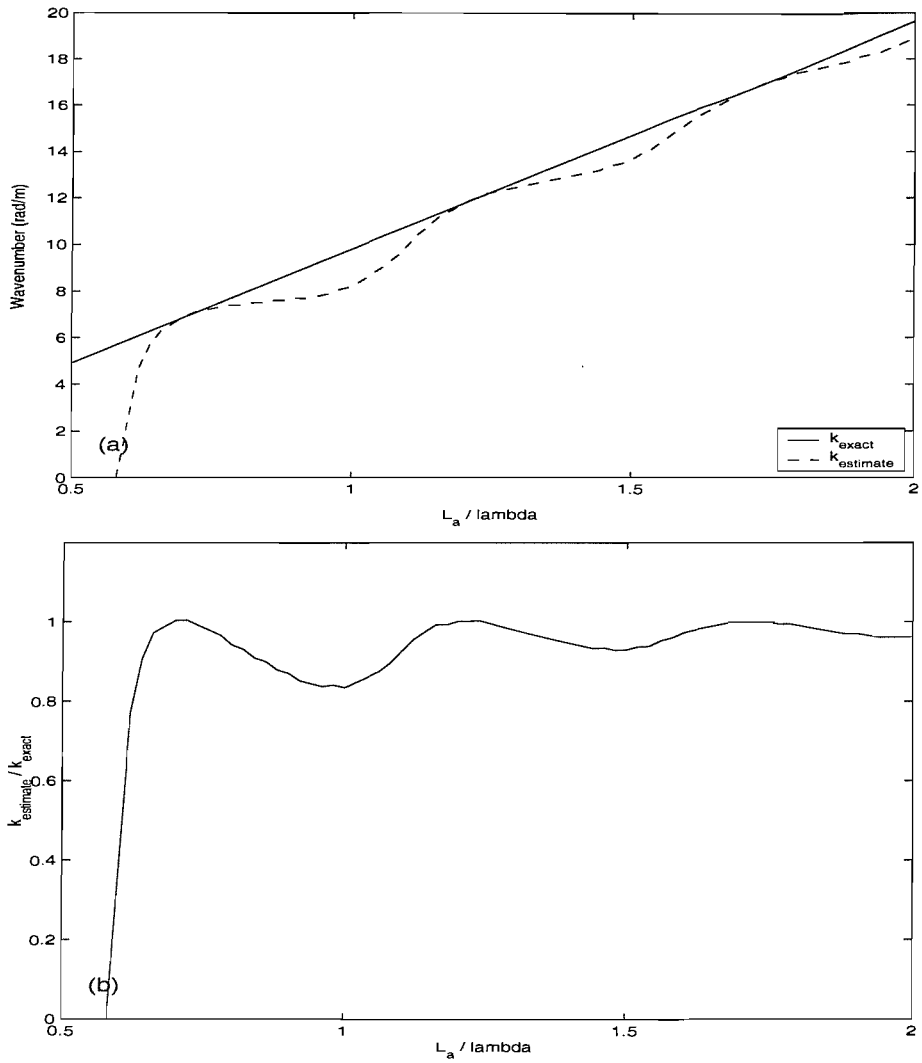

Figure E.5. Comparison of wavenumber estimates and the exact wavenumbers. Motion of the phase change of 0.

The similar results where the phase change of $\pi/4$ is considered are shown in Figure E.6. The errors seem generally smaller than the previous results. A maximum error of 12% is found for the range of L_a/λ considered.

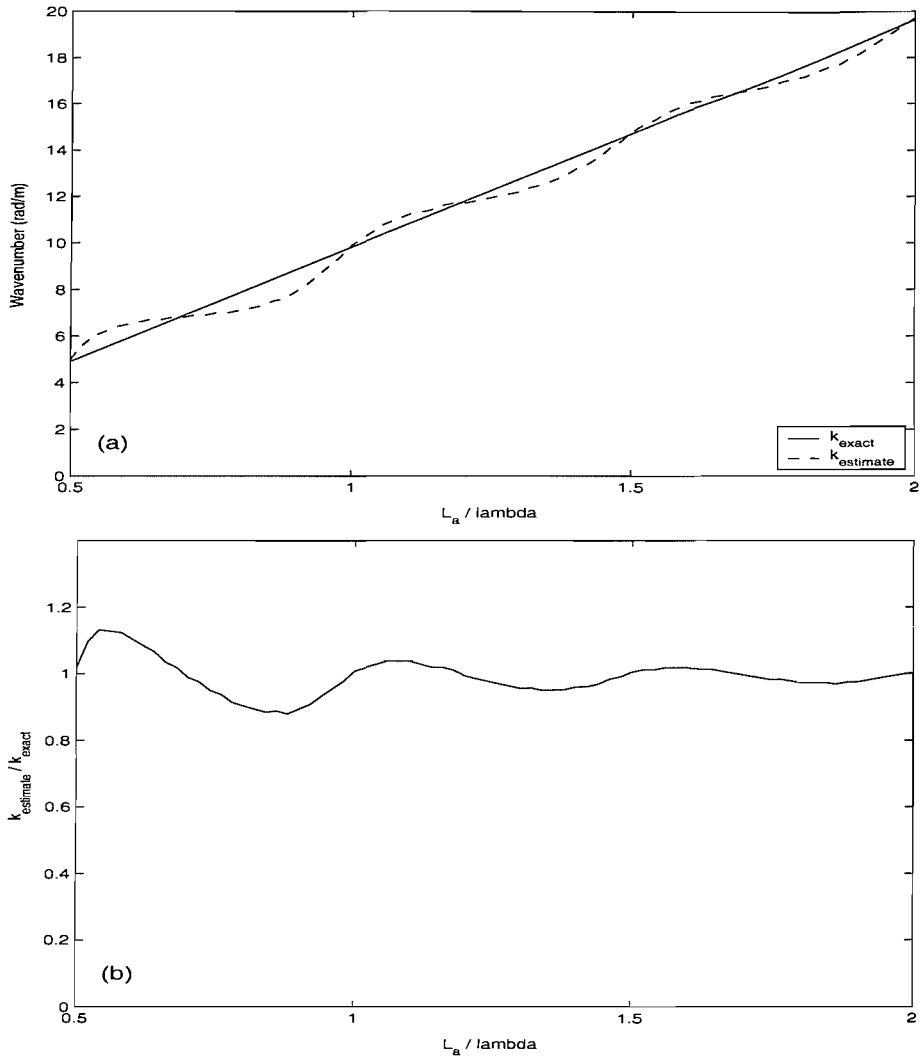

Figure E.6. Comparison of wavenumber estimates and the exact wavenumbers. Motion of the phase change of $\pi/4$.

Next, the motion having the phase change of $\pi/2$ is considered and the results are shown in Figure E.7. The minimum number usable value of L_a/λ is found at 0.53 (error of 13%).

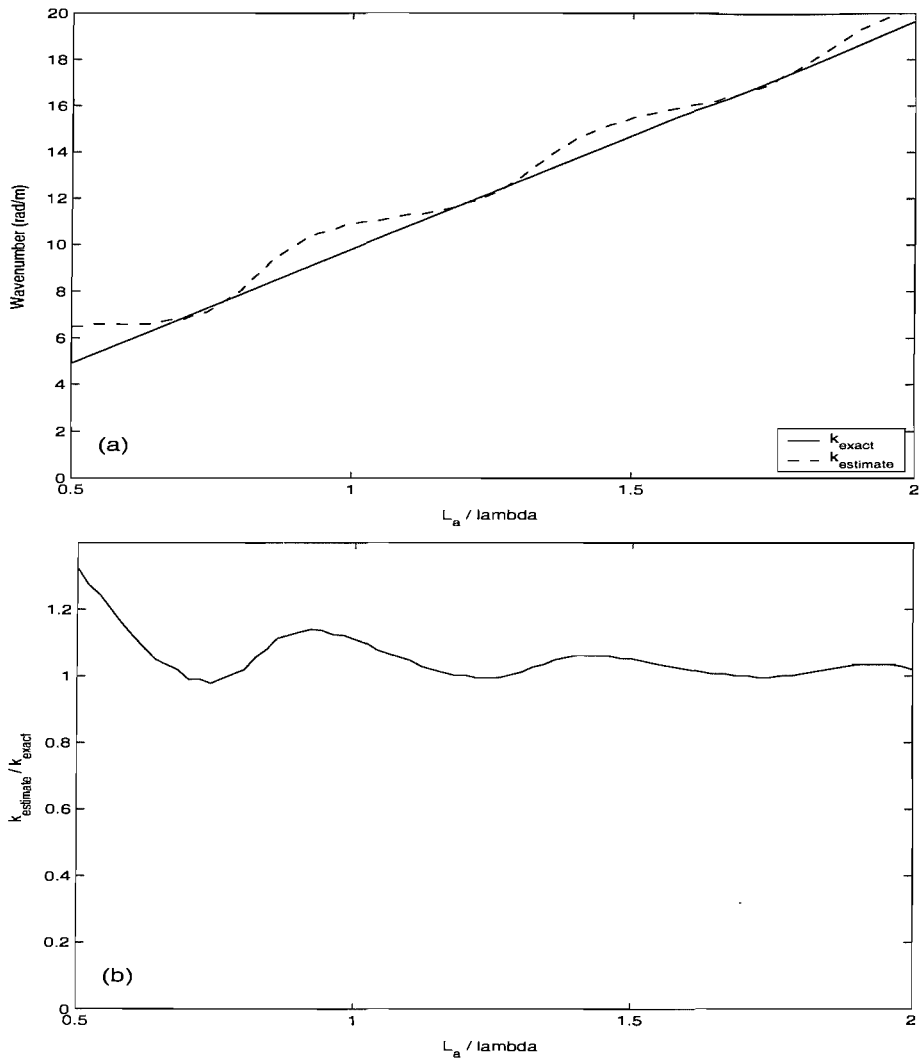

Figure E.7. Comparison of wavenumber estimates and the exact wavenumbers. Motion of the phase change of $\pi/2$.

Summarising the results of the different relative phases, it can be said that the motion having $L_a/\lambda \geq 0.63$, thus 63% of the principal wavenumber ($2\pi/L_a \times 0.63$), can be identified to within 16%. The corresponding wavenumber low limit for the use of equation (7.6) is about 6.2 rad/m. Thus for the present situation, the estimated wavenumber using equation (7.6) may be inaccurate below this wavenumber lower limit.